***Table of contents***

# 1. Introduction

At the present time, the study of biosystems retains a significant relevance in many fields of the scientific research. In particular, the analysis of cells activity 'in vitro' represents a fundamental tool for investigating and understanding complex biological phenomena and it is employed for a number of purposes, such as toxicity studies, vaccines production, the realization of artificial tissues, cell and gene therapies [1]. At the beginning of the 1990's, the first steps toward a deep revolution of the standard experimental methods of traditional biology were taken. This transformation, which has undergone a dramatic acceleration in the last decade, is strongly connected to the development of new miniaturization technologies and to the introduction of new 'smart' materials manufacturing [2]. More specifically, development of micro and nano-fabrication processes and their applications over a new class of soft synthetic biopolymers allowed the production of micro-devices that can implement many of the techniques and functionalities usually employed in traditional biological laboratories' routines are implemented (lab-on-a-chip technologies, LOC). The main advantages of these systems dwell in the use of small amounts of reagents (few hundreds of μL to pL), thus reducing the costs and the amount of polluting wastes, and in the possibility of carrying out single or multiple analysis improving productivity (high-throughput analysis) [3]. The possibility of carrying out fast multi-parametric analysis, manipulating a single cell and realizing spatially controlled cell co-culture on chip also represents a significant improvement in the area of *in vitro* assays [4]. Moreover, based on the experiences acquired with the development and realization of a wide range of micro-electro-mechanical systems, it has been possible to enhance the functional and operational potential of the cells based LOC devices, by integrating mechanical actuators, sensors, electrical and optical components in the chip [5].

From the point of view of the materials employed for the LOCs realization, hydrogels have recently aroused an increasing interest in a variety of cells based applications due to their unique properties. These natural or synthetic hydrophilic polymers present a cross-linked network structure which enables them to imbibe and retain a significantly high amount of

water (from 10 to 100 times their dry weight) still maintaining their solid state [6]. Furthermore, the incorporation of specific co-monomers in the backbone chains during the materials' synthesis can enhance their biocompatibility features and/or confer them a responsive behavior to environmental changes, such as pH, temperature or light intensity (smart hydrogels) [7]. Hydrogels have been previously integrated *in situ* in LOC systems both as substrates for cell culturing and as autonomous sensors (such as biomolecules detectors) and micro-actuators, like valves, pumps, or mixers [8]. The present thesis can be set within the frame of the LOC technologies for the realization of micro-fluidic devices, based on the use of new synthetic hydrogel materials aiming to find a direct application in the 'in vitro' cell culture on chip. The main objective of the research is the development and realization of a manufacturing protocol for producing micro-structured hydrogel based thermo-responsive freestanding thin films (10 to 300 μm thick) that will be subsequently integrated with other micro-fabricated thermoplastic components in order to produce a multilayer LOC device prototype that will operate as a cell sorter by exploiting the stimulus-reactivity of the hydrogel. The specific target application was chosen considering the importance that single cell based assays have gained in the years; their application ranges from stem cells biology, cancer and tumor research, pathological analysis, rare states monitoring to gene expression [9].At the present time, the techniques which are mostly employed for sorting and isolating cells for in vitro single-cell based assays can be divided in three main categories:

*1. Traditional methods:* these sorting strategies rely on sequential dilutions of an original population suspended in the cell medium, that are carried out until a single cell is isolated. The main drawback of this group of methods, which are still widely employed in cell biology (e.g. stem cells clonogenic assay [10]), are predominantly related to its statistical unreliability, lack of reproducibility and its dramatically high time-consuming feature.

*2. Novel techniques:* another family of techniques which are relatively diffused in this field goes beyond the traditional methods in terms of the technology employed for promoting the sorting mechanism and can thus be defined as novel. Laser-capture microdissection [11] or fluorescence activated sorting (e.g. flow citometry [12]) are manual and automated

mechanisms respectively, both relying on the use of extremely expensive equipments which is often complex in use and requires specific and constant technical support.

*3. Sorting on-chip:* LOC systems for promoting cell sorting on-chip have been developed, prototyped and tested using a variety of mechanisms, including magnetic, fluorescence, adhesion, fluidic, acusto-mechanic and electrophoretic based separation [13]. Though the relatively low cost for the production of these devices makes them appealing as an alternative solution for sorting a cell population, there are different disadvantages in using such systems. Firstly, the miniaturized LOC active sorting component is often coupled to, and equipped with, bulky external instrumentation, which could result in cumbersome system implementation procedures; this also requires technical skills which might be too specific for the final users. Furthermore, sorting on-chip mostly relies on a sample labeling procedure before the isolation mechanism takes place (e.g. magnetic sorting) which could damage the cells to some extent or cause collateral effects on the biological specimen which could therefore affect or alter the reliability of the single-cell assay to be carried out. It must also be observed that all of the above mentioned on-chip techniques could not be effectively applied for selecting a specific number of the cells starting from a population of identical cellular units and that it is often difficult to have the sorted cell sample available for analysis in an environment that differs from the device itself, thus eventually limiting the specimen manipulation and related measurements for the user.

In order to meet the requirements of a single cell sorting LOC system, a proposed device was designed and a schematization of its operational functionality is shown in Figure 1.1. The principal component of the device that was to be investigated within the present work for thin films synthesis, fabrication and integration is poly-N-isopropylacrylamide (PNIPAAm), a thermo-responsive polymer hydrogel which undergoes a sharp reversible volume phase transition when the temperature is raised over a threshold value, named the Lower Critical Solution Temperature (LCST), which is around 32°C [14]. If the temperature value of the hydrogel is set above LCST, a shift from its hydrophilic to hydrophobic character is induced, resulting in a coil to globuli transition of the cross-linked chains and in a contextual shrinkage of the polymeric matrix [15]. The idea of exploiting this temperature-triggered mechanism in

the framework of a cell sorting micro-device and the specific operational features of the chip to be realized can be explained as follows. PNIPAAm based thin layers with an array of micro-through-holes (30 to50 µm diameter) are assembled between two fabricated thermoplastic components, the bottom one having cylindrical microwells (100 to 250 µm diameter) aligned with the holes present on the hydrogel and the top one endowed with fluidic ports connected to a chamber which encompase the whole array. The device is initially kept at 37 °C in an incubation cabinet; in this condition, shrinkage of the film takes place and the through-holes diameter will be consequently reduced due to the deswelling of the polymer. After a cell suspension is injected into the top component through the fluidic ports over the array, a pressure difference across the PNIPAAm layer is artificially promoted to capture ("dwell") a single cell on top of each shrunken hole present on its surface. Then, the untrapped cells are washed out by gently perfusing the top chamber with cellular medium. When the temperature of the device is subsequently allowed to reach room temperature due to natural environmental cooling, the swelling of the hydrogel layer will cause the holes to open and the single cell can thus be collected in each well present on the bottom platform. The three components system can then be disassembled to recover the culture plate so that it would be possible to culture single cells in each individual well.

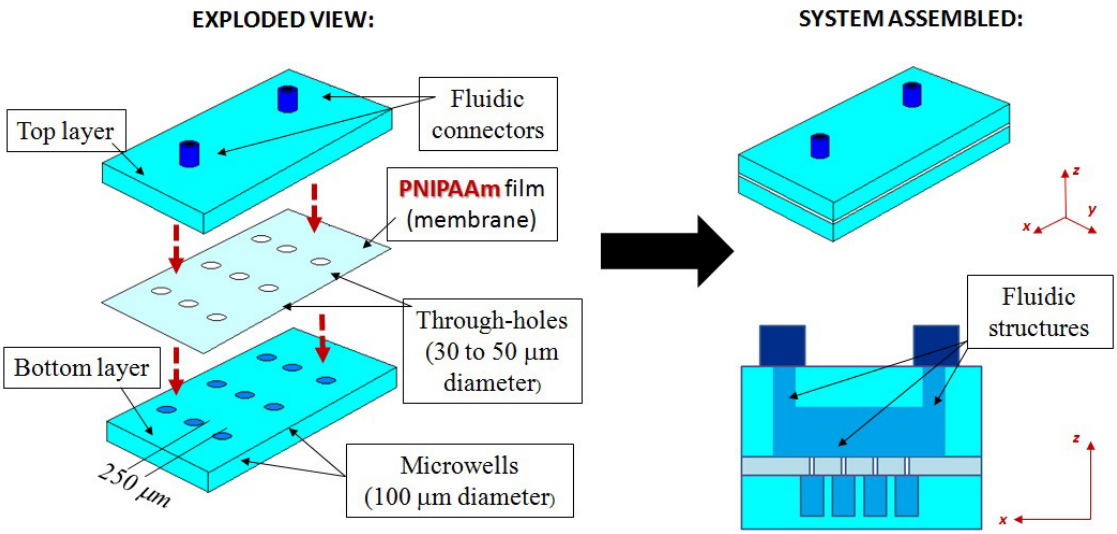


(a)

T = 37 °C > LCST (HOLES ARE CLOSED)
INJECT CELL SUSPENSION IN TOP CHAMBER

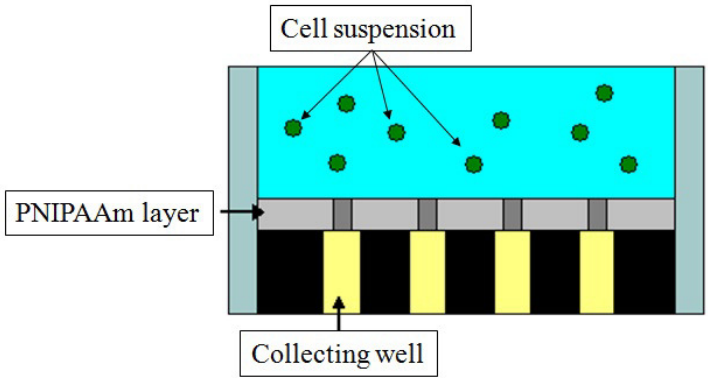


(b)

T = 37 °C > LCST (HOLES ARE CLOSED)
APPLY ΔP THROUGH MEMBRANE TO
CAPTURE A SINGLE CELL PER SINGLE HOLE

'DWELL'

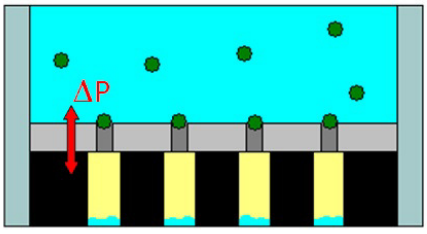


(c)

T = 37 °C > LCST (HOLES ARE CLOSED)
WASH UNTRAPPED CELLS BY
PERFUSION

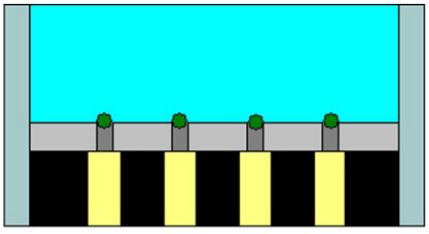

(d)

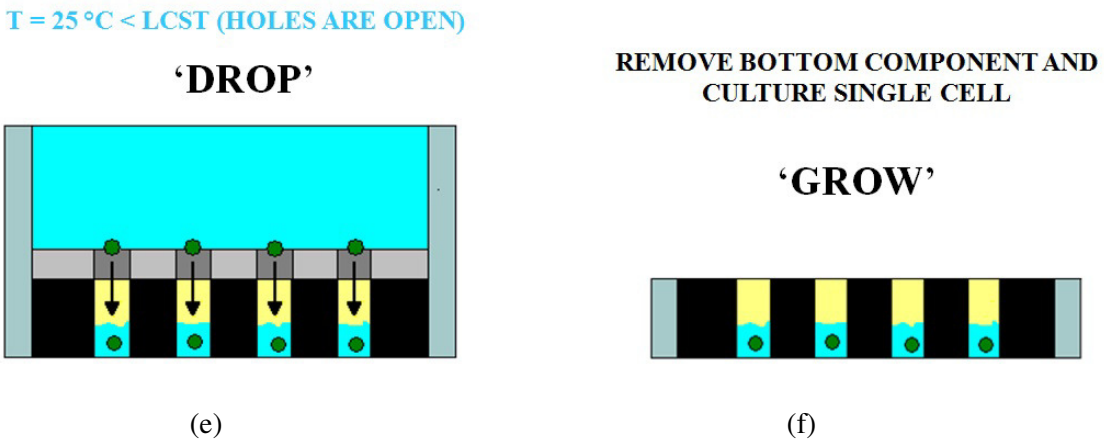


**Figure 1.1.** Schematization of the LOC sorting prototype and its operational principle. a) Exploded view of the chip components and their assembly. b) A cell suspension is injected in the fluidic structure present in the top chamber; the system is kept at 37 °C, so the PNIPAAm layer is beyond the transition point. c) A pressure difference is promoted across the hydrogel film to capture the floating cells in each single hole. d) The cells which are not trapped in the holes are washed by a second perfusion. e) The system is brought back to room temperature so that cells can be dropped in the bottom collecting wells through the opening of the holes. f) The system is disassembled and the bottom component can be used as a multi-well plate for culturing each single cell per well.

The main advantages of this micro-device (DDG i.e. Dwell, Drop and Grow) are:

- The process is time-saving, since the labour for cell sorting is dramatically reduced in respect to the traditional methods which rely on the use of sequential dilution starting from a determined number of cells present in suspension. Furthermore, the reproducibility of the process would eliminate the highly statistical behavior that affects the dilution processes characteristic of the traditional sorting methods.

- The multiple sorting per use determined by the array dimensions (number of holes and corresponding micro-wells) allows a high throughput operation to be carried out.

- The simple user friendly solution which does not require any use of cumbersome or expensive external equipment or any particular technical training to properly put in operation the device also constitute an advantage. Moreover, no labeling of the cellular sample is required prior to sorting.

The research challenges (innovations) required to realize such a device can therefore be identified as:

- The use of freestanding hydrogel layers implemented with other polymeric components and the determination of a suitable packaging process to reversibly assemble the chip. This represents novelty in the area of lab-on-chip applications, since the use of hydrogels materials for this particular applications always relies on moulding and fabrication technique to produce the component directly *in situ* and not *ex situ*, i.e. prior to integration in the device [16].

- As will be explained later, the technique employed for micro-drilling the PNIPAAm based layers was excimer laser machining. Though very few examples of hydrogels structuring using this technique have been reported in the literature [17], micro-hole drilling in thermo-responsive PNIPAAm based material has not been described before. The whole process developed in this research for the moulding and manufacturing of the polymeric freestanding layers is therefore novel.

- The specific sorting mechanism of the device: the temperature controlled dwell, drop and grow procedure using micro-drilled PNIPAAm thin films as an interface between polymeric components is a new way of approaching the sorting process itself in the field of cells-based LOC and sorting operation in general.

The main focus of the present work was to identify the appropriate protocol to realize the PNIPAAm based patterned actuators and to characterize their behavior in order to assess their feasibility in working as smart sorting temperature-triggered interfaces when implemented in a LOC system. In this sense, the work that was carried out extended to the synthesis of the

material and to the development of the layers manufacturing and laser machining protocols, as well as to the characterization of the thermo-responsiveness of the micro-patterned PNIPAAm films and the subsequent layers integration with thermo-plastic components to demonstrate their functionality. The research described in the following chapters therefore developed according to the following methodology:

1. *Materials synthesis:* being initially based on literature methods, PNIPAAm hydrogels were synthesized by tuning the type of chemicals, amount and reaction conditions, in order to produce a library of materials with suitable mechanical properties, such as elasticity, resistance to compressive strain and stress, and optical transparency. These properties were evaluated at a largely qualitative level. Both pure PNIPAAm based hydrogels and PNIPAAm random co-polymers with methylmethacrylate (MMA) or hydroxyethylmethacrylate (HEMA) were synthesized. Characterization in terms of swelling behavior and compositional IR analysis also took place.

2. *Development of the protocol for films fabrication:* an injection/compression molding (ICM) technique was developed and defined on an empirical basis in order to realize a reliable and repeatable protocol with mass production scale up features to produce thin PNIPAAm layers with thickness ranging from 10 to 300 μm. Within this, a study of the hydrogels' adhesion properties to different substrates was conducted to identify the set of conditions for obtaining uniformly flat thin films attached over rigid supports that could also enable the appropriate focusing and normal incidence of the excimer laser when patterning took place. Furthermore, detachment and swelling tests of the layers were carried out by using different chemical treatments to obtain the hydrogel as freestanding components. Then, hybrid poly-HEMA/PNIPAAm layers were molded according to a fabrication protocol inspired by the ICM. These structures were thin films with geometrically defined regions based on different monomers (HEMA and NIPAAm) which were chemically bonded at the interface. Being able to spatially define and control the material properties over the same layer allowed the creation of patterned thermo-responsive PNIPAAm based cores linked to the more elastic PHEMA frame that would operate respectively as the

temperature triggered sorters and the gasket to be compressed by the thermoplastic components in the final DDG prototype.

3. *Excimer laser micro-machining:* patterning of the supported layer was carried out to drill tapered micro-through-holes with entrance holes diameters of 10, 20, 30 and 150 μm depending on the projection mask employed. Machining operational parameters were varied until well resolved features with minimal debris traces were produced. Moreover, different output energy values were explored in order to identify the ablation threshold of the material. The obtained micro-structures were then analyzed by optical and scanning electron microscopy. After detaching and swelling of the layers, tapering characterization was conducted both by optical inverted and confocal microscope to reconstruct a three-dimensional profile of the holes in the PNIPAAm water-swollen state

.

4. *Thermo-responsiveness characterization:* a custom made system which consisted of a thin transparent heater and a thermocouple connected to an electronic proportional integral derivative controller was realized and employed to analyze the behavior of the freestanding machined layers in a liquid environment by regulating the temperature of the water bath they were soaked in. This set up allowed the monitoring of the patterned hydrogel's volume transition by acquiring images in real time using optical inverted microscope images. As a result of the polymer shrinkage, the drilled holes homogeneously reduced their size by a quantity varying from 25% to 50% of their original size depending on the hydrogel structure, thus validating the main idea behind the development of the cell-sorting micro-device. Reversibility of the process was also tested by carrying out multiple cycles and the layers thermo-response characterization under mechanical constraints was conducted as well.

5. *Integration in hybrid materials multilayer micro-devices and DDG prototype development:* poly-methylmethacrylate (PMMA) components were designed and manufactured by computer numerically controlled (CNC) micro-milling to conduct first implementation tests of the hydrogel films in multilayer polymeric devices by

using a screw based compression packaging approach. A Leakage Test Device (LTD) micro-fluidic chip was realized and tested to identify a reasonable pressure range over which PNIPAAm based films could operate as a gasket element, avoiding liquid leakages at the interface between the soft polymer and the thermo-plastic joints without being damaged due to the constraint. A second device was also designed and realized using PMMA micro-milled platforms to demonstrate the proof of principle of the target DDG chip, using a single collecting micro-well instead of a multi-micro-well system on the bottom component.

The potential of the micro-structured and temperature triggered PNIPAAm based smart layers as autonomous interfaces and actuators in the frame of multilayer LOC systems was demonstrated using MG63 cells and the results obtained suggest that these interesting and promising self-regulating micro-structured components represent a valid tool for promoting label-free sorting and filtering on-chip.

## References


[1] Yeon J H Park J-K 2007 *Biochip journal*. **1** 17-27

[2] Li N Tourovskaia A Folch A 2003 *Critical Reviews™ in Biomedical Engineering* **31** 423–488

[3] Paguirigan A L and Beebe D J 2008 *BioEssays* **30** 811–821

[4] Ni M Tong W H Choudhury D Rahim N A A Iliescu C Yu H 2009 *Int. J. Mol. Sci.* **10** 5411-5441

[5] Beebe D J Mensing G A Walker G M 2002 *Annu. Rev. Biomed. Eng.* **4** 261–86

[6] Kopecek J and Yang J 2007 *Polym Int* **56** 1078–1098

[7] Kumara A Srivastavaa A Galaevb I Y Mattiasson B 2007 *Prog. Polym.* Sci. **32** 1205–1237

[8] Becker H and Gärtner C 2008 *Anal Bioanal Chem* **390** 89–111

[9] Ryan D Ren K Wu H 2011 *Biomicrofluidics* **5** 021501-1-021501-9

[10] Fedr R Pernicová Z Slabáková E Straková N Bouchal J Grepl M Kozubík A Souček K **2013** *Cytometry Part A* 83 **472–482**

[11] Frumkin D Wasserstrom A Itzkovitz S Harmelin A Rechavi G Shapiro E 2008 *BMC Biotechnol.* **8** 17-24

[12] Dalerba P Kalisky T Sahoo D Rajendran P S Rothenberg M E Leyrat A A Sim S Okamoto J Johnston D M Qian D Zabala M Bueno J Neff N F Wang J Shelton A A Visser B Hisamori S Shimono Y van de Wetering M Clevers H Clarke M F Quake S R 2011 *Nat Biotechnol.* **29** 1120–1127

[13] Rohin M R Shashi K I Murthy K 2006 *International Journal of Nanomedicine* **1** 3 –14

[14] Otake K Inomata H Konno M Shozaburo S 1990 *Macromolecules* **23** 283-289

[15] Cai S Suo Z 2011 *Journal of the Mechanics and Physics of Solids* **59** 2259–2278

[16] Zhang R Liberski A Khan F Diaz-Mochon J J Bradley M 2008 *Chem. Commun.* **11** 1317-1319

[17] Bryanta J S Cuya J L Haucha K D and Ratner B D 2007 *Biomaterials* **28** 2978-2986

# 2. Literature review

## 2.1. Polymeric Lab-on-a-Chip systems for probing cell biology

Lab-On-a-chip systems (LOC) are becoming increasingly promising tools for probing cell biology at different levels and for addressing more complex and specific questions on biosystems behavior. The application area of this kind of micro-devices is wide and variegate; in this first background section, the application of polymeric miniaturized devices in the most important *in vitro* cell based assays and cell manipulation will be briefly reported before going into details of smart hydrogel based materials and their use in LOCs in the next sections. From an historical point of view, the first miniaturized systems that can reasonably be considered as proper LOCs (as defined in Chapter 1) relied on the use of silicon and glass as the micro-fabricated platforms constituting the device [1]. Though silicon and silicon based materials (e.g. $SiO_2$ and quartz) have the enormous advantage of being suitable for processing using the well established lithographic and etching techniques employed in the microelectronic industry, they do not present high biocompatibility, though some *in vitro* cell culture experiments validate their suitability as culture platforms for cell lines which are not particularly sensitive to the substrate physical and chemical properties [2]. Furthermore, the production costs for realizing miniaturized systems using these materials is relatively high [3]. On the other hand, polymers represent a broad class of materials which can be obtained either in pure form or through polymerization reactions at relatively low costs. They can be manufactured using a wide range of techniques (e.g. printing, replication, laser machining, lithographic processes [4]) and retain a set of properties which enables them to be good candidates to operate as miniaturized platforms and components in the frame of LOC systems which rely on the use of secondary or primary cell lines. These features can be summarized as [5]:

- Biocompatibility; this is an obvious requirement when *in vitro* assays take place, but it has to be highlighted that this fundamental feature is intended as the tendency of the material to mimick the physical and chemical properties of the extracellular matrix, depending on the structural characteristics of the material itself.

- Feasibility and tendency to adaptation to be microfabricated and processed with the available production techniques without being damaged and without degrading, so that reliability and repeatability can be achieved when the manufacturing of the device takes place.

- Optical transparency in the visible range of the electromagnetic spectrum, since most of the throughput screening to be carried out on the cellular samples rely on the use of optical inverted or confocal microscope.

- Suitable mechanical features that render the material easy to handle and not subjected to damages such as breaking, tearing or cracking.

- The possibility of integrating optical, electrical and mechanical components to improve and enrich the functionality of the device.

- Different bonding techniques can be applied for realizing stacking polymeric multilayer devices, such as thermal bonding, solvent assisted bonding and mechanical fastening [6].

- The affinity with the standard sterilization techniques (e.g. autoclave, UV or gamma ray irradiation).

Since it is not trivial for a single material or composite to have all of these properties merging together, a trade-off is often reach by developing multilayer and modular hybrid systems in which a number of components based on different materials is assembled to form a single device. The choice of the materials is typically selected according to the particular application, the experimental set up coupled with the micro-system, the assay to be carried out and the relative equipment for monitoring the process (e.g. fluorescence and confocal microscopy, electro-kinetic studies), and to the specific biological question that the experiment carried out using the micro-system should address. A variety of polymeric materials have been proposed in the literature for developing numerous LOCs covering an enormous range of applications, but the three main groups can be divided into thermoplastics, elastomers and hydrogels [7]. In the next paragraphs examples of devices realized using the

first and second classes of materials are reported, while hydrogel based polymers and their application in LOC systems will be extensively treated starting from section 2.2.

Thermoplastic materials are a family of polymers, with linear or branched structure, which can be heated up above their glass temperature to soften, or melted for processing [8]. This features allows microfabrication routes of these polymers based on injection moulding, hot embossing and microthermoforming [9]. Techniques such as laser ablation (e.g. excimer laser [10]) and micro-milling are also suitable direct methods for realizing micro-structures on thermoplastic substrates [11]. The most widely employed thermoplastics for LOC systems are poly-methyl methacrylate (PMMA), polystyrene (PS), polycarbonate (PC) and cyclic olefin co-polymers (COC). Their low production costs, optical transparency, relatively low water uptake and mechanical properties make these materials particularly interesting in the framework of LOC development [8]. From the cell biology application point of view, all these materials provide a certain degree of biocompatibility [12], but surface physical and chemical functionalization is sometimes required to improve the performance of the polymeric device in respect of a specific analysis. PMMA microchannels have been coated with poly(ethylene glycol) to induce electrophoretic separation of proteins on-chip [13], while both PMMA and PC surfaces have been pristine and UV modified for electrokinetic cell manipulation [14]. A PS microarray for cell culture of HUVEC cells in a miniaturized environment has been treated with low-powered oxygen plasma to confer hydrophilic character to the surface of the chip [15] and thermoformed PC foils have been functionalized by means of heavy ion bombardment to functionalize microcontainers for tissue growth and embryonic stem cells cultivation [16].

For elastomeric LOC devices, the majority of these systems are made of poly-dimethyl siloxane (PDMS). This polymer presents lateral organic $CH_3$ groups covalently bonded to the main backbone that confers a combination of properties to the material which render it particularly suitable for micro-fabrication and for LOC applications [17]. More specifically, its high hydrophobicity, high elasticity, good resistance to high temperatures, optical transparency and low chemical reactivity are the principal features of the elastomer [18]. The easiness to be moulded and its ability to replicate geometrical structures down to 500 nm have given PDMS a crucial role in the development of the soft lithography techniques [19]. A

certain degree of biocompatibility of PDMS has also been observed [20], but the surface functionalization of the silicone substrate with protein and peptides is used to enhance this property [21]. Furthermore, since $CO_2$ gas is able to permeate through thin PDMS layers [22], moulded elastomeric perfusion based microsystems endowed with heaters and gas exchange reservoirs have been prototyped for operating as miniaturized cell incubators, favoring the culture of SupT1 [23] and Hep G2 [24] cells in stand alone LOC devices. In the literature, the examples of microfluidic systems based on PDMS are extremely wide and ranges from electrochemical trans-membrane analysis of cultured cells [25] to micro-bioreactors for stem cell cultivation [26].

## 2.2. Hydrogel materials

As already mentioned in Chapter 1, hydrogels are hydrophilic cross-linked polymer networks able to absorb from 10-20% up to hundreds of times their dry weight in water while still maintaining their solid state [27]. Because of their hydrophilic character, their potential to be biocompatible, their optical transparency and controlled mechanical properties, they have gained an increasing interest in various biomedical applications, such as *in vitro* cell culture platforms and as three dimensional scaffolds for cell encapsulation [28]. Their biocompatible character can be enhanced during the synthesis step, by incorporating bioactive co-monomers in the polymer matrix and by tuning their mechanical properties in order to generate a tissue analogue for the specific cell type involved in the culture [29]. Moreover, hydrogels are degradable non-toxic materials, and this feature renders them a useful tool in the tissue engineering field as a support for cell growth and then for generating an implantable construct [30]. The microfabrication techniques developed for moulding soft polymers are important tools for producing surface microstructured hydrogels that can potentially be used as microfluidic biomimetic components for on-chip cell cultivation and various LOC applications [29]. In this sense, to microfabricate and microengineer this family of polymers a variety of techniques have been developed, such as emulsification, photolithography, microfluidic and micromoulding [30]. Among this family of polymers, the class of the so

called ‘smart’ hydrogels has been revealed to be particularly interesting for LOC applications. These materials are able to undergo a volumetric phase transition in response to environmental stimuli (e.g. pH, temperature, light intensity or electric field variations) due to the presence of reactive co-monomers which confer responsiveness to the whole polymeric matrix [31]. There are a range of smart hydrogels, but one of the most important due to its thermo-responsive character is PNIPAAm which is discussed in the next section.

### 2.2.1. PNIPAAm smart hydrogels

Smart hydrogels can be subjected to macroscopic changes due to a reversible phase transition induced by variations of the surrounding environmental conditions [32]. From a general point of view, they can alter their shape due to modifications in the molecular interactions occurring in the polymeric matrix; for example, a shift from a hydrophilic to hydrophobic character of the hydrogel in response to a physical or chemical stimulus that results in a shrinkage of the material, as a consequence of water loss from the structure [33]. As mentioned in the previous section, hydrogels responding to pH, temperature, light intensity or electric field have been engineered and studied extensively [34]. Regarding thermo-responsive smart hydrogels, PNIPAAm is the most widely studied material; it exhibits a sharp conformational coil to globuli phase transition when the temperature is raised above 32° C [35], resulting in a characteristic shift from a hydrophilic to hydrophobic state which leads to a partial loss of the water embedded in the network with a consequent hydrogel shrinkage [36]. A schematization of the PNIPAAm volume phase transition is shown in Figure 2.1.

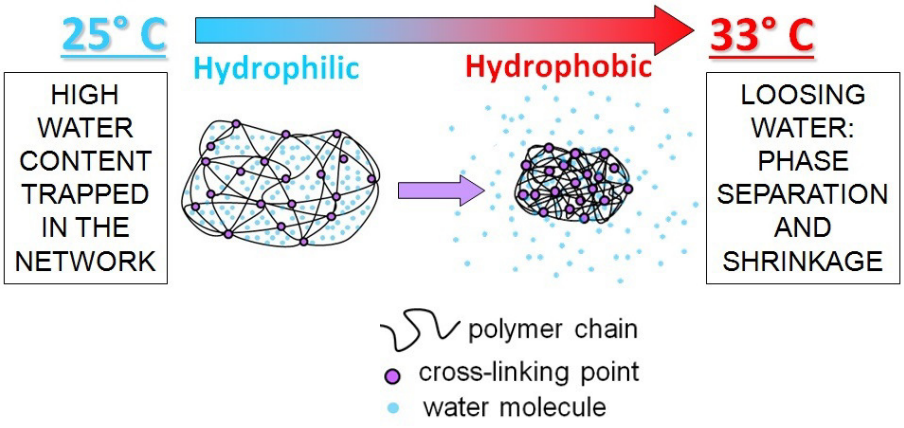


**Figure 2.1.** PNIPAAm hydrogel volumetric phase transition.

The level of shrinkage is known to depend on a number of factors, such as reaction conditions or cross-linker amount [37]. Since the transition temperature is close to the physiological value of 37 °C, PNIPAAm based hydrogels have been synthesized and engineered to be employed in a wide range of biomedical and biotechnological applications in the last decades [38]. Figure 2.2 shows the chemical structure of the PNIPAAm monomer.

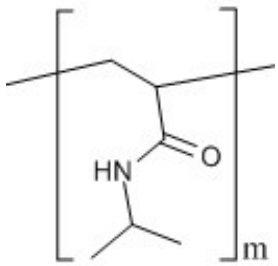


**Figure 2.2.** PNIPAAm hydrogel monomeric unit

As can be seen from the monomeric unit structure, there is a coexistence of hydrophobic backbone and isopropyl groups with hydrophilic acrylamide pendants, which interact with water molecules through different mechanisms. From the thermodynamic point of view, water tends to form a clathrate-like structure around the non polar regions, orientating in such a way that a local order structure is formed around the hydrophobic groups; this results in a

negative value of the mixing enthropy $\Delta S_{mix}$ [39]. On the other hand, water molecules establish hydrogen bonds with the hydrophilic groups, eventually giving a negative value to the mixing enthalpy, $\Delta H_{mix}$ [39]. Defining the Gibbs free energy of mixing for the system as:

$$\Delta G_{mix} = \Delta H_{mix} - T\Delta S_{mix} \quad [1.1]$$

when the temperature is increased over the LCST value, the hydrophobic interaction becomes dominant, the Gibbs free energy reaches a positive value and the de-mixing regime is established, causing water loss and the subsequent hydrogel shrinkage mentioned above [40]. It must also be observed that, as a result of the phase transition, the polymer Young's modulus dramatically increases in its collapsed state, shifting from a few hundreds of kPa to a few MPa [41]. The transition mechanism and kinetics has been experimentally studied in various ways, including thermal measurements (microcalorimetric studies [42] and differential scanning calorimetry [43]), structural analysis (nuclear magnetic resonance [44]) and spectroscopy (fluorescence correlation spectroscopy [45], plasmon resonance [46]). Theoretical modelling based on the poroelastic theory [47] and on classical thermodynamics [48] as well as numerical simulations [49] have been carried out to obtain more detailed information on the phenomenon. Although some general trends have been identified and tracked, since hydrogel materials' mechanical properties and stimuli-responsive behaviour are in general very sensitive to their composition, reagent amounts and synthesis conditions, slight variations in one of those parameters could lead to a material with significantly different properties [50] and that thus should be individually characterized. Some of the aspects to be considered as general properties of PNIPAAm based hydrogels are reported below.

- The transition temperature for single monomer PNIPAAm based hydrogels is 33 °C, but it can be increased or decreased by adding hydrophilic or hydrophobic co-monomers respectively. An excessive amount of co-monomers could hinder the transition [51].
- The shrinkage of the polymer decreases with increasing cross-linker amount [52].
- Reaction temperature during synthesis affects the homogeneity of the hydrogel and the degree of shrinkage. PNIPAAm based hydrogels synthesized at temperature values

close to the LCST show decreased polymer homogeneity (and increases its refractive index) and degree of shrinkage [53].

- A thick skin layer preventing water escape spontaneously forms over the hydrogel surface after the transition takes place at the thermodynamic equilibrium [54].
- The kinetic process of the transition is not fully understood and no comprehensive general theory exists at the present time [55], but the deswelling rate is known to increase when the hydrogel porosity and network mesh size is increased [56].

Before discussing the application of PNIPAAm based materials in the context of LOC systems, microfabrication techniques for processing hydrogel materials will be discussed.

## 2.3 Hydrogel moulding and microfabrication

### 2.3.1. Thin Films

Thin hydrogel films, with thickness ranging from a few nanometers to several hundreds of micrometers, have been produced both *in situ* and as freestanding layers by a number of techniques, including spin coating, layer-by-layer, plasma deposition techniques and capillary driven or direct injection in a mould [57, 58]. The main advantage of having thin films in the context of stimuli-responsive hydrogels is that the response rate can be dramatically increased, to reach values going from a few seconds to one hour [59]; this is predominantly due to the fact that water migration and expulsion from the polymeric matrix is favoured through the small thickness of the layers compared to the bulk systems. More specifically it has been shown that response times can be tailored to less than one second for responsive-hydrogel layers thinner than 10 μm [60]. It should also be noted however, that a substantial difference in response can be found between freestanding and mechanically constrained hydrogel thin layers. In many applications, including LOCs, it is desirable to realize a hydrogel based thin films which adhere or which are covalently bound to a rigid support, thus having an in-plane constraint due to the attachment to the substrate. As a result, these layers can swell only in the direction perpendicular to the constriction plane, thus limiting the 3D

free isotropic and homogeneous swelling typical of the unconstrained configuration [61]; depending on the aspect ratio of the film, deformation effects like side curvatures and bending, can also take place during the swelling - deswelling process [62]. PNIPAAm films have been grafted on a variety of substrates (glass, chemically functionalized plastics) using both UV photo-polymerization and free-radical polymerization techniques [63, 64], while freestanding PNIPAAm based thin brushes have been realized using the layer-by-layer technique [65] or by peeling off the polymerized structure after casting from the preparation substrate [66]. The LOC applications involving PNIPAAm based thin film predominantly rely on coating of the microfluidic structures with the thermo-responsive hydrogel [67], grafting [68] or on *in situ* photo-cross-linking [69], while it appears that no freestanding based PNIPAAm thin layers as a stand-alone component integrated on chip during the device assembly have been reported in the literature. In this framework, the main challenge is to engineer a PNIPAAm based hydrogel film which is able to retain its thermo-responsive properties when mechanically constrained as it would operate as a freestanding component.

### 2.3.2. Soft lithography based techniques

Among the most recent development in micropatterning of smart materials, photo-cross-linking is nowadays one of the principal technique for processing hydrogel layers and stimuli-responsive polymers in general. In this kind of process, formation of the cross-linked network can be promoted and spatially controlled over precisely localized regions by exposing the native polymer mixture to a source of UV radiation through a shadowing mask. This not only allows the production of micro or nano-sized hydrogel structures with controllable geometrical features, like beads, pillars or brushes, but can also be employed for modulating the material properties, such as their degree or rate of reaction to the external stimulus, as well as their mechanical properties [70]. Soft lithography techniques also find a wide range of applications in hydrogel micro-structuring [71]; the approach is based on the realization of a negative mould of the structures that constitute the desired micropattern by employing an elastomeric stamp, usually in PDMS, which replicates the geometrical features previously fabricated on a original master (e.g. etched silicon). The PDMS operates as the

new mould to define the size and shape of the forming hydrogel by embossing the cross-linking gel (replica micromoulding). A schematization of this technique is represented in Figure 2.3.

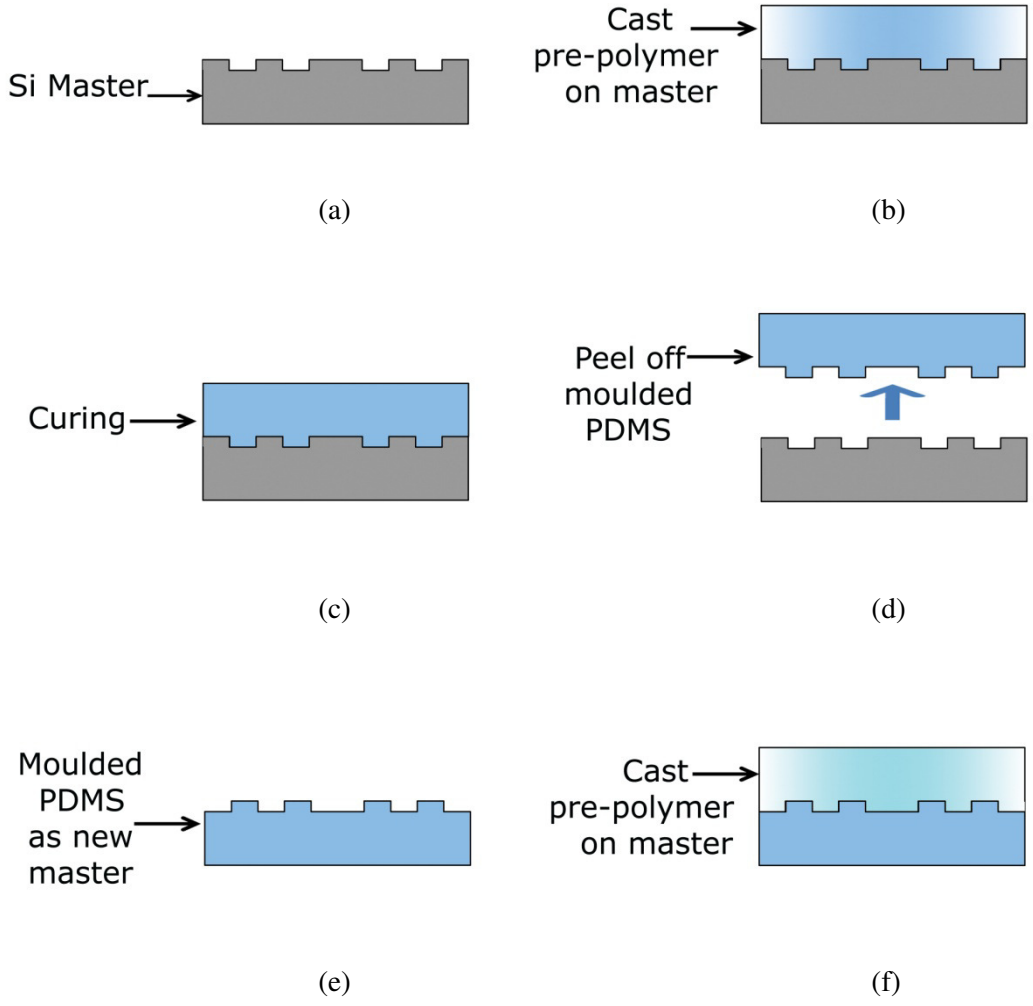

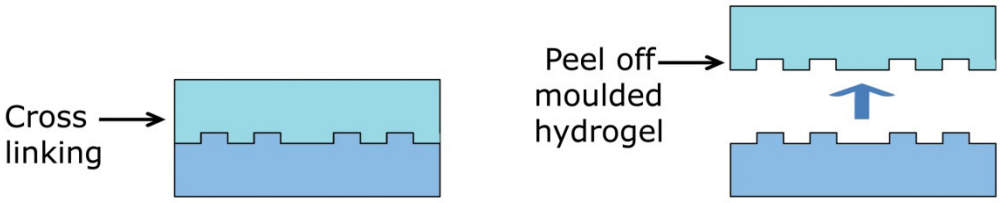


(g) (h)

**Figure 2.3.** Soft lithography and replica micromoulding for fabricating hydrogel based microfluidic components: a) A silicon master is prepared using standard photolithography and etching techniques. b), c) PDMS pre-polymer is cast over the micro-structured silicon master and cured. d), e) After solidification, the PDMS component is peeled off from the master and will subsequently operate as the new master for micromoulding the hydrogel. f), g) The hydrogel pre-polymer is then cast over the microstructured PDMS and cross-linking of the material takes place. h) After solidification of the hydrogel, the polymer is peeled off from the silicone master having the microfluidic structures replicated on its surface.

The main advantages of this technique rely in its low costs, flexibility, time efficiency and simplicity [72] and examples of hydrogels micomoulded via soft lithography are numerous. PHEMA hydrogels have been fabricated using this manufacturing procedure and could replicate rectangular microchannels from a PDMS stamp with features down to 1.5. μm [73], while moulded photo-cross-linked poly (ethylene glycol) (PEG) hydrogel rectangular microstructures (300 μm x 300 μm, 50 μm high) have been used to localize mammalian cells growth for drug screening [74] and similar routes have been employed for generating biosensors and protein immobilization [75]. Micropatterned PNIPAAm moulded via the soft lithography technique has been chemically attached to glass and used for creating cells aggregates in circular and square microwells by exploiting the stimuli-responsiveness of the material [76] and PNIPAAm rectangular structures with height from 1.5 μm to 120 μm were realized to form a microgroove array for Escherichia coli bacteria localization [77]. In addition to the group of soft lithography techniques which rely on the use of a photolithographic processed silicon master to generate or transfer micropatterns onto soft

materials, printing methods such as nano imprint lithography (NIL) and soft embossing (SE) are also suitable techniques for realizing micro and nanostructures on hydrogel surfaces. These methods rely on a manufacturing route which is opposite to the replica micromoulding procedures, since the incompletely cross-linked soft hydrogel is directly molded by using microstructured PDMS stamps, which transfer their features on the forming polymer through a vertical compression [78]. The high throughput and accuracy of NIL and SE have rendered them as interesting tools, with particular attention to those hydrogel materials having Young's modulus from tenths of Pa to a few kPa, where de-molding from the PDMS stamp using soft lithography techniques could damage the moulded material or cause features to wide [79]. Patterns with resolution ranging from 100 μm to 2 μm were transferred from PDMS to poly(acrylamide) hydrogels for genomic applications [80], while optical sensors consisting of size-modulating gratings with periods ranging from 2 to 5 μm fabricated on pH-sensitive hydrogel films grafted on solid substrates have been realized using imprinting with PDMS stamps [81]. Nanostructures with size down to 50 nm were realized with similar fabrication schemes on grafted photo-sensitive PEG based hydrogel layers [82] and hematopoteic stem cells were cultivated on 100 μm diameter microwells (50 μm deep) embossed in the same material [83].

### 2.3.3. Direct writing methods

Direct hydrogels micropatterning methods predominantly rely on the use of electron beam lithography (EBL) and laser based techniques [84]. In the case of EBL, its main advantages are the possibility of realizing highly resolved features down to a few nanometers in size with an extremely high geometrical flexibility, since the electron beam delivered on the sample can be precisely moved over the polymer surface according to a CAD drawing [85]. However, the process is serial and can only be applied to relatively small areas of the sample and thus the applications of the technique are relatively limited [86] but it becomes significantly useful for fine surface topography and chemical modification of the materials along the realized pattern. It was shown that electron dose variations when patterning

poly(amidoamine) based dry hydrogels resulted in a local modification of the swelling properties of the material as a consequence of the chemical modification of the polymer; this effect, coupled with the material surface topography variations, also allowed the selective directional growth of secondary neuron cells axons along the patterned regions [87]. Similar results have been obtained on PEG microgels, where cells adhesiveness could be spatially controlled at the subcellular level [88].

Laser based techniques employed for hydrogel microstructuring include 3D stereolithographic and pulsed laser ablation processes employing Nd:YAG, titanium:sapphire and excimer lasers [4]. Using high power (1 to 10 W) short pulsed laser beams (from $10^{-3}$ to 50 ns) in the UV range allows structures with micrometric resolution to be generated avoiding thermal damages of the polymers due to the 'cold' ablation process involved [89]. Polymeric materials in general are known to present high absorption to light in the UV region of the electromagnetic spectrum [90] and in this particular microfabrication protocol the focused energy delivered by the photons is transferred to the sample to break strong intra-chain covalent bonds [91]. This eventually causes the decomposed material to be expelled from the surface in a time scale of the order of the laser pulse (photochemical ablation [89]). Furthermore, the ablation is confined to the volumetric portion of the material which absorbs the energy and it only takes place for energy values which go above a characteristic ablation threshold [91]. For polymers, the etch rate (etch depth of material removal per laser pulse) can vary from hundreds of nanometers to a few microns, depending on the material properties (e.g. refractive index) and the incident energy value [89]. A schematic view of a typical excimer laser setup is shown in Figure 2.4.

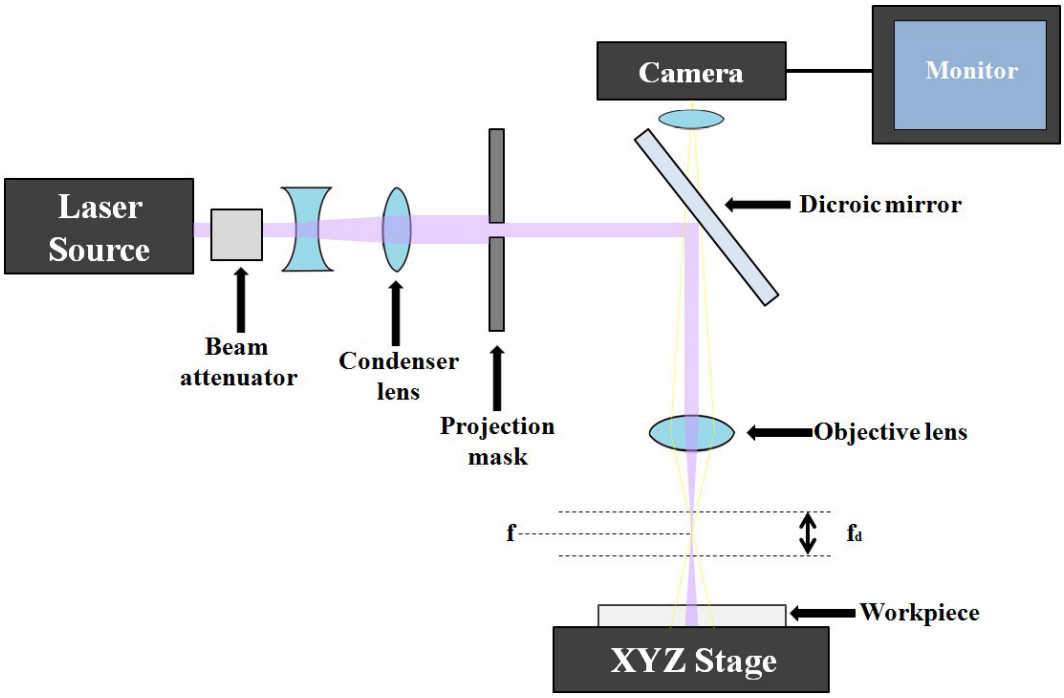


**Figure 2.4.** Scematic drawing of the typical excimer laser setup for polymeric materials micromachining.

The excimer laser beam is generated in the source and it is delivered to a projection stencil mask (usually made of thin metal sheet), which allows the photons to pass only through specific regions which correspond to the desired pattern to be generated on the sample. The original Gaussian beam is homogenized and partially attenuated by an optical system positioned between the source and the mask. A dicroic mirror vertically projects the laser light onto an objective lens, so that the pulses can reach the workpiece imaging the features designed on the mask with a demagnification factor depending on the particular optic element employed. The light intensity reaches its maximum value at the laser focal point f and can be considered constant over a spatial region identified by the laser focal depth $f_d$, which is a function of the laser wavelength, the objective numerical aperture and the projection mask characteristics [89]. The sample is mounted on an automated xyz moving stage and a camera is also usually integrated in the system to allow direct visualization of the workpiece surface. Because of the high ablation efficiency and throughput features, excimer lasers machining of

polymers is playing an increasingly important role in the microelectronic industry, enabling the realization of vertical interconnections for dense 3D wiring network packaging [92] and it has also been applied for the realization of ink jet printer nozzles in polyimide [93]. Moreover, the ablation mechanism of soft biological tissue has been widely investigated and the application of these laser based techniques to clinical ophthalmology is currently used to correct high myopia and in dermatology as well [94]. Since hydrogel based materials possess structural, morphological and mechanical properties which resemble those typical of biological tissues at different levels, the analogy between the two architectures constituted the main motivation to use KrF excimer laser machining for holes drilling in PNIPAAm based layers for the research reported in this thesis. However, there are no examples in the literature of hydrogels micro-hole drilling by means of excimer lasers and only a few reports on their microstructuring using photochemical ablation could be found. These are related to surface topography and chemical surface modification of PHEMA and PNIPAAm hydrogels for corneal epithelial cells attachment and proliferation [95] and for localized bovine artery ES cell attachment and controlled detachment [96] respectively. Agarose hydrogel substrates have been processed with ArF excimer laser to produce 60 x 150 μm microchannels for C2C12 murine mioblast cell growth [97] and machined for realizing spatially controlled cell co-culture onto various micropatterns [98]. Microporous poly urethane tubes have also been designed and realized for tissue engineering applications using KrF laser machining [99]. Furthermore, the effect of hydrogel water content on the ablation rate has been studied for PHEMA and the ablation rate has been observed to slightly decrease with the hydration level of the material [100].

## 2.4. Hydrogels in LOC systems

The majority of examples where hydrogels have been implemented in LOCs have used *in situ* photo-polymerization and photo-patterning of the material as the integration strategy and usually takes advantage of their biocompatibility and stimuli-responsiveness. Bioreactors hybrid microfluidic systems were designed to exploit the properties of PEG hydrogels to culture cells in 3D miniaturized cell laden structures for enzyme extraction, purification [101]

or signaling [102]. In other works, monolithic hydrogel based microfluidic devices have been realized by mean of a sacrificial template technique, in which a soluble pre-moulded solid microfluidic network is embedded in the polymerizing biocompatible hydrogel and subsequently removed by being dissolved after the surrounding material is cross-linked [103, 104]. Smart hydrogel integration on chip is also dominated by photo-polymerization techniques and the examples of these as micro-actuators (e.g. valves and pumps) in LOCs are vast and use a variety of response mechanisms, as previously mentioned. In the next subsection, the most representative PNIPAAm based LOC devices will be presented and discussed.

### 2.4.1. PNIPAAm -based devices

Thermo-responsive PNIPAAm based valves have been realized in situ in microfluidic channels both by mean of free radical polymerization and photo-patterning; the operational functionality of this component is to obstruct the fluid flow inside the duct by exploiting the swelling-deswelling mechanism (corresponding to the valve close-valve open states respectively) induced by the reversible phase transition of the hydrogel [105]. A schematic view of the component is shown in Figure 2.5.

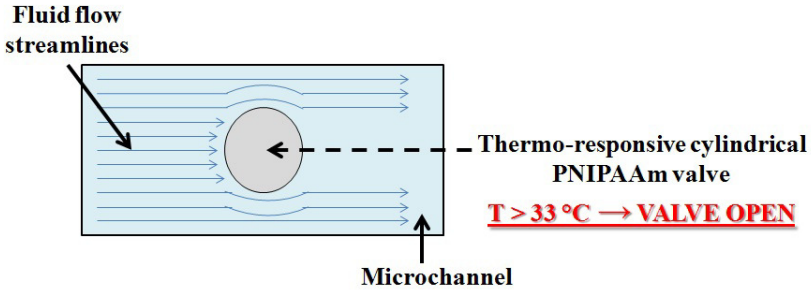


(a)

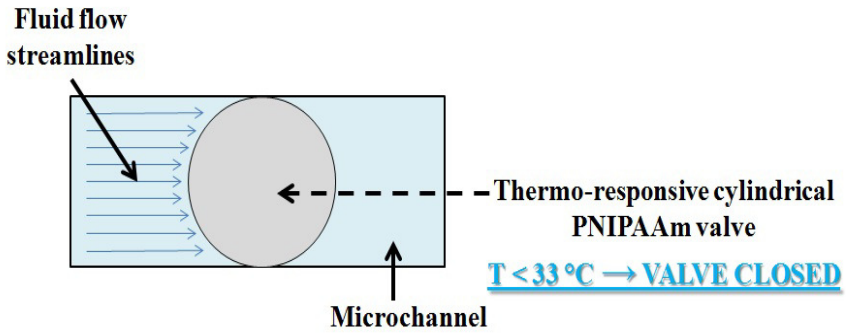


(b)

**Figure 2.5.** Scematic view of a PNIPAAm based hydrogel "valve".

Different fabrication schemes have been adopted to improve this smart actuator design and performances, such as response rate, pressure tolerance and duty cycle. More specifically, the response time has been scale down to 0.3 ms for 50 nm-sized PNIPAAm based valves [106]. Displacement micropumps have also been realized employing *in situ* photo-cross-linking of the hydrogel on different substrates, including glass, plastics and PDMS [107]. The general idea for the development of this type of actuators is to exploit the PNIPAAm transition to control the hydrogel swelling in the direction perpendicular to the support and to move liquids in a top chamber located over the smart polymer. Microheaters, which are typically realized using thin metal film deposition technologies, are integrated in the microfluidic device to controllably induce the transition of this kind of actuators [108]. Another fluid control application of PNIPAAm based hydrogels takes advantage of the modification of the polymer wettabilty below or above the transition point to induce directional switching of a laminar liquid flow in a PNIPAAm surface modified glass capillary [109]. Other examples of smart devices based on the thermo-responsive mechanism include cell based microfluidic chips for cell manipulation and culture. Using a soft lithography approach combined with a focused ion beam, Castellano et al. [110] realized 20 µm trenches on PNIPAAm grafted over PDMS; the system operates as a microfluidic platform for capture and release of biosamples as a function of temperature, while controlled attachment and detachment of mouse fibroblasts from patterened 100 µm PNIPAAm domains realized on PS

using photolithography techniques have been demonstrated [111]. The property of the hydrogel to tune its character from hydrophilic to hydrophobic has also been employed to organize localized cells and protein structures over specific heated areas [112]. The same route can be applied for immobilizing growth factors such as insulin which can stimulate cell growth over PNIPAAm substrates [113]. Furthermore, cell sheets could form on PNIPAAm grafted layers in the hydrophobic state and subsequently be detached by decreasing the temperature down to 20 °C [114]; the process of cell detachment using this mechanism was then hastened by introducing a laminar flow of cold medium in a PDMS microchannel, which was bonded to the hydrogel by partially curing the elastomer over the PNIPAAm surface [115]. To localize this phenomenon into small areas, excimer laser ablated micropits (25 μm depth) were fabricated onto the PNIPAAm grafted layer prior to cell attachment [116]; this is the only example in the literature in which the excimer laser has been used to process PNIPAAm based hydrogels, as mentioned erlier, micromachining of through-holes or microfluidic structures on the material using this technique has not been reported yet.

## 2.5. Cell sorting On-Chip

In this section, the principal techniques employed for promoting cell sorting on-chip will be reported and discussed. As already mentioned in the Chapter 1, the choice of the specific approach can be selected with respect to the particular biological case in terms of the target cell, the measurements and assays to be carried out and the particular information that is required. From the general point of view, the main sorting mechanisms can be identified as magnetic, optical, electrical, fluidic, acoustic and adhesion based [117]. Each of these methods will be discussed below.

*Magnetic sorting*: this popular technique requires a labeling procedure of the target cells by mixing and incubating coated magnetic nanoparticles with the cell suspension, so that they can attach to the biosample membrane by mean of antibodies. A magnetic field is then created in the chip to localize and isolate cells in specific positions, maintaining the viable

microorganism. Labeled eukaryotic organisms have been trapped at the corners of zig-zag structured magnetic microwires in a $Si/SiO_2$ device located at the center of four magnetic coils [118], while micromagnets arrays coated with parylene have been used to drive and assist cell migration to specific locations in a microfluidic device [119]. Magnetophoresis and mobile magnetic traps have also been integrated with microfluidic technology to isolate labeled cells in LOC systems [120, 121]. Although the sorting efficiency of this technique is high, the time-consuming feature of the labeling, the marker type specificity and the potential damage to the biosample that this procedure can induce are still significant drawbacks of this group of sorting methods [122].

*Optical sorting*: this sorting route is also a widely used method for heterogeneous cell populations separation. The criteria underlying this sorting mechanism can be related to cells size, polarizability and refractive index difference and can be promoted both with low intensity and focused laser light [123]. Optical tweezers have been implemented in microfluidic platforms and demonstrated the capability of cell manipulation by exploiting the scattering and electric field gradient force generated by a focused Gaussian laser beam directed to a cell suspension flowing in a micro-channel [124], and single cell analysis could also be carried out *in situ* by controlling different beam parameters, such as polarization and phase [125]. Fluorescence activated sorting can also be considered as an optical technique for sorting marked cells and micro-flow cytometers have been developed to reproduce the conventional macroscopic instrumentation on-chip, overcoming the issues of subjugating the samples to relatively large flow rate and shear stresses [126]. The main disadvantages of this family of methods are related to the relatively complex support equipment, their relatively low efficiency and the underlying mechanism which is not fully understood [125].

*Electrical sorting*: this label-free technique relies predominantly on the use of both direct and alternating current dielectrophoresis on-chip for size based cell separation; an electric polarization is induced on the bioentities so that they can then be trapped in a region where a nonuniform electric field is established [127]. Cell type, density and physiological state can strongly influence the sample response to the forces induced by the electric field. A variety of cells have been sorted using this technique, including blood, breast cancer and murine tumor

cells [117]. One of the main advantages of the application of this technique in LOC systems is the possibility of realizing arrays of individually controlled trapping regions [128]. The separation efficiency can be strongly affected by the balance between the intensity of the force induced by the electric field and the hydrodynamic one derived from the laminar flow driving the samples into the device; if the flow rate value is relatively high, the interaction between the cell and the electric field could take place in a time window which is too short for the sample displacement to take place [125].

*Fluidic sorting*: cell separation and isolation mechanisms based on laminar flow and hydrodynamics phenomena control in microfluidic channels are also suitable sorting techniques. The principal methods belonging to this class take advantage of particular microchannels geometry configurations, like bifurcations, that are designed to guide specific cell types of an original population along the flow stramlines based on size, deformability or other physical biosample properties [117]. The presence of micropillars and other filtering structures in the microfluidic ducts have also been employed for size based sorting [129] while serpentine microchannels forming trapping arrays in conjunction with hydrodynamic flow have been used for localizing single cells on-chip [130]. A PDMS microfluidic network has been sealed to a silicon substrate endowed with vias and ports that can direct cells laminar flow in the chip so that the specimen can be either be finely deposited or moved according to the flow rate value imposed [131]. Photopatterned PNIPAAm hydrogels operating as valves or functional components for flow switch have also been integrated into microfluidic systems for cell sorting; in this type of devices, the transition of the polymer is induced by heating the region of interest using a focused IR laser beam [132, 133]. The main advantages of a purely fluidic based technique dwell in their label-free nature and in the laminar flow regime, which is suitable for guaranteeing the cells viability after separation or localization, but limitations arise from their lack of specificity in terms of number of cells to be selected starting from an original population of identical biosamples and in the fact that having a closed system could reduce the range of possible single cell assays to be carried out by the user.

*Acoustic sorting*: for these on-chip techniques, the specimens are exposed to ultrasound waves and experience an acoustic force which is responsible for their displacement in the nodal or antinodal pressure points of a standing wave generated inside a microchannel, depending on the cells size, density and compressibility [134]. A laminar flow of the cell suspension in a direction orthogonal to the acoustic field has been employed as an alternative effective route to promote cells migration [135]. These acoustic based methods have been tested and finely tuned so that no mechanical and thermal stresses are induced on the specimen, but haven't proved to be able to combine the size-selectivity with rapid high parallelization.

*Adhesion-based sorting*: the specific capture of cells by exploiting the chemical characteristic of their membrane is at the basis of this group of techniques; a cell suspension is usually injected in a microfluidic channel through a laminar flow and the interaction of the biosample with target locally functionalized areas promote the isolation. Different antibody coated arrays have demonstrated an effective local trapping and immobilization of cells over PDMS substrates [136] and aptamers have also been used as suitable capturing agents for prostate cancer cells in a PMMA based LOC device [137]. To favour cell attachment, preliminary modeling and theoretical studies on the correlation between particular surface ligands and cell receptors densities have been carried out and showed a good agreement with the experimental data [117].
The crucial point to be taken into account for realizing effective adhesion-based sorting is to tune the laminar flow rate and the associated shear forces in respect to the adhesion forces in the miniaturized environment [138].

LOC technologies applied to cell sorting is still a rapidly evolving field and though the application for clinical use is still to be proven, the advantages of using these promising devices in respect to the traditional methods still render them appealing for further development and to address more complex biological questions in single cell based assays.

## References


[1] Figeys D and Pinto 2000 A*nalytical Chemistry* **1** 330A-335A

[2] Ni M Tong W H Choudhury D Rahim N A A Iliescu C Yu H 2009 *Int. J. Mol. Sci.* **10** 5410-5411

[3] de Mello A 2002 *Lab Chip* **2** 31N–36N

[4] Becker H Gärtner C 2008 *Anal Bioanal Chem* **390** 89–111

[5] Ratner B D Hoffman A S Schoen F J Lemons J E 2004 *Biomaterials Science*, Elsevier, San Diego, 2nd edn.

[6] Zhang C Xu J Ma W Zheng W 2006 *Biotechnology Advances* **24** 243–284

[7] Beebe D J Mensing G A Walker G M 2002 *Annual Review of Biomedical Engineering* **4** 261-286

[8] M Heckele and W K Schomburg 2004 *J. Micromech. Microeng.* **14** R1-R27

[9] Becker H Gärtner C 2000 *Electrophoresis* **21** 12–26

[10] Wesner D A Aden M Gottmann J Husmann A Kreutz E W 1999 *Fresenius J Anal Chem* **365** 183–187

[11] Spegel C Heiskanen A Henrik L Skjolding D Emne´us J 2008 *Electroanalysis* **20** 680-702

[12] van Midwoud M Janse A Merema M T Groothuis G M M Verpoorte E 2012 *Anal. Chem* **84** 3938–3944

[13] Bi H Meng S Li Y Guo K Chen Y Kong J Yang P Zhong W Liu B 2006 *Lab Chip* **6** 769-775

[14] Witek M A Wei S Vaidya B Adams A A Zhu L Stryjewski W McCarley R Soper S A 2004 *Lab Chip* **4** 464-472

[15] Young E W K Berthier E Guckenberger D J Sackmann E Lamers C Meyvantsson I Huttenlocher A Beebe D J 2011 *Anal. Chem.* **83** 1408–1417

[16] Focke M Kosse D Müller C Reinecke H Zengerle R von Stetten F 2010 *Lab Chip* **10** 1365-1386

[17] Lee J N Park C Whitesides G M 2003 *Anal Chem* **75** 6544-6554.

[18] Weibel D B Garstecki P Whitesides G M 2005 *Current Opinion in Neurobiology* **15** 560–567

[19] Quake S R and Scherer A 2000 *Science* **290** 1536-1540

[20] Lee J N Jiang X Ryan D Whitesides G M 2004 *Langmuir* **20** 11684-11691

[21] Zhou J Ellis A V Voelcker N H 2010 *Electrophoresis* **31** 2–16

[22] Carati S G and Stern S A 1998 *Macromolecules* **31** 5529-5535

[23] ChoiaY H Sonb S U Lee S S 2006 *Key Engineering Materials* **326-328** 879-882

[24] Leclerc E Sakai Y Fujii T 2003 *Biomedical Microdevices* **5** 109-114

[25] Park J H Song Y S J-G Ha Kim Y K S-K Li S J Bai 2013 *Sensors and Actuators: B* **188** 1300-1305

[26] Cimetta E Figallo E Cannizzaro C Elvassore N Vunjak-Novakovic G 2009 *Methods* **47** 81–89

[27] Hoffman A S 2002 *Advance Drug Delivery Reviews* **54** 3-12

[28] Alexander C and Shakesheff K M 2006 *Advance Materials* **18** 3321-3328

[29] Kopecek J and Yang J 2007*Polym Int* **56** 1078–1098

[30] Khademhosseini A and Langer R 2007 *Biomaterials* **28** 5087-5092

[31] Peppas N A Hilt J Z Khademhosseini A and Langer R 2006 *Advance Materials* **18** 1345-1360

[32] Kumara A Srivastavaa A Galaevb I Y Mattiasson B 2007 *Prog. Polym. Sci.* **32** 1205–1237

[33] Mengab H and Li G 2013 *J. Mater. Chem. A* **1** 7838-7865

[34] Kim P Zarzar L D He X Grinthal A Aizenberg J 2011 *Current Opinion in Solid State and Materials Science* **15** 236–245

[35] Hirokawa Y and Tanaka T 1984 *J. Chem. Phys.* **81** 6379-6380

[36] Suzuki A Yoshikawa S and Bai G 1999 *J. Chem. Phys.* **111** 360-667

[37] Gherke S H Palasis and M Akhtar S K 1992 *Polymer International* **29** 29-36

[38] Jeong B and Gutowska A 2002 *Trends in Biotechnology* **20** 305-311

[39] Ueki T and Masayoshi Watanabe M 2007 *Langmuir* **23** 988–990

[40] Ueki T and Masayoshi Watanabe M 2010 *Polymer Preprints* **51** 618-619

[41] Cheng X Canavan H E Stein M J Hull J R Kweskin S J Wagner M S Somorjai G A Castner D G .Ratner B D 2005 *Langmuir* **21** 7833–7841

[42] Principi T Ester Goh C C E Liu R C W Winnik F M 2000 *Macromolecules* **33** 2958–2966

[43] Otake K Inomata H Konno M Saito S 1990 *Macromolecules* **23** 283-289

[44] Rusu M Wohlrab S Kuckling D Möhwald H Schönhoff M 2006 *Macromolecules* **39** 7358–7363

[45] Raccis R Roskamp R Hopp I Menges B Koynov K Jonas U Knoll W Butt H J Fytas G 2011 *Soft Matter* **7** 7042-7053

[46] Harmon M E Jakob T A M Knoll W Frank C W 2002 *Macromolecules* **35** 5999-6004

[47] Yoon J Cai S Z Suo Hayward R C 2010 *Soft Matter* **6** 6004-6012

[48] Colombo I Grassi M Fermeglia M Lapasin R Pricl S 1996 *Fluid Phase Equilibria* **116** 148–161

[49] Cai S and Suo Z 2011 *Journal of the Mechanics and Physics of Solids* **59** 2259–2278

[50] Kopeček J and Yang J 2007 *Polymer International* **56** 1078–1098

[51] Rzaev Z M O Dincer S Piskin E 2007 *Prog. Polym. Sci.* **32** 534–595

[52] Gehrke S H Palasis M Akhtar M K 1992 *Polymer International* **29** 29–36

[53] Kabra B *G* Gehrke S H 1991 *Polymer Commun* **32** 322-323

[54] Matsuo E Tanaka T J 1988 *Chem Phys* **89** 1695–703

[55] Birgersson E Li H Wu S 2008 *Journal of the Mechanics and Physics of Solids* **56** 444–466

[56] Serizawa T Uemura M Kaneko T Akashi M 2002 *Journal of Polymer Science Part A: Polymer Chemistry* **40** 3542–3547

[57] Tokarev I and Minko S 2010 *Advanced Materials* **22** 3446-3462

[58] Tokarev I and Minko S 2009 *Soft Matter* **5** 511-524

[59] Cohen M A Wilhelm S Huck T S Genzer J Müller M Ober C Stamm M Sukhorukov G B Szleifer I Tsukruk V V Urban M Winnik F Zauscher S Luzinov I Minko S 2010 *Nature Materials* **9** 101-113

[60] Tanaka T and Fillmore D J 1979 *J. Chem. Phys.* **70** 1214–1218

[61] Suarez I J Fernandez-Nieves A Marquez M 2006 *J. Phys. Chem. B* **110** 25729-25735

[62] Hong W Liu Z Suo Z 2009 *International Journal of Solids and Structures* **46** 3282–3289

[63] Matsukuma D Yamamoto K and Aoyagi T 2006 *Langmuir* **22** 5911–5915.

[64] Alem H Duwez A S Lussis P Lipnik P Jones A M Champagne S D 2008 *J. Membr. Sci.* **308** 75–86

[65] Estillore N C and Advincula R C 2011 *Macromol. Chem. Phys.* **212** 1552–1566

[66] Maeda S Hara Y Yoshida R Hashimoto S 2010 *Int. J. Mol. Sci.* **11** 52-66

[67] Ebara M Hoffman J M Stayton P S Hoffman A S 2007 *Radiation Physics and Chemistry* **76** 1409–1413

[68] Plunkett N K Zhu X Moore J S Leckband D E 2006 *Langmuir* **22** 4259–4266

[69] Matsukuma DYamamoto K Aoyagi T 2006 *Langmuir* **22** 5911–5915

[70] Liu H and Ito Y 2002 *Lab Chip* **2** 175–178

[71] Weibel D B Garstecki P and Whitesides G M 2005 *Current Opinion in Neurobiology* **15** 560–567

[72] Weibel D B DiLuzio W R and Whitesides G M 2007 *Nature Reviews: microbiology* **5** 209–218

[73] Mukhopadhyay R 2007 *Anal. Chem.* **79** 3248–3253

[74] Koh W-G Itle L J Pishko M V 2003 *Anal. Chem.* **75** 5783-5789

[75] Suha K Y Seonga J Khademhosseini A Laibinisa P E Langer R 2004 *Biomaterials* **25** 557–563

[76] Tekin H Tsinman T Sanchez J G Jones B J Camci-Unal G Nichol J W Langer R Khademhosseini A 2011 *J. Am. Chem. Soc.* **133** 12944–12947

[77] Tsai H-Y Vats K Yates M Z Benoit D S V 2013 *Langmuir **29*** 12183–12193

[78] Nie Z and Kumacheva E 2008 *Nature Materials* **7** 277 - 290

[79] Gillette B Jensen J Tang B Yang G Bazargan-Lari A Zhong M. Sia, S. 2008 *Nat. Mater.* **7** 636-642

[80] Di Benedetto F Biasco A Pisignano D Cingolani R 2005 *Nanotechnology* **16** S165–S170

[81] Ye G and Wang X 2010 *Sensors and Actuators B* **147** 707–713

[82] Fozdar D Y Zhang W Palard M Patrick C W Chen S 2008 *Nanotechnology* **19** 1-13

[83] Kobel S Limacher M Gobaa S Laroche T Lutolf M P 2009 *Langmuir* **25** 8774–8779

[84] Chen L Henein G Luciani V 2011 *Nanomedicine* **6** 1–6

[85] Qin D Xia Y and Whitesides G M 2010 *Nature Protocols* **5** 491 - 502

[86] Sah M K and Pramanik K International 2012 *Journal of Biomedical Engineering and Technology* **9** 101-121

[87] Dos Reis G Fenili F Gianfelice A Bongiorno G Marchesi D Scopelliti P E Borgonovo A Podesta` A M Indrieri Ranucci E Ferruti P Lenardi C Milani P 2010 *Macromol. Biosci.***10** 842–852

[88] Krsko P Sukhishvili S Mansfield M Clancy R Libera M 2003 *Langmuir* **19** 5618-5625

[89] Dyer P E 2003 *Applied Physics A* **77** 167-173

[90] Lazare S Elaboudi I Castillejo M Sionkowska A 2010 *Applied Physics A* **101** 215-224

[91] Lazare S and Granier V 1989 *Laser Chemistry* **10** 25-40

[92] Paterson C Holmes A S Smith R W 1999 *Journal of Applied Physics* **86** 6538-6546

[93] Basting D and Marowsky G 2005 *Excimer Laser Technology* Berlin, Germany, Springer 195-199

[94] Vogel A and Venugopalan V 2003 *Chem. Rev.* **103** 577-644

[95] Bryanta J S Cuya J L Haucha K D and Ratner B D 2007 *Biomaterials* **28** 2978-2986

[96] Akiyama Y Kikuchi A Yamato M Okano T 2004 *Langmuir* **20** 5506-5511

[97] Patz T Narayan R Modi R Chrisey D B 2005 *Mater. Sci. Eng. B* **123** *242–247*

[98] Doraiswamy A and Narayan R J 2010 *Phil. Trans. R. Soc. A.* **368** 1891-1912

[99] Doi K Nakayama Y Matsuda T 1996 *J Biomed Mater Res.***31** 27-33

[100] Feltham M H and Stapleton F 2002 Clin *Experiment Ophthalmol.* **30** 99-103

[101] Heo J Thomas K J Seong G H Crooks R M 2003 *Anal Chem.* **75** 22-6

[102] Heo J and Crooks R M 2005 *Anal Chem.* **77** 6843-51.

[103] Golden A P and Tien J 2007 *Lab Chip* **7** 720-725

[104] Cabodi M Choi N W Gleghorn J P Lee C S D Bonassar L J Stroock A D 2005 *J. Am. Chem. Soc.***127** 13788-13789

[105] Luo Q Z Mutlu S Gianchandani Y B Svec F Frechet J M J 2003 *Electrophoresis* **24** 3694–3702.

[106] Kuckling D Hoffmann J Plötner M Ferse D Kretschmer K Adler H-J PKarl Arndt K-F Reichelt R 2003 *Polymer* **44** 4455-4462

[107] Richter A Klatt S Paschew G Klenke C 2009 *Lab Chip* **9** 613–618

[108] Argentiere S Gigli G Mortato M Gerges I Blasi L 2012 *Smart Microfluidics: The Role of Stimuli- Responsive Polymers in Microfluidic Devices*, Advances in Microfluidics, Dr.Ryan Kelly (Ed.), ISBN: 978-953-51-0106-2, 128-154

[109] Saitho T Suzuki Y Hiraide M 2002 *Analytical Sciences* **18** 203-205

[110] Castellanos A Leffew J Moreno W *Proceedings of the 7th International Caribbean Conference on Devices, Circuits and Systems*, Mexico, Apr. 28-30, 2008, 1-5

[111] Liu H and Ito Y 2002 *Lab Chip* **2** 175–178

[112] Wangl Y Cheng X Hanein Y Shastry A Denton D D Ratner B D Bohringerl K F 2003 *The 12th International Conference on Solid State Sensors, Actuators and Microsystem*, Boston. June 8-12, 979-982

[113] Klouda L and Mikos A G 2008 *European Journal of Pharmaceutics and Biopharmaceutics* **68** 34–45

[114] da Silva R M P Mano J F Reis R L 2007 *Trends in Biotechnology* **25** 577-583

[115] Tang Z Akiyama Y Itoga K Kobayashi J Yamato M Okano T 2012 *Biomaterials* **33** 7405-7411

[116] Kumashiro Y Yamato M Okano T 2010 *Annals of Biomedical Engineering* **38** 1977-1988

[117] Auteberta J Couderta B Bidardb F-C Piergab J-Y Descroixa S Malaquina L Viovy J L 2012 Methods **57** 297-307

[118] Donolato M Torti A Kostesha N Deryabina M Sogne E Vavassori P Hansen M F Bertacco R 2011 Lab Chip **11** 2976-2983

[119] Zablotskii V Dejneka A Kubinová S Le-Roy D Dumas-Bouchiat F Givord D Dempsey N M Syková E 2013 *PLoS ONE* **8**, doi:10.1371/journal.pone.0070416

[120] Gaitas A and French P 2011 *The 16th International Conference on Solid State Sensors, Actuators and Microsystem* doi:10.1109/TRANSDUCERS.2011.5969331

[121] Talasaz A H Powell A A Huber D E Berbee J G Roh K-H Yu W Xiao W Davis M M Pease R F Michael Mindrinos M N Jeffrey S S Davis R W 2009 *PNAS* **106** 10 3970-3975

[122] Radisic M Iyer R K Murthy S K 2006 *International Journal of Nanomedicine* **1** 3 –14

[123] Zhang H and Liu K-K 2008 *J R Soc Interface*. **5** 671–690

[124] Applegate Jr. R W SquierJ Vestad T Oakey J Marr D W M 2004 *OPTICS EXPRESS* **12** 4390-4398

[125] Gossett D R Weaver W M Mach A J Hur S C Tse H T K Lee W Amini H Di Carlo D 2010 *Anal Bioanal Chem* **397** 3249–3267

[126] Wang M M Tu E Raymond D E Yang J M Zhang H Hagen N Dees B Mercer E M Forster A H Kariv I Marchand F J Butler W F 2005[1] *Nature Biotechnology* **23** 83 - 87

[127] Voldman 2006 *Annual review of biomedical engineering* **8** 425-54

[128] Cheng I-F and Chang H-C 2007 *Biomicrofluidics* 1 021503 1-15

[129] Wu Z and Hjort K 2009 *Micro and Nanosystems* **1** 1-8

[130] Di Carlo D 2009 *Lab Chip* **9** 3038-3046

[131] Lovchik R D Bianco F Matteoli M Delamarche E 2009 Lab Chip **9** 1395-1402

[132] Shirasaki Y Tanaka J Makazu H Tashiro K Shoji S Tsukita S Funatsu T 2006 *Anal Chem.* **78** 695-701

[133] Arakawa T Shirasaki Y Izumi T Aoki T Sugino H Funatsu T Shoji S 2006 *Meas. Sci. Technol.* **17** 3141–3146

[134] Dinga X Lina S-C S Kiralya B Yueb H Lic S Chianga I-K Shia J Benkovicb S J Huanga T J 2012 *PNAS* **109** 11105-11109

[135] Agarwal G and Livermore C 2011 *Lab Chip* **11** 2204-2211

[136] Nagrath S Sequist L V Maheswaran S Bell D W Irimia D Ulkus L Smith M R Kwak E L Digumarthy S Muzikansky A Ryan P Balis U J Tompkins R G Haber D A Toner M 2007 *Nature* **450** 1235-1239

[137] Sheng W Chen T Kamath R Xiong X Tan W Fan Z H 2012 *Anal. Chem.* **84** 4199–4206

[138] Didar T F Tabrizian M 2010 *Lab Chip* **21** 3043-53

# 3. PNIPAAm based freestanding layer fabrication

The main objective of this chapter is to describe in detail the experimental protocol developed for the manufacturing of PNIPAAm based freestanding hydrogel layers. As shall be highlighted in the next section, the main purpose of this fabrication process is to produce thin polymeric films (thickness from 10 to 300 μm) for subsequent analysis and testing. These are initially stuck to a rigid substrate, maintaining a flat configuration, which can be useful for handling and processing such as excimer laser micromachining. Chemical treatments of the fabricated PNIPAAm based layers can then be conducted to detach them from the substrates, thus yielding the resulting freestanding components. After the general approach to identify the appropriate conditions and equipment to actually realize the process is explained, the different steps of the technique will be separately analyzed and the results obtained will be contextually discussed for each phase of manufacturing. Several iterations were investigated with the intention to develop a protocol with features adaptable for a subsequent scale up, appropriate for mass production.

## 3.1. Introduction: general and experimental approach

The fundamental requirements of the manufacturing protocol for producing freestanding PNIPAAm based thin films are its reliability and repeatability both in the synthesis of the hydrogel materials and the fabrication process of the films themselves. Although hydrogel materials are known to be very sensitive to variation of their chemical synthesis conditions in terms of the resulting physical properties, a fixed relative amount of the reagents involved should be defined to be able to produce polymers with fixed optical, mechanical and thermo-responsive properties. On the other hand, a suitable technique for fabricating PNIPAAm based layers should ensure that the produced components are identical in terms of shape and size, being particularly focused on obtaining good control over the thickness values. With the

target of eventually employing micropatterned freestanding hydrogel layers integrated with other polymeric components for realizing a cell sorting micro-device prototype, a precise routine for the manufacturing of the layers needed to be established to readily obtain hydrated and flat hydrogel films supported on a platform suitable for laser machining prior to their implementation on the chip. The main steps of the protocol can be summarised by the following sequence of operations:

- *Synthesis of the hydrogels:* a systematic approach for the materials' synthesis is required; this was mainly carried out in CIMaINa laboratories. Thermo-responsive PNIPAAm hydrogels with different cross-linker amounts and PNIPAAm based random co-polymers with the incorporation of both hydrophobic and hydrophilic co-monomers were realized and later characterized in terms of thermo-responsiveness in order to determine a library of materials with different properties suitable for thin layer production.
- *Thin layer realization*: since the specific aim of the lab-on-chip application of PNIPAAm based thin films would require the use of layers with thickness ranging from 10 to 300 μm, an appropriate method for producing such components was identified based on an injection/compression moulding (ICM) technique, similar to that employed for moulding thermoplastic materials. The choice and the operation of the moulding apparatus, in terms of materials type, quantity, as well as the geometry and compression values, were experimentally determined for obtaining the desired hydrogel structures. Spin coating was also tested as an alternative to ICM, as described later in 3.3.1, but the results obtained were not satisfactory, mainly due to issues connected with solvent evaporation of the cross-linking mixture.
- *Excimer laser micromachining:* this microfabrication technique has been previously employed for micro-structuring polymers and polymer based surfaces of different types, including hydrogels, as reported in the literature [1] and here in 2.2.2.5. In the present case, it has been adapted for processing soft materials for the purpose of realizing micro-through-holes in the manufactured PNIPAAm based layers, with entrance diameters ranging from 10 to 30 μm. This machining step was conducted in the optical engineering laboratory of the Wolfson School, Loghborough University. Being able to control the geometrical features of the holes is crucial for the sorting

application on chip; the analysis of the machining parameters' influence over the microstructures morphology is discussed in Chapter 4.

- *Film detachment and swelling:* once the micropatterned thermo-responsive layers are produced on rigid substrates, detachment is promoted by a chemical treatment so that the actual freestanding hydrogels can be easily obtained. The removal of the attached PNIPAAm films should not damage or contaminate the component in any way. A number of tests on non-machined layers employing different solvents and organic compound based aqueous solutions were carried out to find out which could be the most suitable chemicals to detach the films.

These four steps are interconnected and constitute all together the core of the manufacturing protocol. In the next sections of this Chapter, material synthesis, ICM technique and film detachment and swelling will be reported.

## 3.2. Synthesis and materials characterization

The principal source of inspiration for dealing with PNIPAAm based hydrogel synthesis was initially the literature. The polymerization and cross-linking reactions which lead to the formation of the gel matrix are free radical induced and have been described in detail elsewhere [2]. The most significant references adopted as a starting point to rely on for developing the synthesis process could be found in the work of Tanaka et al [3], as well as in [4,5,6]. In this work, the redox initiator chosen was ammonium persulfate (APS) aqueous solution at different concentrations (10 and 20% mol/mol), while cross-linker type and quantity were varied among the synthesis tests. As highlighted before in Chapter 2, a number of variations on the chemical types and amount involved in the reaction must be taken into account for producing hydrogels with the desired physical properties (e.g. transparency, elasticity) but different network structure. More specifically, what determines a specific behavior of the produced materials is the initiator and cross-linker type, as well as the reaction conditions (e.g. temperature of reaction). The monomer to initiator and monomer to cross-linker molar ratio are also crucial parameters in order to control and modulate the resulting material properties. The principal drawback in many applications of PNIPAAm

hydrogels is the weak mechanical properties of the material, which exhibits low elasticity as well as poor resistance to external applied stresses [7]. Moreover, optical transparency is a reliable indicator of the degree of homogeneity of the hydrogel; an increase in opacity of the material is related to the formation of micrometer-sized regions which are randomly located in the polymeric network and in which a globular conformation of the back-bone chains occurs [8]. The presence of these inner micro-structures tends to change the responsiveness of the hydrogel to temperature changes and they are mainly due to the reaction's completion rate [9]. Bearing in mind the target of integrating the fabricated freestanding thermo-responsive PNIPAAm layers in hybrid material lab-on-chip systems, the synthesis tests were carried out focusing on the production of a material which could exhibit both suitable mechanical properties and homogeneity. Within this frame, a library of PNIPAAm based hydrogels with different cross-linker amounts and type, as well as solvent, were realized as moulded cylinders (15 mm diameter, 1 mm height) and qualitatively analyzed in terms of transparency and mechanical strength. Then, PNIPAAm based random co-polymers were also produced and analyzed. Particular emphasis was given to the use of hydroxyethyl methacrylate (HEMA) as co-monomer, and this is due both to the mechanical features characteristic of the PNIPAAm/HEMA co-polymers (3.2.2.) and the development of hybrid Poly-hydroxyethyl methacrylate (PHEMA)/PNIPAAm thin films (3.4.). An infrared spectroscopy characterization was carried out on pure PNIPAAm samples and PNIPAAm/HEMA co-monomers, as well as on PHEMA. Before going into detail describing the ICM technique employed for producing the layers, the synthesis and structural characterization of the hydrogels are discussed.

## 3.2.1. PNIPAAm based hydrogels

A general reaction scheme leading to the formation of the molecular unit of PNIPAAm hydrogel is shown in Figure 3.1. The polymerization reaction using APS as redox initiator was carried out adding the chemicals in the following order:

1. *N-Isopropylacrylamide (Monomer,* NIPAAm*, powder)*
2. *Ethanol (Solvent,* EtOH*, liquid)*
3. *MilliQ or de-ionized water (Solvent,* $H_2O$*, liquid)*

4. *Ethylene glycol dimethacrylate (Cross-linker,* EGDMA*, liquid)*
5. *N,N,N',N'-Tetramethylethylenediamine (Catalyzer,* TEMED*, liquid)*
6. *10% w/w Ammonium persulfate (*APS*, powder) aqueous solution (Initiator,* APS%$_{w/w}$*, liquid)*

All reagents (purchased from Sigma Aldrich) were properly weighed (if powders) or injected with calibrated pipettes (if liquids) and must be completely dissolved and homogenized in the mixture before the next one is added. After the initiator was added, the tube was vigorously shaken for 10 seconds and then tilted from time to time for the next minute before injection in silicone rubber cylindrical moulds using a micropipette.

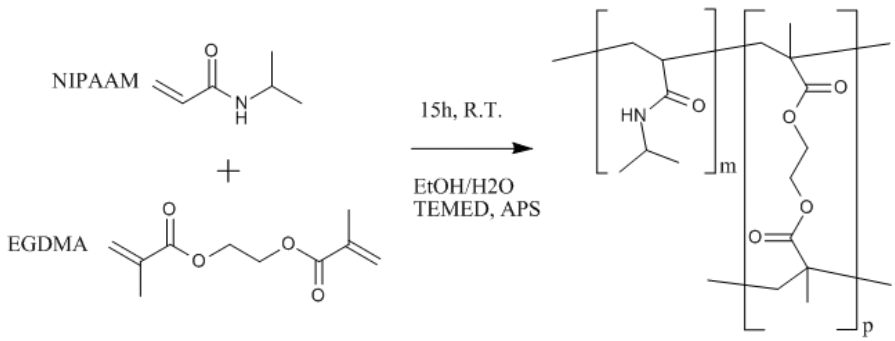


**Figure 3.1.** Scheme of the cross-linking reaction leading to PNIPAAm hydrogel molecular unit

After synthesis and removal from the mould, hydrogels were soaked in ethanol to wash out unreacted chemicals and then slowly swollen in MilliQ water, by decreasing the ethanol aqueous solution concentration by 30% every 2 hours by gradually adding pure water to the mixture. The synthesis parameters and conditions for producing a homogeneous transparent hydrogel, which exhibits suitable mechanical properties, at least at the level of being handled with laboratory tweezers, stretched and compressed without any damage, were found to be:

- *Monomer to cross-linker ratio:* NIPAAm: EGDMA = 1: 0.05 mol/mol
-*Monomer to initiator ratio:* NIPAAm : APS = 1 : 0.003 mol/mol

The reaction temperature was varied in the range 4°C – 28°C and it was found not to affect the final hydrogel film's properties. For this particular recipe, gelation occurred in 4 hours, while the polymerization and cross-linking took 15 hours to complete. These values are the result of a systematic optimization of the reaction protocol for the hydrogel synthesis, being focused on the target of realizing thin PNIPAAm layers. Throughout the remainder of this thesis this composition will be referred to as the **PNIPAAm standard mixture**. An example of the quantity used for producing 0.5 g of PNIPAAm hydrogel according to this recipe is reported in table 3.1.

| | Tot. Quantity | 0.5 | G | | | | | | | |
|---|---|---|---|---|---|---|---|---|---|---|
| | **NIPAAM** | | **EtOH** | | **$H_2O$** | | **EGDMA** | | **TEMED** | | **APS** |
| **Molecular weight (a.m.u.)** | 113.16 | | 41.03 | | 18 | | 198.22 | | 116.2 | | 228.2 |
| **Density ($g/cm^3$)** | - | | 0.789 | | 1 | | 1.051 | | 0.775 | | 1 |
| **Pureness** | 0.97 | | 0.99 | | 1 | | 0.98 | | 0.99 | | 0.98 |
| **mmoles** | 1.667 | | 5.373 | | 3.062 | | 0.088 | | 0.073 | | 0.004 |
| **µL used** | - | | 279.425 | | 55.1 | | 16.61 | | 11.02 | | 10.05 |
| **mg used** | 188.7 | | 220.5 | | 55.1 | | 17.5 | | 8.5 | | 10.1 |
| Weight fraction | 0.377 | | 0.441 | | 0.110 | | 0.035 | | 0.017 | | 0.029 |

**Table 3.1.** Example of relative reagent amounts for producing 0.5 g of PNIPAAm hydrogel.

The swelling ratio defined in equation (1) in 2.2.1 was determined by weighing the samples using a precision balance immediately after the reaction was completed ($W_d$) and after they had been water swollen (corresponding weight is $W_s$). By averaging the values obtained for a set of 10 samples, the swelling ratio was evaluated to be:

$$W_s/W_d = 1.5 \qquad [3.1]$$

Variation of the standard mixture was carried out to try to further improve the mechanical properties of the hydrogel; this issue was particularly important for the handling of swollen thin layers with thickness below 100 μm and this specific aspect will be discussed later on in section 3.3.2. The main variations to the standard mixture that were investigated to give different PNIPAAm hydrogels are reported below.

### 3.2.1.1 Increasing the cross linker amount

EGDMA was added in multiple quantities in respect of the amount used in the standard mixture. These hydrogels will be identified with the name PNIPAAmXR, where R = 1.3, 1.5, 1.7, 2, 4 indicates the multiple employed. PNIPAAmX1.3 did not exhibit significant differences in respect to the materials obtained with the standard mixture. In the range between 1.5 and 2, a slight improvement of the elasticity seemed to take place, but at the same time an enhancement of the opacity suggested that the resulting hydrogels were more heterogeneous. The swelling ratio was decreased by a factor that could be estimated to be about 25% in respect to the standard mixture derived samples. PNIPAAmX4 was characterized by a strong opaque look and no appreciable volume changes showed up in respect to its relaxed state when swollen in water.

### 3.2.1.2. Changing the cross-linker type

Methylene-bis-acrylamide (MBAA) was employed instead of EGDMA as a cross linker, keeping the same monomer to cross-linker amount employed in the standard mixture. The resultant water-swollen hydrogels showed good transparency, but a significant decrease in mechanical resistance.

#### 3.2.1.3 Changing the solvent type

Ethylene glycol was used instead of ethanol as the solvent for the mixture, keeping invariant all the relative chemical amounts. The obtained hydrogels were characterized by poor optical and mechanical properties.

### 3.2.2. PNIPAAm based random co-polymers

PNIPAAm based co-polymers appeared as a valid alternative solution for modulating the mechanical properties of pure PNIPAAm hydrogels. To explore this possibility, two different kind of monomers were taken into account and tested for realizing the bi-component networks; hydroxylethylmethacrylate (HEMA) and methylmethacrylate (MMA). In this context, the main difference between the two co-monomers relies on their hydrophilic/hydrophobic behavior. Although the production of PNIPAAm based random co-polymers using MMA and HEMA has been previously reported in the literature [10, 11], the author adopted a specific variation on the standard recipe for PNIPAAm based hydrogel synthesis, in order to adapt the established protocols to the synthesis of new materials and being confident of the previous results obtained with pure PNIPAAm. The random co-polymers obtained are separately described below.

#### 3.2.2.1. PNIPAAm/MMA co-polymers

MMA is known to be a rather highly hydrophobic monomer [12]. Since the polymer derived from this unit (Poly-MMA i.e. PMMA) exhibits very good mechanical properties [13] and at the same time it is known that the main effect of hydrophobic monomers is to lower the transition temperature when mixed with PNIPAAm [14], the percentage of MMA employed for realizing random PNIPAAm/MMA co-polymers is relatively high: 10% and 20% mol/mol of MMA in respect to the NIPAAm amount. In both cases, the MMA was added to the mixture before the initiator is added. The molecular unit that is formed is represented in Figure 3.2.

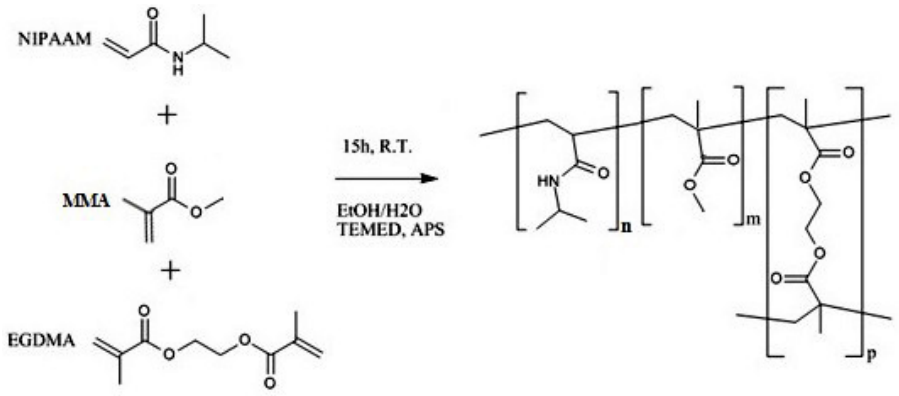


**Figure 3.2.** Scheme of the cross-linking reaction leading to the PNIPAAm/MMA co-polymers molecular unit

The hydrogels thus obtained were quite transparent and exhibited good elasticity (when 10% of MMA was used), while the 20% MMA based sample was too stiff and relatively heterogeneous.

### 3.2.2.2. PNIPAAm/HEMA co-polymers

On the other hand, HEMA is known to be highly hydrophilic [15]. Thus, its main influence on the resulting PNIPAAm based co-polymers should be that of increasing the critical transition temperature value above 32°C. PHEMA hydrogels are widely studied and produced for a number of applications [16] and they are also known to exhibit high elastic properties and good resistance [17], and thus HEMA was an exceptionally good candidate to be incorporated in the PNIPAAm based hydrogel structure to confer suitable mechanical features to the final hydrogel. A synthesis protocol was developed in house for producing pure PHEMA hydrogels which exhibits good elasticity and high resistance to compressive stresses. The determined reaction sequence is reported below:

1. *2-Hydroxyethyl methacrylate (Monomer,* HEMA*, liquid)*
2. *MilliQ or de-ionized water (Solvent,* $H_2O$*, liquid)*
3. *Ethylene glycol dimethacrylate (Cross-linker,* EGDMA*, liquid)*
4. *N,N,N',N'-Tetramethylethylenediamine (Catalyzer,* TEMED*, liquid)*

5. *20% w/w Ammonium persulfate (*APS*, powder) aqueous solution (Initiator,* APS% $_{w/w}$*, liquid)*
6. 

To obtain the material with the desired properties, the monomer to cross-linker and monomer to initiator ratios were set as 1 : 0.06 and 1 : 0.01 (mol/mol) respectively. The molecular unit of PHEMA is shown in Figure 3.3.

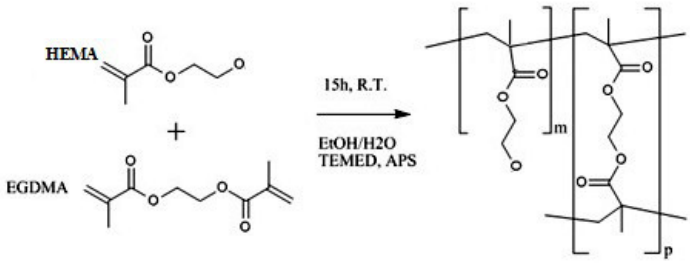


**Figure 3.3.** Scheme of the cross-linking reaction leading to the PHEMA molecular unit

PNIPAAm/HEMA co-polymers, the recipe developed for obtaining the hydrogels required the use of 20% concentration APS solution as the initiator and the addition of the chemicals was carried out according to the following sequence:

1. *Hydroxyethylmethacrylate (Co-Monomer,HEMA, liquid)*
2. *Ethanol (Solvent,* EtOH*, liquid)*
3. *MilliQ or de-ionized water (Solvent,* $H_2O$*, liquid)*
4. *Ethylene glycol dimethacrylate (Cross-linker,* EGDMA*, liquid)*
5. *N,N,N',N'-Tetramethylethylenediamine (Catalyzer,* TEMED*, liquid)*
6. *N-Isopropylacrylamide (Monomer,* NIPAAm*, powder)*
7. *20% w/w Ammonium persulfate (*APS*, powder) aqueous solution (Initiator,* APS% $_{w/w}$*, liquid)*

The molecular unit forming the hydrogel is depicted in Figure 3.4.

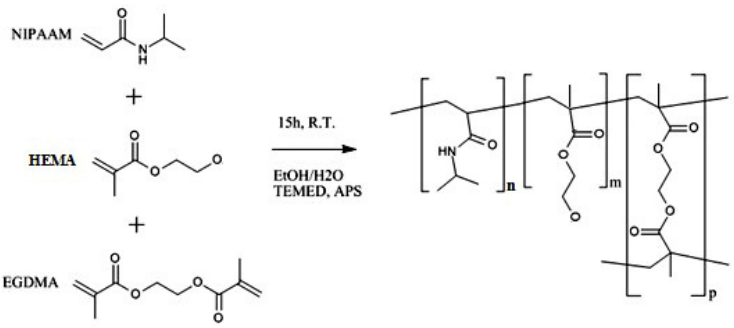


**Figure 3.4.** Scheme of the cross-linking reaction leading to the PNIPAAm/HEMA co-polymer molecular unit

The co-polymers that were realized contained a HEMA : NIPAAm ratio which varied from 5% to 40%, starting from the amount of chemicals employed. As expected, results showed a dramatic increase of elasticity of the water swollen network along with the increasing HEMA amount. Homogeneity depended weakly on the co-monomer concentration and all the samples obtained exhibited acceptable transparency. As will be explained in 3.2.2.3, HEMA (and PHEMA based hydrogels in general) will be fundamental for the development of a family of hybrid hydrogel structures in which precisely defined regions of the same layer will be based on different types of monomer: thermo-responsive PNIPAAm (or PNIPAAm/HEMA) and PHEMA.

## 3.2.3. IR spectroscopy

A quantitative characterization of the hydrogel composition was carried out using infrared spectroscopy (IR) on dry powders of pure PNIPAAm, PHEMA and random PNIPAAm/HEMA co-polymers previously described. The instrument employed was a JASCO spectrometer (model FT/IR-300E). Samples were prepared starting from moulded hydrogel films of the three types that were then dried in a vacuum chamber for one day. For IR spectra acquisition, the layers were pulverized using a ceramic mortar and then mixed with KBr powder (purchased from Sigma Aldrich). After mixing, the resulting compound was compressed using a custom device, in order to realize 1.5 mm thick tablets. The relative amounts, in weight, were: hydrogel powders : KBr powders = 30 : 70 w/w. KBr is known to

be transparent to IR radiation in the range of interest and it is usually employed for this kind of measurement; however, a background baseline relative to this buffer compound only was acquired each time prior to measurements on the hydrogel samples and then subtracted from the resulting spectra, in order to delete possible undesired contributions. Considering the relatively high thickness of the samples and the presence of possible inhomogeneities that could lead to an attenuation of the detected signal, the obtained results were cross-checked using attenuated total reflectance (ATR) spectroscopy on dry hydrogel films of the same composition. A Jasco ATR PRO 450-S accessory was assembled to the spectrometer to carry out this analysis on the moulded layers directly. The advantage of this technique is that it requires a minimal preparation of the samples; prior to measurement, the fabricated hydrogel films were only dried in vacuum for one day and then immediately used for IR characterization. The results obtained using IR reflection based spetroscopy, which gave the clearest spectra to be easily interpreted, are reported in Figure 3.5. T is the transmittance and it is calculated as $I/I_0$, where $I_0$ is the incident light intensity and I is the detected light intensity coming out from the sample.

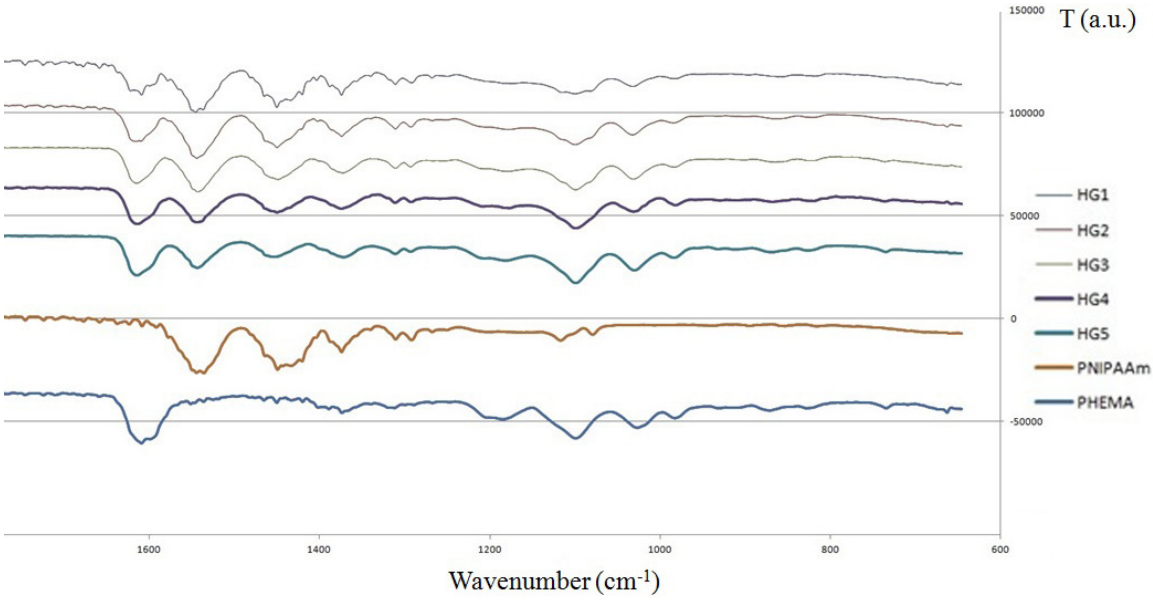


**Figure 3.5.** IR spectra of PNIPAAm, PHEMA and PNIPAAm/HEMA co-polymers. The composite hydrogels are named HG1, HG2, HG3, HG4 and HG5 and correspond to HEMA : NIPAAm molar ratio of 5,10,20,30 and 40% respectively.

The aim of the measurement is to trace the increasing amount of HEMA in the random co-polymers; in order to do so, the peak intensity relative to the contribution of the O-C=O and C-OH groups present in the side chain of the monomer are monitored. All the IR spectra showed two strong amide absorption bands at about 1650 $cm^{-1}$ (ν O=C-NH, peak 1) and 1540 $cm^{-1}$ (ν N-H, peak 2) related to NIPAAm monomeric unit [18]. Peaks at 1730 $cm^{-1}$ (νO=C-O, peak 3) and 1150 $cm^{-1}$ (ν C-OH, peak 4), are related to the HEMA monomeric unit [19], and show an increase in intensity with increasing HEMA content as expected.

## 3.3. Manufacturing protocol

The main topic of this section will be the development of the ICM technique employed for PNIPAAm based thin films realization, its experimental set up and the results obtained with this process. Before entering into details, the outcome of spin coating tests conducted before ICM was developed and applied are also presented and discussed.

### 3.3.1. Spin coating tests

The spin coating technique applied to hydrogel layer fabrication of both thin films (thickness >200 nm) and ultrathin films (thickness < 200 nm) has already been covered in Chapter 2; since the process is reliable in terms of film uniformity and thickness control, it has been the first choice for the purpose of realizing PNIPAAm based layers. The tests conducted using a standard spin coating apparatus are reported below; the spin coater used was a Laurell WS-400B-6NPP/LITE. A picture of the instrument is shown in Figure 3.6.

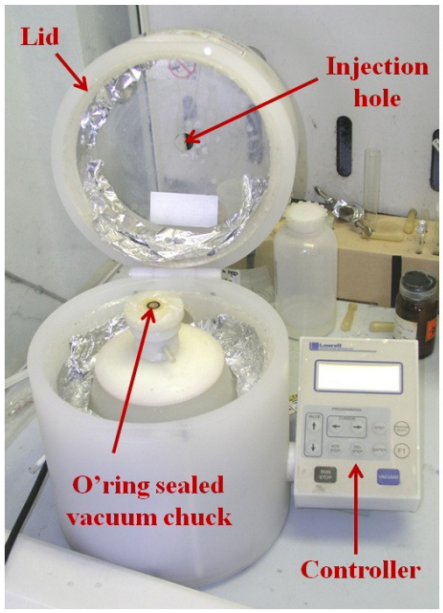


**Figure 3.6.** Spin coating apparatus employed for PNIPAAm based layers fabrication tests

The film fabrication protocol was developed in order to produce hydrogel layers of the desired thickness (between 10 and 300 μm) and having the possibility of obtaining the freestanding component by promoting its detachment from the polymer coated substrate. The substrates employed for the coating were 3.5 cm diameter polystyrene (PS) Petri dishes and a 60 μm thick commercial polyvinyl alcohol (PVA) foil was interposed between the rotating substrate and the injection drop; PVA is soluble in water and so it operates as a sacrificial layer, which can be removed after PNIPAAm hydrogel films are formed by soaking the sample in MilliQ water. Before applying PVA to PS, the surface of the dishes were wetted by a 1:1 ethanol aqueous solution. The PNIPAAm standard mixture was tested first; unfortunately, no film formation was observed during the tests carried out. The main issue which led to failure of the spin coating tests appeared to be the high evaporation rate of ethanol, which happens in a few minutes after the drop is injected in the apparatus and spun, preventing the mixture from cross-linking properly. For this reason, a number of solvents with higher boiling point, including ethylene glycol, were tested to promote the cross-linking in a reasonable time (< 5 min). Another requirement was that the solvents employed should

not dissolve PVA. Results of the tests, including the effects of the chemicals on the PVA film and solvent viscosities are reported in Table 3.2.

| Solvent | Dissolve PVA | Viscosity at 25 °C (cP) | Cross-linking time |
|---|---|---|---|
| *Ethylene glycol* | No | 16.100 | < 5 min. |
| *Isopropyl alcohol* | No | 2.048 | No cross-linking |
| *1,4-dioxane* | No | 1.177 | 30 to 40 min. |
| *Dimethyl sulfoxide* | Yes | 1.987 | 2 h |
| *Tetrahydrofuran* | No | 0.480 | No cross-linking |

**Table 3.2.** Reaction tests of PNIPAAm cross-linking using different solvents. The dissolving effects on the PVA and viscosity values at room temperature [20] are also included.

Ethylene glycol showed up as the best candidate to carry on testing the spin coating technique. To avoid problems connected with common spin coating defects, such as heterogeneous coating, bubbles, streaks and swirling pattern formation, the amount of polymerizing mixture as well as the spinning plate's acceleration and rotation speed were varied with a series of tests until a uniform layer was reached. The best parameters were found to be:

-*Plate acceleration time:* from 0 to 5000 rpm in 30 seconds
-*Plate rotation speed:* 5000 rpm
-*Rotation time:* 30 seconds
-*Polymerizing mixture volume:* 1 ml
-*Drop injection time:* 0 to 10 seconds after rotation started

With these operational parameters, PNIPAAm layers could be fabricated only using ethylene glycol as the solvent; after the PVA was removed, the thickness of the hydrogel films obtained were measured with a caliper and found to be 15 μm. Due to the difficulties encountered with this method, an alternative technique for producing PNIPAAm based thin films was investigated; this was to promote compression of the polymerizing mixture

between two rigid plates, separated by a hollow thin spacer, in order to define the shape and thickness of the hydrogel formed. This would enable the full range of desired thickness to be prepared and led to the ICM technique, as explained in the next section.

### 3.3.2. Injection/compression moulding (ICM) of PNIPAAm based layers

The first tests for exploring the suitability of moulding PNIPAAm based films with an injection/compression mechanism were conducted using a three component basic equipment setup. Standard PNIPAAm polymerizing mixture was injected onto the surface of a glass plate into a region defined by a hollow metallic spacer, then closed with a second glass plate and then compressed with a 10 kg weight covering the entire surface of the system. A schematization of the first version of ICM is shown in Figure 3.7.

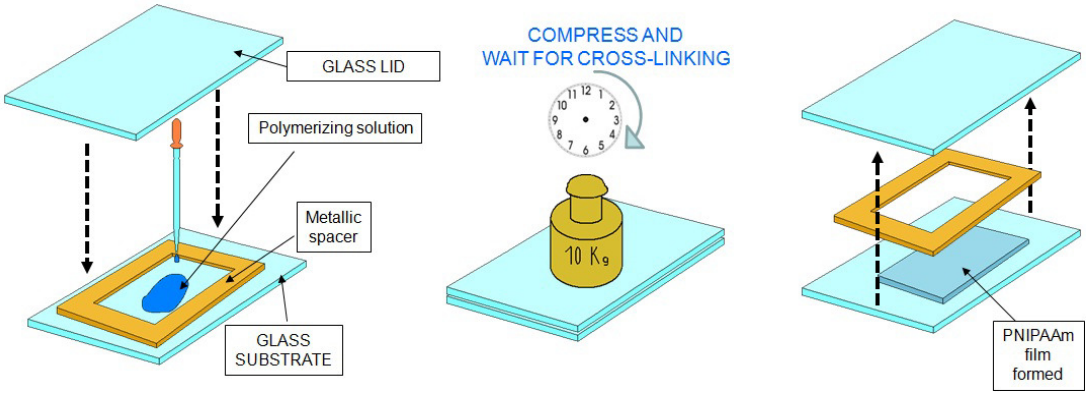


**Figure 3.7.** Schematization of the first version of ICM. a) Polymerizing PNIPAAm standard mixture is injected into the region defined by the metallic spacer and a glass lid is placed on top of it. b) Compression is promoted employing a 10 kg weight positioned over the lid. c) The system is opened and the hydrogel film is formed.

The metallic foils employed were obtained from commercial rolls which were then cut and shaped with a shearing knife. The thickness of the spacers available, which also defines the

actual thickness of the hydrogel films, were 10, 20, 25, 50, 75, 100, 200 and 300 μm. Glass plates were 5 mm thick rectangular slabs (10 x 10 $cm^2$), treated with a piranha solution prior to the moulding ensuring cleanliness of the components. The first results obtained with this method showed the possibility of realizing uniform films of the desired thickness (measured with calipers) for all the spacer thickness values available. However, the technique suffered from a number of difficulties; first, one third of the samples produced each time gave only a partially formed layer, covering not more than 60% of the surface defined by the hollow mould. The main reason for this was thought to be due to massive liquid leakages around the metallic spacer due to the presence of burrs at its edges, generated from the cutting of the foil, and the relatively low viscosity of the polymerizing mixture. Even by reducing the presence of the asperities by cutting the metal foils on rigid surfaces and by refining the surface using sand paper, the productivity of the process remained limited, mainly because of liquid leakages still occurring due to the low sealing properties of the metal; a quantity of the PNIPAAm mixture equal to two times the volume defined by the mould was needed and the surface of the formed films covered not more than about 80% of the desired area. Another difficulty was the fact that, by using glass slides for both lid and substrate, the probability of having the formed film stuck to one of them was 50%; this would cause problems when the film fabrication process was subjected to automation in a scaled up manufacturing protocol. The two main improvements that enabled the realization of the actual ICM were then:

-*Use of shaped silicone rubber thin sheets instead of the metal foils as spacers:* silicone rubber materials exhibit excellent sealing properties when operating as a gasket. Polydimethylsiloxane (PDMS) thin layers were produced in house (thickness from 50 to 300 μm), using the technique described in 3.3.3, and tested as the moulding element employed in ICM. This significantly limited the amount of leaked liquid and allowed the production of PNIPAAm based layers of the desired area. Since PDMS is a rather soft material, it is subject to compliance when compressed; a precise control over the hydrogel film thickness was achieved by the designed of a screw based system described later. Furthermore, silicone based components used in industry have elastic and sealing properties similar to the ones exhibited by PDMS, which therefore represents a good model for further scale up features of the ICM method.

-*Study of PNIPAAm adhesion to different materials:* a systematic study to identify which materials would be best for operating as an adhesive substrate and non-adhesive lid for PNIPAAm was carried out experimentally. This screening was conducted both by observing the behavior of the single material in contact with the PNIPAAm cross-linked layer and by applying ICM to different pairs using silicone PDMS sheets as spacers, in order to define a scale of adhesion. The materials employed were: glass, PDMS, polished aluminum (Al-lux), commercial aluminum film (Al-film), sandpaper treated rough aluminum (Al-rg), silanized glass (Gla-Si), glass functionalized with N-vynilpyrrolidone (Gla-NVP), glass functionalized with styrene (Gla-St), commercial Parafilm layers (para-film), Polyvinyl chloride (PVC), commercial paper stickers (Pap-E), commercial Parafilm paper layers (Pap-P), PS and sandpaper treated rough PVC. The area defined by the mould is to be considered as a rectangular shape, with thickness of 200 µm and surface area of 10 x 2.5 $cm^2$. All tests involving different plates were carried out two times, inverting the positions of the plates in order to exclude possible gravity effects. Every film-like or paper based material was glued to a rigid substrate. The relative couplings tested are reported in Table 3.3.

| MATERIALS | *Glass* | *PDMS* | *Al-lux* | *Al-film* | *Al-rg* | *Gla-Si* | *Gla-NVP* | *Gla-St* | *para-film* | *PVC* | *Pap-E* | *Pap-P* | *PS* | *PVC-rg* |
|---|---|---|---|---|---|---|---|---|---|---|---|---|---|---|
| *Glass* | X | | | | | | | | | | | | | |
| *PDMS* | X | X | | | | | | | | | | | | |
| *Al-lux* | X | X | X | | | | | | | | | | | |
| *Al-film* | | | | X | | | | | | | | | | |
| *Al-rg* | | | X | X | | | | | | | | | | |
| *Gla-Si* | | | | X | | | | | | | | | | |
| *Gla-NVP* | | | X | | | | | | | | | | | |
| *Gla-St* | | | X | X | | | | | | | | | | |
| *para-film* | | X | X | X | | X | | | X | | | | | |
| *PVC* | | X | | | | | | | | X | | | | |
| *Pap-E* | | | | | | | | | | | X | | | |
| *Pap-P* | | | | | | | | | | | | X | | |
| *PS* | | | X | X | | | | | X | | | | X | |
| *PVC-rg* | X | | X | | | | | | | | | | | |

**Table 3.3.** Study on adhesive properties of different materials with ICM fabricated PNIPAAm layers. Each box labeled with an X identifies a specific couple tested.

Here are reported the behavior of the single materials:

- Paper based layers tended to absorb the mixture and to consequently deform, so they could not be used.
- Glass, NVP functionalized glass, styrene coated glass, PVC, and PS showed a similar behavior: PNIPAAm film tended to adhere to this surfaces and a layer curling followed by a spontaneous detachment happened after it dried out over time.
- Rough aluminum and rough PVC were the materials to which PNIPAAm layers tended to adhere the most; the best grit interval of the sandpaper to obtain the best adhesion properties was identified to be between 400 and 800. It was noted that PVC showed completely inert behaviour to the chemical composition of the cross-linking solution, while rough aluminium was partially damaged, exhibiting white regions on its surface, when films were detached. In this sense, while PVC could be recycled for further fabrications, aluminium plates must be changed each time.
- Aluminum film, Parafilm, polished aluminum, silanized glass and PDMS showed non-adherent behavior.

The tests conducted on different materials couples were comparable with the single material characterization. Within this frame, the most appropriate pair satisfying the conditions of a reproducible adhesive/non-adhesive behavior to form the actual ICM apparatus were found to be rough PVC as substrate and polished aluminum as the lid; this choice also relied on the fact that the materials employed are relatively cheap and easy to process. Once the plates and moulding spacer materials were chosen, the methodology for setting up the apparatus and the fabrication protocol were identified for carrying out a reliable and reproducible ICM as follows:

1) PVC flat rectangular plates (15 x 5 $cm^2$ surface area, 2 mm thick) are treated on one surface with waterproof sandpaper (200, 400 and 800 grit), continuously washing the component with MilliQ water during the roughening process, then thoroughly washed in a 1:1 water and ethanol solution.
2) PDMS moulds of the desired thickness and having a hollow rectangular region (10 x 2 $cm^2$) are soaked in acetone for 2 hours, then rinsed in water and positioned and gently pressed over the PVC when dried, in such a way that a good adhesion between the two materials is guaranteed.

3) The polymerizing PNIPAAm standard mixture is injected in the hollow region defined by the silicone layer in a quantity corresponding to 1.3 to 1.5 times the volume defined by the region itself. The system is then closed with the polished aluminum lid and held in compression by applying a brass weight (2 to 5 kg) on top of it.
4) After the time for completing the reaction is reached, the molding apparatus is disassembled with the formed film attached to the PVC plate.

PNIPAAm based thin films were then realized in a high-throughput process, according to the scheme represented in Figure 3.8.

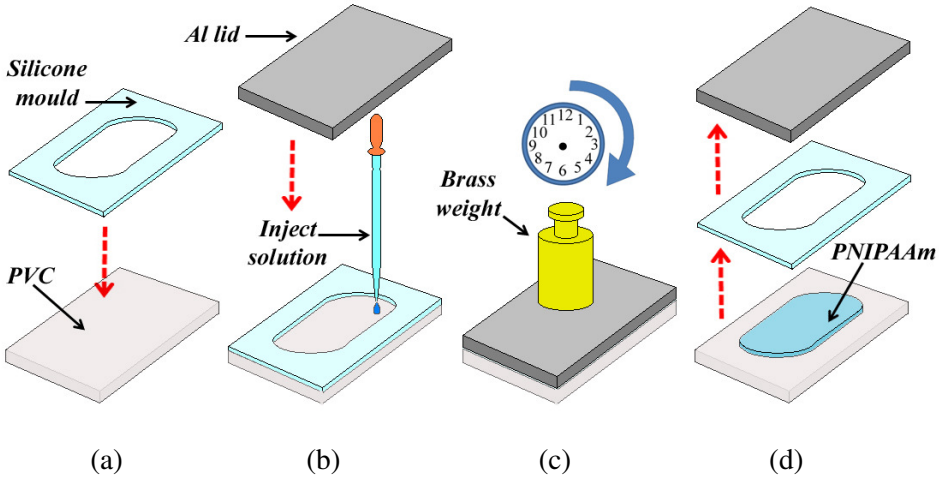


**Figure 3.8.** ICM scheme for PNIPAAm layers realization. a) Silicone mould is positioned over a rough PVC layer. b) The polymerizing mixture is injected into the mould and the system is closed with the polished Al lid. c) Compression is promoted by using a brass weight for the time necessary for the reaction to complete. d) The formed hydrogel film is recovered on top of the rough PVC.

With the protocol described, it was possible to obtain layers with thickness values which had variations of about 10 to 20% with respect to the PDMS mould thickness; as already mentioned, this was due to the compliance of the silicone rubber when under compression. All measurements of hydrogel layer thickness were carried out with a set of calipers. To decrease this discrepancy and thus improve the control over the PNIPAAm layer thickness, a screw-based system working on the same injection/compression principle was designed and

realized with the help of the mechanical workshop of the department of Physics in Milan. The apparatus consisted of two 5 mm thick rectangular slabs (15 x 5 $cm^2$) of PVC and polished aluminium, endowed with threaded through-holes drilled at their corners, and an aluminum jig of the same dimension of the two components, which could be aligned to them. A set of metallic spacers (50, 75, 100, 200 and 300 µm thick) were produced by a numerically controlled milling process, in order to create a hollow frame to be aligned with the other components and being able to host the shaped PDMS moulding. The main idea was to carry out ICM having the metallic spacer interposed between the rough PVC and the polished aluminum defining the final thickness of the film and embracing the PDMS moulds, which would only define the form of the hydrogel layers and guarantee the sealing during the process. For the gasket to work properly, silicone components must be at least 20 to 30% thicker than the metallic frame. Here, compression was promoted by screwing the components together using M4 bolts, as depicted in the scheme of Figure 3.9.

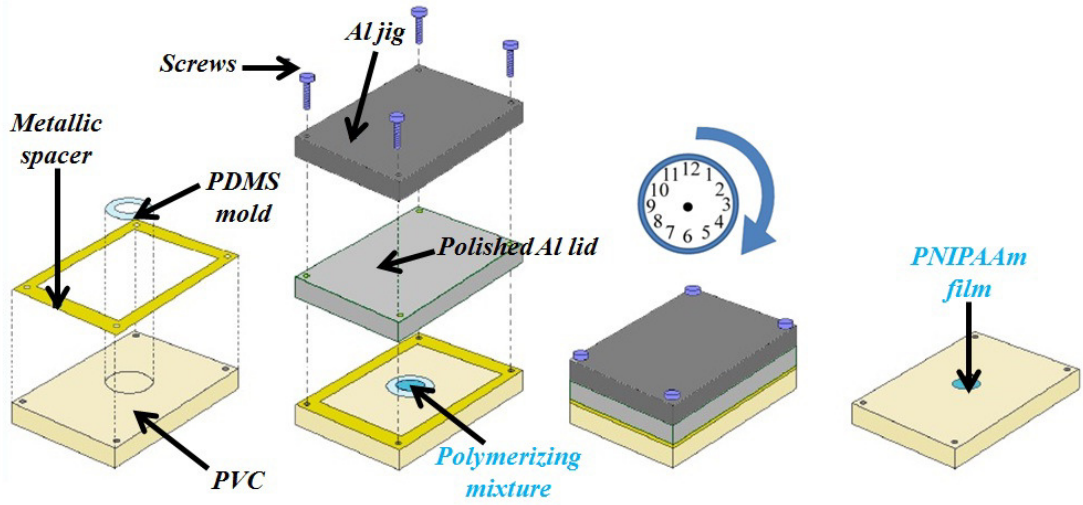


**Figure 3.9.** Screw based ICM device schematization for improving control over thickness for PNIPAAm layers fabrication. a) Silicone mould is positioned over a rough PVC layer, with a thinner metallic spacer embracing it. b) The polymerizing mixture is injected in the PDMS mould and the system is closed by the polished Al lid via an aluminum jig. PVC and aluminum components are easily aligned by the threaded holes. c) Compression is promoted by screwing the bolts in each thread and the system remain closed for the time necessary for the reaction to complete. d) The formed hydrogel film is recovered on top of the rough PVC.

Results obtained both on rectangular and circular films showed that PNIPAAm layer thickness values were always kept within 10% of the respective metallic layers employed. Rough aluminum could also be used instead of rough PVC. The PNIPAAm based layers realized with ICM embraced all the materials described in section 3.2, but the PNIPAAm standard mixture was mostly employed (almost 70% of the total samples). An observation concerning circular hydrogel films was made; while for large surface area rectangular films the percentage of success (layer with desired extension and thickness) was > 95% of the whole sample tested, circular films could only be realized with a percentage of success of 50% per array due to the relatively small amounts of liquid injected. Furthermore, for samples with diameter below 5 mm, a spontaneous detachment from the substrate of the hydrogel structures frequently occurred a few minutes after the system was opened. Detachment tests of the PNIPAAm based layers from PVC substrates were carried out on the freshly fabricated film, in order to determine, prior to the laser machining, how to obtain the freestanding hydrogel components without exercising a mechanical removal that would damage or ruin the structure. The idea was to determine a chemical treatment that would induce detachment of the hydrogels by soaking the film still stuck on the PVC plate in a solution containing water and a certain percentage of organic solvents in order to induce the swelling of the film and thus promote its removal from the substrate. Since all the synthesis reaction for PNIPAAm based hydrogels, as well as for the random co-polymers, involved ethanol as the solvent, aqueous solution containing different ethanol percentage as well as pure ethanol were tested. Soaking the films in pure ethanol resulted in a very effective technique for removing all the hydrogels; within 30/45 minutes rectangular films were completely detached from the PVC, while small disks could reach a freestanding state much earlier (5 to 10 minutes). Swelling of the films was conducted as already described in 3.2. It was observed that films with thickness less than 50 μm could not be handled without causing tears or lacerations that would irreversibly damage the structures; the main problem was that 10, 20 and 25 μm thick films cannot stand their own weight when removed from water, irrespective of their particular chemical composition. Moreover, they exhibited a folded structure when completely water swollen, leading to spontaneous curls from the borders of the films towards their centers. This limited the range of thickness available from 50 to 300

μm. The next section is dedicated to the fabrication protocol developed for realizing the PDMS moulds that have been employed in the ICM technique.

### 3.3.4. Silicone rubber thin film realization

As mentioned before, silicone thin sheets for realizing the gasket elements employed in ICM were produced in house, though industrial silicone foils are sometimes available for the desired thickness (> 200 μm). The process for fabricating PDMS thin layers was also based on a molding technique; the established protocol is described here. PDMS silicone (Sylgard 184, Dow Corning), was obtained by mixing the high viscosity elastomeric component and the related liquid curing agent in a glass beaker, with an elastomer : curing agent ratio of 10:1 w/w. This choice allows the realization of soft stretchable highly elastic components [21]. The solution obtained by mixing the compounds was then stirred by hand using a Pasteur pipette until the liquid appeared to be milky and it was then degassed under vacuum for 2 hours. Typical weights of the solution prepared for realizing one 15 x 5 $cm^2$ rectangular sheet of thickness between 50 and 300 μm was around 1.5 g. The fabrication of the silicone moulds is carried out employing the system shown in Figure 3.10. First, metallic thickness sheets (the same type as employed earlier in the ICM technique) were positioned over an aluminum slab (10 mm thick) in order to define a region which would shape the silicone. The PDMS was then poured directly from the beaker on top of it; the system was then closed using an aluminum lid and a weight (~ 20 or 30 kg) applied. Such relatively high values of the weights were employed in order to minimize the viscous liquid's infiltration between the brass thickness sheets and the bottom aluminum slab, which would lead to massive deviation from the desired thickness values. To hasten the curing process, the whole molding system was placed on a pre-heated hot plate (120 °C); in such a way, it took only 30/40 minutes for the PDMS to solidify, while at room temperature the time needed for solidification would have been 48 hours. After the solidification, the silicone sheet was formed and ready to be detached.

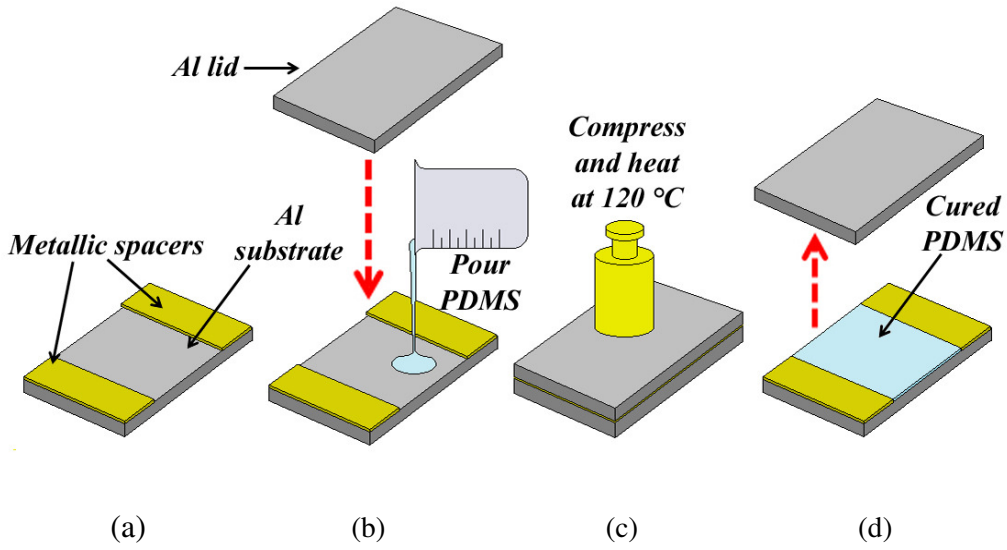


**Figure 3.10.** Silicone mould fabrication: a) Metallic spacers are placed over the bottom aluminum slab. b) Liquid PDMS is then poured directly on the substrate from the beaker. c) A 20 to 30 kg weight is placed on the lid to seal the system until PDMS solidification occurs (30 - 40 min, at 120 °C). d) The lid is removed and then the silicone film is recovered.

During the disassembly of the system, ethanol could be used to favor lubrication of the component interfaces. PDMS films can be detached from the aluminum slab by promoting the polymer's swelling by soaking the system in highly non-polar organic solvents, like acetone, hexane, or petroleum ether. After the film was detached, the mould was shaped by using a cutter or a hole-punch. Silicone moulds with circular holes were produced by hole-punching PDMS layers; arrays of circles with different diameter (2, 3, 4, 5 and 7 mm), as well as single circular moulds with the same dimensions, were tested for producing PNIPAAm films with different geometry both by using the screw-based device and the traditional fabrication protocol.

## 3.4. Hybrid hydrogel thin film development

As mentioned in 3.2., the role of PHEMA was particularly important not only for modulating the mechanical properties of PNIPAAm based layers when incorporated in the network as a co-monomer, but also for the realization of hybrid PHEMA/PNIPAAm thin films; this section is dedicated to this particular smart structure developed in house. The main idea for generating this structure was born after first integration and thermo-responsiveness tests had been carried out, showing issues about the use of pure PNIPAAm when integrated with other thermoplastic components. The thermo-responsive behavior of the film is discussed in Chapter 5, while integration tests will constitute a section of Chapter 6. Since the present chapter deals with the fabrication techniques developed for realizing hydrogel layers, discussion about the methods developed for producing hybrid PHEMA/PNIPAAm structures is carried out in 3.4.2, while preliminary basic concepts as well as a brief summary of the main reasons driving the development of the hybrid films will be contained in the next section.

### 3.4.1. The use of hybrid structures: the role of PHEMA

The synthesis of PNIPAAm based hydrogels and co-monomers combined with the development of the ICM technique led to the possibility of producing a library of smart materials with different optical and mechanical properties in the form of a thin layer, with thickness ranging from 50 to 300 μm. Some of the synthesized hydrogels were identified through a qualitative characterization to be the most suitable materials, in terms of mechanical and optical properties, for the target of hybrid material cells-on-chip application. PNIPAAm thin films obtained with the developed standard mixture, as well as PNIPAAm-co-HEMA (PHEPAAm), were particularly promising as smart materials to be able to endure long term static compression when integrated with harder polymeric materials. However, when temperature changes around the critical transition temperature occurred and the layers were mechanically constrained in the chip at the same time, their elastic behaviour would not guarantee reversible deswelling/swelling without damaging the films. This qualitative

expectation was confirmed by the first integration tests carried out on PNIPAAm based layers as a basis for further developments and which are discussed in section 6.3. Here it is only necessary to say that the PNIPAAm based material layers developed are not sufficiently elastic to stretch without breaking when constrained under compression. Without entering into details, Figure 3.11 shows the tearing occurring at the compression edges when a 7 mm water swollen patterned PNIPAAm disk, compressed between two hollow PMMA slabs endowed with axi-symmetrical aligned cylindrical through-holes at their center, is subjected to the volumetric transition.

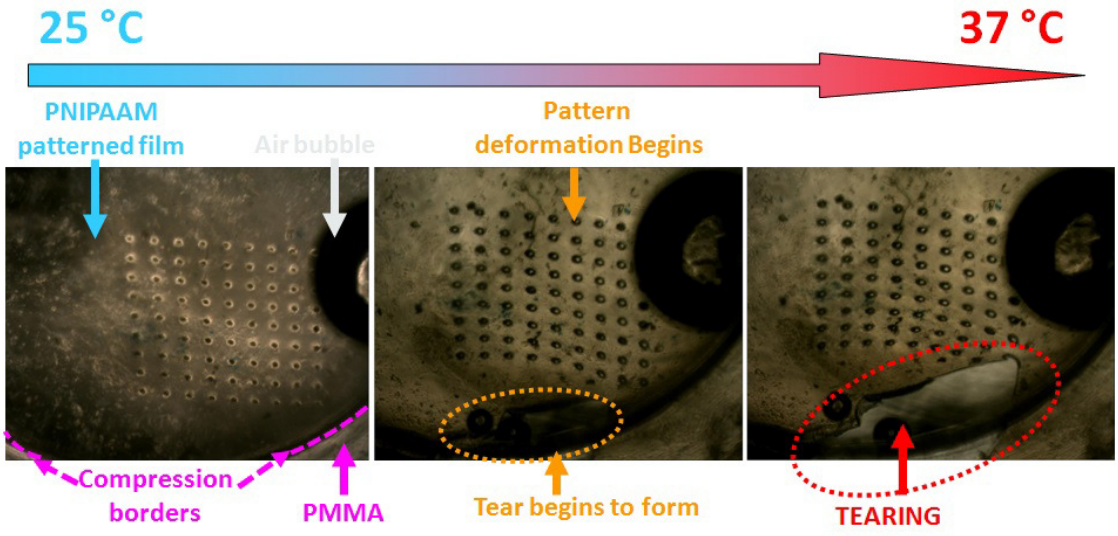


**Figure 3.11.** Deformation and tearing of PNIPAAm disk compressed between 5 mm thick PMMA layers. a) At room temperature the system is static. Pink dashed lines identify the borders where compression of the film ends because of the beginning of the hollow regions in PMMA. b) When the transition starts to occur, tearing begins. c) A big laceration is present in the disk beyond the critical temperature.

It was clear that PNIPAAm based hydrogels should be integrated with harder polymeric components in such a way that their thermo-responsiveness behaviour could still be manifested by shrinking exactly (or similarly) in the same way as the polymer would when in

a freestanding state and without causing tearing or lacerations. Within this frame, a method for realizing inter-penetrating PHEMA/PNIPAAm networks with defined geometrical features was developed. PHEMA presents good elastic properties and could operate as a gasket when integrated with thermoplastic platforms, while PNIPAAm would represent the functional 'free' thermo-responsive component. The only mechanical constraint on the PNIPAAm based component in the chip would be the chemical bond with the HEMA based region of the hybrid layers. A representation of the desired structures and the temperature triggered mechanism that is expected to be observed is reported in Figure 3.12.

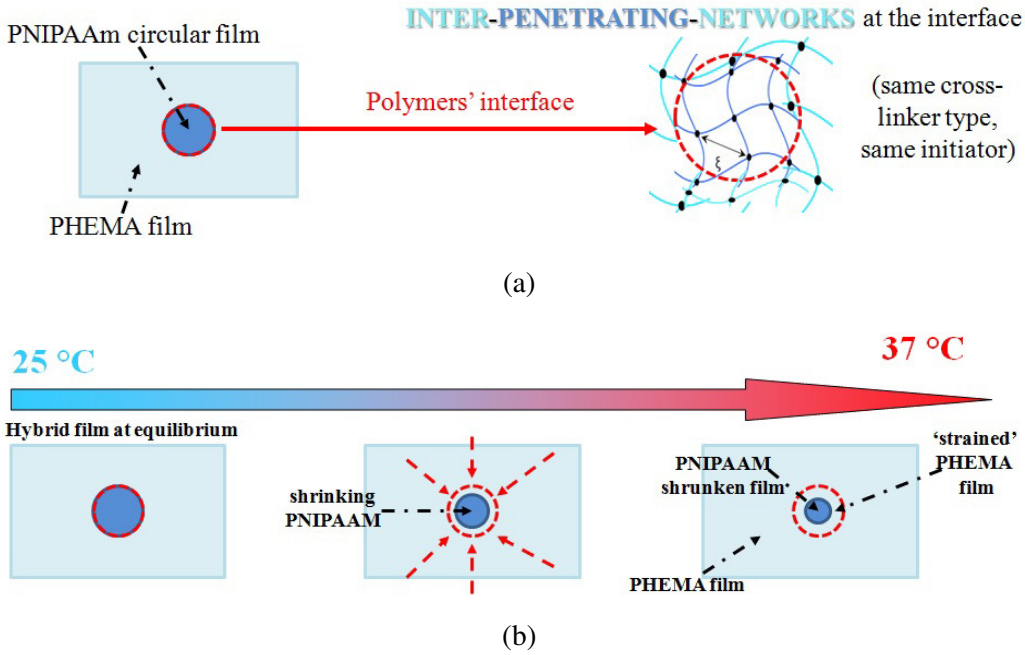


**Figure 3.12.** Structure of hybrid PHEMA/PNIPAAm networks and expected temperature triggered volume phase transition. a) The hydrogels' different structures are cross-linked together in a narrow interface region. b) When the transition is induced by changing the temperature above LCST, only PNIPAAm shrinks, while straining the PHEMA frame along its shrinking path until equilibrium is reached again.

From a general point of view, since both PHEMA and PNIPAAm are acrylic based materials, it is possible to chemically link the two hydrogels together. Furthermore, by exploiting the reaction kinetic of the polymers, it is possible to create a 'hybrid' structure in which regions based on different types of monomers are well defined and they only interpenetrate each other in a narrow interface zone. The main idea underlying the fabrication of these hybrid films is to partially cross-link in a mould one of the two materials, so that it reaches the solid state but it is still able to form strong chemical bonds at the same time, since the reaction is not completed. In this situation, if the shape of the forming hydrogel is modified between the gelation point and 80% of the reaction's completion, the new shape is maintained and then the link of the other material to the forming network could be promoted in an effective way, by controlling both the bonding degree and the geometry. More specifically, two techniques were developed and represent the starting point for PHEMA/PNIPAAm based hybrid film fabrication. Based on the results obtained with these two manufacturing protocols, a third technique was introduced and then optimized to be employed for the actual hybrid hydrogel layers manufacturing.

## 3.4.2. Hybrid PHEMA/PNIPAAm layer fabrication

The fabrication techniques were based on the ICM protocols developed for pure PNIPAAm thin layer realization. Material synthesis was still based on the chemically induced free-radical polymerization using ammonium persulfate (APS) as the initiator. Three methods were sequentially introduced and tested and they are described below. The first two protocols (METHOD 1 and METHOD 2) rely on similar fabrication schemes, which is the injection of the polymerizing solutions on the flat substrates before compression takes place. The third method (METHOD 3), which was shown to be the most repeatable and reliable for producing these type of hybrid layers with high consistency and high-throughput features, was based on a slightly different scheme, as it will be discussed later. Hybrid hydrogels moulded with this manufacturing protocol were used for testing the cell sorting prototype, as described in Chapter 6.

- **METHOD 1:** the first method is based on the fabrication of thin PHEMA layers first, by using the standard ICM technique previously developed. Once the gel is formed, the mould is opened and the partially cross-linked film is hole-punched. A PNIPAAm polymerizing solution is then added into the punched regions, so that PHEMA itself acts as the new mould to give shape and thickness to the forming thermo-responsive component. This process is schematized in Figure 3.13.

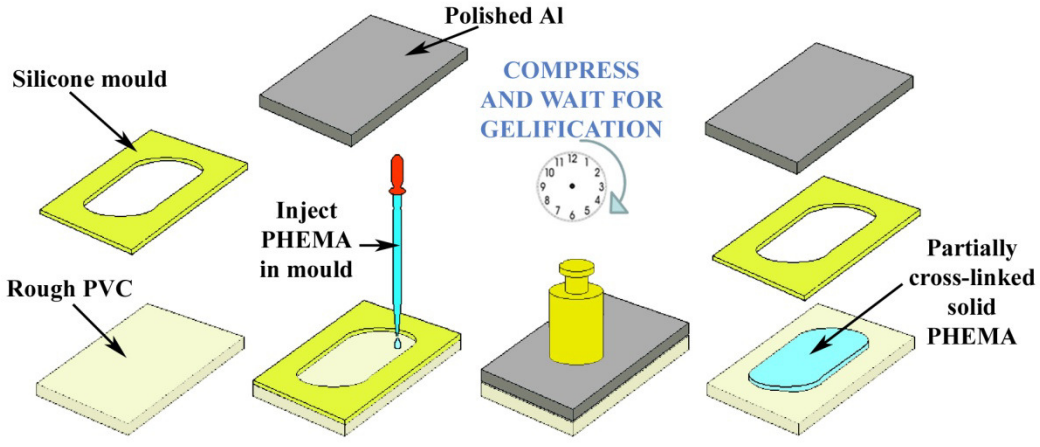

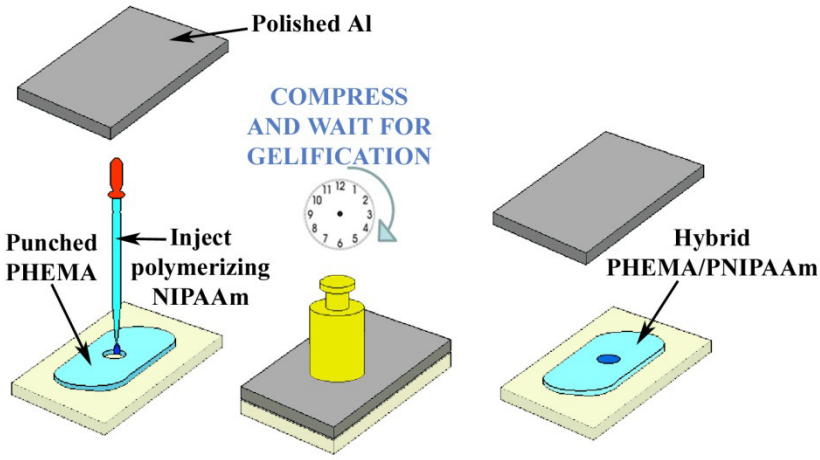


**Figure 3.13.** Method 1 for hybrid films fabrication based on the ICM technique. a) PDMS mould is positioned over rough PVC plate. b) PHEMA polymerizing mixture is injected into the mould and the system is closed with the polished aluminum lid. c) Compression is promoted by putting a weight over the system. d) The system is disassembled when the PHEMA film is formed, but only partially cross-linked. e) PHEMA is hole-punched and PNIPAAm mixture is injected in the circular regions. f) Compression is once more promoted until PNIPAAm hydrogel is formed. g) The hybrid PHEMA/PNIPAAm film is recovered on the PVC when the system is disassembled.

- **METHOD 2:** the second method is based on the fabrication of small thin disks of PNIPAAm (3 to 4 mm diameter) at first, by using the standard injection/compression moulding technique previously developed. After disks are formed and the gelification point is reached, a hollow silicone mould is placed around them in order to define the region in which PHEMA must be injected. After the injection, compression is promoted once again and the hybrid structure is formed. A representative scheme describing METHOD 2 is shown in Figure 3.14.

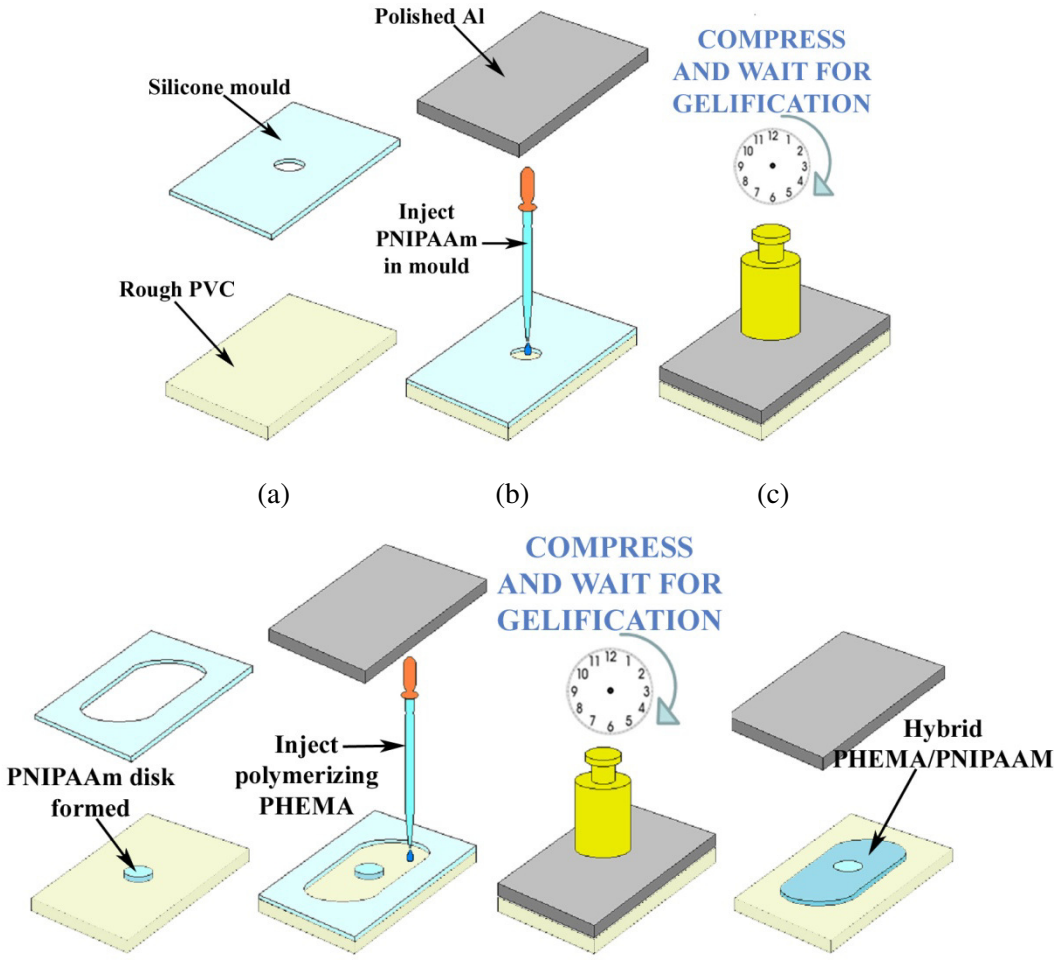


**Figure 3.14.** Method 2 for hybrid films fabrication based on the ICM technique. a) PDMS mould is positioned over the rough PVC plate. b) PNIPAAm polymerizing mixture is injected in the hollow circular region of the mould and the system is closed with the polished aluminum lid. c) Compression is promoted by putting a weight over the system until gelification of PNIPAAm is reached. d) The system is disassembled and the PNIPAAm thin disk is formed but only partially cross-linked. A hollow silicone mould is then placed on PVC. e) PHEMA is injected in the region defined by the PDMS spacer around the PNIPAAm structure and the aluminum plate closes the system. f) Compression is once more promoted until PNIPAAm and PHEMA completely cross-link. g) The hybrid PHEMA/PNIPAAm film is recovered on PVC when the system is disassembled.

Both methods present advantages and disadvantages that can be summarized as follows:

- ✓ **Advantages:** the protocol has been well defined in terms of use of materials employed (hydrogels, substrate and lid) and equipment (silicone spacers, weights) and it has been shown to be reproducible and reliable, at least at the single monomer based component level. The simplicity of the minimal equipment required also represents an advantage. Moreover, the PNIPAAm based hydrogels employed are exactly of the same type as the ones which have been previously characterized in terms of thermo-responsivity after laser micro-patterning, so their behavior at the phase transition is already a reference to rely on when analyzing the hybrid films' response to temperature changes. Having a set of information on their thermo-responsive behavior constitutes and advantage because it avoids the need of further analysis on the pure material itself.

- ✓ **Disadvantages:** once the reaction is induced by the initiator, it will carry on to its end with no possibilities of stopping it. An accurate knowledge of the kinetics of the reactions involved and an appropriate time schedule is required to work out the protocol properly. Furthermore, METHOD 1 suffers from the inconvenience that the NIPAAm polymerizing solution will be injected in a porous mould (PHEMA), so it is likely to diffuse at a certain rate in the mould itself; since the gelification time for the standard PNIPAAm is about 4 hours, diffusion phenomena can lead to massive leakages. On the other hand, the production of small PNIPAAm disks described in METHOD 2 was shown to only have a success of about 50% of the samples tested. Moreover, in METHOD 2, a PHEMA layer could possibly cover the PNIPAAm disks at their top due to the second compression and this could potentially hinder the thermo-responsive behavior of the disks.

Theoretically, problems connected with both methods could be overcome by properly tuning the synthesis conditions of the hydrogels in order to produce PNIPAAm based films with the same cross-linker and initiator couple, same monomer to cross-linker ratio and a slight difference in monomer to initiator ratio, without thus significantly altering the properties of

the gel in respect to the standard material (METHOD 1) or by making minimal variations to the moulding apparatus (METHOD 2). Fabrication of the hybrid films using the techniques described are treated separately in sections 3.4.2.1 and 3.4.2.2.

- **METHOD 3:** METHOD 3 was determined after METHOD 1 and 2 were developed and tested. More specifically, the introduction of a third method was necessary in order to overcome the issue associated with the coverage of the PNIPAAm disks by the PHEMA, which was observed in the layers realized by using METHOD 2. The new fabrication scheme started with the preparation of the PNIPAAm components first (same as METHOD 2). After the disks were formed, a horseshoe-shaped silicone spacer was positioned on the PVC, so that it could surround the PNIPAAm. Then, a polytetrafluoroethylene (PTFE) component was assembled to the moulding system using clamps, to ensure that the PNIPAAm regions were compressed to about 10% of their initial thickness. The PHEMA polymerizing solution was then injected in the gap between the PVC and PTFE components in order to fill the free volume between the PVC substrate and PFTE lid, determined by the PDMS mould. The fabrication protocol is depicted in Figure 3.15. The choice of the use of PTFE instead of aluminum will be clarified in the next section.

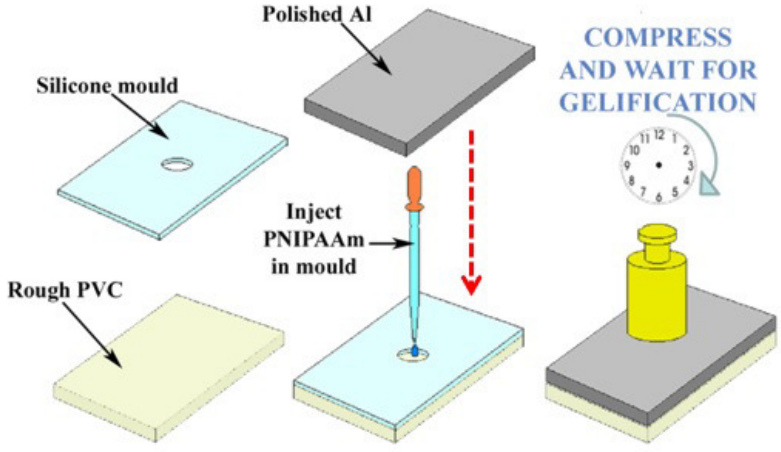


(a) (b) (c)

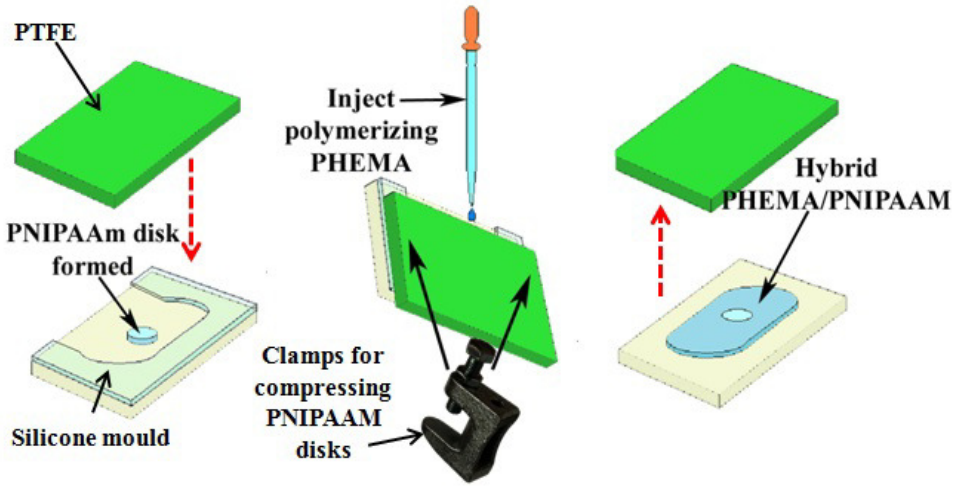


**Figure 3.15.** Method 3 for hybrid films fabrication based on the ICM technique. a) PDMS mould is positioned over rough PVC plate. b) PNIPAAm polymerizing mixture is injected in the hollow circular region of the mould and the system is closed with the polished aluminum lid. c) Compression is promoted by putting a weight over the system until gelification of PNIPAAm is reached. d) The system is disassembled and the PNIPAAm thin disk is formed but only partially cross-linked. A horseshoe-shaped silicone mould is then placed on the PVC. e) The PNIPAAm disks are compressed by the PTFE component using a system of clamps and the PHEMA solution is injected into the gap between the substrate and lid; the thickness is determined by the silicone spacer. f) Compression is once more promoted until PNIPAAm and PHEMA are completely cross-linked. f) After the polymerization and cross-linking of the PHEMA, the hybrid PHEMA/PNIPAAm film is recovered on the PVC when the system is disassembled.

This technique has all the advantages of METHOD 1 and 2 (use of materials and minimal equipment, simplicity), but, as a plus, it can avoid the overmoulding of the PHEMA on the PNIPAAm regions, depending on the appropriate positioning and configuration of the clamps to compress the rigid components.

### 3.4.2.1. Investigation of Method 1

The main problem of METHOD 1 was identified to be the slow polymerization of the PNIPAAm component, resulting in hybrid films lacking or partially missing the PNIPAAm component, due to diffusion of the polymerizing liquid within the porous punched PHEMA mould. Problems connected with evaporation of ethanol could also have affected the process if the aluminum lid was not immediately positioned after injection. In order to overcome these issues, gelification tests of the PNIPAAm hydrogels using different APS amounts were carried out starting from the standard mixture recipe. Furthermore, gelification tests on standard PHEMA solutions were also done to monitor the viscosity evolution of the mixture. Once the reaction mixtures' viscosity is controlled over time for both hydrogels, it is possible to set an appropriate time schedule to inject the liquids in the moulds for hybrid PHEMA/PNIPAAm films fabrication, avoiding diffusion phenomena to interfere. The essential requirements on the materials' properties for the fabrication protocol are:

- PHEMA solution should be viscous enough not be easily dispersed or subjected to massive leakages underneath the silicone mould when compressed by the lid.
- Immediately after gelification takes place, the partially cross-linked PHEMA film should be hole-punched and PNIPAAm should be injected; PHEMA punching should occur in a reasonable time (15 min to 10 min) according to the 60 min required for the reaction to complete to its 98%.
- PNIPAAm solution should be viscous enough and sufficiently near to the gelification point when injected in the hole-punched PHEMA frame so that it won't have time to diffuse into the forming elastic hydrogel matrix and hence not be dispersed; PNIPAAm gelification should occur in a reasonable time (30 min to 90 min) to avoid cumbersome time differences between the reactions of the two hydrogels.
- PNIPAAm component of the hybrid film should be transparent and homogeneous to preserve the thermo-responsivity properties previously characterized.

Gelification tests are reported below.

*1) PHEMA gelification tests*

Samples realized for these tests were 0.5 g of PHEMA hydrogel; reagents were mixed in a 5 ml glass test tube according to 3.2.2. After the APS solution was added, the test tube was shaken by hand for 30 seconds/1 minute to promote the mixing of the chemicals. The initiator solution was injected at time 'zero' and the viscosity of the solution was then monitored by continuously tilting the test tube and observing changes in the rapidity of the flow. A hand-shaking of the mixture was carried out from time to time. The viscosity values attributed to the mixture are referred to a qualitative observation of the behavior of the liquid in time. The semi-quantitative test showed the results depicted in Figure 3.16.

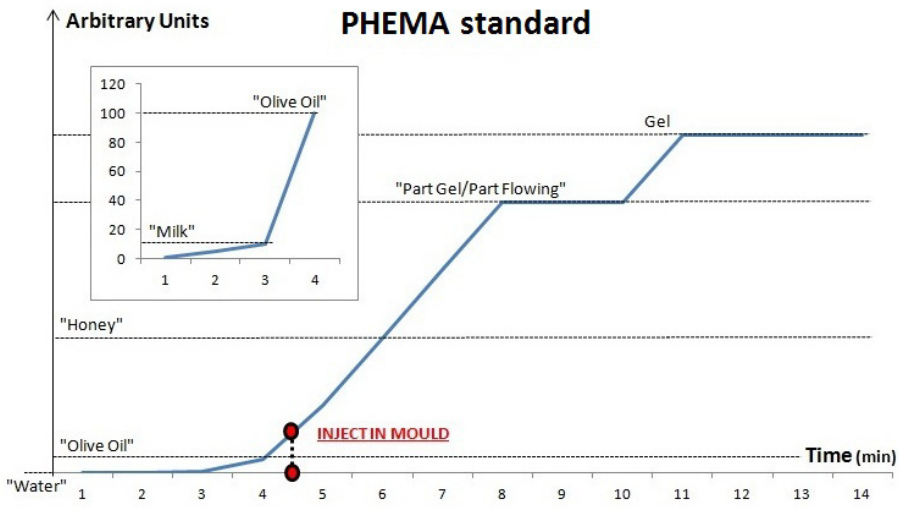


**Figure 3.16.** Gelification tests carried out for PHEMA hydrogels. Value of viscosity based on a qualitative observation of the polymerizing liquid flow when the tube was tilted in time.

The proper timing for injecting the solution in the silicone mould and then compressing the forming gel appeared to be between 4 and 5 minutes; the appropriate time to open the molding system and to hole-punch the partially cross-linked film was between 11 and 15 minutes.

*2) PNIPAAm gelification tests*

Using the standard reaction protocol, samples of 0.5 g were produced; gelification takes place in 4 hours and the viscosity changes happened only within the last half an hour prior to solidification, usually in the very last few minutes. This timing was cumbersome for the manufacturing of the film, since it was much larger than the time required for PHEMA to reach the gel state. First tests for increasing the reaction speed in ethanol were carried out by adding APS solution into the mixture reported above varying the initiator amount (larger APS solution volumes, keeping the 10% ratio): 40 µl (4x), 60 µl (6x), 80 µl (8x). The reason why larger volumes of the 10% APS solutions rather than higher concentration (e.g. 20%) were chosen is because an excessive APS concentration could cause a rapid polymerization reaction leading to a heterogeneous hydrogel or to a 'local' polymerization of the drop of initiator solution in the mixture. The test's protocol is identical to the one reported for PHEMA. However, it was observed that when using the 4x, 6x and 8x APS amounts, if the tube was not shaken in the first 30 second/ 1 minute, an almost instant gelification of the APS drop within the solution occurred, typically concentrated at the tube's bottom. Results are reported in Figure 3.17.

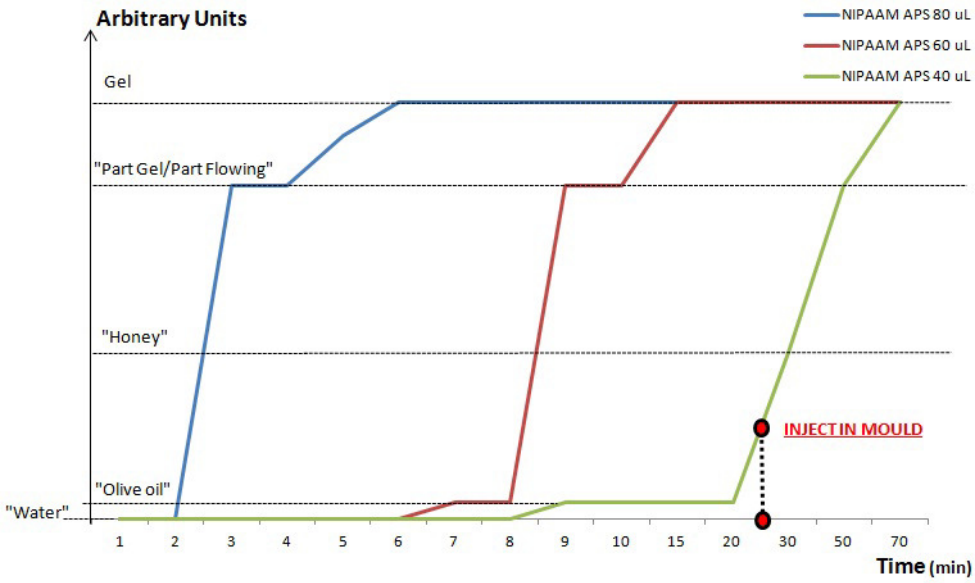


**Figure 3.17.** Gelification tests carried out for PNIPAAm hydrogels having different initiator solution amount at the same concentration (10%). Value of viscosity are referring to a qualitative observation on the polymerizing liquid flow when the tube was tilted in time

The sample obtained by adding 40 µl of APS solution (PNIPAAm4x) was the best candidate since:

- The resulting gel appeared with a good transparency/homogeneity, while the others were opaque.
- The hydrogel exhibited mechanical properties similar to standard PNIPAAm at a qualitative level.
- The time required for viscosity changes and gelification to happen were comparable to PHEMA

These reaction kinetic tests for PNIPAAm hydrogels were cross-checked by experiments carried out in Fondazione Filarete by the research group in Milan (F. Martello, March 2012) by employing a different apparatus consisting of a syringe containing the polymerizing solution under a constant weight and by measuring the time in which a fixed number of mixture drops were collected. The experimental set up is shown in Figure 3.18.

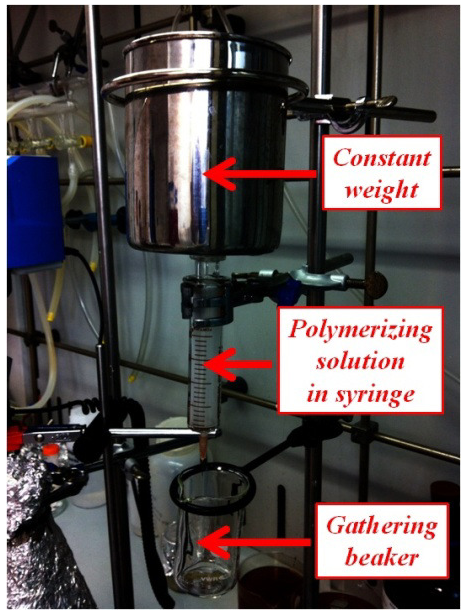


**Figure 3.18.** Experimental apparatus employed in Fondazion Filarete to cross-check the PNIPAAm gelification tests.

According to the results obtained, the most reasonable time schedule for the hybrid film realization was therefore set as the following:

| 0 min | 10 min | 15 min | 30 min | 40 min |
|---|---|---|---|---|
| Inject APS in PNIPAAm4x | Inject APS In PHEMA | Inject PHEMA in mould | Open mould and punch PHEMA | Inject PNIPAAm4x in punched PHEMA |

The equipment employed for realizing the hybrid films with METHOD 1 was the same as for the ICM apparatus described in 3.4. Before injecting the PHEMA polymerizing solution according to the time schedule previously reported, PVC substrates were treated with sandpaper of different grits as previously defined and thoroughly washed in de-ionized water. Silicone moulds were soaked in acetone for an hour and then left to dry in air for half an hour. Before assembling the polished aluminum lids to the molding system, they were washed with hand soap and water, then repeatedly washed with 2-propanol. Compression was promoted by using weights between 2 and 5 kg according to the fabrication process developed for pure PNIPAAm layers. Tests were carried out producing four hybrid structures each time, each one bearing three circular PNIPAAm films within the PHEMA frame. It was

noted that a critical time of about 15 minutes after APS injection was required to discriminate whether the PHEMA stuck to the Al lid ($t < 15$ minutes) or onto the PVC ($t > 15$ minutes). To avoid issues deriving from this critical time, 5 mm thick PTFE slabs were used instead and in this way it was possible to obtain PHEMA layers on PVC with a percentage of success of 100%. Furthermore, the insulating properties of this plastic were able to keep the forming hydrogel soft and wet enough to be easily processed by a hole-punch tool, unlike the ones produced by using Al as a lid, which showed dry and stiff properties that rendered it difficult to be processed late. Measured thickness values were within 20% of the silicone spacer thickness, according to the values of the compression weights employed and based on previous results obtained on pure PNIPAAm layers. Brass-based hollow spacers could also be used as an outer frame embracing the PDMS moulds to help keep the error of the thickness lower.

After PHEMA films were obtained, hand-made plastic hole-punches with diameters of 1, 3 and 5 mm were used to cut the material using present in an aluminum alignment stencil mask, placed directly in contact with the layer. The mask was fabricated by milling. Regions of a reasonable circularity aligned along the film could be obtained; diameters of 3 mm were the minimum size obtainable for such features. Sharper tools could be used in future, though the risk of ruining the PVC substrates would rise considerably. The hole-punching step took about 3 to 5 minutes per film on average. A time of 5 to 10 minutes before gelification takes place was the ideal moment at which the PNIPAAm mixture injection should take place, according to the data from the gelification tests. Diffusion of the PNIPAAm mixture within the porous frame was thought to commence almost instantly and then tended to carry on steadily at a rate which could be approximately estimated as about 1 to 3 μl/minute. Within this frame, a volume of PNIPAAm polymerizing mixture which is at least between 1.5 and 2 times higher than the circular region of injection is required. Furthermore, a rather viscous phase of the mixture would help considerably to slow the diffusion process down. In the employed protocol, compression molding of the thermo-responsive element is always carried out without the presence of the PDMS spacers previously used; polished Al or PTFE are still used as lids and compressive weights are also the same. Once the PHEMA frame is punched as previously depicted, PNIPAAm4x is injected, with the volumetric amount of about 1.5 to 2 times the volume required to completely fill the mould. Instead of immediately closing the

molding system with the lid, diffusion of the polymerizing solution is monitored for the next 5 to 10 minutes after the injection and supplementary amounts are provided from time to time to re-establish the complete filling of the circular structures. After a critical time (around 10 minutes) diffusion effects are strongly damped, probably due to different phenomena occurring:

- The formed circular rings (1 to 2 mm size) of diffused PNIPAAm solution around the punched region may constitute an obstacle for further liquid to penetrate in the porous mould; in other words there is a threshold for PHEMA to locally absorb liquid in its matrix.
- By the time liquid is continuously injected, polymerization of the solution takes place and the pure macromolecular component of the mixture may not easily penetrate into the PHEMA anymore.
- The reaction happening in contact with oxygen and nitrogen in the air may play a role for hastening the process.

After the critical time, compression is applied to the forming film and the hybrid layer is recovered on PVC after leaving the system to polymerize overnight. Results obtained with the assisted ICM technique appeard to look promising, since the hydrogels exhibit the expected characteristics in terms of transparency, shape and bonding strength (see swelling tests in section 3.3.3.). An optical microscope image of a hybrid PHEMA/PNIPAAm film is reported in Figure 3.19; it shows the presence of a defined line over which the two hydrogel layers present a slight difference in thickness.

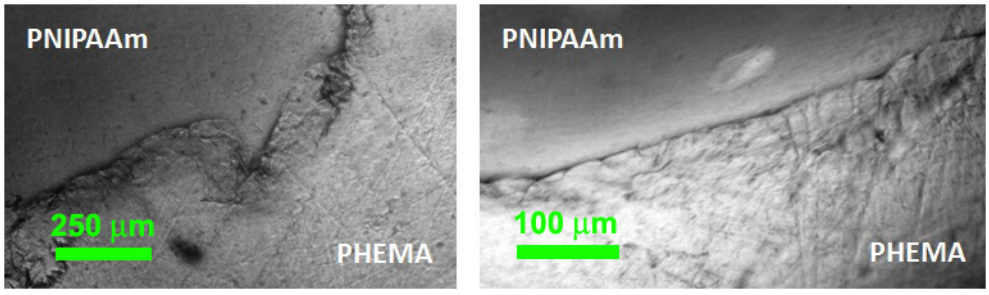


(a) (b)

**Figure 3.19.** Microscope images of the PHEMA/PNIPAAm interface region. a) Low magnification. b) Higher magnification.

Changing the viscosity of the polymerizing PNIPAAm solution is another way of overcoming the diffusion problems; since the rate of the PNIPAAm cross-linking reaction is not affected by viscosity changes or by reaction condition (e.g. temperature), the introduction of co-monomers in the original mixture could be an effective alternative. In this sense, three possibilities should be considered for further work in future:

- The introduction of polyethylene glycol diacrylate (PEGDA) co-monomers; these particular kind of molecular chains have the effect of enhancing the PNIPAAm viscosity without interfering with its final thermo-responsive properties (separate tests on thermo-responsivity on PNIPAAm/PEGDA random co-polymers should be carried out anyway).
- The introduction of small amounts of HEMA; though the thermo-responsive features of the final hydrogel could be slightly affected, the synthesis conditions of this material have already been set and could be further developed by gradually diminishing the HEMA amount until the proper trade-off between the high viscosity of the polymerizing liquid and final thermo-responsive properties is reached.
- The introduction of NIPAAm oligomers; by increasing the molecular units of the chains, viscosity will be increased. If NIPAAm oligomers are separately prepared and then added to the cross-linking mixture, the final PNIPAAm solution will have an increased viscosity. Tests on the synthesis of NIPAAm olygomers and their effects on the final mixture's gelification should be carried out separately.

Within this scheme of possible solutions, some initial tests on PHEPAAm10 (NIPAAM : HEMA = 90 : 10 mol/mol) copolymer as the thermo-responsive component for producing the hybrid films were carried out (total number of samples tested was 5). Despite PNIPAAm4x, the intrinsic viscosity of the solution is rather high due to the presence of HEMA. The percentage of success using PHEPAAm compared to PNIPAAm was > 80% in this case and the diffusion of the thermo-responsive polymerizing mixture through PHEMA was not significant.

### 3.4.2.2. Investigation of Method 2

As a brief reminder, METHOD 2 can be summarized as:

1) PNIPAAm small thin disks fabricated by injection/compression moulding
2) PHEMA frame injection around formed disks
3) Detach PHEMA/PNIPAAm hybrid film

As previously mentioned, thin PNIPAAm based small disk fabrication was already applied, giving an average success rate of about 50% of the total attempts per array. For the production of hybrid hydrogel layers, silicone moulds employed were 3.5 x 8 $cm^2$ rectangular PDMS sheets (100 and 200 μm thick) over which 3 x 6 arrays of hole-punched circles were present; the diameters of the circles was 4 mm and the center to center distance between the circles was 10 mm. Experiments were conducted using rough PVC as substrates and PTFE and polished Al as lids. Weights employed and the treatment of PVC and lids were the same as used in METHOD 1. PNIPAAm4x was prepared as highlighted before and the solution was injected in the arrays by a micropipette 5 to 10 minutes after the initiator was added. When the polymerizing solution was injected in the circular form, liquid leakages occurred underneath the silicone spacer; supplementary liquid was then further added until the edge of the silicone was completely filled by the PNIPAAm solution. A time between 90 and 120 minutes was found to be appropriate for the PNIPAAm4x disks to be formed in the moulding system. Considering that the polymerization reaction would be completed in a time of about 10 hours, the time established for opening the mould and injecting PHEMA was reasonable since the reaction was between the gelification point and 50% of its completion. A percentage of success of about 50% was still achieved; around half of the circles of the arrays were filled with the shaped gel, while others showed significant imperfections (holes due to bubble formation or a half-moon shape due to partial leakage), others showed no gel was formed in the circular moulds. The main problem regarding this fabrication step leading to such a low reproducibility was probably due to the relatively small edge to edge distance between the holes of the array that prevented a proper sealing between the mould and the PVC, thus leading to massive leakages of the polymerizing solution. Since the liquid volume per circle

involved was rather small (few µl, as defined by the circles in the mould), the effect of leakage often resulted in total or partial dispersion. To try to solve this issue, two strategies were defined and actuated at the same time:

- Operating on the mould: larger edge to edge distances between the circles were realized in new silicone moulds to increase the surface available for adhesion between the substrate and the spacer.
  A silicon based grease layer (vacuum type) could also be spread on the spacer to improve the sealing. Furthermore, increasing the weight of compression could help avoid leakages that would happen later after the injection.

- Operating on the material: an increased viscosity would help the polymerizing solution not to leak underneath the silicone. Viscosity could be increased according to the observations drawn when discussing METHOD 1 (use of PEGDA, HEMA co-monomers or PNIPAAm oligomers in the polymerizing solution)

The first tests in which the presence of a silicone grease was introduced to enhance the sealing gave very good results; over 80% of the circles in the array were successfully realized per sample. Furthermore, in order to avoid any issue connected with discrepancies in thickness between the spacers employed for fabricating the two hydrogels, silicone spacers (one for disk formation, one for PHEMA molding) were cut from the same PDMS sheet by means of a $CO_2$ laser. Tests using the laser fabricated silicone spacers and the sealing grease gave encouraging results showing good repeatability of the process in fabricating the disks (percentage of success around 100%). However, 2 mm diameter PNIPAAm4x disks had the natural tendency of detaching from the PVC substrates at their borders after about 30 min, which was similar to the previous results. Another possible solution for improving the technique in future was considered in relation to the PHEMA injections; a sacrificial layer could be fabricated over the disks in order to cap their top surface and avoid PHEMA overmoulding; compression moulding would then be applied with a lid provided with through-holes corresponding to the disk locations. Problems with alignment and tolerances for the fitting of the lid would probably arise. PVA as the sacrificial material could be a good

choice, since it dissolves in pure water, which does not significantly influence the hybrid films detachment.

### 3.4.2.2. Investigation of Method 3

As a brief reminder, METHOD 3 can be summarized as:

1) PNIPAAm small thin disk fabrication by injection/compression moulding
2) Compression of the disks using a PTFE lid clamped to the PVC
3) PHEMA frame injection around formed disks
4) Detach PHEMA/PNIPAAm hybrid film

An array of 10 disks (5 mm diameter) were produced for each PVC plate by standard ICM. Silicone grease was used to fix the PDMS on the PVC, minimizing leakages of the PNIPAAm4x solution. Different spacer thicknesses were employed (100, 200 and 300 μm), but the thickest ones were predominantly employed because they could confer high robustness to the solid films. The silicone moulds were configured and hole-punched so that the edge to edge distance between the PNIPAAm regions was 15 mm. In this way, 90% of the disks present in the array were formed for each fabrication. Furthermore, 5 mm PVC plates were used to guarantee good mechanical stability of the final clamped assembly for PHEMA injection. After moulding of the thermo-responsive components, diethyl ether was used to remove grease traces left on the substrate and to properly clean the PVC where leakage of the solution occurred. The PTFE plate was then assembled to compress the disks according to the time schedule reported in 3.4.2.2 (METHOD 2). Different configurations of the clamping system were tested in order to identify the optimum position to avoid leakages when the PHEMA solution was vertically injected in the gap between PTFE and PVC. A picture of the most effective clamping system, which was then employed for high-throughput fabrication of the hybrid layers, is shown in Figure 3.20.

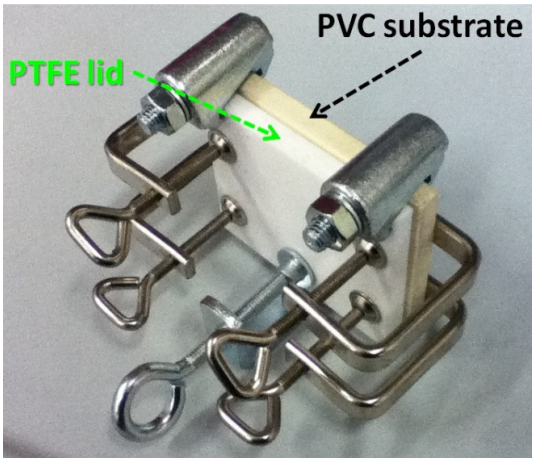


**Figure 3.20.** Moulding apparatus assembled with clamps for PHEMA injection after PNIPAAm disks are formed. The clamping configuration employed ensured no leakages of the polymerizing solution.

This moulding system could be replaced by a screw based apparatus similar to the one presented in 3.3.2 (Figure 3.9) in order to have better control on the compression and a simpler assembly solution. The introduction of a pair of aluminium jigs to homogeneously compress the PTFE could also be a suitable route to improve the fabrication performance. Hollow brass based spacers were employed as outer frames surrounding the PDMS moulds the same way as depicted in 3.3.2. to provide a defined compression strain of the PNIPAAm disks. After the PHEMA was formed, the apparatus was disassembled and the film remained attached on the PVC plate. A percentage between 80% and 90% of the disks were surrounded by PHEMA and the inter-penetrating network formed at the interface between the hydrogels appeared to be more homogeneous than in the previous cases; the thickness difference observed between the two hydrogels was seen to be less pronounced than the one obtained with METHOD 1 and 2. All the information related to synthesis procedures and timing as well as the correct choice of the material played a crucial role for the development of METHOD 3, which at this stage is still considered the best choice for a reliable and reproducible hybrid layer fabrication. However, if the compression of the PTFE over the PNIPAAm disks was not accurately set by operating the clamps to promote a uniform pressure, the samples could either present a weak bonding at the interface between the hydrogels or a partial coverage of the PNIPAAm disks by PHEMA; in this sense, the

introduction of a screw based system was necessary to optimize the manufacturing protocol. Alternative methods that were preliminary tested to produce hybrid PHEMA/PNIPAAm layers and that constitute a promising opportunity for further development are discussed in Appendix A at the end of the thesis, while in the next section the experimental work on the detachment and swelling of the obtained hybrid films is reported.

### 3.4.3 Hybrid film detachment and swelling

Detachment of the films produced with both METHOD 1 and METHOD 2 was first carried out on the best samples obtained with these techniques as preliminary tests. The results obtained for these families of specimens were then applied to detach all the samples produced with METHOD 3. Since the detachment protocol of the hydrogel layers was previously determined for pure PNIPAAm films only, before testing the behavior of the hybrid PHEMA/PNIPAAm samples, pure PHEMA layers were also individually tested in different organic solvents and aqueous solution in order to observe their detachment. The results obtained are reported in Table 3.4.

| SOLVENT | Observation |
|---|---|
| **Acetone** | Film detachment happens in 30 min, but PVC is ruined |
| **DCM** | It breaks PVC |
| **Ethanol (EtOH)** | It breaks the film |
| **EtOH 50% in $H_2O$** | It breaks the film |
| **$H_2O$** | Film is removable only after applying mechanically assistance |
| **EtOH 20% in $H_2O$** | Good for films with area inferior to 1 $cm^2$ |
| **EtOH 10% in $H_2O$** | Film doesn't detach |
| **Methanol** | Good for films with area inferior to 1 $cm^2$ |
| **Isopropanol** | Film doesn't detach |

**Table 3.4.** Detachment tests on pure PHEMA layers; tests were carried out by soaking the films stuck to PVC in different solvents and solutions. Their behavior was monitored for 2 hours.

According to the results obtained, the most promising candidates to be tested were ethanol aqueous mixtures (concentration between 10% and 50%) and acetone aqueous solutions at different concentrations. The first attempt to detach a PHEMA/PNIPAAm4x hybrid film was carried out using a 30% ethanol aqueous solution; this value was chosen because it represents an intermediate between the extreme points of the alcohol's concentration range to be tested. The sample was soaked in a crystallizer containing 200 ml of the solution. As can be seen in Figure 3.21, there was a large difference between the two polymers' swelling degree in this mixture; in a time of 10 minutes, the PNIPAAm swelled much more than the PHEMA did, leading to a curvature of the thermo-responsive component with respect to the hydrogel frame it was attached to, which remained flat instead. This result also suggested that the two hydrogels were chemically attached, since PNIPAAm disks did not completely detach, but remained stuck to the PHEMA at their borders.

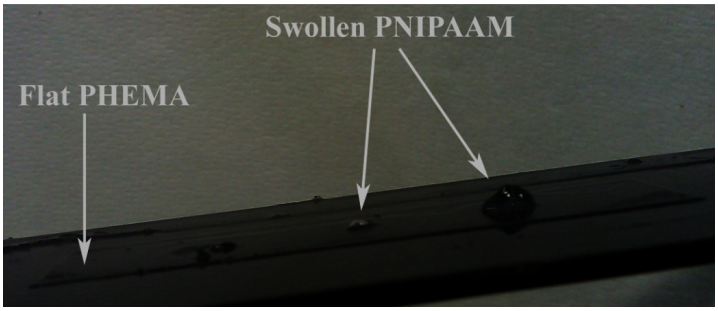


**Figure 3.21.** Detachment tests on PHEMA/PNIPAAm4x using a 30% ethanol aqueous solution. PNIPAAm based regions swelled more with respect to the PHEMA based ones, resulting in a partial detachment only.

Other tests on hybrid PHEMA/PNIPAAm4x films were carried out using acetone/water solution. Since PVC is strongly attacked by pure acetone, low concentrations of the organic solvents were required. In the first tests, a 25% acetone concentration was used; the sample was soaked in a crystallizer containing 200 ml of solution. Wrinkles occurred to the PHEMA frame in the first half an hour and partial detachment was observed. After 40 minutes, the behavior of the hybrid film was found to be reversed compared to the ethanol/water case; the PNIPAAm remained attached to the PVC, while the PHEMA was almost completely

detached from the substrate. To help the PNIPAAm swell, ethanol was gradually added to the mixture until an aqueous solution containing 15% of acetone and 35% of ethanol was reached. After one hour, no complete detachment was observed and the PHEMA frame looked partially damaged, showing diffused thin lacerations. Mechanical removal of the hybrid film was then promoted to save the film, but the sample was highly damaged already.
No further tests could be carried out on pure PHEMA/PNIPAAm based hybrid layers fabricated with the 'traditional' METHOD 1, because of lack of samples; further tests could only be carried out on PHEMA/PHEPAAm10. As a basis for these detachment tests, separate experiments were carried out on pure PHEPAAm10. It was observed that pure PHEPAAm10 layers could be easily detached from PVC substrates by soaking the sample in ethanol; this behavior was compatible with the one of pure PNIPAAm thin films, since NIPAAm constitutes almost 90% of the molar mass of the hydrogel. Based on this, a hybrid PHEMA/PHEPAAm10 film is expected to behave similarly to the PHEMA/PNIPAAm samples previously tested. The approach for detaching these samples, was to start with a higher concentration of acetone in the solution, in order to promote a more aggressive treatment of the thermo-responsive component. To not ruin the PVC substrate, a 40% acetone aqueous solution was chosen. In 30 minutes, PHEMA was almost completely detached, while PHEPAAm10 took 45 minutes to start reacting to the treatment; after 1 hour of soaking the samples, complete detachment of the hybrid layer was observed. Little damage, such as thin lacerations or cracks, showed up to be present in the films, mainly at the PHEMA/PHEPAAm10 interface. These were probably due both to the slight swelling difference of the two hydrogels which was still occurring and to the mechanical stress induced by the manipulation of the detached layers when they were transferred from the crystallizer to the sample box. It was also observed that smaller films (PHEMA circles of 10 mm diameter) were much easier to detach compared to the larger layers defined by the mould previously shown. A picture of the hybrid PHEMA/PHEPAAm10 layers soaked in pure ethanol after being detached and hole-punched into 10 mm disks is reported below.

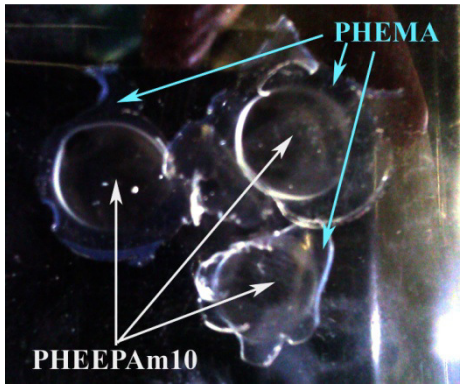


**Figure 3.22.** Hybrid PHEMA/PHEPAAm films soaked in pure ethanol.

Swelling tests were then carried out by adopting the usual routine established for PNIPAAm or PHEMA based hydrogels. The films were hydrated by gradually adding water to ethanol every 2 hours, in amounts equal to the 30% of the total volume of the solution, until pure water was reached. This procedure caused a massive bending of the PHEPAAm10, due to its higher swelling degree in respect to PHEMA, at least at the rate of hydration imposed by the standard routine. A picture of the curved hybrid films in pure water is reported in Figure 3.23, showing what can be described as a 'jellyfish' effect, due to the particular form the films assumed.

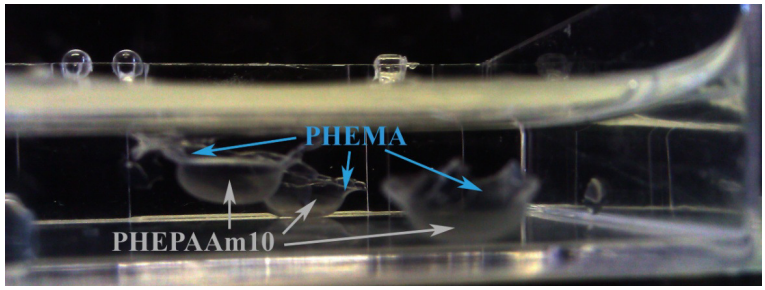


**Figure 3.23.** Hybrid PHEMA/PHEPAAm10 films hydrated in water. The curvature of the thermo-responsive part, absorbing more water than the PHEMA frame at the swelling rate imposed, gives rise to a jellyfish-like shape of the films.

To explore the reversibility of the process, the samples were then brought back to pure ethanol at the same rate and then the solvent was repeatedly rinsed. After one day a quasi-flat configuration was reached; a slight curvature was still present, probably due to the fact that some water was still embedded in the hydrogels. Further experiments both on the swelling rate and the dehydration process were carried out. More specifically, detachment tests using acetone aqueous solution containing a small percentage of ethanol (10 to 20% of the total mixture volume) were used and found to be applicable. For samples obtained with METHOD 2, the detachment protocol used was identical to that for the PHEMA/PHEPAAm10 samples fabricated using METHOD 1 i.e. by soaking the samples in a 40% acetone aqueous solution. The process was quite successful and effective, but some damages to the samples was present. Again, smaller samples were easier to be detached by the chemical treatment. After freestanding samples were obtained, they were soaked in the same solution employed for detachment and stored. No swelling tests were carried out. Since the amount of water contained in the 40% acetone solution is relatively high, a useful strategy for not damaging the samples could be a gradual reduction of the amount of acetone until pure water is reached at a rate of 10% every 2 hours. Figure 3.24 shows a detached sample positioned over a PVC support.

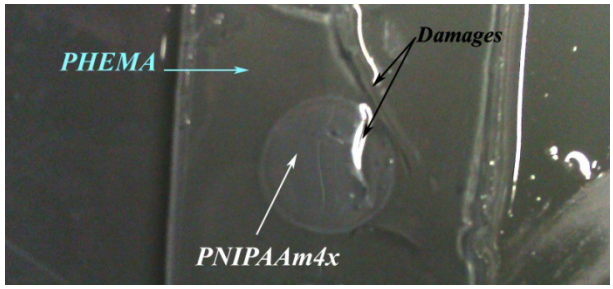


**Figure 3.24.** Hybrid PHEMA/PNIPAAm4x films produced with METHOD 2 detached from PVC substrate using a 40% acetone aqueous solution.

To reveal the presence of an overlaid PHEMA film on the disks, the surface of PNIPAAm was scratched until the upper extra layer was removed, as shown in Figure 3.25.

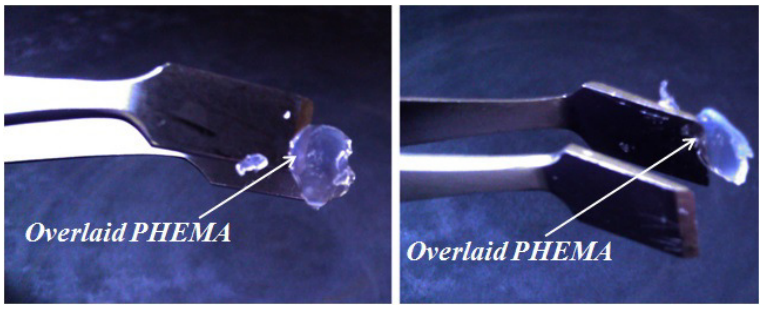


**Figure 3.25.** Circular parts of the hybrid PHEMA/PNIPAAm4x films produced with METHOD 2 detached from PVC substrate using a 40% aqueous solution. On both sides of the layer, the presence of an overlaid PHEMA film is shown.

According to the detachment and swelling results obtained on the hybrid hydrogels produced with METHOD 1 and METHOD 2, an appropriate strategy for removing the layers realized with METHOD 3 was established. A 40% acetone aqueous solution, with 10% of ethanol, was employed. Detachment of the layers happened in two hours, which is a reasonable time based on the relatively wide surface area of the moulded array. After the hybrid films were available as freestanding, they were soaked in pure MilliQ water directly; every 1 hour, the water was changed in order to wash out all the unreacted monomers. After ten hours of being in the water bath, a curvature of the PNIPAAm disk was present, but it appeared to be less pronounced than the PHEEPAm10 one shown in Figure 19. This is probably due to the slow swelling rate of the PNIPAAm4x and its lower swelling ratio. It was then observed that the stress generated by the different swelling behavior of PHEMA and PNIPAAm4x did not damage or tear the layer, indicating that the bonding between the hydrogels was sufficiently strong to prevent breaking at their interface. Furthermore, as it will be shown in CHAPTER 5 and 6, the presence of a slightly curved PNIPAAm component in the hybrid film did not affect either the thermo-responsiveness of the layers or their integration in the sorter prototype.

## References


[1] Brynata J S Cuya J L Haucha K D and Ratner B D 2007 *Biomaterials* **28** 2978-2986

[2] Rzaev Z M O Dincer S and Piskin E 2007 *Prog. Polym. Sci.* **32** 534-595

[3] Hirokawa Y and Tanaka T 1984 *J. Chem. Phys.* **81** 6379-6380

[4] Otake K Inomata H Konno M and Saito S 1990 *Macromolecules* **23** 283-289

[5] Zhang X Z Yang Y Y Chung T S and Ma K X 2001 *Langmuir* **17** 6094-6099

[6] Suzuki A Yoshikawa A and Bai G 1999 *J. Chem. Phys* **111** 360-367

[7] Jiang Y Li B Wu Y and Zhu M 2010 *Journal of Macromolecular Science Part B: Physics* **49** 843-853

[8] Gherke S H Palasis M and Akhtar S K 1992 *Polymer International* **29** 29-36

[9] Zhang X Z and Chu C C J 2003 *Mat. Chem* **13** 2457-2464

[10] Rzaev Z M O Dincer S and Piskin E 2007 *Prog. Polym. Sci.* **32** 534-595

[11] Zhang X Z and Zhuo R X 2002 *Materials Letters* **52** 5-9

[12] Lu H Zhang S and Knauss W G 1997 *Polymer Engineering and Science* **37** 1053-1064

[13] Aranaz I Carrasco S Tardajos M Elvira C Reinecke H Lopez D and Gallardo A 2011 Polym. Chem 2 709-713

[14] Yildiz B IsikB and Kis M 2001 *Polymer* **42** 2521-2529

[15] Jung Y P Kim J H Lee D S and Kim Y H 2007 *Journal of Applied Polymer Science* **104** 2484-2489

[16] Mabilleu G Stancu I C Honoré T Legeay G Cincu C Basle M F and Chappard D 2006 *J Biomed Mater Res A* **77** 35-42

[17] Rosellini E Cristallini C Guerra G Barban N and Giusti P 2010 *Biomed. Mater.* **5** 1-9

[18] Demirelli K Coskun m and Kaya E 2001 *Polymer Degradation and Stability* **72** 75-80

[19] http://www.wolframalpha.com/ , created by Wolframalpha Inc. , 100 Trade Center Drive, Champaign, IL, 61820, USA,217-398-0700 | 1-800-WOLFRAM

[20] Lee J N Jiang X Ryan D and Whitesides G M 2004 *Langmuir* **20** 11684-11691

# 4. Excimer laser micromachining of PNIPAAm based thin films

This chapter considers the excimer laser micropatterning of the PNIPAAm based layers prepared by the ICM technique explained in Chapter 3. After an introductory section that explains the specific purpose and requirement to properly develop the machining process, as well as to briefly depict the phenomena involved in the process, a description of the equipment will be provided and then results for the manufacturing of the hydrogel will be discussed.

## 4.1. Introduction: general and experimental approach

As explained in Chapter 1, the objective of the laser fabrication process is to achieve micrometer diameter sized through-holes in the PNIPAAm layers, when they are still attached to the flat substrates that they are moulded on. A schematic diagram of the excimer laser set up is shown in Figure 4.1.

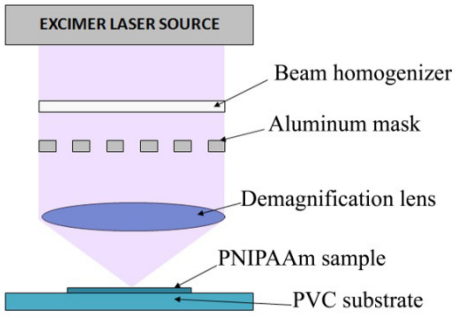


**Figure 4.1.** Schematization of the excimer laser set up employed for machining PNIPAAm based thin films.

In principle, the laser beam is focused normally on the top flat surface of the sample and is characterized by a depth of focus, along which the intensity of the light delivered should be spatially uniform; this feature depends on the beam homogenizer present in the optical

system. If the sample is positioned at a distance which is beyond the depth of focus, the machined structures will reflect non-uniformity in the laser beam energy profile. When the beam is incident on the sample, UV photo-ablation causes the direct breaking of the chemical bonds of the material, resulting in the removal of a thin layer for each single pulse; this etch rate, for polymeric materials in general, can vary from hundreds of nanometers to a few microns per pulse [1]. The theoretical explanation of the ablation mechanism induced by the pulses is still under debate, since the fundamental physico-chemical phenomena involved are rather complex and are defined by multiple factors, such as pure photochemical and photothermal etching, non-linear absorption and radiation screening effects [2]. However, for what concerns biological tissue and soft polymers, the removal of material layers using this technique has found a wide range of applications and the lack of damage on the areas surrounding the machined features constitute one of the main advantages of the process [3, 4]. Taking into account the relatively high complexity in modeling the radiation/polymer interaction, obtaining reliable predictions on the machined features characteristics can be time consuming, especially when new materials are processed. The realization of micro-holes on PNIPAAm based layers (that would operate as sorting capillaries in the target cells-on-chip) was therefore achieved on an empirical basis by controlling the excimer laser machining parameters, such as fluence and number of shots and monitoring the material behaviour in respect to the UV ablation mechanism.

The appropriate configuration and geometrical features of the created pattern should reflect the characteristics of a multiwell plate; in this sense, the diameter of the desired structures were initially sized to the typical length scale of the most representative cell lines. Cell diameters vary depending on the particular nature of the cell, which exhibits, during its evolution state, a specific phenotype when cultured; a range therefore between 10 and 30 microns was initially considered to be acceptable for realizing the micro-though-holes as a first attempt [5]. To be confident with the dimensions of the cell lines available for the first sorting tests (Chapter 6), three different cell types were taken into account and a characteristic length representative of the cell dimensions (cellular diameter) were measured by acquiring optical inverted microscope images and processing them with calibrated measuring software after three days of culture on traditional Petri dishes. Without going into

details referring to the characteristics of the specific cell lines used, the results obtained on MCDK, PC12 and MG63 cells are reported in Table 4.1.

| Cell line | Average (µm) | ST DEV | n | Max | Min |
|---|---|---|---|---|---|
| **MDCK** | 20,40 | 2,16 | 55,00 | 25,89 | 16,51 |
| **MG63** | 24,05 | 2,33 | 43,00 | 29,32 | 18,49 |
| **PC12** | 16,03 | 2,14 | 39,00 | 21,74 | 12,14 |

**Table 4.1.** Measured average cellular diameter and standard deviation (ST DEV) for MDCK, MG63 and PC12 cells. Total number of cells measured (n) and maximum (Max) and minimum (Min) values observed are also indicated.

The optical setup of the excimer laser employed a fixed linear demagnification of the pattern present on the projection mask at a ratio of 10 : 1. Taking into account this feature, three aluminum masks (250 µm thickness) were designed to carry a 9 x 9 array of through-holes, having diameters of 100, 200 and 300 µm and a centre to centre distance of 1 mm; the entrance hole diameters which could be obtained on the dry hydrogel surface were therefore expected be 10, 20 and 30 µm respectively. Masks were fabricated by etching at DEK international (U.K.). The layout of the projection mask design and optical microscope images of the realized mask are shown in Figure 4.2.

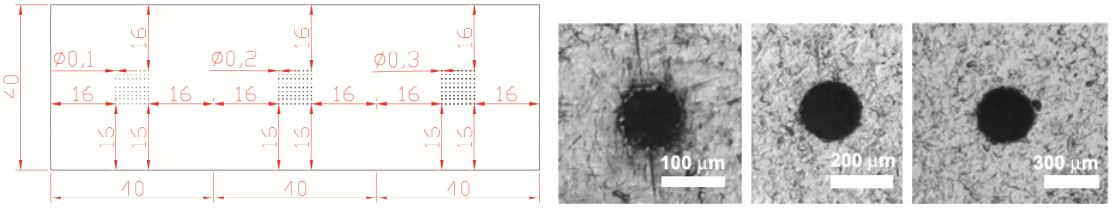


(a) (b) (c) (d)

**Figure 4.2.** Aluminum projection masks employed for PNIPAAm excimer laser machining. a) CAD design of the component. b) Optical microscope image of a 100 µm diameter hole. c) Optical microscope image of a 200 µm diameter hole. d) Optical microscope image of a 300 µm diameter hole.

Masks were then cut into squares with a surface area of 4x4 $cm^2$ and used individually in each patterning process. Hydrogel thickness available (50 to 300 μm) and mask projection characteristics would allow the formation of micro-holes with different aspect ratio (entrance hole diameter to depth), varying from 3 : 5 to 1 : 30. The metrology characterization section will consider how the machined structures change their size after film hydration is promoted, according to the swelling ratio previously determined. As will be shown later in the section dedicated to the analysis of the laser machining of the hybrid PHEMA/PNIPAAm hydrogel layers, a fourth aluminum mask having a single hole of 1.5 mm diameter was also introduced in order to be able to fabricate only one micro-capillary in the thermo-responsive core of the layers. In this case, the mask thickness was 2 mm and the hole was manufactured by mechanical drilling.

### 4.1.1. UV/Vis spectrophotometry on PNIPAAm samples

UV/Vis absorption spectra acquisition was carried out on PNIPAAm solutions and thin films to provide quantitative information on the material absorption in the UV range of interest for the laser ablation process. The spectrophotometer employed was a UV/Vis JASCO-l7850. At first, 500 mg of NIPAAm were dissolved in 1 ml of ethanol and its UV/Vis absorption spectrum was recorded in a wavelength range from 190 nm to 900 nm. Since no absorption was observed in the region beyond 290 nm, all other spectra acquisition was limited from 190 nm to 300 nm. The spectrum of the NIPAAm solution showed a wide saturation region going from 220 nm to 275 nm, indicating a strong absorption band as shown in Figure 4.3. The absorbance A is calculated as:

$$Abs = - \log (I/I_0) \qquad [4.1]$$

where $I_0$ is the initial light intensity delivered on the sample and I is the detected transmitted intensity.

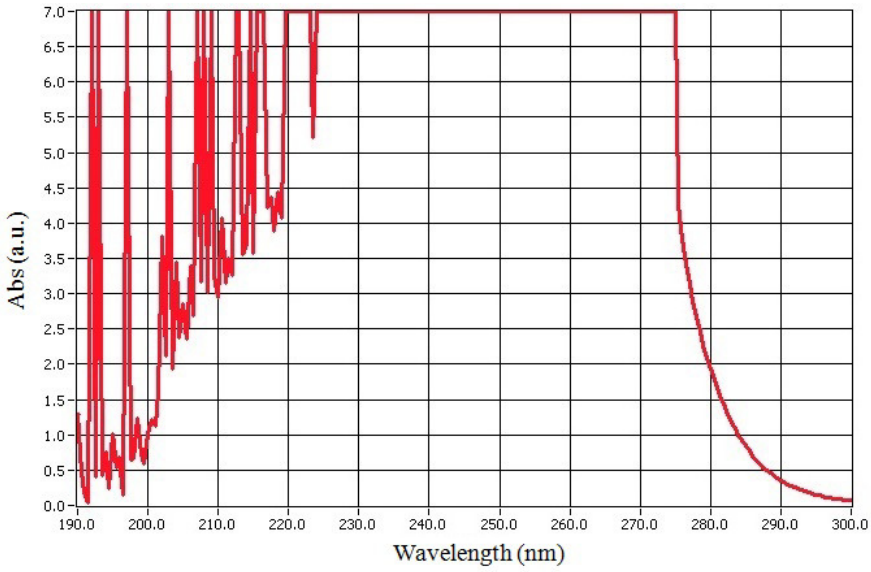


**Figure 4.3.** UV/Vis absorption spectrum of a 1 ml ethanol solution in which 500 mg of NIPAAm was dissolved; a wide saturation region in the transmitted intensity profile indicates a strong absorption of the mixture in the range going from 220 nm to 275 nm.

To provide a clear spectrum profile without saturation effects, the initial solution was diluted in ethanol so that a sample having 50 mg of NIPAAm could be analyzed. The absorption was dramatically reduced as expected, but a broad maximum could be identified at 225 nm and the overall intensity graph resembled the features of the one previously acquired, as shown in Figure 4.4.

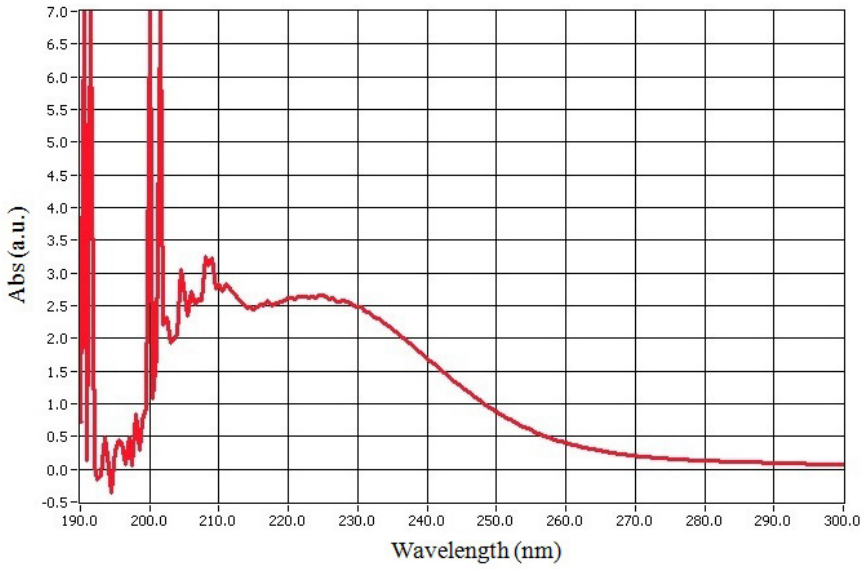


**Figure 4.4.** UV/Vis absorption spectrum of a 1 ml ethanol solution in which 50 mg of NIPAAm was dissolved; a maximum intensity peak is present at 225 nm.

In order to evaluate the possible contributions of the cross-linker to the spectrum and to have a more realistic picture of the polymeric material behavior to UV light absorption in its solid state, a 100 µm thick layer of PNIPAAm was prepared using the standard recipe discussed in 3.2.1 and analyzed using the spectrophotometer. This sample represented a good model for all the specimens that underwent laser machining in terms of relative amounts of the reagents involved and it was moulded starting from a solution having 200 mg and 18.5 mg of monomer and cross-linker respectively. During measurements, the sample was supported by a hollow rectangular aluminium frame. The absorption spectrum is reported in Figure 4.5.

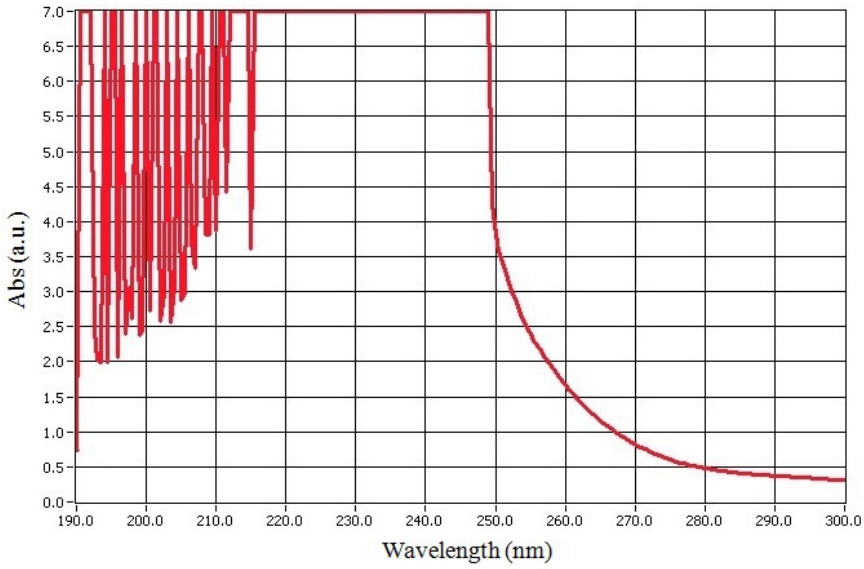


**Figure 4.5.** UV/Vis absorption spectrum of a 100 µm thick PNIPAAm layer (prepared using 200 mg of NIPAAm, 18.5 mg of EGDMA).

A saturation band going from 215 nm to 250 nm was still present, while a dramatic drop from 250 nm to 275 nm was observed; the spectrum profile is in accordance with the one previously measured for NIPAAm. Based on these results, it is reasonable to expect a high efficiency of material ablation when using an excimer laser system for patterning the layers.

## 4.2. Equipment and experimental set up

The KrF excimer laser employed is a computer-controlled LPX 100i Exitech series 7000, Lambda Physik, with a UV pulsed beam at 248 nm wavelength. A picture of the system (S7000) and its two compartments is illustrated in Figure 4.6.

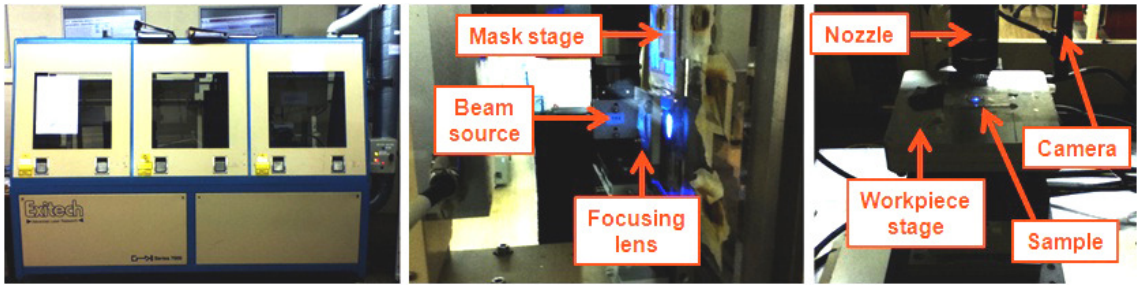


(a) (b) (c)

**Figure 4.6.** Pictures of: a) The S7000 system. b) Mask and laser source compartment. c) Sample compartment.

The S7000 can be controlled both in external and internal mode; this means that it can be run both directly by the user and by running custom-designed programs in a remote mode. The initial output energy of the pulse can be set to values ranging from 0 to 250 mJ, while the repetition rate varies from 0 to 40 Hz. The duration of the pulse is 20 ns. An energy attenuator allows control over the laser beam reducing the amount of energy delivered per pulse according to its position . Projection masks are located on a software controlled stage and their relative coordinates are identified by moving the stage with respect to the focusing lens. For locating the machining point of the samples two different approaches are available. If there are no specific locations over the sample surface area over which the pattern must be projected, it is sufficient to run the laser internally and move the workpiece stage using the jog function via software until the beam reaches one of the substrate's edges; the actual coordinates of the sample's regions to be machined could then be obtained by properly increasing the values previously identified. The second approach relies on the use of the alignment camera; the specific region of interest is imaged by the instrument and its relative coordinates are then determined. The fixed distance between the nozzle and the camera

allows the appropriate position in which the sample must be moved for the machining to be calculated. Once masks and sample coordinates are known, the first operation to carry out is the focusing of the beam on the workpiece. For this purpose, an empirical method is used. The focal distance of the laser (*f*) is fixed by the optics of the system. The sample is machined in a fixed number of regions chosen by the user and each machining is carried out by moving the stage with a fixed step rate along the zenithal direction, so that the workpiece's top surface moves through *f*. Once the process is over, samples are then observed using an optical microscope to evaluate the quality of the ablation in terms of how the shape of the geometrical features of the pattern are reproduced and defined on the specimen's surface. Once the mask and sample coordinates and the focal position are determined, machining of the hydrogels can be carried out.

### 4.2.1. Energy measurements

Energy per pulse was measured at the focal plane by employing a pyroelectric sensor (J-50MUV-248, Coherent) connected with a digital energy meter (LabMax-TOP, Coherent). The projection mask employed was the one with 200 μm diameter holes. The energy range available was explored by fixing the initial energy output of the laser (250, 225, 200, 175, 150 and 125 mJ were the values used) and by changing the position of the beam attenuator, expressed in arbitrary units, from 0.8 (low attenuation) to 0.3 (high attenuation), with a step of 0.1. For each measure, the number of shots delivered was 100 and a statistical calculation of the energy values over the total number of pulses was automatically carried out by the instrument, giving the minimum and maximum energy per pulse ($E_{min}$ and $E_{max}$ respectively), the average energy <E> and its relative standard deviation $\sigma_E$. The repetition rate was kept constant at 5 Hz. Overall measurement accuracy could be calculated according to the sensor's calibration and manufacturer's specifications as 5%. A graph of the energy per pulse delivered over all the holes in the array and measured at the focal plane against the beam attenuator position is shown in Figure 4.7.

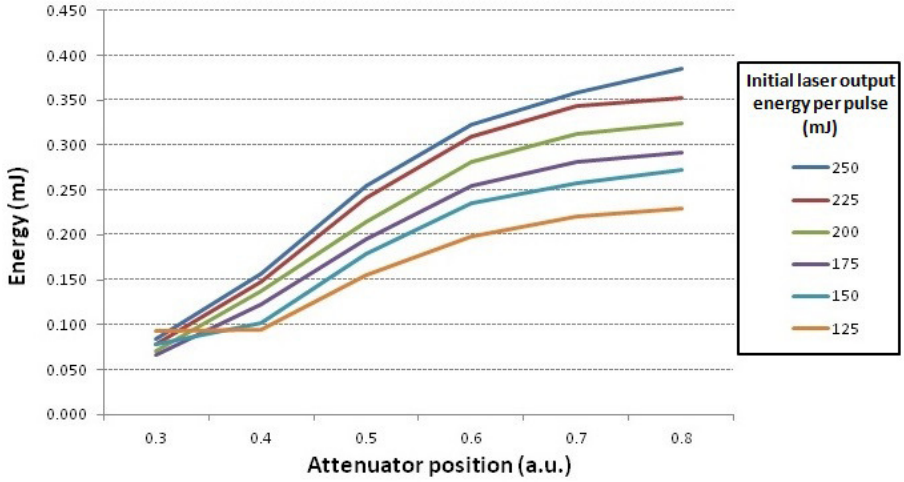


**Figure 4.7.** Energy per pulse measured at the image plane against attenuator position for the 200 µm diameter holes projection mask.

The first observation is that massive energy losses take place along the optical physical path of the beam from the source to the image plane, predominantly due to the mask blocking some of the beam. It is also noticeable that for low initial energy values, the standard deviation (data not shown) is relatively high for each of the attenuator positions explored. Furthermore, a 'low light' regime was found to be established for energy values of 150 and 125 mJ with the attenuator position fixed at 0.3; in this situation, the electrical discharge required for generating low initial energy outputs is below the threshold of the voltage required for the laser to operate properly (15 kV). For the same reason, initial energy values below 125 mJ could not be tested due to the laser instability. Considering the array geometry and the demagnification optic, the beam spot size at the focal plane is defined by 81 holes of 20 µm diameter, with a total surface area equal to $\Sigma = 25.4 \times 10^{-5}$ cm$^2$. Defining the laser fluence as $F = \langle E \rangle / \Sigma$, the range explored in terms of fluence goes from 1.5 J/cm$^2$ (initial energy of 250 mJ, attenuator position of 0.8) to 0.26 J/cm$^2$ (initial energy of 175 mJ, attenuator position of 0.3), according to the measurements. The same protocol was then applied for evaluating the energy at the focal plane using the 300 µm diameter mask. According to the wider area through which the laser light passes, all the obtained <E> values were found to be higher than the ones obtained in the previous case. More specifically, the

maximum value available using this stencil mask, corresponding to an initial energy of 250 mJ and an attenuator position of 0.8, was 0.58 mJ, while the minimum, corresponding to an initial energy of 175 mJ and an attenuator position of 0.3, is 0.11 mJ. As expected, when using these values to calculate the maximum and minimum fluences achievable, the results were found to be comparable with the ones previously obtained for the 200 μm diameter hole mask.

## 4.3. PNIPAAm based layer micropatterning

The thickness of the PNIPAAm based thin films machined ranged from 50 to 300 μm. First tests to explore the features of the fabrication process with respect to the material were carried out on pure PNIPAAm films of 100 and 200 μm thickness, attached on PVC substrates, using the mask with 200 μm diameter holes. Before the machining took place, both the thickness of the films and PVC plates were measured using calipers in over 20 regions and a variation not greater than 10 μm was found across the samples. Since the depth of focus of the S7000 is 80 μm, these relatively low differences in the thickness values of the hydrogel films would not affect the machining process in terms of reproducibility of the pattern present on the masks. The focal position was determined by firing the laser at the hydrogels with 10 shots per mark over eight different regions located in the film, moving the sample stage elevator 0.1 mm in each step. Then, each mark on the samples was analyzed by optical microscopy to identify which one correctly reproduced the in-focus pattern. This procedure sometimes required further refinement around a specific stage position to improve the quality of the pattern produced; in this case the stage elevator was moved 50 μm for each mark. Using an energy value of 150 mJ as the initial laser with the attenuator position set at 0.3 did not produce any result on the films; this suggested that an increase of the laser output energy to 250 mJ was required in order to overcome the ablation threshold of PNIPAAm. The attenuator position was then set at 0.8, while the repetition rate was fixed at 5 Hz. When patterning of the samples was carried out, six regions were machined, each corresponding to a different number of shots. This parameter did not appeared to have a significant influence

on the amount of debris generated around the machined structures, but did cause a tapering effect, as will be explained later. Optical microscope images of a patterned 200 μm thick PNIPAAm layer are shown in Figure 4.8.

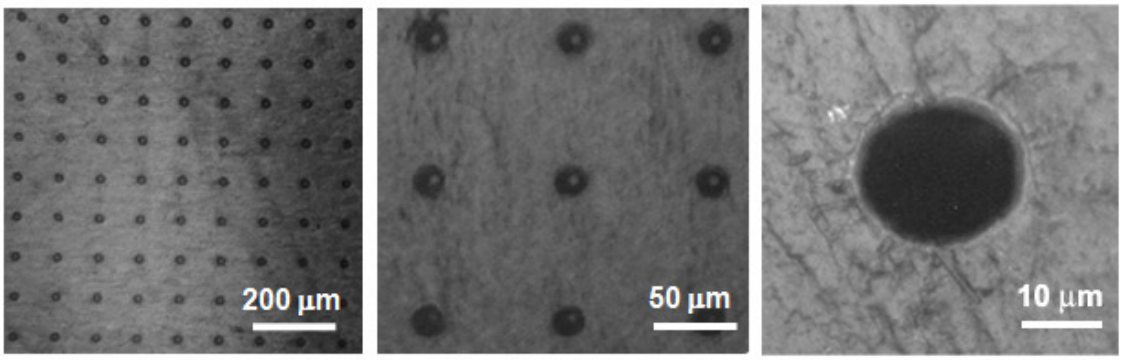


(a) (b) (c)

**Figure 4.8.** Optical microscope images of a laser machined PNIPAAm film (200 μm thick, number of shots 1600). a) Low magnification . b) Higher magnification image. c) View of a single aperture.

The identification of the parameters to achieve well resolved features without damaging the sample and keeping a minimum amount of debris around the structures was carried out. A scanning electron microscope (SEM) image of a hole machined using 1600 shots is shown in Figure 4.9.

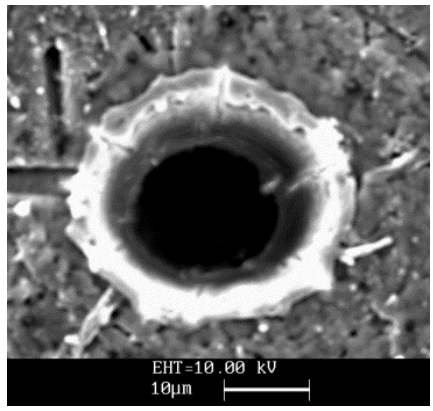


**Figure 4.9.** SEM image of a hole from an array machined in a 200 μm thick PNIPAAm film (number of shots 1600).

As mentioned before, the influence of the number of shots on the debris around the structures was negligible. In Figure 4.10, optical microscope images of holes machined with different numbers of pulses delivered over the same film (200 μm thick) are shown.

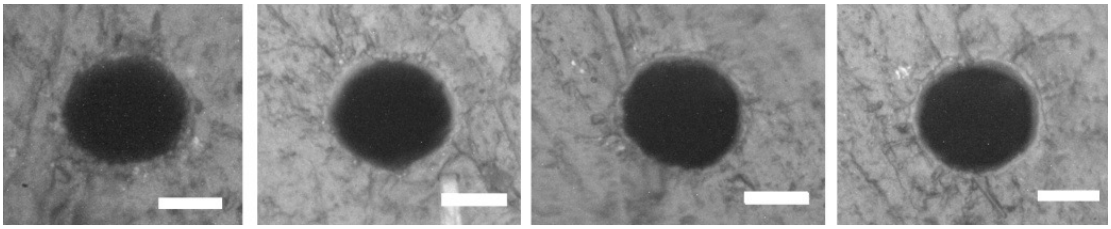

(a) (b) (c) (d)

**Figure 4.10.** Machined holes present on a PNIPAAm 200 μm thick layer produced using different number of shots (N). a) N = 100. b) N = 400. c) N = 800. d) N = 1000. Scale bar in each picture is 10 μm.

Once the machining conditions for obtaining well resolved micro-holes was fixed (initial energy ouput equal to 250 mJ, attenuator position as 0.8 and repetition rate fixed at 5 Hz), PNIPAAm of different film thickness (50, 75 and 300 μm) and PNIPAAm/MMA and PNIPAAm/HEMA co-polymers as well as PNIPAAm with a double cross-linker were also laser processed. The fabrication features in terms of resolution and debris deposition on all the hydrogels produced showed similar characteristics to those identified for pure PNIPAAm layers. Figure 4.11 shows microscope images of the patterns obtained on the different families of materials and also 50 and 75 μm pure PNIPAAm machined layers.

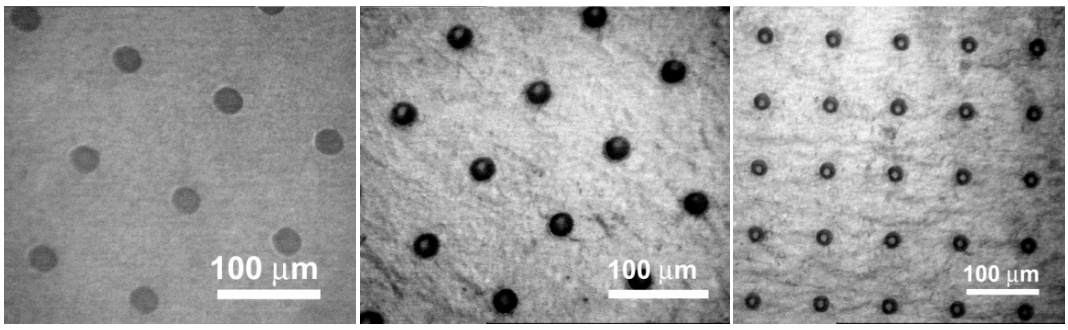


(a) (b) (c)

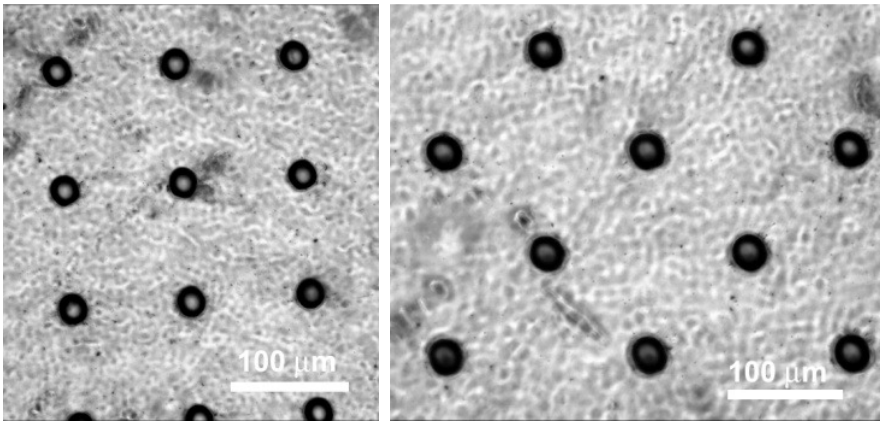


(d) (e)

**Figure 4.11.** Microscope images of the micropatterned hydrogels (N=400). a) PNIPAAm/PHEMA co-polymer (NIPAAm : HEMA = 90 : 10 mol/mol) 200 µm thick. b) PNIPAAm/MMA co-polymer (NIPAAm : MMA = 90 : 10 mol/mol) 100 µm thick. c) PNIPAAm with double EGDMA amount (100 µm thick). d) PNIPAAm 50 µm thick. e) PNIPAAm 75 µm thick.

Laser machining of PNIPAAm layers (100 and 200 µm thick) was also carried out employing masks with 100 and 300 µm diameter holes and using the same set of operation parameters. For the larger diameter holes, no effects due to the different projection features were revealed in the machined films; the structures were well defined and resolved as in the case of the 200 µm diameter mask holes (Figure 4.12 – a). On the other hand, 100 µm diameter projected holes were slightly less resolved (Figure 4.12 – b and c); this is probably due to the mask itself, which did not have perfectly circular etched edges, as shown before in Figure 4.2. For this reason, the metrology characterization that will be the core of the next section was focused on the micro-holes obtained with the 200 and 300 µm diameter hole projection masks and will also consider the 1.5 mm diameter one for the hybrid layers.

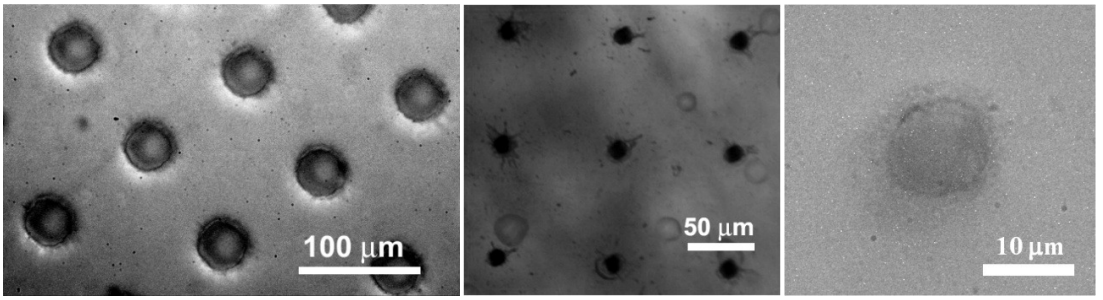


(a) (b) (c)

**Figure 4.12.** PNIPAAm layers machined using different projection mask. a) 300 μm diameter holes projected on a 150 μm thick PNIPAAm film. b) and c) 100 μm diameter holes projected on a 100 μm thick PNIPAAm layer.

## 4.3.1. PNIPAAm ablation threshold

Laser output energy values ranging between 125 and 250 mJ were explored in order to evaluate the actual ablation threshold of PNIPAAm. For this purpose, excimer laser machining of a 100 μm layer was initially carried out in 6 different regions of the sample by varying the initial energy values over all the range available. The projection mask employed was the one with 200 μm diameter holes. The attenuator position was fixed at 0.8, while the initial laser output energy values were 250, 225, 200, 175, 150 and 125 mJ, that, according to the energy measurements reported in 4.2.1., corresponded to energy values per shot at the focal plane of 0.385, 0.353, 0.324, 0.292, 0.272 and 0.229 mJ respectively. In this energy range, no difference in the pattern formation was observed and all the circular features produced were equivalent. For this reason, a refinement of the measurement was carried out; 5 different regions of the layer were machined, employing a fixed value of the initial energy output equal to 125 mJ while varying the attenuator position from 0.7 to 0.3, corresponding to maximum and minimum energy per pulse at the focal plane of 0.221 and 0.080 mJ respectively. The patterned features obtained for the different energy values are reported in Figure 4.13 and it clearly shows how the ablation starts to decline for energy values per pulse below 0.156 mJ (attenuator position of 0.5).

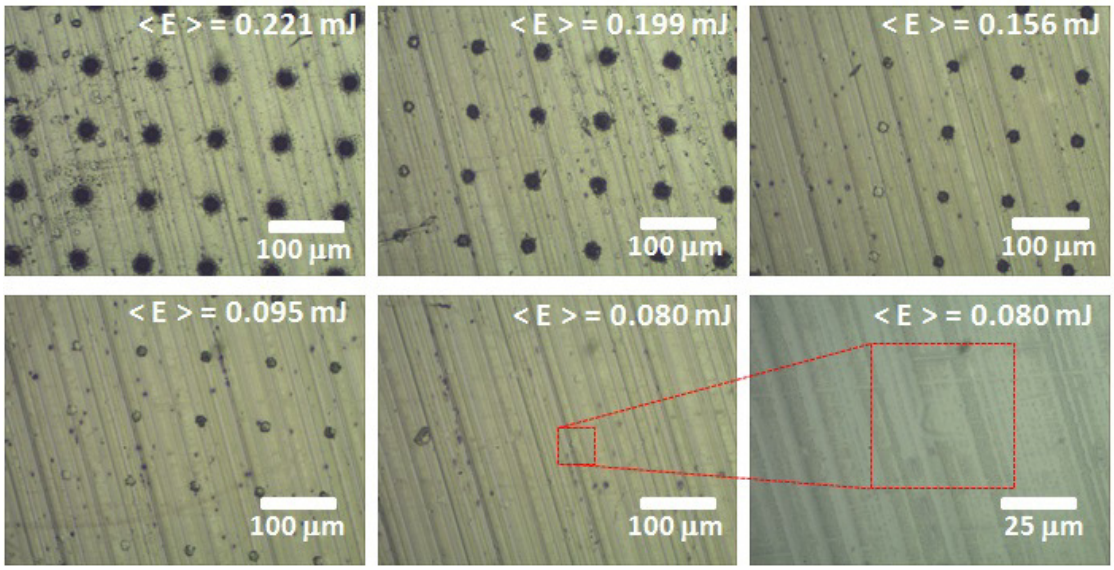


**Figure 4.13.** Optical microscope images of the pattern evolution for decreasing laser energy values. Marks start to disappear for mean energies <E> < 0.156 mJ and are completely abstent when <E> = 0.080 mJ.

As can clearly seen from the pictures, two effects dominate when approaching the ablation threshold: the first is that the Gaussian intensity profile of the beam, lead to higher intensity values at the centre of the pattern, which causes the lateral circular features to disappear first rather than the micro-structures located at the centre. Secondly, the shape of the holes through the whole pattern is also affected, so that the circularity is gradually lost, and the resulting dimension of single holes decrease significantly with lower energy values. Furthermore, as pointed out in 4.2.1., since the 'low light' regime was established in the laser pulse generator when the initial energy and attenuator position values were set at 125 mJ and 0.3 respectively, it was not possible to characterize the material behavior below this intrinsic instrumental limit. For this reason, it was possible to identify an ablation threshold range only rather than a single value; this range of values, in which the actual ablation threshold is located, was determined to be from 0.095 mJ to 0.080 mJ. This information was useful when laser machining of the PNIPAAm layers at low energies just above 0.095 mJ to investigate the effect this low energy regime could have on the tapering of the holes.

# 4.4. Hybrid PHEMA/PNIPAAm film micropatterning

The same machining protocol was applied to pattern hybrid PHEMA/PNIPAAm films; the projection masks employed were the ones with 200 and 300 µm diameter holes as well as the single 1.5 mm hole one. In order to facilitate the location and laser focusing on the thermo-responsive regions in the hybrid structure, hybrid films were moulded in systems with fixed geometry that were manufactured by $CO_2$ laser cutting of PDMS layers (50, 100 and 200 µm thick) and PVC substrates (2 mm thick) to obtain the required geometry shown in Figure 4.14.

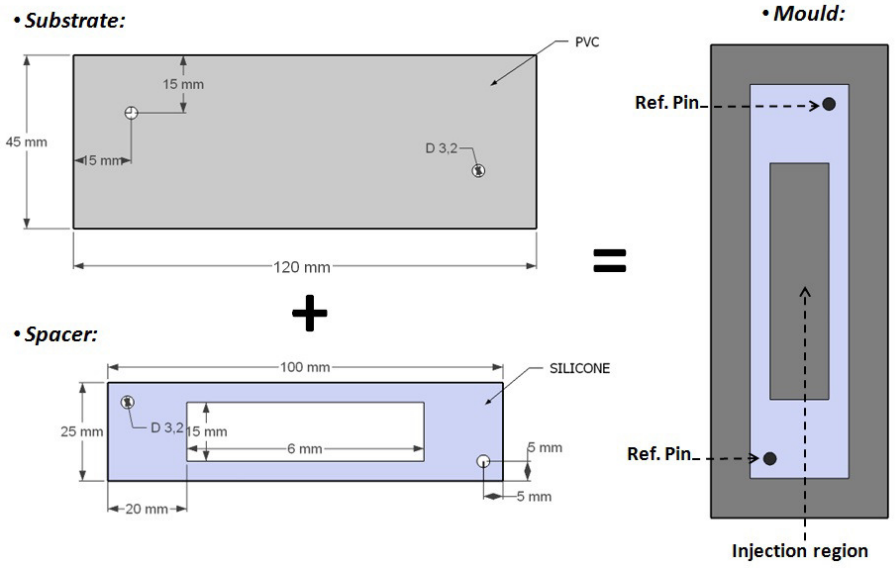


**Figure 4.14.** Geometrically controlled mould for preparing hybrid PHEMA/PNIPAAm layers to be easily aligned with the laser beam by moving the stage a fixed amount in X and Y.

Polished aluminium lids were fabricated by milling; the obtained slabs were easily positioned with respect to the other moulding components by aligning the through-holes drilled at their corners with the reference dowel pins fixed on the PVC. Two aluminium stencil masks were also realized in order to hole-punch the PHEMA in fixed positions to define both the circular region to inject PNIPAAm and the outer PHEMA final disks, as shown in Figure 4.15; the final hybrid films obtained after laser machining and detachment from the PVC were circles

with an outer diameter of 10 mm (defined by the PHEMA frame) and inner diameter of 1, 3 or 5 mm (defined by the thermo-responsive component).

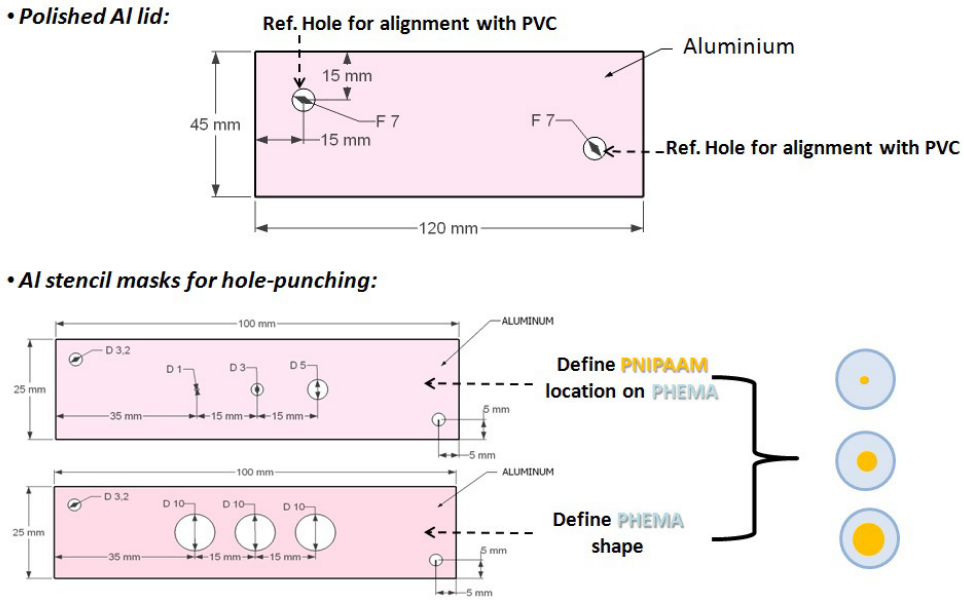


**Figure 4.15.** Aluminium component to be assembled with the geometrically controlled mould employed for realizing hybrid PHEMA/PNIPAAm.

The focusing process was carried out on the outer PHEMA frame using the same procedure previously described; results of the machining showed that, due to the relatively large depth of focus of the S7000, the slight height difference encountered between the thermo-responsive and the elastic component present on the samples realized with METHOD 1 did not affect the focus projection of the holes on the films. Figure 4.16 shows optical microscope images of the samples prepared both with METHOD 1 and METHOD 2.

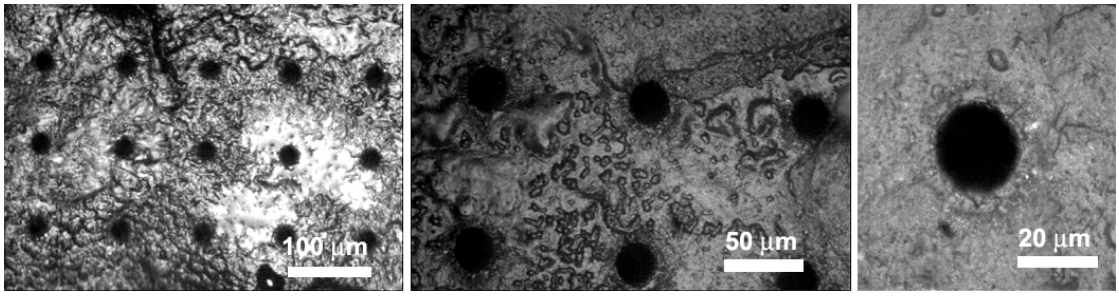


(a) (b) (c)

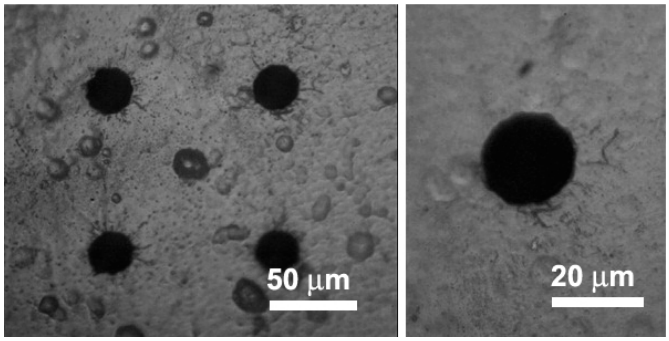


(d) (e)

**Figure 4.16.** Hybrid PHEMA/PNIPAAm films (100 μm thick) laser machined using the 200 μm diameter hole mask. a) Samples produced using METHOD 1, low magnification. b) Higher magnification. c) Hole details at higher magnification. d) Samples produced using METHOD 2, high magnification. e) Hole details at higher magnification.

The samples produced with METHOD 3 were laser machined using the 1.5 mm diameter hole mask only. As mentioned in the previous Chapter (3.4.2.), the layers moulded with this manufacturing protocol were the ones that were integrated and tested in the cell sorting prototype (Chapter 6), having a single through-hole with a relatively large entrance (150 μm when the hydrogel is dehydrated), and this significantly improved the optical quality of the system when both the film transition and the chip operation were observed and monitored at 37 °C using an inverted optical microscope. The focal position determination procedure was carried out the same way as it for the samples produced with METHOD 1 and METHOD 2, while the appropriate sample coordinates to project the laser light passing through the single hole at the center of the thermo-responsive core were always identified using the alignment camera. Figure 4.17 shows an optical microscope image of the 150 μm entrance hole machined in a 200 μm thick PHEMA/PNIPAAm hybrid layer manufactured using METHOD 3. The sharp edges and the good circular shape of the fabricated feature reflect the good quality of the machining, as previously reported.

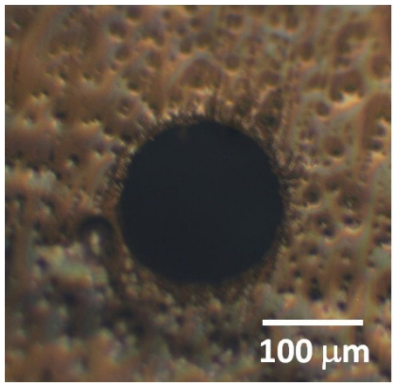


**Figure 4.17.** 150 μm diameter hole laser machined on a hybrid PHEMA/PNIPAAm hydrogel produced with METHOD 3.

## 4.5. Metrology characterization

Dry PNIPAAm machined layers attached to PVC substrates were first analyzed by optical microscope to evaluate the reliability of the process in terms of demagnification of the pattern at the sample image plane. Calibrated imaging process software was employed to measure the average diameter of the holes in the fabricated array; the calculations were initially carried out on all of holes present in the pattern using images obtained with the 20x objective lens and the standard deviation was evaluated using the set of measurements acquired. Depending on the projection mask employed, all the samples showed holes with a diameter error going from ±0.7 μm to ±1.2 μm of the expected values of 10, 20 and 30 μm. After this basic characterization was conducted, samples were detached from the PVC plates by soaking the hydrogels and substrates in ethanol, as indicated in Chapter 3. The standard protocol was then used for hydrating the films and, after complete swelling, the water of the hydration bath was changed three times a day for two days. The hydrated water-swollen samples were then analyzed both by optical inverted and confocal microscope to obtain information on the hole shape and size according to the different number of shots delivered to the layers. Results reported in subsections 4.5.1 and 4.5.2 relate to pure PNIPAAm layers, while the hybrid films characterization is reported in 4.5.3.

## 4.5.1. Optical inverted microscope characterization

After swelling, the holes' size uniformly changed according to the swelling ratio of 1.5 determined by the blot and weighing method described in 3.2.1. Furthermore, it was noticed that the swelling and rinsing procedure carried out on the hydrogels resulted in a substantial removal of some of the debris traces generated by the laser machining. Figure 4.18 shows inverted microscope images of a swollen 100 μm thick PNIPAAm film machined using the 200 μm diameter hole mask, at equilibrium in a MilliQ water bath at room temperature (number of shots employed in this case was 800). The entrance holes present an average diameter equal to 31.8 ± 1.6 μm, thus showing a diameter increase of about 50% with respect to the dry state.

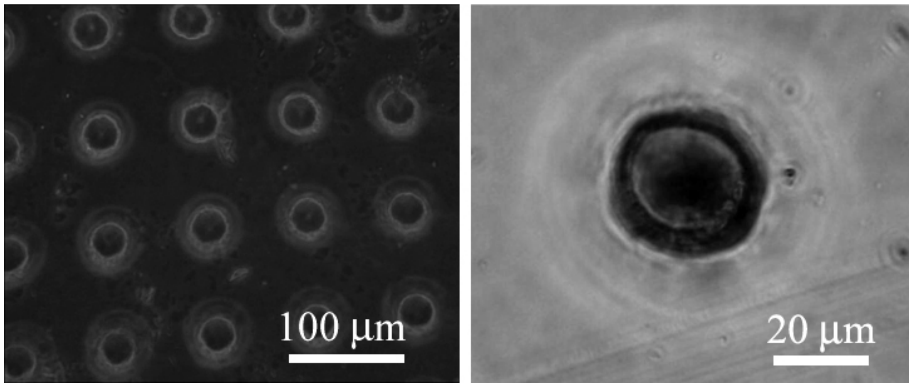


(a) (b)

**Figure 4.18.** Optical inverted microscope images of the entrance holes of a 100 μm thick PNIPAAm film, machined with the 200 μm diameter hole mask. a) Image acquired using the 20x objective lens. b) Image of a single hole.

To examine the influence on the tapering of the holes and on the exit hole diameter due to the different number of shots delivered, patterned films were observed using the inverted microscope, focusing on both the top and bottom surfaces of the transparent layer during the same observation (strategy 1). As an alternative, the sample was flipped over in the water bath to measure the holes on both surfaces (strategy 2). By measuring the exit hole diameter, a calculation of the taper angle and a 3D CAD reconstruction of the hole shape were carried

out. A metrology characterization using the first strategy on a 100 µm thick PNIPAAm sample machined with 1600 shots is reported in Figure 4.19.

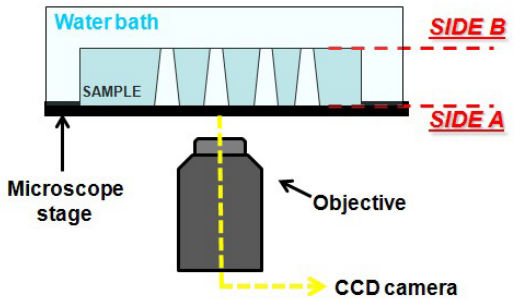


(a)

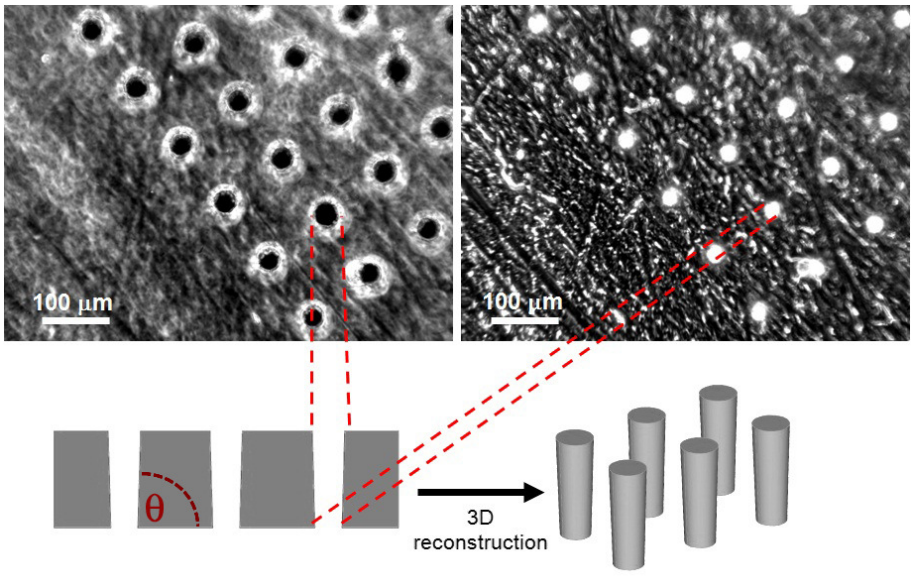


(b)

**Figure 4.19.** a) Experimental set up for inverted microscope characterization of water-swollen PNIPAAm samples. b) Microscope images acquired for SIDE A (left) and SIDE B (right). 2D and 3D reconstructions have also been provided.

The average entrance hole diameter was determined for the holes present in the image and found to be $\langle d_{ent} \rangle$ = (28.3±1.8 µm), while the exit hole diameter was $\langle d_{ext} \rangle$ = (17.2±1.5 µm); from the diameter values obtained and using error propagation, the taper angle θ was found to

be (83.7±0.7)°. A 250 µm thick sample machined using the 300 µm hole diameter mask and a number of shots equal to 3200 is reported in Figure 4.20; this sample was characterized using the second strategy (Figure 20 - a and b).

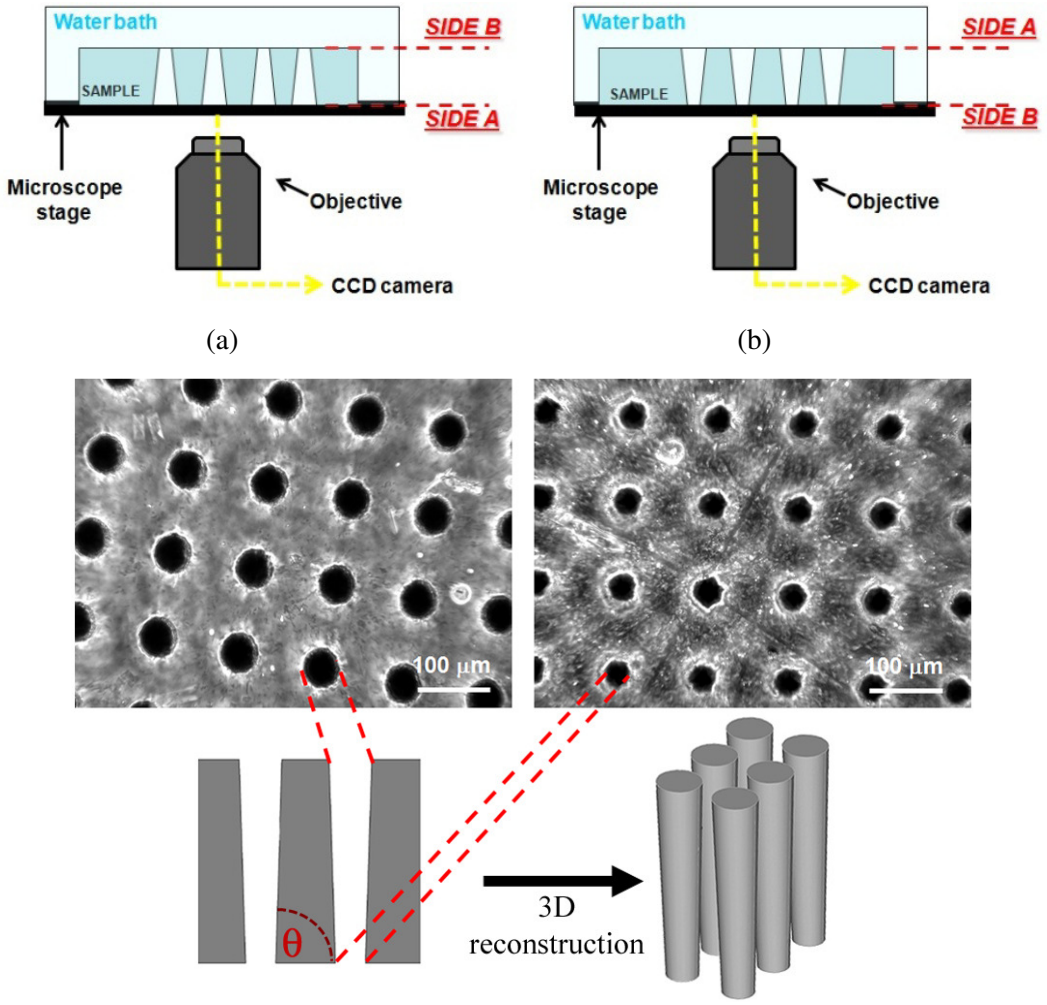


**Figure 4.20.** a) Experimental set up employed for measuring entrance and exit holes using an inverted microscope over a 250 µm thick PNIPAAm film machined with 3200 shots. b) Sample is flipped in the water bath and the opposite surface is directly imaged. c) Results obtained on SIDE A (left) and SIDE B (right); both images have the same magnification.. 2D and 3D reconstructions of the film have also been carried out.

Measurements on the entrance and exit holes gave $<d_{ent}>$ = (47.4±1.9 μm) and $<d_{ext}>$ = (35.6±2.0 μm) respectively, while the taper angle was (87.3±0.6) °. It can be seen from the images that when 3200 shots were used, traces of debris were slightly enhanced and spread over the sample surface; a similar behavior was not observed for samples obtained with N ≤ 2400. Another issue to be taken into account is the shape of the exit holes; their circular profile appears rather distorted with respect to the entrance holes and this can be due to the excessive relatively high number of shots delivered, that may cause overetching of the hydrogel. A similar defect appeared on a 250 μm sample machined with the same projection mask and 2400 shots; microscope images of entrance and exit holes of this sample are shown in Figure 4.21.

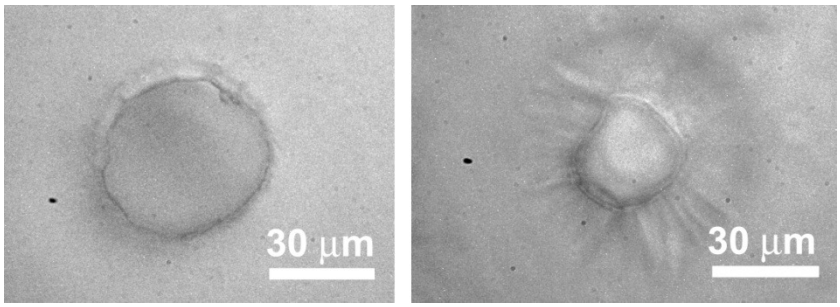


(a) (b)

**Figure 4.21.** Microscope images of a water-swollen 250 μm PNIPAAm film machined using the 300 μm diameter holes' projection mask, with N = 2400. a) Entrance hole. b) Exit hole.

In this case, $<d_{ent}>$ = (48.0±2.1 μm) and $<d_{ext}>$ = (27.5±1.6 μm) while the taper angle was (82.2±1.0)°. As expected, the number of shots had some influence over the tapering, although only slight variations encountered for a relatively high number of shots, probably related to the fact that the fixed initial energy of 250 mJ was high. It has been shown that the influence of the number of shots on tapering is typically magnified at the lower fluence values just beyond the ablation threshold of the material [6] and it is also verified and accepted that fluence itself plays an important role in determining the taper of the machined structures [7]. In this sense, tests were also run on 200 μm thick PNIPAAm layers, but did not gave satisfactory results, since the number of shots delivered to obtain an exit hole diameter of

about 20 µm in the swollen state was high (N = 4000) and led to poor quality machining in terms of the circular profile of the structures and eventually in partial burning of the material. The results obtained so far enabled a good control over the entrance and exit hole dimensions; Figure 4.22 reports the exit hole diameter as a function of the number of shots for a water swollen 250 µm thick PNIPAAm film machined with the 200 and 300 µm diameter holes stencil masks, using the set of optimized machining parameters. Due to the difference in the energy per shots delivered at the focal plane, as reported in 4.2.1, the diameter values obtained with the mask endowed with larger features are relatively higher as expected. There is further scope for investigation of the machining parameters, including creening effects due to the ablation plume generated by the laser beam; varying the repetition rate between 1 and 10 Hz would be interesting to examine how it affects the influence of the number of shots on tapering.

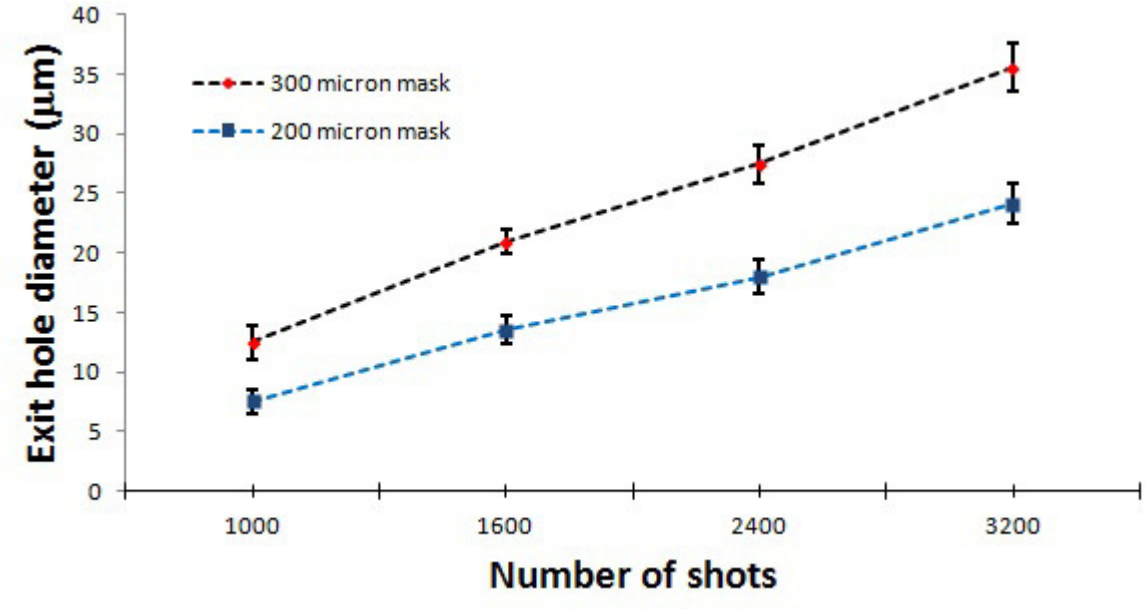


**Figure 4.22.** Graph of the exit hole diameter for the 200 and 300 µm hole diameter hole masks as a function of the number of shots for a 250 µm thick PNIPAAm film patterned with the optimized machining parameters.

## 4.5.2. Confocal microscope characterization

The effects of scattering, absorption and multiple reflections of the laser beam that could occur during the etching process of the deepest layers inside the machined structures, may have the effect of deviating the final shape of the hole from the one of a truncated cone, especially when a high number of shots is delivered. To highlight the tapered shape of the machined through-holes and thus validate the 3D reconstruction provided in 4.5.1, confocal microscope characterization was also carried out. Confocal microscopy has found employment in a wide range of applications, such as tracking and labeling of biomolecules, cells imaging and fluorescence correlation spectroscopy [8, 9, 10]. The working principle of confocal microscopy is the same as standard fluorescence microscopy, in which a fluorescent sample is excited by a laser light of the appropriate wavelength and the emission signal is collected by the optics of the system to image the specimen. The crucial difference in the confocal microscope set up is the presence of a pinhole aperture, positioned between the fluorescence detector (typically a photomultiplier) and the objective, that selects only the emission rays corresponding to contributions from a defined focal plane. At a basic level related to pure imaging processes, the main advantage of this instrument is the possibility of providing a three-dimensional reconstruction of the samples from the individual stacks acquired at each in-focus detection. The idea behind confocal microscopy measurements applied to water-swollen PNIPAAm based patterned films was to exploit the intrinsic permeability characteristics of the hydrogel layers to incorporate a small fluorescent dye in their sieve-like structure in order to confer fluorescent characteristics to the whole polymer matrix. Using this, when the laser light is shone onto the machined films, the fluorescent emission signal collected will be due to the excitation of the dye absorbed in the hydrogel thus revealing the empty regions defined by the holes, which will not contribute to the overall emission; in each stack, the holes are expected to result as dark spots surrounded by the emitting coloured dye background. By acquiring in plane focused images throughout the whole thickness of the sample, it was be possible to reconstruct the machined structure's shape by processing the different stacks via software. PNIPAAm samples were soaked in a Rhodamine B aqueous solution (20% v/v) overnight, to qualitatively evaluate the characteristic permeability of the network in respect to this dye, which is typically employed

as a fluorescent probe in biological assays and which presents a strong absorption peak at 555 nm and a fluorescence emission peak at 581 nm [11]. After being submerged in the solution, the films appeared coloured pink as the molecule was absorbed in the hydrogel network. Before each measurement took place, films were briefly rinsed in pentane in order to eliminate any residual trace of the dye in the holes. During imaging acquisition, the samples were kept between two glass microscope slides and each measurement was conducted within 30 minutes in order to avoid dehydration of the samples. The instrument employed for the measurements was a Leica DMIRE2 HC Fluo TCS 1-B-UV confocal microscope, fitted with Ar and HeNe lasers. In plane image acquisition of a 100 µm thick PNIPAAm film, machined with the 200 µm hole diameter mask and with N = 1000 is shown in Figure 4.23.

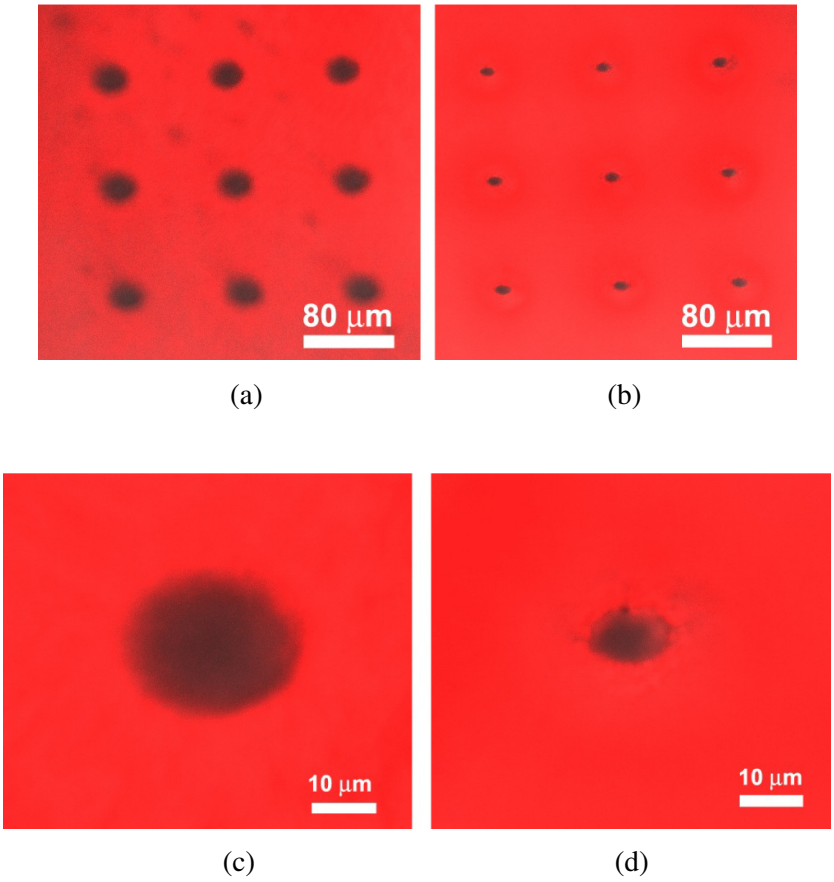


**Figure 4.23.** Images acquired using the Leica confocal microscope showing: a) top and b) bottom stack of PNIPAAm based film at low magnification. c) Entrance hole. d) Exit hole.

As expected, the darkest regions of the image representing the holes are clearly visible and easy to identify in respect to the fluorescent background. The height step rate used for selecting the in focus stacking was set as 0.5 μm, as a trade-off between the resolution and reliability of the final reconstruction and the time required for the acquisition process. The software ImageJ was later employed for realizing the 3D image; Figure 4.24 shows the results obtained after the stacks had been processed. The image reported is a negative representation in which the tapered holes appear bright on a dark background.

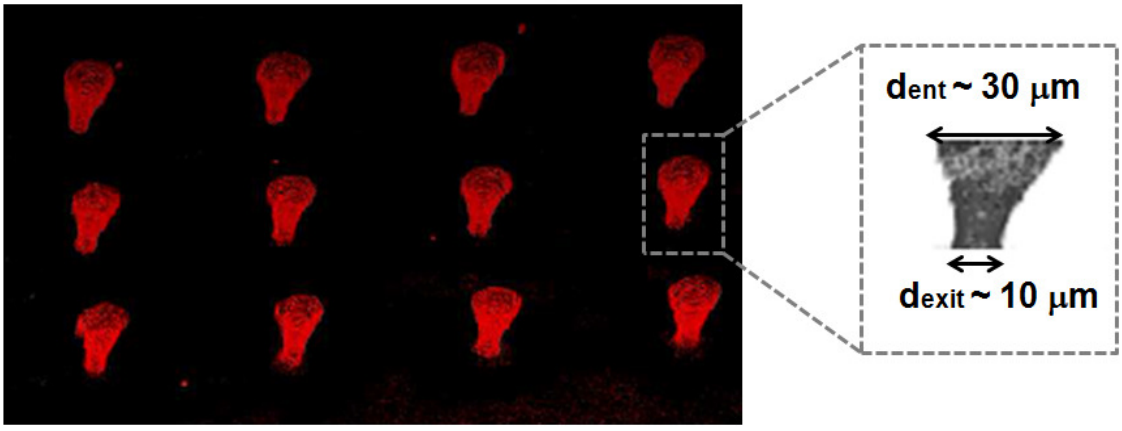


**Figure 4.24.** 3D reconstruction obtained by processing individual stacks acquired by the Leica confocal microscope.

The difference between the entrance and exit holes is evident and measures over the array gave the values $\langle d_{ent} \rangle$ = (30.0±1.7 μm) and $\langle d_{ext} \rangle$ = (10.5±1.0 μm) respectively with taper angle θ calculated as (78.6±1.1)°. This value is consistent with the higher taper angle and higher exit hole diameters observed for the PNIPAAm 100 μm thick film machined with N = 1600. These measurements suggest the possibility of employing the confocal microscope characterization to other PNIPAAm based layers in the swollen state.

## 4.5.3. Patterned hybrid hydrogel layers metrology characterization

As mentioned in 4.4. , hybrid PHEMA/PNIPAAm layers manufactured with METHOD 1 and METHOD 2 were machined using the 200 and 300 μm hole diameter masks, while the samples produced with METHOD 3 were patterned using the 1.5 mm diameter single hole mask. All the water swollen hybrid layers were characterized using the procedure discussed in 4.5.1. Figure 4.25 shows inverted microscope images of a 200 μm hybrid sample moulded with METHOD 2 and then machined with the 200 μm hole diameter masks with 1600 shots. The values of the entrance and exit hole diameters are $\langle d_{ent} \rangle$ = (32.4±1.1 μm) and $\langle d_{ext} \rangle$ = (10.5±0.9 μm) and were found to be in agreement with the results previously obtained from metrology measurements on the water swollen pure PNIPAAm layers. Using the CAD reconstruction of the holes, the evaluated tapering angle θ is (87.2±1.0)° and its value is also compatible with the results obtained in the previous cases.

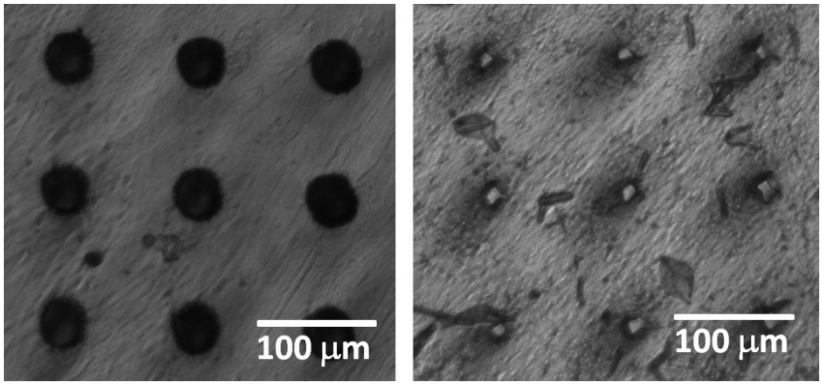


(a) (b)

**Figure 4.25.** Water swollen hybrid PHEMA/PNIPAAm film (200 μm thick) laser machined using the 200 μm hole diameter mask. a) Entrance holes. b) Exit holes.

For the single holed hybrid layers moulded with METHOD 3, optical microscope images of the machined structure on a dry 250 μm thick sample (number of shots equal to 200) are shown in Figure 4.26. The sample was mechanically removed from the substrate in order to visualize and measure the diameter of the circular features in the dry state prior to swelling and then swelled in water to carry out metrology measurements in its hydrated state; the

diameter of the structure increased by a factor equal to 1.5 when the polymer was water swollen.

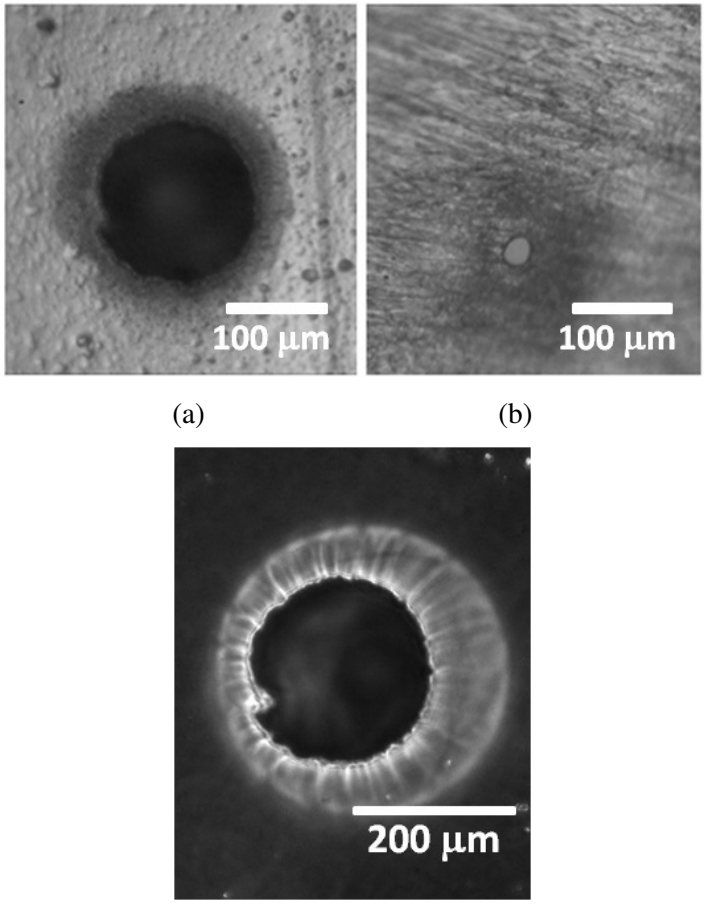


**Figure 4.26.** Single hole machined on a PHEMA/PNIPAAm hybrid layer moulded with METHOD 3. a) Entrance hole in the dry state; the diameter was measured as $<d_{ent}>$ = (148.1±1.6 µm). b) Exit hole in the dry state; the diameter was measured as $<d_{ext}>$ = (23.0±1.3 µm). c) Entrance hole in the water swollen state; the diameter was measured as $<d_{ent}>$ = (218.1±2.0 µm) , revealing a diameter increase of a factor equal to 1.5. In the swollen state, the reconstructed tapering angle θ was (70.3±1.2)°.

The imperfection observed on the circular profile of the entrance hole reflects the imperfect shape of the hole in the mask, which was produced by mechanical drilling. The determination of the hole diameter was carried out by taking 10 measurements for each picture and then

averaging over all the obtained values; the standard deviation was then calculated accordingly. A calibration curve showing the exit hole diameter as a function of the number of shots for a water swollen 250 μm thick hybrid PHEMA/PNIPAAm film machined with the 1.5 mm hole diameter mask is reported in Figure 4.27. All the values are relative to different micro-features machined on different thermo-responsive PNIPAAm regions of the same hybrid film, using the set of optimized machining parameters.

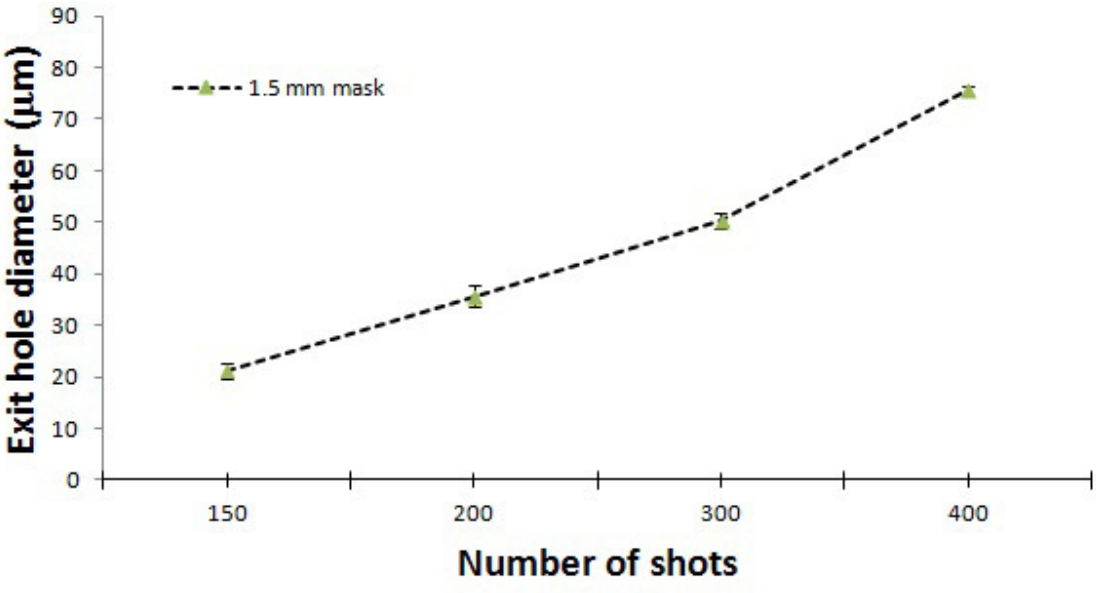


**Figure 45.** Graph of the exit hole diameter for the 1.5 mm diameter hole stencil masks as a function of the number of shots for a 250 μm thick PHEMA/PNIPAAm film patterned with the optimized set of machining parameters.

Due to the higher energy values on the focal plane, deriving from the large aperture hole present on the mask, a relatively small number of shots is required to achieve higher values of the exit hole diameters in respect to the previous cases. The machining was therefore found to be more efficient and less time consuming than for the 200 and 300 μm hole diameter masks. These single holed samples were subsequently chosen for the cell sorting on-chip application; in this case, the exit hole of the machined capillary would operate as the trapping hole for the cells, that could then be released into the bottom component of the device exiting through the relatively wide entrance hole.

## References


[1] Lippert T Hauer M Phipps C R and Wokaun A 2003 *Appl. Phys. A* **77** 259–264

[2] Dyer P E 2003 *Appl. Phys. A* **77** 167–173

[3] Vogel A and Venugopalan V 2003 *Chem. Rev.* **103** 577-644

[4] Lazare S Elaboudi I Castillejo M and Sionkowska A 2010 Appl Phys A **101** 215–224

[5] Ozcan A and Demirici U 2008 *Lab Chip* **8** 98-106

[6] Hsieh Y S Yang C R Hwang G Y and Lee Y D 2001 *Macromol. Chem. Phys.* **202** 2394-2401

[7] Paterson C Holmes A S and Smith R W 1999 *Journal of Applied Physics* **86** 6538-6546

[8] Andersson S B 2005 *Appl. Phys. B* **80** 809-816

[9] Schneckenburger H Weber P Wagner M Bruns T Richter V Schickinger S and Witting R 2012 *Photon Laser Med* **1** 35-40

[10] Hess S T Huang S Heikal A and Webb W W 2002 *Biochemistry* **41** 697-705

[11] Shao Y Wang L Zhang J and Anpob M 2006 *Journal of Photochemistry and Photobiology A: Chemistry* **180** 59-64

# 5. Thermo-responsiveness characterization of patterned PNIPAAm based layers

## 5.1. Methodology

After discussing the manufacturing protocol developed to realize micro-patterned PNIPAAm based hydrogel layers in Chapters 3 and 4, this chapter is dedicated to the characterization of the stimuli-responsive behaviour of the polymeric components produced from these materials. Both freestanding pure PNIPAAm films synthesized with the standard recipe (3.2.1) and samples fabricated using different cross-linker and initiator amounts (3.2.1.1. and 3.4.2.1.) were subjected to thermo-responsiveness tests in pure water. The aim was to determine the amount of shrinkage of the laser machined structures when the temperature is raised above the critical transition value employing two different techniques that will be described in the next section. Using the same equipment and procedures, freestanding micro-structured PNIPAAm co-polymer based hydrogels (3.2.2.1 and 3.2.2.2.) and hybrid PHEMA/PNIPAAM thin films (3.4.2.2. and 3.4.2.3.) were then tested. To obtain further information on how the mechanical constraints caused by the mounting of the films could affect the transition of the hydrogels, a PMMA framework, which was already mentioned in 3.4.1., was employed to compress the elastic PHEMA frame region of the hybrid hydrogels when subjected to the temperature transition. The experimental results obtained on all hydrogels are treated separately starting from section 5.3 and then are compared and discussed at the end of the Chapter, in section 5.7.

## 5.2. Freestanding PNIPAAm film characterization: experimental approach and set-up

To achieve a complete picture of the freestanding machined layers' response to temperature changes, two approaches were considered. In the first instance, PNIPAAm based films were monitored in real time using a temperature controlled water bath and the pattern shrinkage was recorded by acquiring optical microscope images of the holes as the temperature was varied from 18 °C to 39 °C. In this way, the sharpness of the phase transition could be analyzed and multiple cycles could also be easily carried out to explore the reversibility of the process and observe any fatigue effects induced by the transition at each loop. The second set of experiments was done by increasing the water bath temperature from 18 °C to 37 °C and then observing the natural relaxation of the polymers toward their initial state induced by the natural environmental cooling to room temperature; this test could give a reliable indication of the rate of re-swelling when no external heating or cooling mechanism is supplied. In order to carry out the first group of tests, a system was developed to precisely regulate the temperature of the cell. This consisted of a Proportional Integral Derivative (P.I.D.) controller (CAL9500), a heating element and a k-type thermocouple (KTC). The patterned films were immersed in 2.5 ml of MilliQ water, then heated. To hold the specimens in place during imaging, a 150 μm thick glass slide was placed over the hydrogels, in order to maintain planarity with only a mild compression so that the films would not endure any severe mechanical constraint. A 120 μm thick transparent heater (MINCO, model H6700R9.0, 9 Ohm, power supply 5 V) was embedded in a moulded PDMS box and connected to the output port of the P.I.D. controller. The heating element was positioned at the bottom of the box, 1 mm underneath the container surface, in order to ensure homogeneous heating of the water bath. The thermocouple was held in place, suspended in the liquid and the measured temperature values were continuously processed by the P.I.D. system. A feedback loop between the heater and KTC ensured accurate control over the water temperature (±0.5 °C), which could be directly set from the controller. A schematic diagram of the in house realized piece of equipment and its working principle is shown in Figure 5.1.

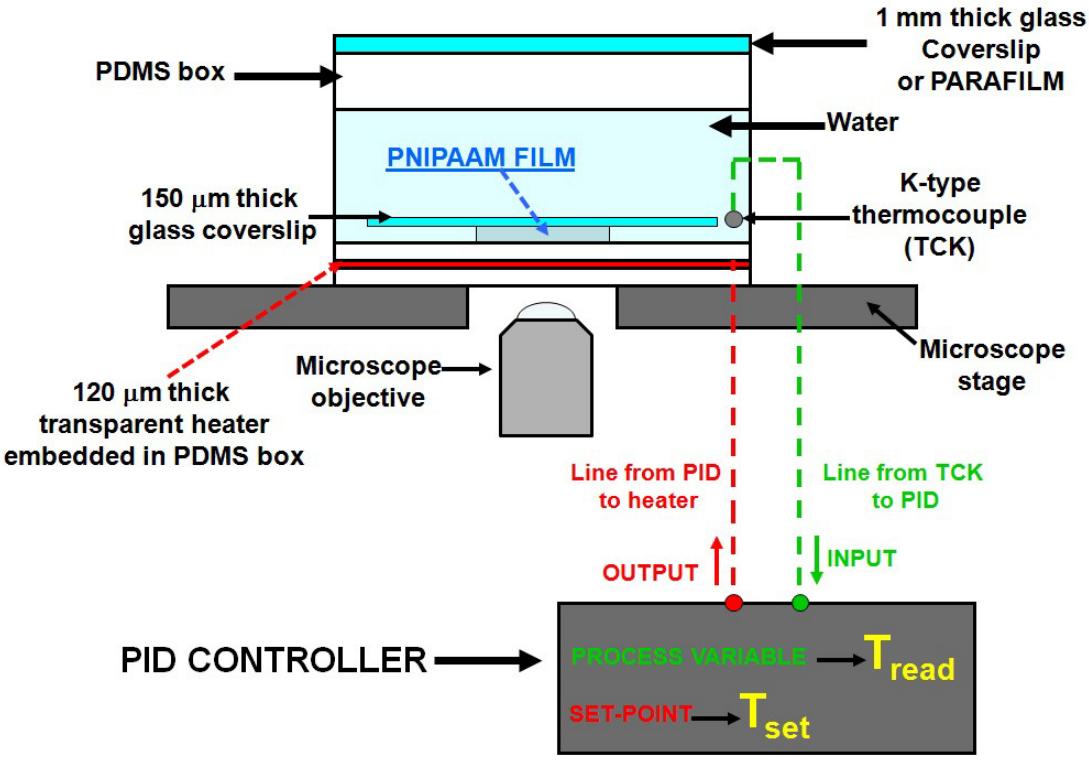


**Figure 5.1.** Experimental setup for thermo-responsiveness characterization of the PNIPAAm based freestanding films.

The temperature set points at which snapshots of the layers were acquired were chosen as 18, 25, 33, 37 and 39 °C. By setting the P.I.D. controlling parameters, such as integral and derivative time, the heating rate could be changed. To not thermally stress the samples, a heating rate of 1 °C per minute was chosen for these tests. Once each set point was reached, the temperature value was maintained constant for 15 minutes so that the hydrogels could be considered in thermal equilibrium with the water bath and the shrinking behavior was then monitored using the inverted optical microscope. The number of cycles each sample underwent using this heating system was three, and the same temperature values were selected at each loop, using the same timing and heating rates. In the second set of experiments the temperature increase of the water bath from 18 °C to 37 °C and the subsequent cooling to room temperature to observe the polymer's relaxation were promoted using a different strategy. To thermalize the PNIPAAm based layers at the physiological

temperature, samples were soaked in a water filled Petri dish (10 mm diameter) and positioned in a cell incubator at 37 °C, which provided a highly controlled environment in terms of temperature stability. Again, a 150 μm thick glass slide was placed over the hydrogels (Figure 5.2).

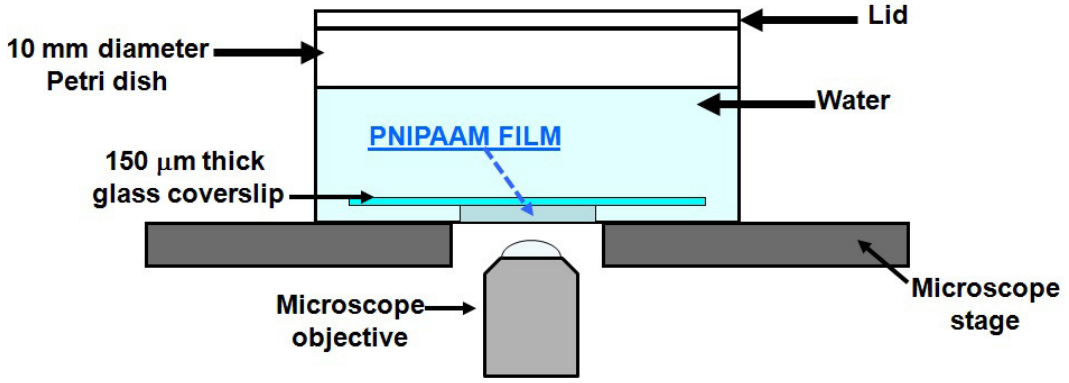


**Figure 5.2.** Schematic diagram of the PNIPAAm based freestanding film in a Petri dish soaked in MilliQ water. The system was then positioned in the cell incubator.

Samples were left in the incubation cabinet for 1.5 hours in order to ensure that the value of 37 °C was reached and maintained for 0.5 hours and then the dishes were extracted to be immediately positioned on the microscope stage. Image acquisition took place in real time so that the patterned feature dimensions were continuously monitored over time while the system temperature decreased. The laboratory temperature was kept at 25 °C using an air conditioning system.

## 5.3. Freestanding micro-patterened PNIPAAm based hydrogel layers thermo-responsive behavior

### 5.3.1. P.I.D. temperature controlled water bath tests for pure PNIPAAm films

Pure PNIPAAm layers were manufactured, patterned, detached and swelled in MilliQ water according to the procedures described in Chapters 3 and 4. After swelling, disks were cut from the layers using hole punches of 5 and 7 mm diameter, so that the resulting hydrogel disks had the patterned features at the center. The layers were produced using all the silicone and brass based spacers available as discussed in 3.3.2., so that the whole thickness range could be explored. Figure 5.3 shows a 100 µm thick PNIPAAm film in the swollen state, machined using the 200 µm diameter hole projection mask, undergoing the volumetric phase transition at the set points of 18, 25, 33, 37 and 39 °C.

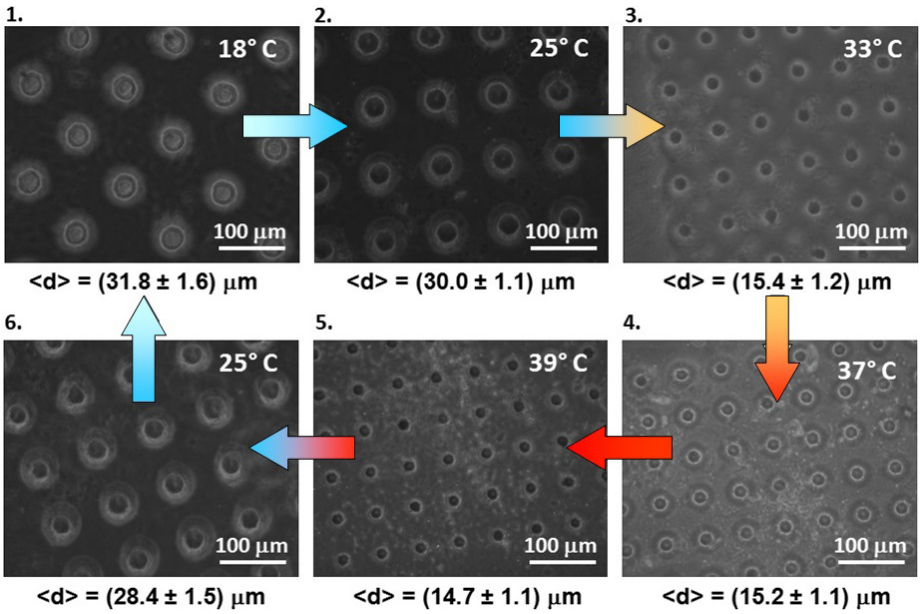


**Figure 5.3.** Inverted microscope thermo-response characterization of a micro-patterned water swollen 100 µm thick freestanding PNIPAAm layer. Measured average entrance hole diameter < d > is reported.

No appreciable changes in the sample dimensions or transparency were observed for temperatures below 27 °C. A slight decrease in the disk's dimensions (~10 to 15% of its initial diameter) and a mild opacity of the hydrogel started between 28° and 30 °C, followed by an abrupt shrinkage that brought the polymer to its equilibrium collapsed state in a few seconds after 32 °C was reached. It was observed that when the hydrogel's temperature was driven beyond the transition point, pattern shrinkage occurred throughout the whole film, thus leading to a significant reduction in the through-hole size. The average entrance hole diameter was measured to decrease from about 30 μm to about 15 μm for the sample imaged in Figure 5.3, as shown in the graph reported in Figure 5.4.

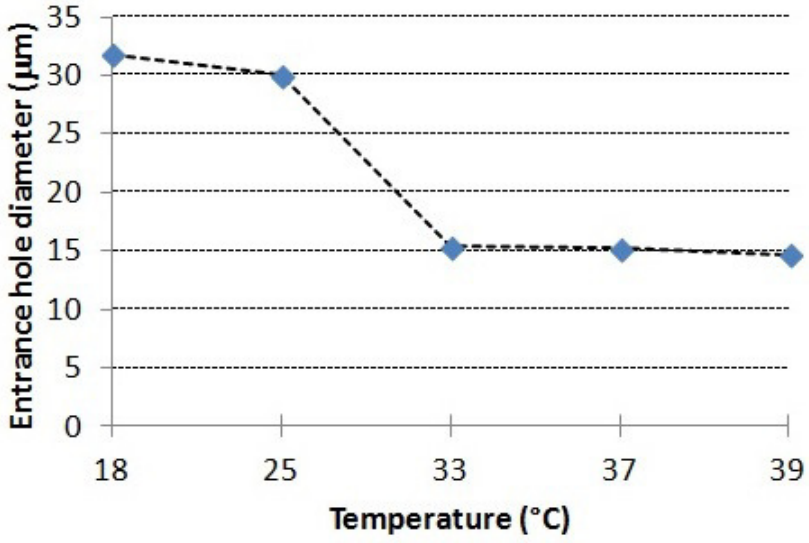


**Figure 5.4.** Temperature vs entrance hole diameter plot for the 100 μm thick freestanding PNIPAAm layer; the sharp feature of the phase transition is revealed from the steep profile between 25 and 33 °C.

No significant deformations of the micro-capillaries' shape were observed during shrinkage and compatible changes could be observed for the exit holes, according to the hole tapering values. A similar behaviour was also observed for samples with different thickness (250, 200 and 150 μm) which were also machined employing different projection masks; for the thickness range explored in these tests, no effects on the shrinking behaviour were observed and the shrinking degree of the micro-structures was also invariant, as shown in Figure 5.5.

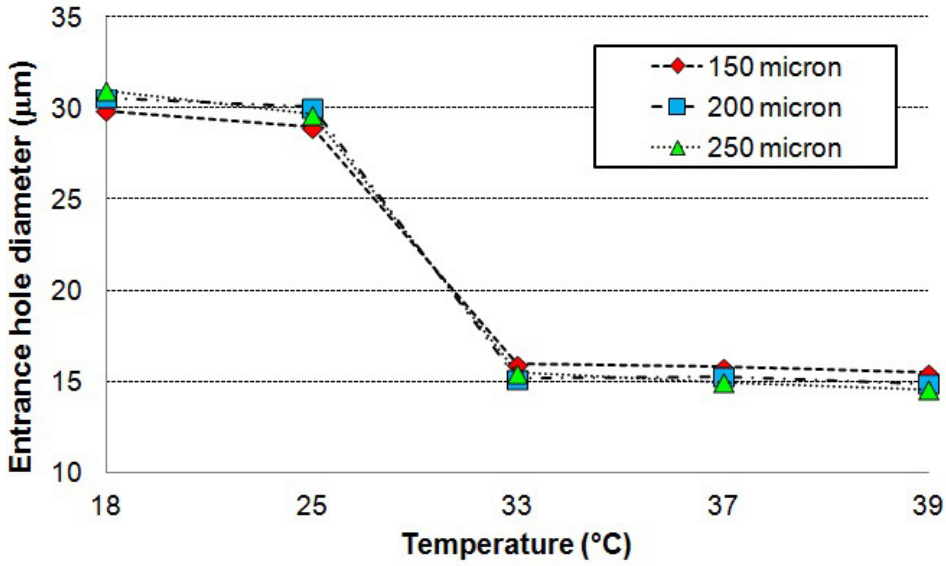


**Figure 5.5.** Temperature vs entrance hole diameter plot for the 150, 200, 250 µm thick freestanding PNIPAAm layers.

Supplementary thermo-sensitivity experiments were later conducted on thinner micropatterned PNIPAAm layers, approaching a minimum thickness of 50 µm; the deswelling mechanism still showed the same phenomenology, preserving the holes' diameter changes. Figure 5.6 shows inverted microscope images at low magnification of the whole pattern shrinkage for a 50 µm thick PNIPAAm layer machined using the 200 µm hole diameter projection mask.

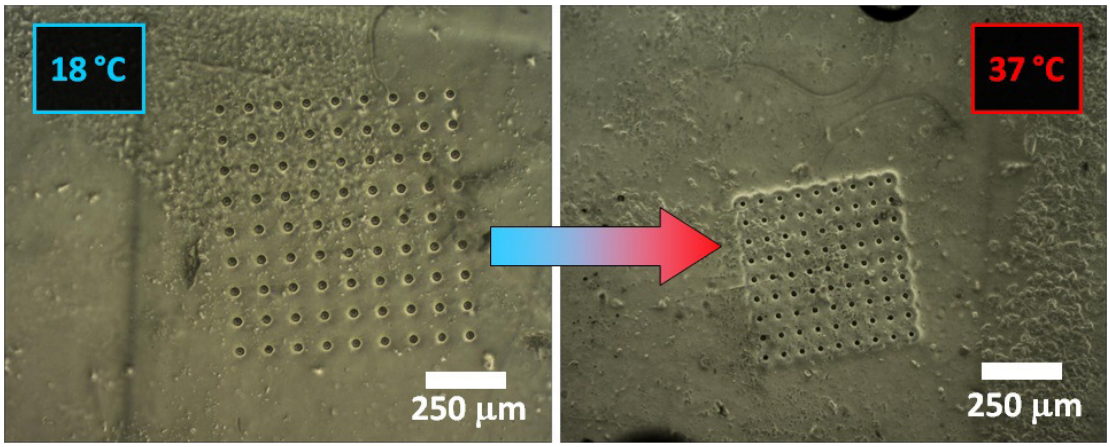


**Figure 5.6.** Low magnification inverted microscope images at 18° (left) and 37 °C (right) of a micro-patterned water swollen 50 µm thick freestanding PNIPAAm layer. Samples are viewed from the entrance hole side. No significant deformations affect the overall pattern shape.

Furthermore, the reversibility of the process was demonstrated when multiple cycles were carried out. In this group of experiments, the cooling rate was set at 1 °C per minute. The results of the swelling-deswelling kinetics over each cycle showed identical characteristics in terms of response rate and relative hole dimension changes when the temperature was varied from 18 °C to 39 °C, but exhibited a slower re-swelling process for the film to recover its initial state. This could be interpreted as a consequence of the reduced mobility of the hydrophobic polymer chains in their globular conformation in respect to the coil-like hydrophilic state, as also pointed out in [1]. The typical recovery behaviour of the hydrogels is represented in Figure 5.7, where the evolution of the entrance hole diameter as a function of time along the cooling of the sample is reported for the 100 µm thick PNIPAAm layer previously characterized.

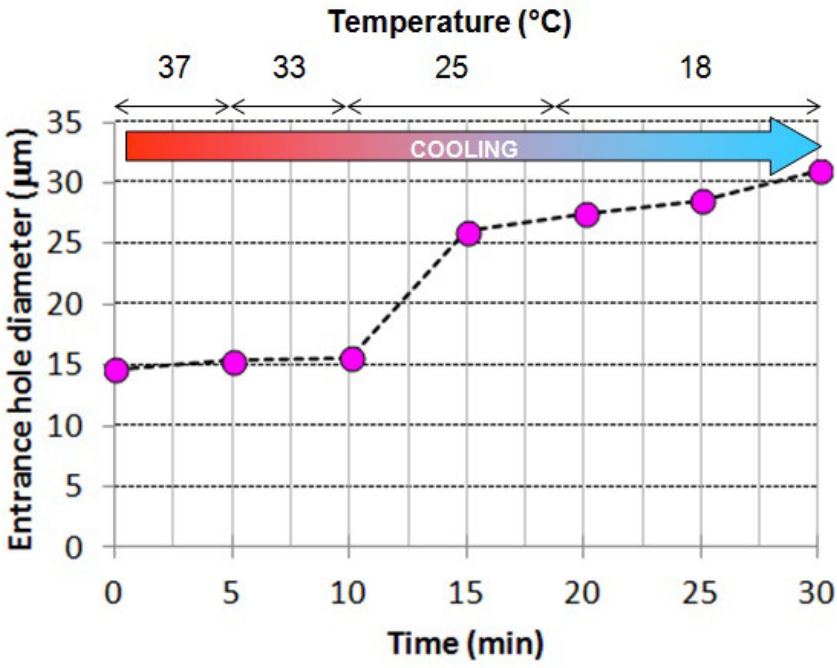


**Figure 5.7.** Time vs entrance hole diameter plot for the 100 µm thick freestanding PNIPAAm layer throughout the cooling cycle.

It can be reasonably deduced from the observations that the freestanding character of the fabricated films not only enables the homogeneous and substantial isotropic restriction of the machined geometrical features, but it also promotes buckling-free deformation of the through-holes and avoids significant distortion phenomena affecting their shape, at least at the meso-scopic scale. Figure 5.8 shows inverted optical microscope images of the entrance and exit holes at 18° and 37 °C for a 250 µm thick water swollen freestanding PNIPAAm layer patterned using the 300 µm hole diameter mask (number of shots equal to 3200). Measured average entrance and exit hole diameters and the relative standard deviation are reported as well. In agreement with the previous cases, the hole diameters were reduced to about half their original size when the film transition occurs.

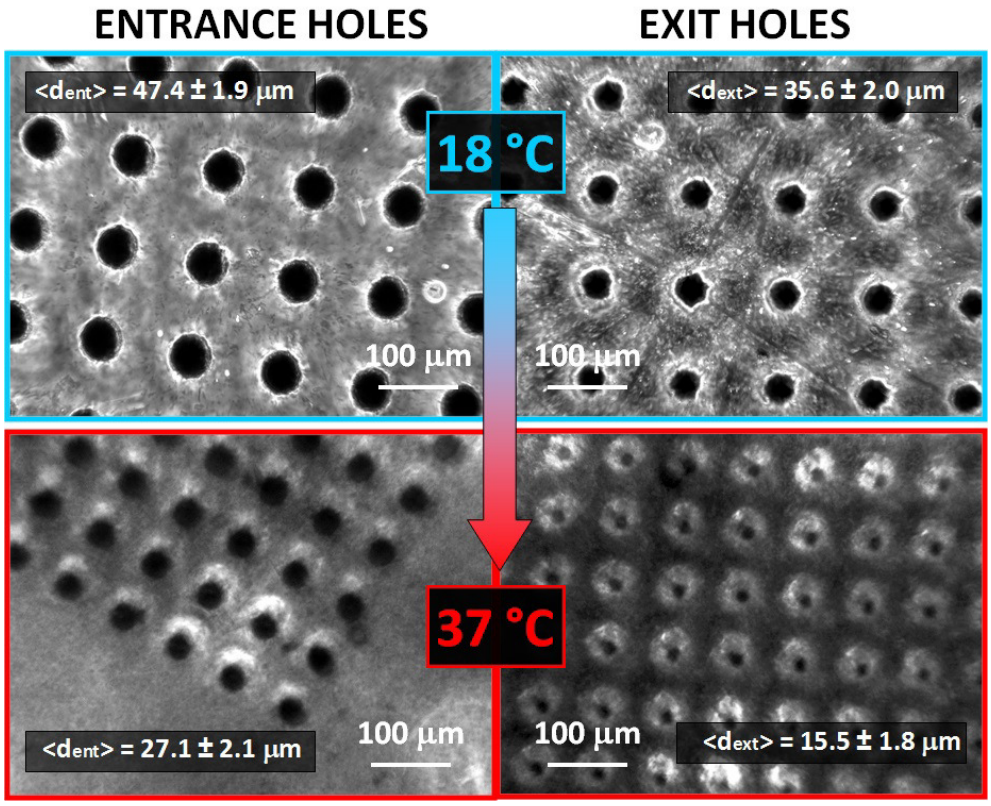


**Figure 5.8.** Inverted microscope images at 18 (top) and 37 °C (bottom) of a micro-patterned water swollen 250 µm thick freestanding PNIPAAm layer.

## 5.3.2. Cell incubator tests for pure PNIPAAm films

Pure PNIPAAm samples of the same size and with the same features as the ones analyzed in 5.2.1. were tested using the cell incubator with the procedure described in 5.1. Figure 5.9 reports inverted microscope images of a water swollen 200 μm PNIPAAm sample, laser machined using the 200 μm hole diameter mask, prior and before incubation at 37 °C.

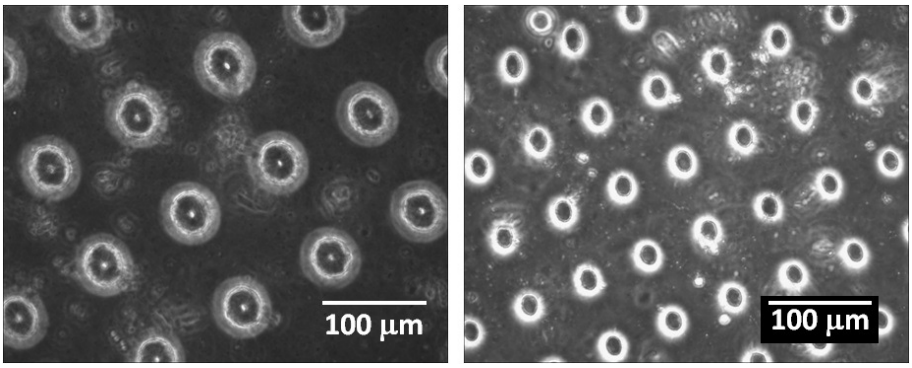


(a) (b)

**Figure 5.9.** Inverted microscope thermo-response characterization of a micro-patterned water swollen 200 μm thick freestanding PNIPAAm layer. a) Film entrance holes before incubation at 18 °C. b) Film entrance holes after 1.5 hours incubation at 37 °C.

The behavior of the tested layers was in accordance with the phenomenon previously observed when employing the P.I.D. controlled water bath at set points of 18 °C and 37 °C; entrance hole diameters for the PNIPAAm film shown in Figure 5.9 were measured as $<d_{t0}>$ = (32.0±1.5 μm) and $<d_{t1}>$ = (15.8±1.9 μm) before and after incubation respectively, thus reproducing the hole shrinkage value of about 50% its original size. This phenomenon showed the same features for layers machined both with the 200 μm and 300 μm hole diameter masks, thus not revealing any dependency from the initial diameter value. More interestingly, the cooling of the layers at room temperature was monitored in real time. Figure 5.10 reports the most significant phases of the hydrogel relaxation to its initial state for the PNIPAAm film shown in Figure 5.9.

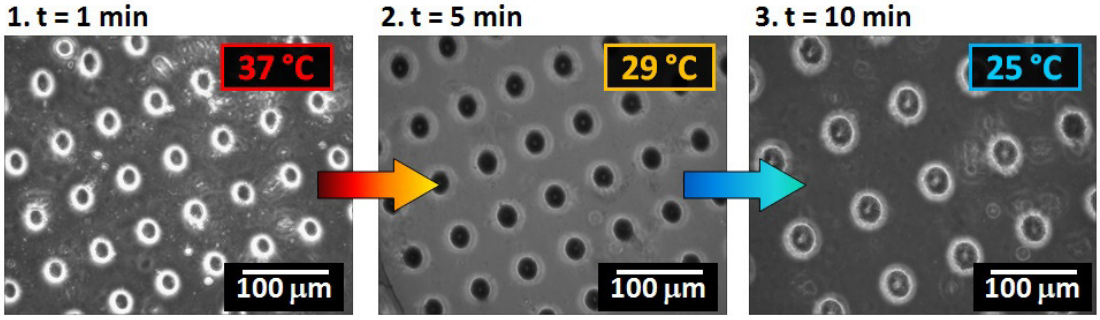


**Figure 5.10.** Micro-patterned water swollen 200 µm thick freestanding PNIPAAm layer cooling at room temperature after 1.5 hours incubation time. The images show the entrance holes after 1 minute (t = 1 min, left), 5 minutes (t = 5 min, center) and 10 minutes (t = 10 min, right) after the layer was removed from the cell incubator.

After 5 minutes, the water in the Petri dish had begun cooling down and the entrance holes partially recovered their original size; the measured average diameter was $\langle d_{t5} \rangle$ = (25.2±1.6 µm), corresponding to a measured temperature value of 29 °C. After 10 minutes, room temperature was reached and the film was almost completely recovered, giving a measured average diameter of $\langle d_{t10} \rangle$ = (29.4±1.2 µm). This was slower than when heating due to the characteristic delay caused by the conformational features of the polymeric chains, which slowly return from a globular to a coil-like structure. In the 10 minutes time window, snapshots were acquired with a time lapse of 10 seconds, which could give an estimate of the average reswelling rate of about 2 µm per minute. The trend of the hydration process of the layers in terms of entrance hole diameter size as a function of time is reported in Figure 5.11.

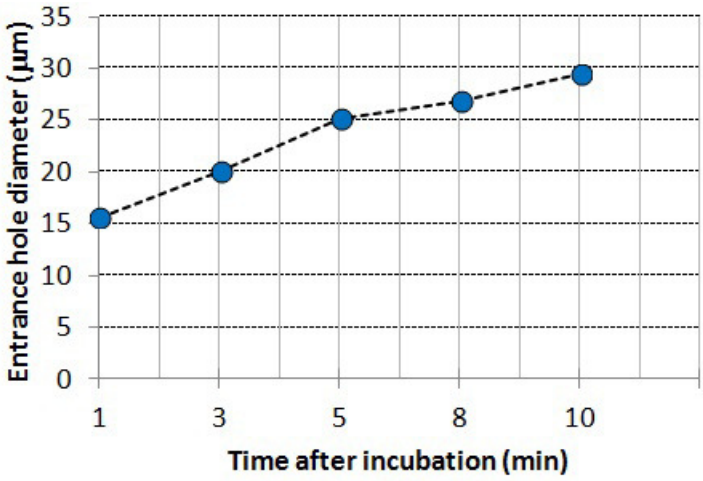


**Figure 5.11.** Time vs entrance hole diameter plot for the 200 µm thick freestanding PNIPAAm layer after removal from the incubator at 37 °C.

The results obtained on all the layers tested using the incubator thermalization were reproducible and compatible. The main information that can be derived from these observations combined with the results collected employing the P.I.D. set up is:

- After the transition takes place, the final size of the patterned holes does not depend on the heating rate imposed and keeps its value of about 50% its original size.

- Using the set up employed (cell incubator for stabilizing the temperature at 37 °C, 10 mm diameter Petri dish), the natural recovery of the polymer at room temperature happens relatively quickly toward the initial state, but the slow globular chain relaxation process brings the same time lag before the original configuration is reached, as was observed in the experiments carried out using the P.I.D.

Keeping in mind the high reliability and thermal stability of the incubation system when employed as a thermostat, using this method constituted an easy and effective way for monitoring the stimuli-responsive behaviour of all the PNIPAAm based and hybrid PHEMA/PNIPAAm layers realized.

# 5.4. Thermo-responsive behavior of freestanding PNIPAAm based hydrogel layers prepared using alternative routes

This section is dedicated to the stimuli-responsiveness characterization of the freestanding PNIPAAm based hydrogel layers synthesized by varying the standard recipe, either by changing reagent amounts or by introducing different co-monomers. All of the samples tested were characterized using both the P.I.D. system and the cell incubator thermalization process. Results of the pattern shrinkage of the PNIPAAm layers synthesized using different cross-linker and initiator amounts are reported in the next subsection, while PNIPAAm-co-HEMA and PNIPAAm-co-MMA thermo-responsive behavior is reported in 5.4.2. To identify the degree of the patterned layers' shrinkage, a shrinking ratio S will now be considered; this quantity is defined as:

$$S = (1 - (< d_{ent} >_{37} / < d_{ent} >_{18}) ) \times 100\% \qquad [5.1]$$

Where $< d_{ent} >_{37}$ and $< d_{ent} >_{18}$ are the measured average entrance hole diameters at 37 °C and 18 °C respectively.

## 5.4.1. Layers with different cross-linker or initiator amount

### 5.4.1.1 PNIPAAm layer with double cross-linker amount: PNIPAAm - EGDMA 2x

PNIPAAm samples with double cross-linker amount (PNIPAAm – EGDMA 2x) were qualitatively described in 3.2.1.1. The main differences in respect to the standard pure PNIPAAm films were the opacity and swelling degree of the hydrogel. PNIPAAm – EGDMA 2x was less transparent, thus suggesting a lower degree of homogeneity, while its lower swelling degree was a manifestation of the fact that the relatively highly cross-linked polymer could retain a lower quantity of water. Since the temperature-triggered shrinkage is

related to the amount of water incorporated in the polymeric matrix, it was expected that the hole dimension above the critical temperature would be larger than the one observed for the standard PNIPAAm layers. Figure 5.12 shows a water swollen 200 μm thick freestanding PNIPAAm – EGDMA 2x film patterned using the 200 μm hole diameter projection mask before and after 1.5 hours incubation.

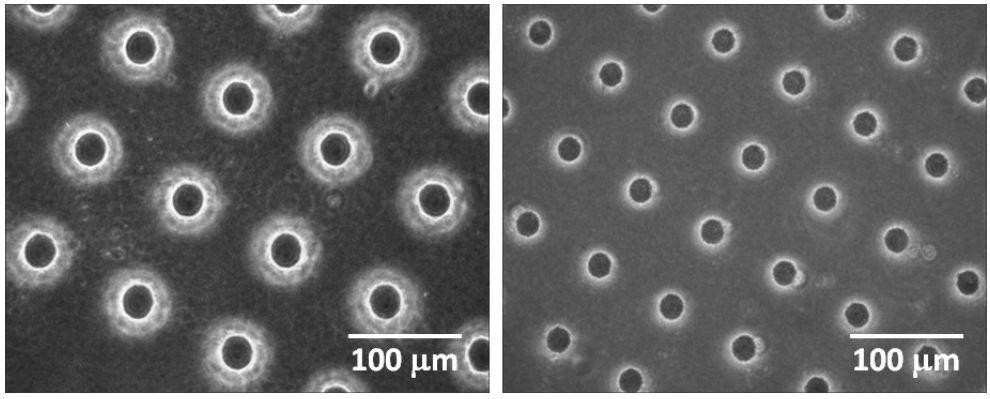


(a) (b)

**Figure 5.12.** Inverted microscope thermo-response characterization of a micro-patterned water swollen 200 μm thick freestanding PNIPAAm – EGDMA 2x layer. a) Entrance holes before incubation at 18 °C. b) Entrance holes after 1.5 hours incubation at 37 °C.

Entrance hole diameters were measured as $\langle d_{ent} \rangle_{18}$ = (31.2±1.3 μm) and $\langle d_{ent} \rangle_{37}$ = (23.3±1.2 μm), thus confirming the lower shrinking ratio of the holes, which was about 25%, rather than 50% as in the cases previously discussed in 5.3. On the other hand, the recovery of the hydrogel toward its initial state during cooling was relatively quicker, but still maintained the delay effect due to the reduced mobility of the globular structure of the chains, slowly relaxing to a coil-like configuration, as shown in Figure 5.13.

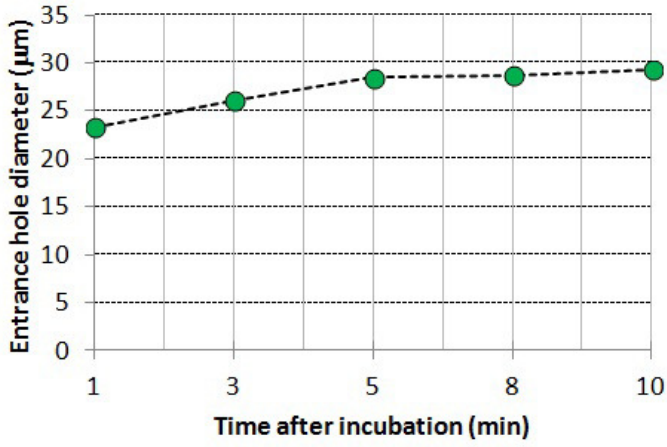


**Figure 5.13.** Time vs entrance hole diameter plot for the 200 µm thick freestanding PNIPAAm – EGDMA x2 layer after incubation at 37 °C.

Using the P.I.D. system, tests with multiple cycles were also carried out on the sample; no significant differences in the shrinking rate features were observed with respect to the results reported in 5.3.1. Though the PNIPAAm – EGDMA 2x based samples had the advantage of having an improved elasticity in respect to the standard PNIPAAm layers, as observed at a qualitative level, the weak shrinking behaviour induced by the temperature transition strongly limits the possibility of modulating the size of the machined structures, which constitutes a disadvantage from the application point of view.

### 5.4.1.2. PNIPAAm layer with increased initiator amount: PNIPAAm4x

The class of PNIPAAm based hydrogels synthesized using 4 times the initiator aqueous solution amount with respect to the standard recipe (namely PNIPAAm4x , described in 3.4.2.1.) are extremely important from the application point of view, because of their involvement in the hybrid PHEMA/PNIPAAm layer fabrication. As mentioned in Chapter 3, PNIPAAm4x disks constitute the thermo-responsive cores of the hybrid structures, so their stimuli-responsive behavior will be determinant for any filtering or trapping operations on-chip related to the shrinkage/enlargement mechanism of the patterned holes. Figure 5.14 shows a water swollen 250 µm thick freestanding PNIPAAm4x layer, machined using the 300 µm hole diameter projection mask, before and after 1.5 hours incubation.

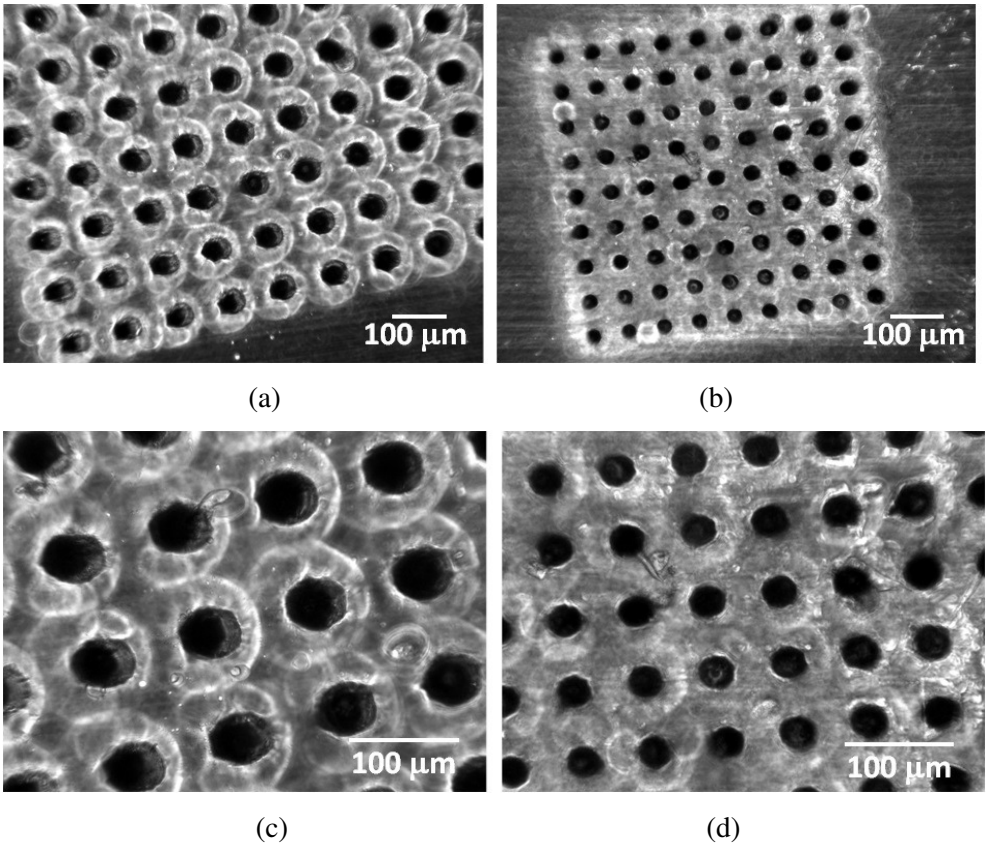


**Figure 5.14.** Inverted microscope thermo-response characterization of a micro-patterned water swollen 250 µm thick freestanding PNIPAAm4x layer. a) Entrance holes at 18 °C. b) Entrance holes after 1.5 hours incubation at 37 °C. c) Higher magnification of (a). d) Higher magnification of (b).

Entrance hole diameters were measured as $\langle d_{ent} \rangle_{18}$ = (46.4±1.9 µm) and $\langle d_{ent} \rangle_{37}$ = (28.1±1.6 µm), before and after incubation respectively. The resulting shrinking ratio was 40%, which can be considered as a reasonable value, taking into account that, at the macroscopic level, the swelling degree of the PNIPAAm4x layers is similar to the one exhibited by the pure PNIPAAm based films. The slight reduction from 50% to 40% could be caused by the presence of regions of higher heterogeneity in the cross-linker distribution due to the higher reaction speed and higher reaction temperature developed during the polymerization and solidification. P.I.D. tests were also run and, as in the case of the PNIPAAm – EGDMA 2x based samples, the observations were compatible with the ones collected and dicussed in

5.3.1. As expected, the observed stimuli-responsive behavior makes micro-patterned PNIPAAm4x hydrogel based components appropriate for operating as thermo-responsive cores in the hybrid PHEMA/PNIPAAm structures.

## 5.4.2. PNIPAAm based random co-polymers

PNIPAAm-co-HEMA and PNIPAAm-co-MMA based layers were characterized. As already pointed out in 3.2.2., the value of the transition temperature of PNIPAAm based co-polymers can be increased or decreased to a certain extent depending respectively on the hydrophilic or hydrophobic character of the co-monomer introduced and on its relative amount with respect to the NIPAAm polymeric unit. For this reason, the characterization was first carried out employing the P.I.D. system set up in order to identify any shift in the value of the critical temperature.

### 5.4.2.1. PNIPAAm-co-HEMA

PNIPAAm/HEMA co-polymers were synthesized in different molar ratios and characterized by IR spectroscopy measurements as reported in 3.2.3. Qualitative swelling characterization was then carried out on the hydrogel disks to determine any macroscopic evidence that an excessive amount of HEMA in the co-polymer might dramatically decrease the water absorption of the polymeric matrix, which could then hinder the phase-transition. In the water swollen state, no appreciable volume changes were noted with respect to their relaxed state for PNIPAAm-co-HEMA with HEMA : NIPAAm molar ratio equal to 20, 30 and 40%. Since the PNIPAAm/HEMA co-polymer having a HEMA : NIPAAm molar ratio of 5% did not qualitatively exhibit any significant improvement in the elastic properties in respect to the PNIPAAm standard mixture, hydrogels with monomer molar ratio HEMA : NIPAAm = 1 : 10 mol/mol (PHEPAAm10) were chosen as the best candidates for thermo-responsive characterization. The temperature range and set points fixed by the P.I.D. system were the same as in 5.2.1. Figure 5.15 shows a water swollen 200 μm thick freestanding PHEPAAm10

layer machined using the 200 μm hole diameter mask at the temperature set points of 18 °C and 37 °C.

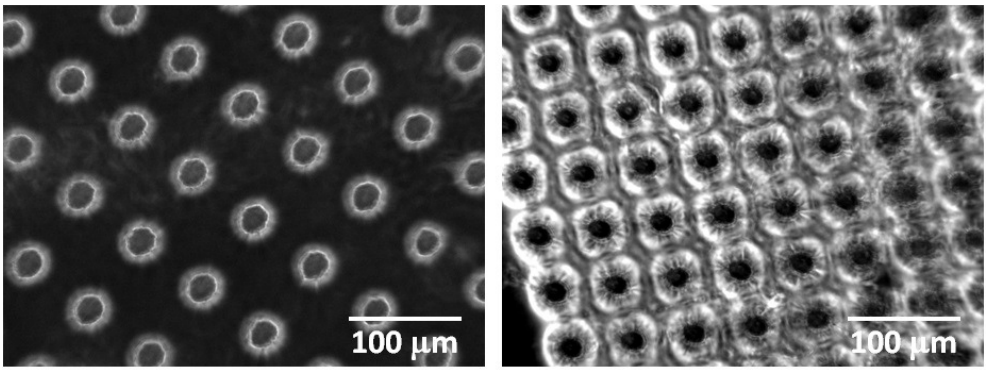


(a) (b)

**Figure 5.15.** Inverted microscope thermo-response characterization of a micro-patterned water swollen 200 μm thick freestanding PHEPAAm10 layer. a) Entrance holes at 18 °C; the measured average diameter is $\langle d_{ent} \rangle_{18}$ = (30.7±2.1 μm). b) Entrance holes after 1.5 hours incubation at 37 °C; the measured average diameter is $\langle d_{ent} \rangle_{37}$ = (21.0±1.8 μm).

From the observations collected using the P.I.D. controlled water bath, the relatively small molar ratio of the monomers did not dramatically affect the transition temperature, which was determined to be around 34 °C. These results are compatible with those reported in the literature [5]. After thermalization at 37 °C, the machined holes were homogeneously shrunk, but the shrinking ratio was determined to be around 30%, a value which is relatively higher than the one found for the PNIPAAm – EGDMA 2x based layers. Overall, the introduction of the hydrophilic co-monomer did not appear suitable for applications requiring a high degree of shrinkage of the thermo-responsive films.

### 5.4.2.2. PNIPAAm-co-MMA

PNIPAAm hydrogels incorporating MMA as co-monomer were synthesized with a molar ratio equal to MMA : NIPAAm = 1 : 10 mol/mol and the laser machined layers were then characterized in terms of thermo-responsiveness using the P.I.D. based temperature

controlled water bath. Figure 5.16 shows a water swollen 200 μm thick freestanding PNIPAAm-co-MMA film machined using the 200 μm hole diameter projection mask at the temperature set points of 18 °C and 37 °C.

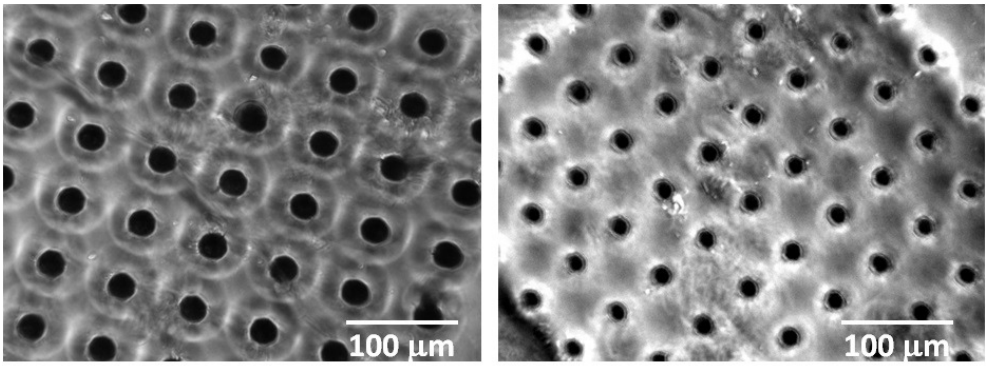


(a) (b)

**Figure 5.16.** Inverted microscope thermo-response characterization of a micro-patterned water swollen 200 μm thick freestanding PNIPAAm-co-MMA layer. a) Film's entrance holes at 18 °C: the measured average diameter is $<d_{ent}>_{18}$ = (31.9±1.2 μm). b) Film's entrance holes at 37 °C: the measured average diameter is $<d_{ent}>_{37}$ = (18.8±1.5 μm).

A change in the temperature transition was observed from 32 °C to 29 °C. This result is also in agreement with that reported in the literature [6]. The deswelling rate wasn't affected by the introduction of the hydrophobic monomer and the shrinking ratio was found to be S = 35%, a value which is higher than that observed for the PHEPAAm10 based layers; this is probably due to the hydrophobic interaction between the side groups of the monomers, which facilitates the co-polymer shrinkage to a certain extent [7]. PNIPAAm-co-MMA layers were shown to have a stimuli-responsive behavior similar to that exhibited by PNIPAAm4x and this renders this family of co-polymers good candidates for employment as thermo-responsive cores for the realization of hybrid hydrogel smart layers.

## 5.5. Freestanding micro-patterened PHEMA/PNIPAAm hybrid hydrogel layers thermo-responsive behavior

As pointed out in 3.4.2., three methods to manufacture hybrid PHEMA/PNIPAAm layers were developed. A brief summary is reported here below:

- **METHOD 1:** this technique relied on the moulding of the PHEMA frame first and on the subsequent realization of the thermo-responsive core. The protocol showed lack of reliability and low reproducibility, so films realized with METHOD 1 were not taken into account for thermo-responsiveness tests, although a few samples produced with this method were laser machined.

- **METHOD 2:** this fabrication protocol is based on the PNIPAAm components realization first, after which the moulding of the PHEMA frame takes place. The technique was more reliable and repeatable than METHOD 1, but the inconvenience of having the thermo-responsive core partially covered by the PHEMA outer layer did not allow a high-throughput reproducible realization of the hybrid films. However, the highest quality samples obtained using METHOD 2 were laser machined using the 200 and 300 μm hole diameter mask and thermo-responsiveness characterization was carried out. The moulding technique was then improved by the introduction of METHOD 3.

- **METHOD 3:** this process is equivalent to METHOD 2 in terms of the fabrication scheme (the first step is PNIPAAm moulding, then the outer PHEMA is realized) but was more reliable and reproducible, so that the number of stimuli-responsive cores covered by PHEMA was dramatically reduced. The hybrid samples obtained with this technique were laser machined using the 1.5 mm single hole mask and then characterized in terms of thermo-sensitivity.

Thermo-responsiveness characterization of the hybrid PHEMA/PNIPAAm layers produced with both METHODS 2 and 3 are reported. The samples were analyzed in pure water as freestanding components with both the experimental setups described in 5.2. As previously pointed out in Chapter 3 and here in 5.4.1.2., all the hybrid layers were realized by employing PNIPAAm4x as the thermo-responsive component. Figure 5.17 shows the results obtained using the P.I.D. system for a 250 µm thick hybrid PHEMA/PNIPAAm film manufactured with METHOD 2 and laser machined using the 200 µm hole diameter projection mask. During the experiments, the curved side of the PNIPAAm4x could be kept in touch with the bottom of the heated PDMS container, so that good optical quality images of the pattern could be acquired for relatively low magnification (5x and 10x objectives).

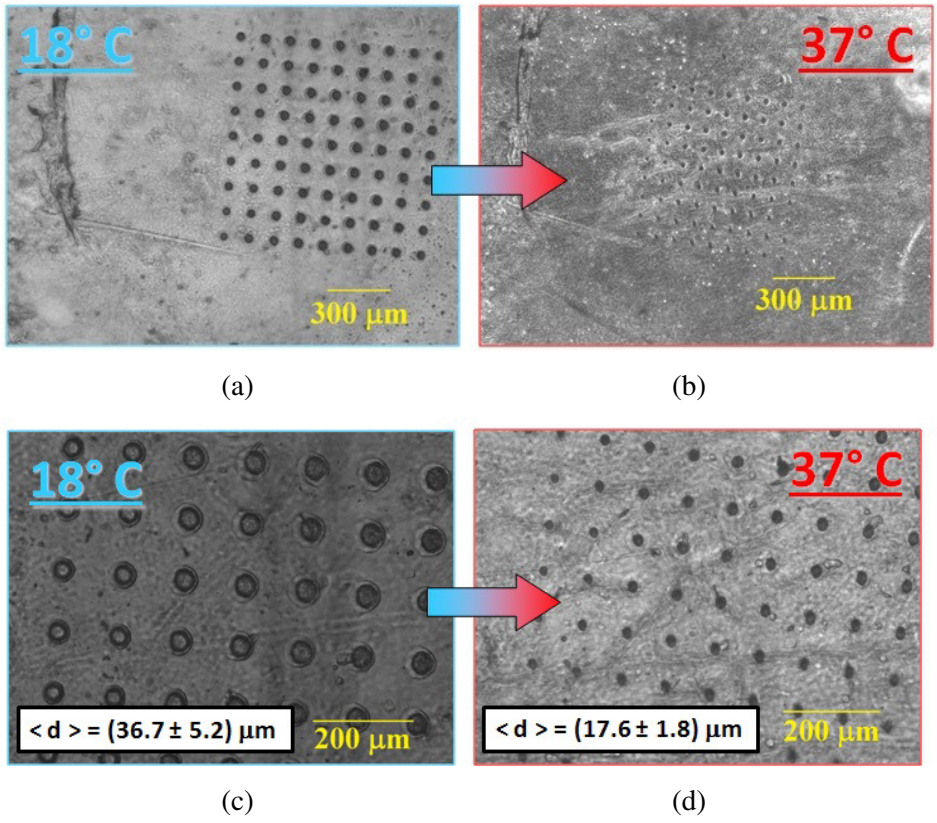


**Figure 5.17.** Inverted microscope images of a micro-patterned water swollen 250 µm thick freestanding hybrid PHEMA/PNIPAAm layer manufactured with METHOD 2. a) Entrance holes at 18 °C. b) Entrance holes after 1.5 hours incubation at 37 °C. c) Higher magnification of (a). d) Higher magnification of (b).

From the higher value of the standard deviation obtained for the hole diameter measurements at 18 °C with respect to the one obtained at 37 °C it can be deduced that a slight deformation of the pattern is induced by the PNIPAAm4x curvature due to the hydrogel swelling and that the shrinking of the thermo-responsive core after transition flattens the PNIPAAm4x layer, allowing measurements of the hole diameter with higher consistency. This behaviour, i.e. the PNIPAAm4x flattening at 37 °C, is also observed at the macroscopic level. The reduction of the machined hole size is between 50% and 40%, in agreement with the stimuli-responsive characterization of the freestanding PNIPPAm4x layers reported in 5.3.1.2. Another macroscopic effect which is caused by the transition is that the PHEMA frame tends to bend and deform along with the PNIPAAm4x shrinkage. Figure 5.18 shows a schematic view of the observed phenomenon. As will be reported in the next section, this will influence the pattern shrinkage of the hybrid layer when it is subjected to external compression.

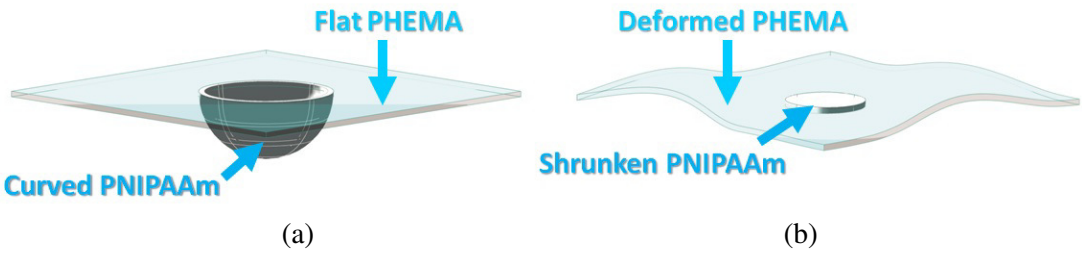


**Figure 5.18.** Schematic view of the PHEMA bending phenomenon when the hybrid layers undergo the phase transition. a) Film at 18 °C. b) Film at 37 °C. Drawing not into scale.

The bending of the elastic frame was also present when the single holed hybrid layers moulded with METHOD 3 were tested using the P.I.D. setup. However, in this case, since the machined feature is relatively small (entrance hole surface area is 0.0225 $mm^2$) compared to the dimension of the array of holes patterned on the samples manufactured with METHOD 2 (pattern surface area is 1 $mm^2$), the deformation induced by the PNIPAAm4x curvature was reduced. Figure 5.19 shows optical microscope images of a 250 μm PHEMA/PNIPAAm hybrid layer manufactured using METHOD 3 undergoing the phase transition.

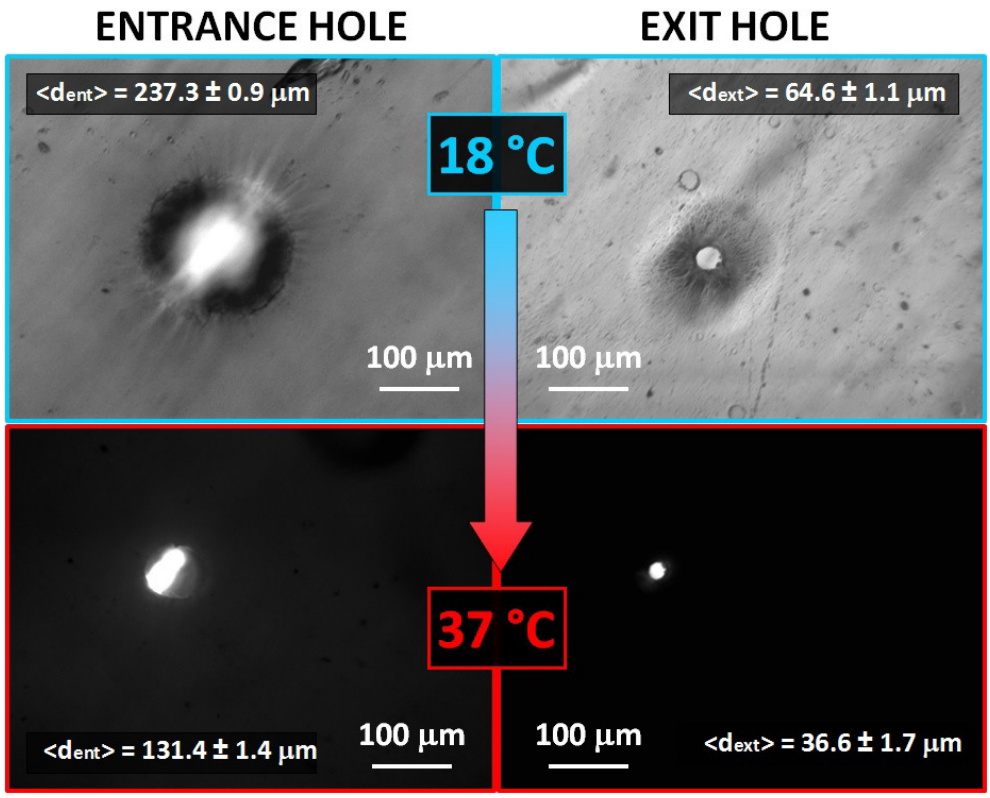


**Figure 5.19.** Inverted microscope images at 18 °C (top) and 37 °C (bottom) of a single holed 250 µm thick freestanding hybrid layer. Entrance ( left) and exit (right) holes. Measured average diameters are reported.

The observed thermo-responsive behavior of the laser machined layers manufactured with METHOD 3 can be considered the more appropriate to be exploited as the trapping and sorting actuator on-chip. In fact, they were shown to consistently preserve the shrinking ratio of the PNIPAAm4x and the high optical quality properties of the imaged features facilitated a direct real time visualization of the phase transition along the whole process both for entrance and exit hole, even for relatively high thickness values, with no significant distortions due to the PNIPAAm4x curvature below the critical temperature. As will be shown in the next section, when the single hole layers are subjected to mechanical compression of the elastic PHEMA region, there is a slight difference from this ideal situation, but these smart layers could be employed for testing the developed lab-on-chip prototype without losing their operational functionality.

## 5.6. Micro-patterened PHEMA/PNIPAAm hybrid hydrogel layers thermo-responsive behavior under mechanical constraint

This section is dedicated to a set of preliminary tests that were carried out to monitor the behavior on the hybrid PHEMA/PNIPAAm layers when clamped between two thermoplastic components designed to grip the elastic PHEMA region only. These experiments were not intended to quantitatively assess the feasibility of the hydrogels as sealing components, but to qualitatively evaluate the influence of the mechanical constraint on their thermo-responsive behavior. Specific systematic tests on their sealing properties were later carried out prior their integration on chip as will be shown in Chapter 6. As already pointed out in 3.4, PNIPAAm based material layers are not sufficiently elastic to stretch without breaking or tearing when constrained under compression (Figure 3.11); for this reason, the hybrid hydrogel layers concept was introduced and developed. The system employed for checking the effect of constraint on the hybrid films when undergoing the phase transition is the same as mentioned in 3.4.1. Briefly, two hollow PMMA slabs with axi-symmetrical aligned cylindrical through-holes at their center were sandwiched using four M4 screws and nuts to lock the water swollen PHEMA/PNIPAAm hydrogel in between them, so that compression could be exercised on the elastic PHEMA only. The three component assembly was then positioned into a water filled Petri dish so that the layers could be kept hydrated continuously. Stimuli-responsive tests were carried out by inserting the closed plate into the incubator for 1.5 hours and subsequently extracted to monitor the relaxation toward their initial state at room temperature as previously described in 5.2.2. Both layers moulded with METHOD 2 and METHOD 3 were subjected to these experiments. Since layers with thickness below 200 µm were found to be relatively fragile and difficult to handle when integrated in the assembly, hybrid films having thickness of 200 and 250 µm were characterized only. Figure 5.20 presents a schematic view of the assembly and photographs of the realized system.

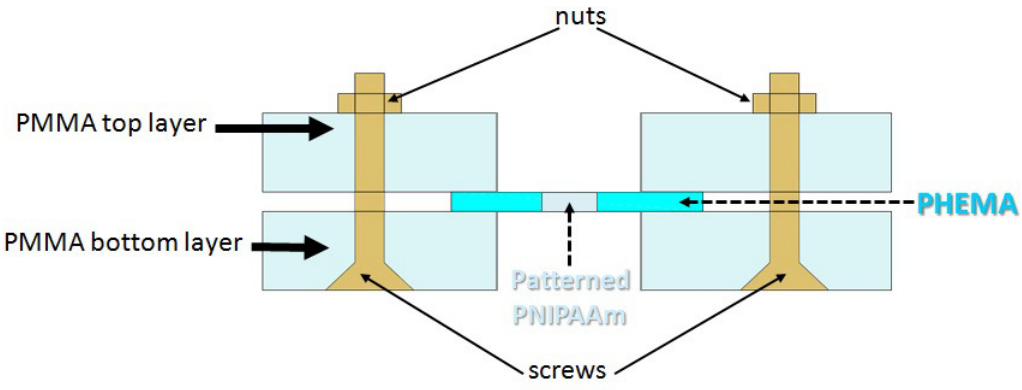


(a)

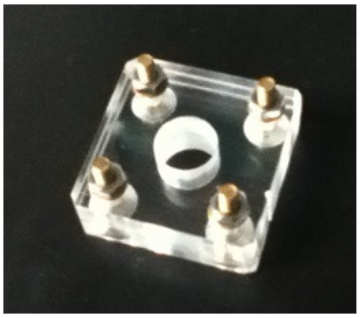

(b)

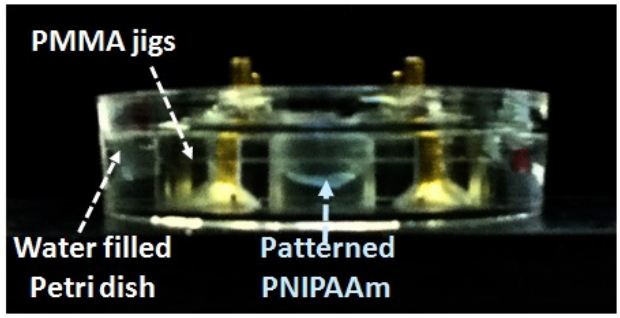


(c)

**Figure 5.20.** Experimental setup for the thermo-responsive characterization of hybrid PHEMA/PNIPAAm layers under mechanical constraint. a) Schematic view of the final assembly. b) Photograph of the PMMA jigs assembled together with M4 screws. c) Photograph of the compressed hybrid layer in the water filled Petri dish.

The homogeneous pressure applied by the screws for promoting the assembly sealing was set at 0.25 MPa using a dynamometric wrench for fastening. Figure 5.21 presnts the results obtained on a 250 µm thick PHEMA/PNIPAAm layer moulded with METHOD 2 and machined with the 300 µm hole diameter projection mask. As can be seen from the image acquired from the bottom side of the layer, the optical quality for imaging the layers at the focal plane where the exit holes are located at high magnification was poor. This situation showed up both at 18 °C and 37 °C, but the stronger distortion effects were seen above the transition temperature, when the film was less transparent and the holes shrunk.

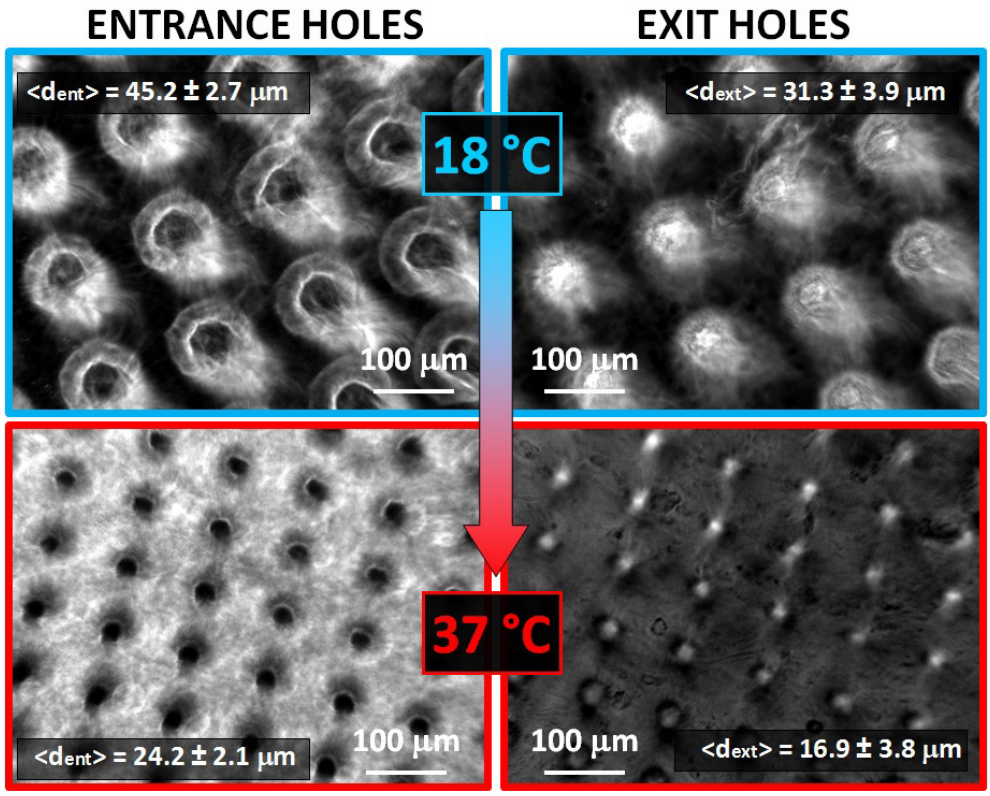


**Figure 5.21.** Inverted microscope images at 18 °C (top) and 37 °C (bottom) of a 250 µm thick mechanically constrained hybrid layer machined with the 300 µm hole diameter mask. Entrance (left) and exit (right) holes measured average diameters are reported.

Similarly, a relatively poor imaging quality was also found for the entrance holes both at 18 °C and 37 °C; this is probably due to the curvature effect discussed in 5.5. coupled with the fact that in this specific case the pattern is not in contact with the bottom of a container, but a thick water layer (around 5 mm) is interposed between the latter and the film. At 37 °C, the entrance holes are more defined, but it could be observed that the machined features, though reducing their size by about 40%, were slightly deformed and assumed the shape of an ellipse; this is probably due to the mechanical constraint which is holding the deforming PHEMA (Figure 5.18 –b) in place during the transition and thus generating anisotropic stresses that affected the thermo-responsive core and its patterned structures. This effect could be visualized in a much clearer way when single hole hybrid layers were analyzed

using the same setup reported above. Figure 5.22 shows optical microscope images of a single hole 250 µm PHEMA/PNIPAAm hybrid layer manufactured using METHOD 3 before and after 1.5 hours of incubation at 37 °C. The high quality of the imaging available for this family of layers is preserved as in 5.5. (freestanding hybrid layers); this will allow the possibility of satisfactorily monitoring the transition throughout the whole process when the hydrogels will be integrated on chip (Chapter 6).

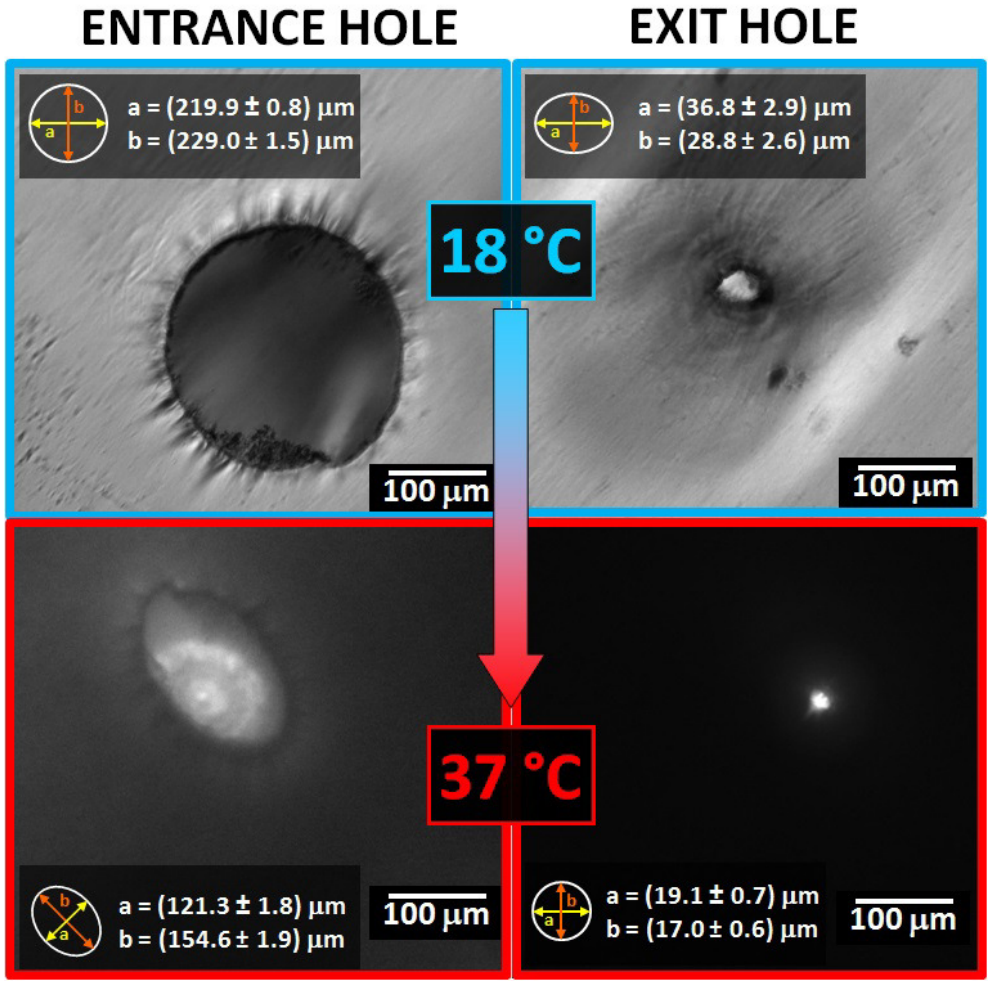


**Figure 5.22.** Inverted microscope images at 18 °C (top) and 37 °C (bottom) of a 250 µm thick mechanically constrained hybrid layer machined with the 1.5 mm hole diameter mask. Entrance (left) and exit (right) hole. Measured average diameters are reported.

The shape of both entrance and exit holes before and after the transition were affected by the PHEMA constraint, but the shrinking of the machined features demonstrates the feasibility of using these temperature triggered actuators that can be size-modulated for the trapping and sorting mechanism. In fact, according to Figure 5.22, the shrinking ratio was around 40% and 30% for the a and b axis respectively. The time required for the PNIPAAm4x core to fully recover to its initial state was comparable with the results discussed in 5.2. At this level, single hole machined layers manufactured with METHOD 3 were revealed to be best candidates for being integrated on-chip as smart self-regulating micro-structured interfaces.

## 5.7. Discussion

The experimental observations on the thermo-responsive behaviour of the manufactured PNIPAAm based layers can be compared with those reported in the literature concerning the behaviour of in-plane mechanically constrained thermo-responsive micro-printed PNIPAAm based films. Khademhosseini et al. [2], as well as Eiichi et al. [3], realized micro-patterned PNIPAAm grafted thin films, chemically anchored to solid substrates; due to the *in situ* fabrication methods employed, for these systems the deswelling mechanism was confined only to the thickness direction and an increase in the holes' diameter when the temperature was raised beyond 32 °C was observed. Conversely, fully three-dimensional swelling/de-swelling, in the absence of planar stresses at the film-substrate interface [4], allows the temperature-triggered freestanding surfaces to completely transfer their volumetric transition behaviour to the micro-features. This means that a reduction in the whole film's size does not promote an increase in the holes' geometrical dimension but rather favours their shrinkage, according to the overall macroscopic de-swelling process in agreement with the observations reported here.

The reproducible phase transition of the micro-patterned PNIPAAm layers validate the original idea of employing these promising and interesting tools in lab-on-chip systems for size-dependent sorting operation, such as filtering, or those which are engineered for

promoting cell sorting and cell isolation mechanisms for biotechnological applications. The results obtained on the thermo-responsiveness characterization of all the families of micro-patterned hydrogel layers tested are reported below. Table 5.1 summarizes the observed stimuli-responsive behavior of the freestanding films based on pure PNIPAAm and the synthesized co-polymers. Along with the relative shrinking ratio value ($S = (1 - < d_{ent}>_{37} / < d_{ent}>_{18} ) \times 100\%$), the potential to be employed as an effective temperature-triggered size-modulated interface on-chip is reported. It was arbitrarily set that layers having a shrinking ratio above 35% are considered to have a high potential for the designed lab-on-chip application.

| Hydrogel | Shrinking ratio S | Potential as size-modulated actuator |
|---|---|---|
| PNIPAAm | 50% | *High* |
| PNIPAAm-EGDMA x2 | 25% | *Low* |
| PNIPAAm4x | 40% | *High* |
| PHEPAAm10 | 30% | *Low* |
| PNIPAAm- co -MMA | 35% | *Medium* |

**Table 5.1.** Summary of thermo-responsive characterization for the micro-structured freestanding PNIPAAm based layers tested.

Pure PNIPAAm layers realized using the standard recipe were shown to have the highest shrinking ratio (S = 50%), while variation in the relative reagent amounts or the introduction of co-monomers reduced the thermo-responsiveness of the hydrogels to some extent. In this sense, the cross-linker increase (double the amount of the original EGDMA quantity) and the introduction of the hydrophilic HEMA monomer in the hydrogels (HEMA : NIPAAm = 1 : 10 mol/mol) strongly hindered the deswelling behavior when layers were subjected to the transition (S = 25% and 30% respectively). On the other hand, the incorporation of the hydrophobic MMA co-monomer in the polymeric matrix (HEMA : NIPAAm = 1 : 10 mol/mol) lowered the films shrinking ratio by only 15%, and thus represents a threshold case, in which the temperature transition is not excessively modified (S = 35%). Accelerating the polymerization reaction rate using four time the amount of initiator solution in respect to the

original synthesis conditions does not dramatically affects the shrinking performance of the layers (S = 40%); this family of hydrogels could therefore be introduced as the fundamental stimuli-responsive component for the realization of hybrid PHEMA/PNIPAAm based layers. In Table 5.2 a summary of the stimuli-responsiveness of the PNIPAAm4x based hybrid hydrogel films moulded with METHOD 2 and 3, both freestanding and mechanically constrained, is reported. The optical quality of the layers undergoing the transition, which affects their potential to be employed as temperature-triggered actuators on-chip, is also considered. High optical quality features are determined as those corresponding to entrance hole diameter standard deviation values below 2.0 μm.

| **Moulding technique** | **Mechanical constraint** | **Shrinking ratio S** | **Optical quality** | **Potential as size-modulated actuator** |
|---|---|---|---|---|
| METHOD 2 | NO | 40% | *Medium* | *Medium* |
| METHOD 3 | NO | 40% | *High* | *High* |
| METHOD 2 | YES | < 40% | *Low* | *Low* |
| METHOD 3 | YES | 40% | *High* | *High* |

**Table 5.2.** Summary of thermo-responsive characterization for the micro-structured PHEMA/PNIPAAm4x hybrid layers manufactured with both METHODs 2 and 3.

Freestanding layers moulded with METHOD 2 and machined using the 9x9 array of holes exhibited thermo-responsiveness features similar to those observed for the pure PNIPAAm4x films, but optical distortion phenomena due to the PNIPAAm4x curvature induced by the different swelling ratio of the stimuli-responsive core and the elastic PHEMA frame affected the diameter measurements. This situation did not show up when freestanding single hole PNIPAAm4x based hybrid layers were observed when subjected to temperature changes; furthermore, transition features of the responsive component were also preserved in this case (S = 40%). When a mechanical constraint was introduced by promoting homogeneous compression on the PHEMA region, employing the assembly described in 5.5., observation of the exit holes before and after transition became unreliable for the family of hydrogels

moulded with METHOD 2, at least for the film thicknesses tested (200 and 250 μm). On the other hand, the whole transition process could be monitored in real time both for entrance and exit holes when compressed single hole hybrid layers manufactured with METHOD 3 were subjected to temperature changes. The mechanical constraints affected the micro-capillary shape beyond the transition point, but the shrinking ratio remained at a value around 40% and 30% in the a and b axis of the ellipse respectively (Figure 5.22).

## 5.8. Conclusions

All the manufactured micro-patterned PNIPAAm based hydrogel layers were characterized in terms of thermo-responsiveness using two alternative techniques. The group of hybrid films manufactured with METHOD 3 and endowed with a single through-hole located at the centre of the thermo-responsive core were shown to have high potential to be employed as the self-regulated actuators in the frame of multilayer lab-on-chip systems based on different types of materials, due to their relatively high shrinking ratio (40%) and good optical quality. As previously mentioned, the designed prototype will rely on the on-chip integration of this family of hybrid layers, as will be shown and discussed in the next Chapter. It must also be observed that all the hydrogels, both the freestanding single monomer based and the hybrid layers, showed the same characteristics in terms of transition sharpness, which was always revealed to happen abruptly beyond the critical value. More specifically, the final size of the machined structures did not depend on the heating rates imposed and consistently led to the same geometrical configuration without altering the through-hole shape. When left to cool at room temperature after the transition point is reached, the relaxation of the hydrogel layers toward their initial state showed the same properties for all the polymer families realized, showing a characteristic lag time for the complete recovery of their original shape. Furthermore, different thickness of the layers and machined hole size did not affect the shrinking ratio, which rather depended on the physical and chemical properties of the hydrogels (e.g. cross-linker and initiator amount, co-monomers) and was only slightly influenced by the mechanical constraints of the films in the configuration tested.

## References


[1] Wu X S Hoffman A S and Yager P 1992 *Journal of Polymer Science: Part A Polymer Chemistry* **30** 2121-2129.

[2] Yildiz B Isik B and Kis M 2001 *Polymer* **42** 2521–2529

[3] Aranaz I Carrasco S Tardajos M G Elvira C Reinecke H Lopez D and Gallardo A 2011 *Polym. Chem.* **2** 709–713

[4] Zhang X and Zhuo X 2002 *Materials Letters* **52** 5–9

[5] Tekin H Tsinma T Sanchez J G Jones B J Camci-Unal G Nichol J W Langer R and Khademhosseini A

2011 *J. Am. Chem. Soc.* **133** 12944–12947

[6] Eiichi T Yoshiyuki Y Satoshi F Katsumi T Atsushi M Hiroyuki K Yoshiharu T Shohei Y *Chip provided*

*with film having hole pattern with use of thermoresponsive polymer and method of producing the same*

EP1942179 (patent) 2008

[7] Hong W Liu Z and Suo Z *International Journal of Solids and Structures* 2009 **46** 3282–3289

# 6. Freestanding hybrid hydrogel films integration in Lab-On-a-Chip devices

## 6.1. Introduction

This chapter is dedicated to the implementation process of the thermo-responsive excimer laser micro-machined hybrid PHEMA/PNIPAAm layers realized with METHOD 3 in multilayer lab-on-a-chip devices, to operate as temperature-triggered actuators for cell biology applications. According to the scheme reported in Chapter 1 (Figure 1.1.), the chosen target application is related to an on-chip cell trapping and sorting mechanism based on the deswelling/swelling behavior of the micro-structured hydrogel, induced by the phase transition above 32 °C. From the general point of view, the multilayer system should be sealed, relatively compact to be easily handled and provided with appropriate chip-to-the-world tubing connections both for flowing the cell suspension and for promoting suction across the hydrogel film. Another fundamental characteristic of the device is that of ensuring that microscope characterization at relatively high magnifications (20x objective at least) could be carried out having good optical quality; in this sense, limitations on the thickness of each individual layers arise. The methodology adopted to prove the feasibility of the hydrogel based micro-structured freestanding component operation on-chip was developed throughout five main points, as reported below.

1. *PHEMA mechanical characterization:* prior the implementation of the patterned hybrid hydrogel films with other micro-structured polymeric layers, mechanical properties of PHEMA under compression were investigated through compressive testing, in order to measure the ultimate strain of the material and to achieve a picture on the hydrogel behavior according to our particular recipe by extracting the compressive stress-strain relationship (6.2). Some computational aspects were also included to compare the experimental data to mathematical models based on the

hyperelastic theory; the key results of this approach will be also reported. These two sets of analysis were due to the collaboration with W. Zhao and Prof. C. Liu, from which the publication of a journal paper [1] originated.

2. *Choice of the materials:* as mentioned in Chapter 2, thermoplastics are suitable materials for the realization of micro-fluidic components. The advantage of using these polymers, such as PMMA, for the stacking system layers fabrication firstly dwells in the vast options available for machining them, either mechanically (e.g. micro-milling [2]) or with laser based techniques (e.g. $CO_2$ laser [3]) as well as in their transparency which allows a real time optical microscope visualization of the processes taking place in the chip. The convenience of using PMMA for micro-fluidic components realization is also reported in literature [4]; both the device employed for preliminary leakage tests (6.3) and the final sorting prototype (6.4) will be realized using this material as the 'hard' component.

3. *Identification of the appropriate system packaging technique:* the main requirement for developing hybrid multilayer micro-fluidic devices having the realized micro-structured PHEMA/PNIPAAm based components integrated as autonomous actuators is to identify a packaging strategy which would allow multiple disassembly and re-assembly by the user, so that the costs and efforts for rapid prototyping would be minimized. In other words, the bonding between the hydrogel layers and the other components of the device should not be permanent, but should have reversible features. Furthermore, a bonding technique that could be carried out at room temperature and without involving the employment of solvents or adhesives could also be suitable. The method that was developed for integrating freestanding hydrogel layers in LOC micro-devices was then based on mechanical fastening, using a system of bolts and nuts to promote reversible compression and sealing of the components. This conventional assembly technique, which has been extensively used in various industrial applications, in particular for large component construction (e.g. aircraft), presents a number of advantages that can be summarized as follows:

- Ease of manufacture of the individual layers before assembly; compression moulding for hydrogel film fabrication and micro-milling for machining thermoplastic platforms are reliable and reproducible strategies for component fabrication. Injection moulding could also be considered for the hard material platform realization for other thermoplastics (e.g. polystyrene, cyclic olefin co-polymers).
- Bonding/assembly takes place in a relatively low temperature environment since no heating is required for.
- A user defined and user-friendly approach to enable different degree of joint tightening is available, thereby the system can be subjected to different internal pressures, required for specific applications.
- The possibility of easily disassembling and reassembling the system allows easy replacement of the hydrogel film, without changing any other component.
- The manufacturing and packaging processes are free of contaminations and can be implemented in a clean environment; no glues or chemicals which exhibit toxicity to cells are involved.
- UV sterilization procedure could be easily carried out directly on the packaged device.

4. *Leakage tests:* various challenges arise when it comes to apply mechanical fastening as the assembly technique at small scales; in particular, providing an effective sealing (or isolation) through an optimum management of the layers packaging compression in respect to the flowing fluid pressure is critically important in order to prevent liquid leakages in any part of the system, which could lead to its malfunctioning or to unreliable measurements. For this latest reason, leakage tests to assess the feasibility of the hydrogel component to operate as a gasket in sealed stacking micro-fluidic devices were carried out using a test micro-system that was designed and realized. More specifically, the test device was used for implementing PHEMA hydrogel membranes, with thickness ranging from 100 to 220 μm, with two PMMA components, which present micro-milled fluidic circuits on the surface that seals the

soft polymer sheet. The optimization of the mechanical fastening technique proved through these leakage tests gave birth to two conference papers ([5], [6]) in collaboration with W. Zhao and Prof. C. Liu.

5. *Cell sorting prototype design and test:* a four component micro-fluidic device prototype having the sealed smart actuators integrated using a system of bolts and nuts was realized and tested as it will be discussed in details in section 6.4. It must be underlined that although the original idea of the device for the target application, as it was expressed in the introductive part of the thesis (Chapter 1), should require a minimal use of equipment in its optimized version, the developed prototype is relying on the use of a bulky support instrumentation for demonstrating the trapping/sorting proof of concept. Moreover, the experiments conducted for proving its functionality limit to the determination of the best conditions for promoting the temperature-triggered mechanism (i.e. handling the cell line by mean of the size-modulating micro-structures) and do not aim to probe cells viability of the sorted sample or to asses long-term stable repeatability features in the system performance at this stage. MG63 cells were used as the biosample to be sorted and the feasibility of the hydrogel based layers as smart micro-structured actuator integrated in the prototype could then be assessed.

## 6.2. Mechanical characterization of PHEMA layers

Although the compressive behavior of PHEMA has already been experimentally analyzed and reported in the literature [7], since hydrogel based material mechanical properties are very sensitive to variations of the reagents' relative amounts as well as to reaction conditions, compression testing was carried out on PHEMA samples synthesized with the recipe employed for hybrid film fabrication as reported in 3.2.2.2. The target of these experiments was to identify the ultimate strain value the polymer could undergo before mechanical failure occured when subjected to uni-axial compression; the determination of this threshold was fundamental to carry out the PHEMA layer integration with the PMMA components using mechanical fastening without damaging the film. Experimental results on the compressive behavior of the hydrogel were then used to select the most appropriate description of PHEMA under compression based on two different mathematical models implemented using the acquired stress-strain data. Since the computational aspects and the modeling of the material are not strictly related to the present thesis work, a brief summary of the main ideas underlying the analysis and the relative results will be reported, while a detailed description of the whole simulation procedure and mathematical tools involved can be found in [1].

### 6.2.1. PHEMA compressive tests

#### 6.2.1.1. Sample preparation and experimental setup

Due to the sensitivity of the compression testing machine (positional accuracy could reach up to $\pm 0.05\%$), using a thin film (100 to 200 μm thick) as the test sample would be problematic because of the intrinsically small compression displacement involved, which could not be recorded accurately because of the apparatus resolution (10 μm was the minimum displacement that could be read). Therefore, PHEMA samples in this experiment were produced as thick cylinders, without any affect on the geometry independent mechanical features to be measured. PHEMA samples were produced by injecting the polymerizing

mixture prepared as reported in 3.2.2.2 into punched silicone rubber moulds; two flat polished aluminium layers were employed to close the system on both sides using a clamping system, thus conferring the proper cylindrical geometry to the solidifying hydrogel. The complete polymerization and cross-linking of the material took place in less than 2 hours, according to 3.4.2.1, then the shaped polymer could be extracted from the moulds. In order to investigate any geometrical effects that could possibly affect the compressive behavior of the hydrogel, two different moulds were employed; cylinders with 18 mm and 32 mm diameter, both with the same thickness (12.5 mm), were fabricated and used. After extraction from the moulds, samples were washed in an ethanol aqueous solution to remove the unreacted monomer and then swelled according to the protocol reported below. Hydrogels were firstly kept in a 50% ethanol aqueous solution and the ethanol concentration was then gradually reduced to 30% and 10% by adding water to the mixture after 4 and 8 hours respectively, until the sample could be completely soaked in pure water. Normally, the bigger the sample is, the more sensitive to the ethanol concentration changes it is and this would require the solvent rinsing to be slower and milder; for this reason, sample preparation protocol took up to 3 weeks, showing a time consuming but effective route for sample preparation. An Instron Series 3366 Model universal testing machine, equipped with 2kN load cell, was used for measuring the mechanical properties of PHEMA hydrogel samples under compression. The position accuracy is ensured by a screw-driven actuator and, as previously mentioned, it could reach up to $\pm 0.05\%$ of displacement display reading, while loads could be measured to within $\pm 0.5\%$ of the indicated force at $25\ ℃$. This accuracy is accepted as a reasonable value for flexible hydrogel compression testing [7]. To preserve swelling and hydration conditions of hydrogels, tests were conducted in an aqueous environment. The experimental setup (Figure 6.1) consisted of the actuator (load cell), sample (PHEMA cylinder), water container (polystyrene dish) and the stage (testing machine fixed plate).

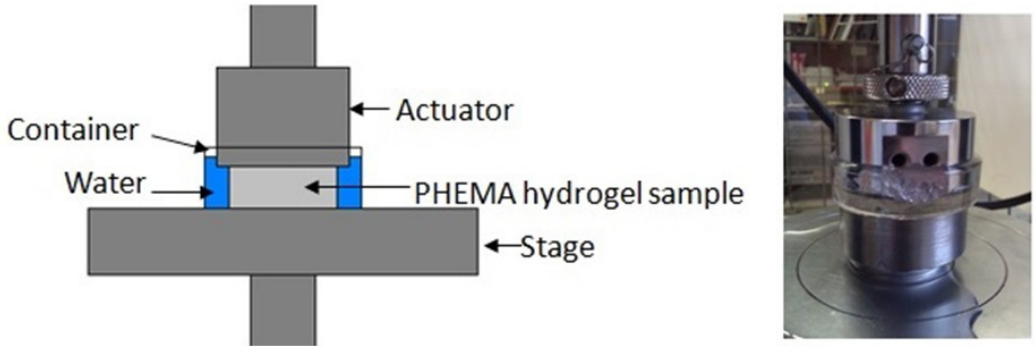


(a) (b)

**Figure 6.1.** Experimental setup for PHEMA mechanical testing. a) Schematic view of the equipment employed. b) Photograph of a PHEMA sample undergoing compression tests.

The water filling the container offered the proper aqueous environment for hosting the PHEMA hydrogel samples during the whole testing process. A compressive force was applied at 6 mm/min until the sample break point was reached; the establishment of this situation was reflected by the beginning of a non-smooth region of the curve in compressive stress vs compressive strain graph, as will be shown in section 6.2.1.2. The goal of the experiment was to extract the stress-strain relationship up to the point where the ultimate strain was reached. On the basis of ideal compression theory [8], compression stress has to be read in a slow-speed static testing condition frame, in order to reduce the affect on the measurements caused by the damping of the material. Therefore, the time to reach the maximum strain of the specimen was set to 120 sec, while the corresponding speed was 100 $\mu m/s$. According to this speed of testing, compressive loads (N) versus compression (mm) values were recorded by the data acquisition system (50 sets of data per second). It must be considered that the surfaces of the hydrogel in contact with the actuator or with the bottom of the container could expand because of the material Poisson's ratio, thus bringing undesired boundary stresses or machine deflections, which may affect the accuracy of the results. In order to minimize these effects, a Dow Corning silicone based lubricant was applied on the PHEMA cylinder base during testing; the compound is moisture resistant and is highly water repellent and it does not affect the actual measurements [9].

### 6.2.1.2. Results

Compressive stress-strain curves for the PHEMA samples are shown in Figure 6.2; engineering stress-strain were chosen as the relevant variables to reduce the affect of the sample size on the data by normalizing the diameter difference. The graphs show that the ultimate engineering strain could be approximately 45% for the 32 mm diameter sample and 55% for the 18 mm diameter sample, as revealed by the non-smooth profile of the curves ('sample failure' points), corresponding to an ultimate yielding strength of 0.45 MPa to 0.7 MPa respectively.

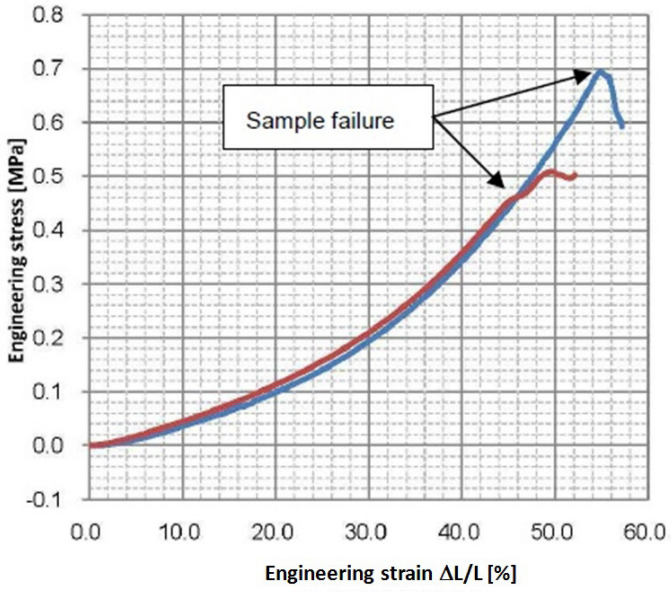


**Figure 6.2.** Engineering stess-strain curve for the moulded hydrated PHEMA cylinders under compression. The blue line refers to the 32 mm diameter sample, while the red one is for the 18 mm diameter one. L is the cylinder thickness.

## 6.2.2. Hyperelastic behavior of PHEMA

PHEMA hydrogel is considered as a hyperelastic solid at room temperature, with features similar to rubber. In order to simulate the behaviour of PHEMA under mechanical deformations, in the specific case of uni-axial compression, a hyperelastic model can then be reasonably used [10]. According to the hyperelastic theory, there are several constitutive laws that could be employed. In the present analysis, two widely used models were taken into account and compared: the Mooney-Rivlin (MR) model [11,12] and Neo-Hookean (NH) model [13], which offer a numerical solution for analyzing hyperelastic materials behavior. Without entering into details of the calculation and of the mathematical theory involved (which are extensively reported in the collaborative paper published with Zhao and Liu [1]), the engineering stress-strain curves obtained from the compressive tests were compared to the ones obtained by solving the MR and NH models' constitutive equations using the COMSOL Multiphysics software to obtain a simulation of the polymeric material behavior under compression. In order to make the comparison between the experimental data with the MR and NH simulations more quantitative, the analysis of mean squared error (MSE) was included in the calculation [1]. The comparison between stress-strain curves derived from the compression experiments and the simulations for both the specimens tested are reported in Figure 6.3 and 6.4 for the 18 mm and 32 mm diameter samples respectively.

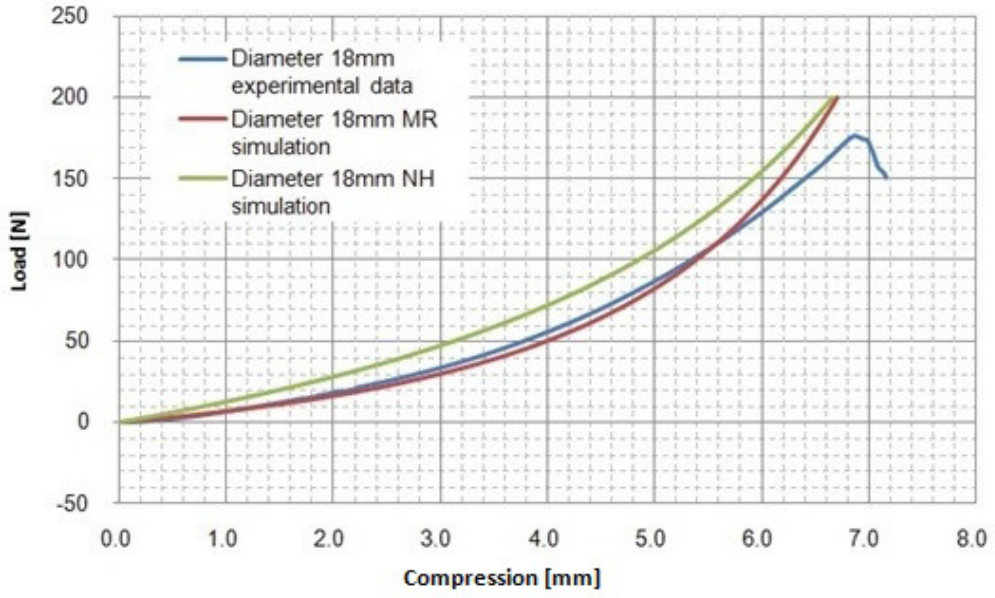


**Figure 6.3.** Comparison between the experimental results obtained from the compression tests for the 18 mm diameter sample and the Mooney-Rivlin and Neo-Hookean models.

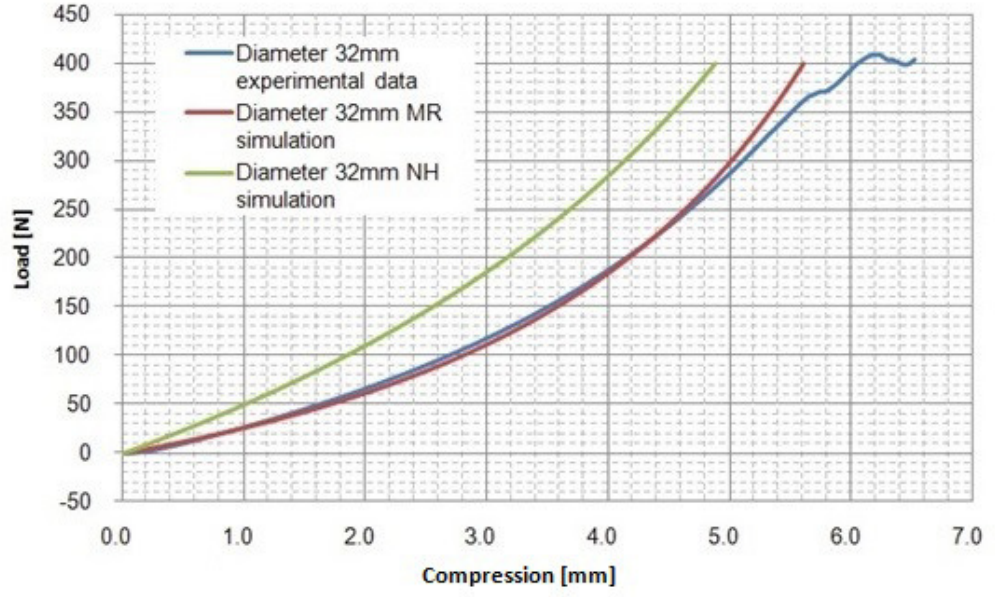


**Figure 6.4.** Comparison between the experimental results obtained from the compression tests for the 32 mm diameter sample and the Mooney-Rivlin and Neo-Hookean models.

At this level, the MR model was revealed to be reliable for describing the response of PHEMA hydrogels to compressive deformations, since the accuracy between the experimental data acquired and the simulation points generated by applying MR could be kept within 5%. For this reason, thanks to the collaboration with W. Zhao, the behavior of PHEMA hydrogel layers undergoing uni-axial compression could be modeled prior to the on-chip integration tests. The setup and results of the simulation are reported in the next section.

### 6.2.3. Modeling PHEMA films under mechanical constraint

The MR model was used to simulate the compressive response of a 250 μm thick PHEMA hydrogel layer in order to provide information on how the stress induced by compression of the film could affect the region located at its the center. This information was useful to understand whether the compressive strain of the elastic frame could affect the thermo-responsive core located at the central region of the PHEMA/PNIPAAm hybrid hydrogel layer when assembled in the prototype. More specifically, thermo-responsive tests carried out on the hybrid film under mechanical constraint were already discussed in 5.6. and showed that uni-axial compression of the PHEMA caused a non-isotropic deformation of the machined hole when temperature was increased above the transition threshold. According to the set up employed for these tests (PMMA jigs, reported in Figure 5.20) and to the final prototype design that will use a similar geometry (as described in 6.4.1) the component dimensions and configuration considered for modeling were chosen as described below. The hydrogel layer is a 22 mm diameter 250 μm thick cylindrical layer of hyperelastic PHEMA, fixed on a rigid support consisting of a hollow disk, having the same outer diameter and a 10 mm diameter through-hole at its center. A second disk, having the same dimensions and characteristics of the one acting as a substrate, is considered to compress the hydrogel layer promoting a fixed value of the soft material compressive strain. In the static configuration, when PHEMA is sandwiched between the hollow cylinders, the MR model is employed to predict the material response in terms of compressive stresses along the radial and zenithal direction of the hydrogel disk by running a simulation using COMSOL Multiphysics, with mesh size, boundary conditions, geometrical domain symmetry and other simulation parameters chosen according to [1]. Figure 6.5 shows a 3D representation of the configuration and set of

coordinates employed for simulating PHEMA behavior under compression, as well as the resulting stress-strain curves along the radial and zenithal axis as functions of the r coordinate which were obtained by fixing the strain values equal to 10 and 20% of the initial value of the layer thickness.

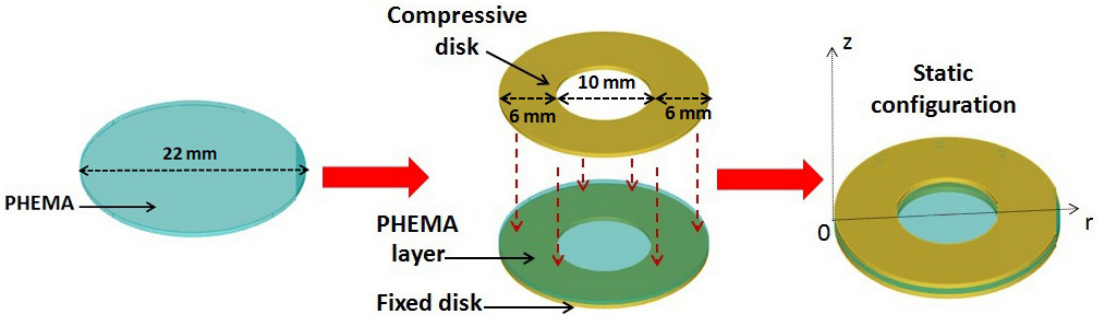


(a)

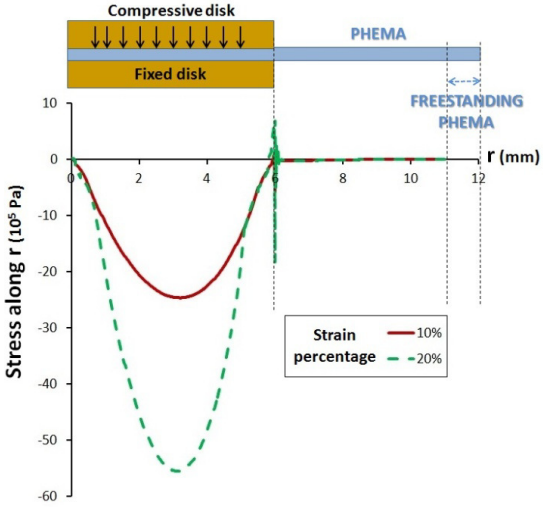


(b)

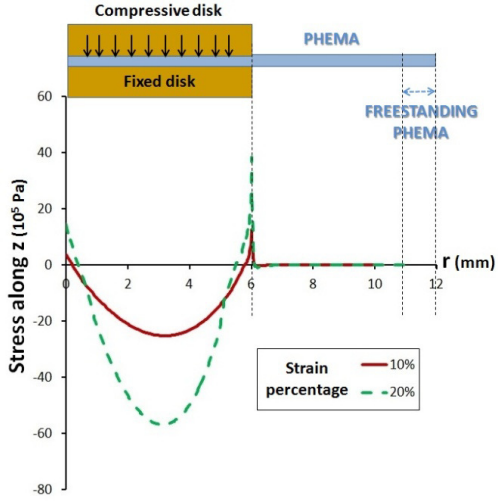


(c)

**Figure 6.5.** Schematization of the spatial configuration used for modelling the PHEMA hydrogel behaviour under mechanical constraint. a) 3D reconstruction of the assembly. b) Stress along the radial direction induced by the compression exercised on the hydrogel as a function of radial distance. c) Stress along the zenithal direction induced by the compression exercise on the hydrogel as a function of radial distance.

As shown in the stress-strain curves in Figure 6.5-b and c, both radial and zenithal stresses showed a peak in the middle region of the compressive disk ($0 < r < 6$ mm); the corresponding Von Mises stress values, to be compared with the ultimate strength thresholds identified in 6.2.1.2. are 0.05 and 0.21 MPa for 10 and 20% strain respectively, which are both below the failure regime of the sample. For $r > 6$ mm, both the stress profiles reduced rapidly to very low values and beyond 11 mm reduced to zero. Considering that the hybrid PHEMA/PNIPAAm layers moulded with METHOD 3 and employed for thermo-responsive tests under constraint, as well as the ones that will be integrated in the sorting prototype, are endowed with a 6 mm diameter circular thermo-responsive region located at the centre of a 22 mm diameter PHEMA frame, the results obtained from the simulation show the influence of the mechanical constraint on the PNIPAAm region in the static assembly. More specifically, compressive radial and zenithal stresses are both lower than 100 Pa for $r > 8$ mm, while they are extremely low when approaching the centre of the hydrogel disk, showing to be lower than 20 Pa for $8.5 \text{ mm} < r < 11$ mm and lower than 5 Pa for $r > 11$ mm. Having separate information about the PNIPAAm compressive stress-strain curves would help to give a more detailed picture of the effects induced by mechanical constraint on the hydrogel, but the obtained results can be considered satisfactory for a semi-quantitative analysis of the hybrid layers when PHEMA is undergoing compression, using a configuration which is recalling both the experimental setup used in 5.6 and the prototype geometrical features.

## 6.3. Freestanding hybrid hydrogel layers integration on-chip: mechanical fastening and leakage tests

### 6.3.1. General and experimental approach

This section is dedicated to the reversible compression based packaging technique of mechanical fastening, able to promote sealing between micro-fabricated thermoplastic components and freestanding thin hydrogel films for the realization of hybrid material cell-based multilayer microfluidic devices. A leakage test device micro-system (LTD) was realized in order to evaluate the reliability of the technique in implementing PHEMA hydrogel layers, with thickness ranging from 100 to 220 μm, with PMMA components that included micro-milled fluidic circuits on the surface that sealed against the soft polymer sheet. Coloured dye aqueous solutions were continuously pumped into the PMMA micro-fluidic structures at different flow rates and any liquid leakage at the interface between the materials was observed near the conduits by optical microscope imaging, showing that the packaging technique was suitable for typical liquid pressure values developing in perfused lab-on-a-chip devices.

### 6.3.2. Leakage tests

#### 6.3.2.1. Device design and experimental setup

A representative scheme of the core of the mechanical fastening technique employed for leakage tests is reported in Figure 6.6. The functional microfluidic chip components are top and bottom thermoplastic layers, a freestanding hydrogel membrane and a metallic frame that operates as a rigid spacer between the plastic parts. A system of screws is set around the hollow region defined by the spacer hosting the soft polymer membrane. The thickness difference between the hydrogel membrane and the spacer is a fixed value (Δt), thus

compression can be controlled when the system is assembled by controlling the hydrogel thickness. The interface between the plastic top component and the hydrogel film is therefore properly sealed such that the microfluidic structures machined in the hard polymer slab can endure continuous liquid flow with no leakage.

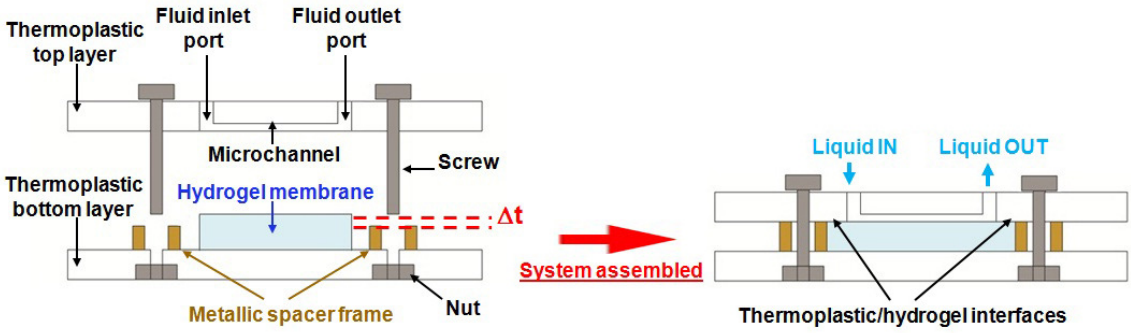


**Figure 6.6.** Schematic diagram of the mechanical fastening technique for LTD realization. The hydrogel film is positioned over the thermoplastic bottom layer, at the centre of the metallic frame (left); Δt represents the thickness difference between the spacer and the soft polymer membrane. The assembly is then sealed by screwing the plastic components together (right).

To realize the actual LTD employed for visualizing possible liquid leakages at the thermoplastic/hydrogel interfaces, 3 mm thick PMMA slabs were micro-milled with a computer numerical controlled (CNC) routine in the mechanical workshop of the Physics department in Milan. Rectangular cross-section micro-channels (1 mm width, 500 μm height) were machined on the bottom surface of the thermoplastic top layer with a precision within 3%; micro-channel lengths varied according to the different geometries of the circuits and the whole fluidic structure was machined in order to cover a surface area of (30 x 20 $mm^2$). Three different geometries were milled to check possible anomalous liquid leakage behavior. Inlet and outlet fluidic ports were machined with 3 mm diameter and threaded to host tubing connectors. Around the primary fluidic circuits (‘fluidic channels’), circuits of the same geometrical features embracing the whole perfused liquid path (‘sink channels’) were milled with a side-to-side offset of 500 μm from the fluidic channels, in order to easily collect any

fluid that leaked at the interface (Figure 6.7). Through-holes for hosting the sealing screws and reference dowel pins for alignment were also machined.

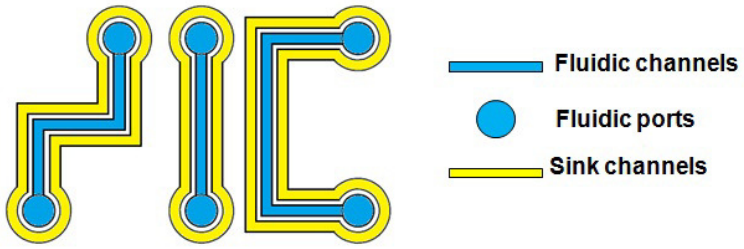


**Figure 6.7.** Schematizatic diagram of both fluidic and sink channels. The two classes of circuits are separated by a side-to-side distance of 500 µm. Fluidic ports are also shown.

The metallic spacer frames for controlling the PHEMA strain during compression were made of brass with thickness ranging from 70 to 200 µm and were milled in order to be aligned to the PMMA components in such a way that the hollow region of 30 x 20 $mm^2$ present at the centre could hold the hydrogel film. Taking into account the ultimate engineering strain values identified from the compressive tests reported in 6.2.1.2 (from 45% for the 32 mm diameter sample to 55% for the 18 mm diameter sample), and the corresponding values of the ultimate yield strength (0.45 MPa to 0.7 MPa respectively), the $\Delta t$ between PHEMA and metallic spacer was always kept below 40% of the film thickness, in order to ensure that no sample mechanical failure took place when sealing the LTD. Two aluminium jigs were also fabricated to avoid the PMMA cracking due to the high compression values reached during tests; both components presented an optical window with the same linear dimensions as the region defined by the hydrogel film, in order to allow optical microscope observations. The pressure range applied by the screw system for promoting sealing was from 0 (no sealing) to 0.35 MPa. However, a value of 0.25 MPa was set as a threshold in order to avoid deformation of the metal spacer and to minimize bending effects that would curve the PHEMA at the bottom of the fluidic structures toward the inside of the channels. The complete configuration schemes of the hydrogel films employed with the relative metallic spacer thickness is reported in Table 6.1. Each leakage test was carried out two times for each set.

| *PHEMA film thickness (µm)* | *Spacer thickness (µm)* | *Compression (kPa)* |
|---|---|---|
| 100 | 75 | 250 |
| 120 | 100 | 200 |
| 200 | 175 | 150 |
| 220 | 200 | 100 |

**Table 6.1.** Summary of PHEMA layers and corresponding brass-based spacer thickness employed for leakage tests using the LTD.

Figure 6.8 shows the process of LTD assembly; the system could be easily aligned due to the presence of reference dowel pins.

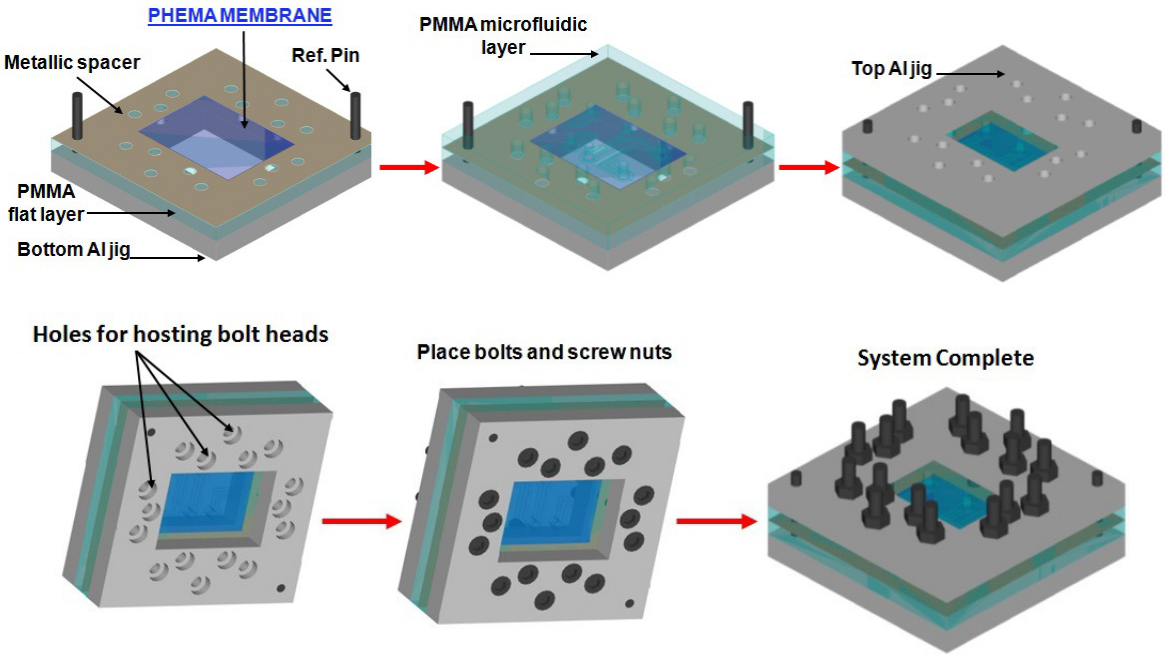


**Figure 6.8.** 3D model of the actual LTD assembly process previously shown in Figure 6.6. The aluminium jigs were introduced in order to avoid breaking or damaging of the PMMA components during mechanical fastening.

Threaded fluidic connectors (SMC) were screwed to the LTD's fluidic inlet and outlet ports and could host 2 mm outer diameter polyurethane tubes. A diaphragm micropump (ThinXXs microtechnology) was connected to a reservoir containing red colored dye (E122-Azorubine) aqueous solution (25 mmol) and the volumetric flow rate was varied in the range from 10 µL/min to 10 mL/min, according to the pump's duty cycle. In order to give a quantitative analysis of the resulting leakage tests, the volumetric flow rate values (Q) employed and the corresponding pressure differences ΔP expected to be developed in the channels in respect to the atmospheric pressure considered in the static configuration are reported in Table 6.2. ΔP values are calculated according to the fluidic resistance of each micro-channel, as reported in [14].

| **Q = (ml/min)** | **0.1** | **0.5** | **1.0** | **3.0** | **5.0** | **10.0** |
|---|---|---|---|---|---|---|
| **Channel 1(left): ΔP (Pa)** | 3.81 | 19.0 | 38.1 | 114 | 190 | 381 |
| **Channel 2 (middle): ΔP (Pa)** | 2.82 | 14.1 | 28.2 | 84.5 | 141 | 282 |
| **Channel 3 (right): ΔP (Pa)** | 5.46 | 27.2 | 54.6 | 134 | 272 | 546 |

**Table 6.2.** Volumetric flow rates and expected pressure differences for the three microchannels tested during leakage experiments. Left, middle and right labels refer to the fluidic conduits shown in Figure 6.7.

Leakage tests took place at room temperature on the stage of an inverted optical microscope. Since typical values of the fluid pressure developed in microfluidic systems range from < 1 Pa to hundreds of kPa [15], the experimental set up configuration was considered reliable for reproducing the behavior of a wide family of perfusion micro-systems. The average duration of each test was around 30 minutes for each of the flow rate values explored and no further characterization was carried out to explore long-term stability effects on the hydrogel components; this is due to the fact that the cell-sorting prototype based on the hybrid PHEMA/PNIPAAm film developed is conceived to be operating over a time of < 30 min.

### 6.3.2.2. Results

The principal focus of these leakage tests was to identify a range of pressure which could be endured by a water swollen PHEMA film operating as a gasket element when interposed between two harder PMMA based polymeric layers. Figure 6.9 shows a picture of the LTD's central straight micro-channel perfused with the dye solution pumped at the maximum flow rate. Real time microscope images were acquired every 30 seconds. No leakages were observed, as shown from the microscope images reported in the inset of Figure 6.9. The PHEMA film employed in this case was 100 µm thick, while the metallic spacer thickness was 75 µm. Sealing compression value was therefore 0.25 MPa.

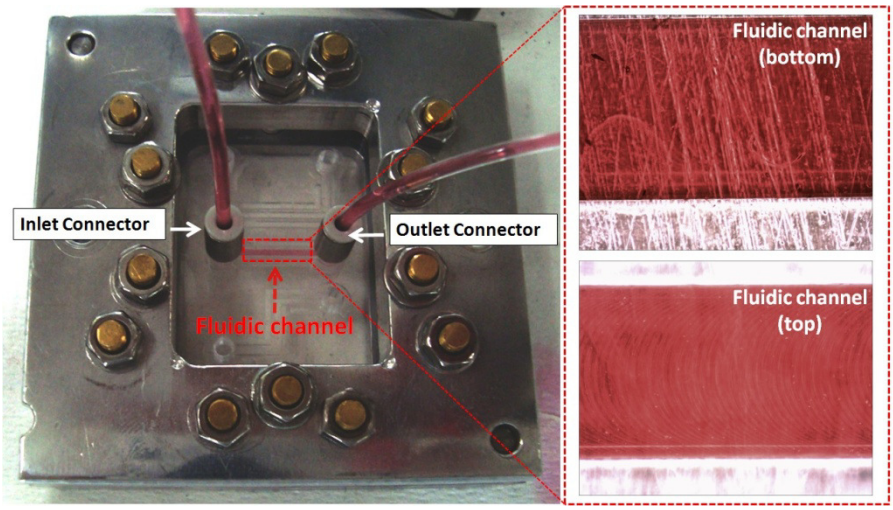


**Figure 6.9.** Perfusion test in the straight fluidic channel located at the centre of the LTD. A photograph of the experimental setup is reported (left). On the right hand side of the picture, microscope images of the coloured liquid filled fluidic channel are shown, focussing both at the PHEMA/PMMA interface (top) and at the top of the micro-milled channel (bottom).

The other micro-fluidic circuits were tested under analogous operating conditions and showed similar behavior for the flow rate values tested (0.1, 0.5, 1.0, 5.0, 10.0 mL/min). Liquid leakage was monitored both in the sink channels and at the interface between PMMA and PHEMA. No dye traces were observed in any of those regions of the device for all the

fluidic regimes explored, thus confirming that mechanical fastening is a suitable packaging solution in respect of these hybrid material platforms. Figure 6.10 shows the LTD with all of the micro-channels filled after being perfused at 10 mL/min.

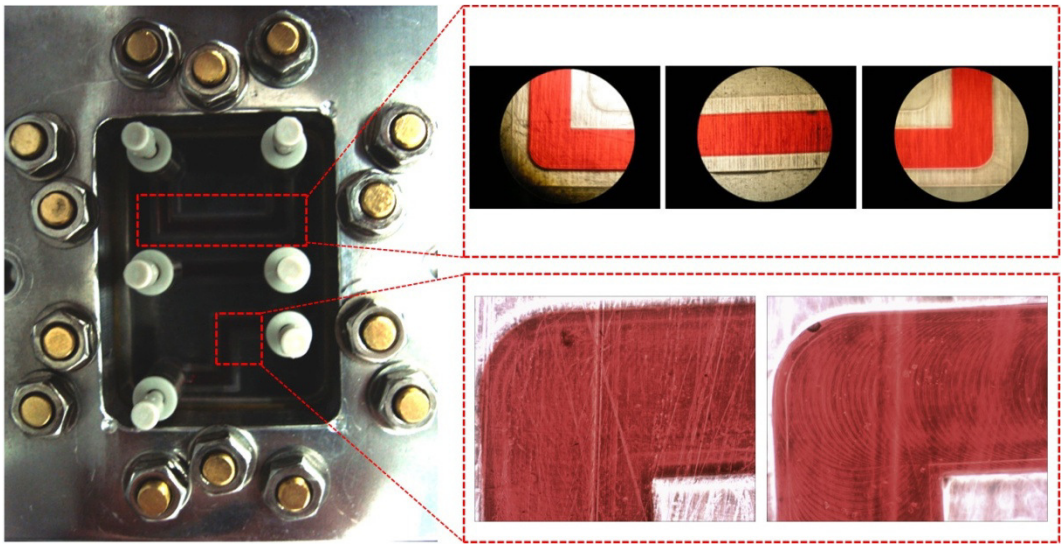

**Figure 6.10.** LTD after perfusion test in all the fluidic structures. A photograph of the liquid filled device is reported (left). On the right hand side of the picture, microscope images of the fluidic channels are reported, focussing both at the PHEMA/PMMA interface (top row and bottom left) and at the top of the micro-milled channel (bottom right).

During tests, the tight joint between the different material layers, as well as the fluid flow and contextual diffusion of liquid in the hydrogel matrix, prevented the film from dehydrating, thus preserving its water-swollen state properties. After disassembling the system, no significant traces of embossing on the PHEMA membrane due to compression contacts with the micro-channels milled on the PMMA were observed, thus suggesting that no relevant deformation of the film took place within the fluidic microstructures because of the system bonding.

# 6.4. Prototype temperature-triggered cell-sorting-on-chip

In this section, the cell-sorting prototype based on hybrid PHEMA/PNIPAAm hydrogels and thermoplastic components will be discussed in terms of design, operational principle and functionality. Trapping and sorting tests carried out using MG63 cells will be then reported and discussed.

## 6.4.1. Design of the device

As already mentioned in Chapter 5, the hybrid hydrogel layers that will be implemented in the chip are endowed with a single micro-hole, laser machined at the center of the PNIPAAm core, with the exit hole (diameter ranging from 25 to 60 μm at room temperature) acting as the trapping site for the cells and having a relatively large entrance hole (220 μm diameter at room temperature) operating as the end of the via through which the trapped cell is released into the bottom chamber. Since at the present stage the best manufacturing conditions, in terms of repeatability, consistency and reliability, that were determined for moulding the hybrid layers using METHOD 3 (3.4.2.3) allow the realization of a circular thermo-responsive core having a diameter of 6 mm in the swollen state, the dimensions of the fluidic chambers for cell flowing and collection machined on the thermoplastic components were dimensioned accordingly. Based on all the basic requirements and taking into account the fabrication limitations, the resulting prototype was designed as a stacking four component micro-system. A 3D model of the system layers and their assembly using mechanical fastening is reported in Figure 6.11. The multilayer chip comprises (from bottom to top in the stacking):

- A transparent heater
- A bottom PMMA component (for applying suction and for collecting the sorted cell)
- A single hole hybrid PHEMA/PNIPAAm hydrogel (smart sorting actuator)
- A top PMMA component (for injecting and flowing the cell suspension)

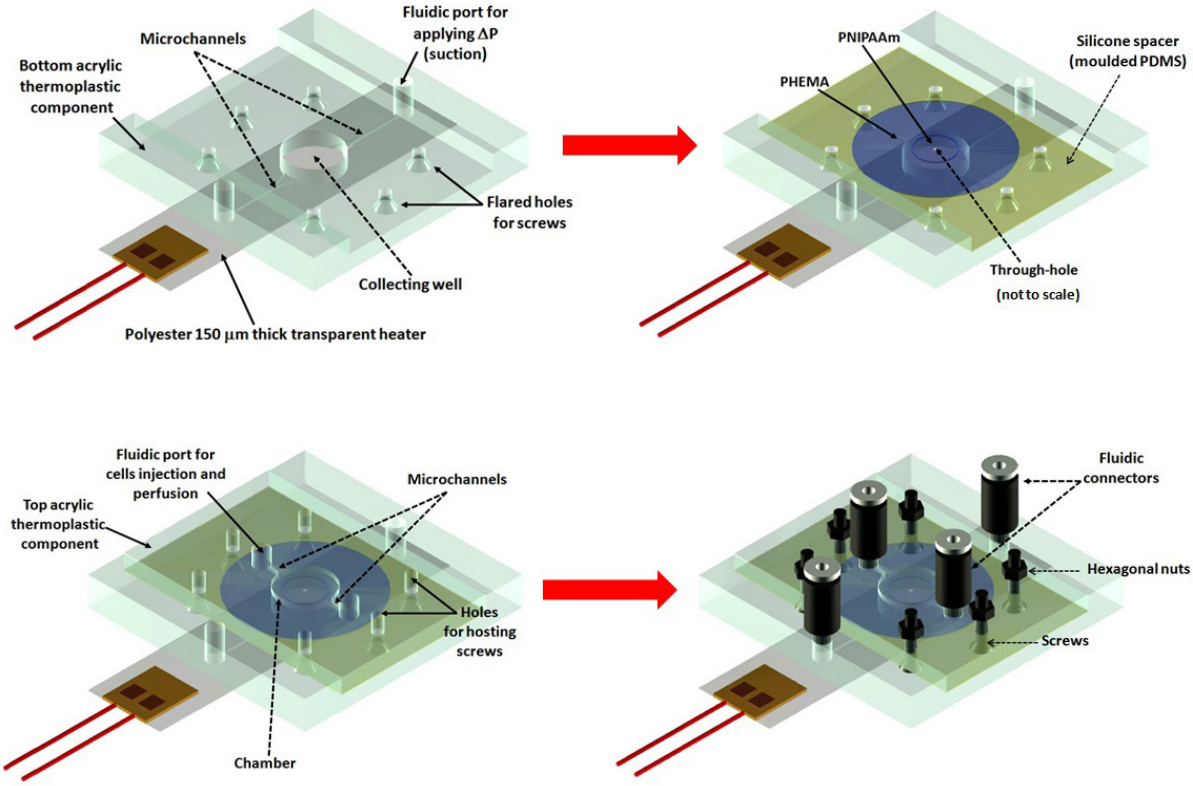


**Figure 6.11.** 3D model of the prototype components and assembly process. Drawings are to scale, unless reported otherwise.

Each layer of the system and its functionality are described below.

1. *Transparent heater:* an external heating element of the same type as the one employed for thermo-responsiveness tests using the P.I.D. (5.1.) constituted the basis of the stacking device. It was connected to a variable voltage power supply and promoted the temperature of the system to increase and stabilize at 37 °C. To confer higher robustness to the thin resistor, it was embedded in a PDMS slab using a moulding procedure similar to the one employed for realizing the thermostatic bath (5.1.) The resulting layer had a thickness of 1 mm, having the heating element fixed at its center.

2. *Bottom PMMA component:* a 45 x 45 $mm^2$ and 6 mm thick acrylic thermoplastic layer providing the chamber for collecting the sorted cell and the connecting fluidic conduit for applying a pressure difference across the hydrogel film was micro-milled. The micro-fluidic structure on one of its surfaces comprised a 38 mm long straight rectangular cross-section channel (height x width = 0.5 x 0.5 $mm^2$) milled across the center of the slab, in parallel to one of its sides, with two 3 mm threaded through-holes for the fluidic connectors located at the terminal points. A 10 mm diameter through-hole was drilled at the centre of the micro-channel. A 45 x 30 $mm^2$ and 3 mm deep recess was machined in the central region of the PMMA component on the opposite surface where the fluidic channel was located; this region will operate as a support for the hybrid layer, while the 10 mm diameter and 3 mm deep cylindrical hollow region will constitute the side walls of the well where the sorted cell will dwell. The thermoplastic component was then chemically bonded to the PDMS block embedding the heater using a chemical functionalization procedure of both layers (which was replicated from [16]) so that the flat surface of the elastomer closed the micro-channels, the collecting chamber and the fluidic ports for applying suction. The PMMA component was also provided with through-holes for hosting 6 M2 screws, drilled in the central region where the recess was and symmetrically located around the cylindrical well.

3. *Hybrid hydrogel layer:* the water swollen PHEMA/PNIPAAm layer having the excimer laser machined through-hole at the center of the thermo-sensitive core was punched in a 22 mm outer diameter disk and then positioned onto the bottom PMMA component, at the central zone of the recess present on the thermoplastic. In this way, the 6 mm circular PNIPAAm region was located on top of the cylindrical well drilled in the PMMA. A punched hollow silicone gasket hosting the PHEMA/PNIPAAm film was used for promoting a better sealing between the soft material and the plastic components.

4. *Top PMMA component:* the fourth assembled layer is a 45 x 30 $mm^2$ and 3 mm thick micro-structured PMMA slab, which was positioned and sealed by the screw system

onto the hydrogel layer, fitting the recess that was present on the bottom plastic component. Its role is to convey the cell flow across the hydrogel, above the PNIPAAm region. The fluidic circuit machined at the centre of one of its surfaces comprised a central cylindrical recess (10 mm diameter, 1 mm height) aligned with the bottom collecting well and two micro-milled 2.5 mm long straight rectangular cross-section channels (height x width = 1 x 0.5 $mm^2$) that operated as inlet and outlet for the flowing cell suspension. The orientation of the channels is perpendicular to those milled on the bottom plastic layer. Two 3 mm threaded through-holes for fluidic connectors are located at the terminal points of each channel. The fluidic structure only seals to the PHEMA region.

Due to the relatively high thickness of the hydrogels employed (200 and 250 μm) and the screws configuration, the compression bonding between PHEMA and thermoplastic components (0.25 MPa) was sufficiently strong to prevent any liquid leakages when the fluidic structures were filled or perfused using the flow rate range explored in 6.3.1.2. This also confirmed the good sealing properties of PHEMA as already observed during leakage tests; for this reason, the silicone spacer was not found to be necessary and removed. Furthermore, hybrid films having the PHEMA frame with a rectangular geometry were used instead of the 22 mm outer diameter disks previously mentioned. This change of configuration allowed a better fitting of the hydrogel film to the recess present in the bottom PMMA component, so that it properly sealed the fluidic structure of the top plastic layer at the same time. Moreover, no geometrical effects due to different PHEMA shapes were observed to affect the thermo-responsiveness of the layer when integrated on-chip, as will be shown later. As observed in the case of the leakage tests, the hydrogel layer was kept hydrated both because of the sealing promoted by mechanical fastening and the liquid filled micro-structures of the stacking system. A photograph of the assembled prototype having the fluidic circuits filled with pure water is shown in Figure 6.12.

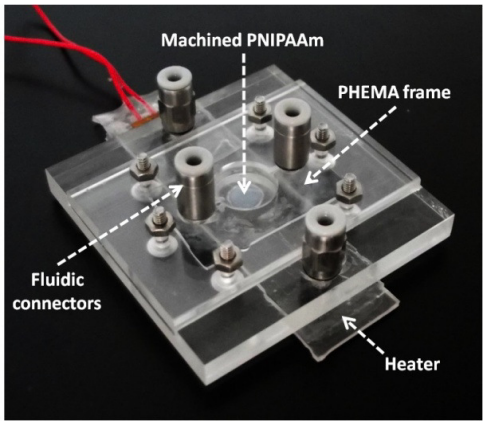


**Figure 6.12.** Picture of the water filled assembled prototype.

## 6.4.2. Prototype operational principle

The concept of the cell-sorting device functionality was already mentioned in Chapter 1. A brief summary of the main steps that characterize its working principle is reported below.

1. A cell suspension is injected in the top fluidic structure machined in the thermo-plastic component over the hydrogel layer. The system temperature is kept at 37 °C, so the micro-holes are closed.

2. In this configuration, a pressure difference is promoted across the hydrogel film and, as a consequence, cells are trapped on top of the holes.

3. Keeping the suction active to hold the cells in their trapping sites, cell medium is flowed in the top chamber to wash away the cells which are not trapped.

4. The temperature of the system is brought back below 32 °C, so that the PNIPAAm hydrogel recovers its initial state. In this configuration, the micro-holes are open and the cells are sorted through each micro-capillary into the bottom well.

A 3D model schematizing how the prototype would function is reported in Figure 6.13.

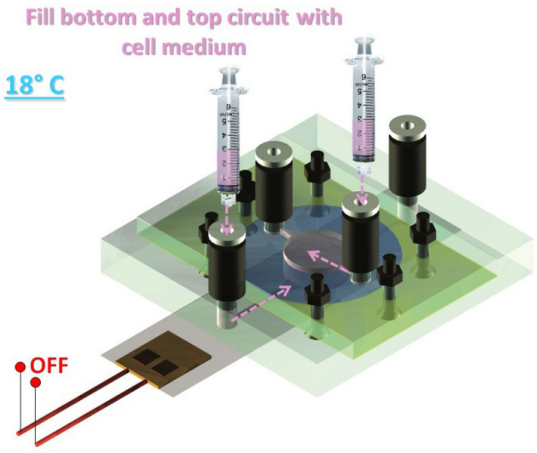
Fill bottom and top circuit with cell medium
18° C
OFF

(a)

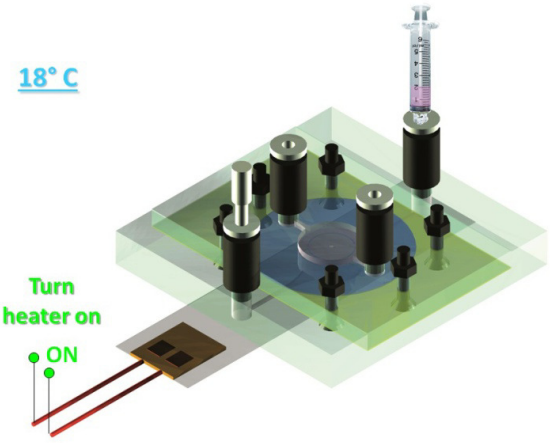
18° C
Turn heater on
ON

(b)

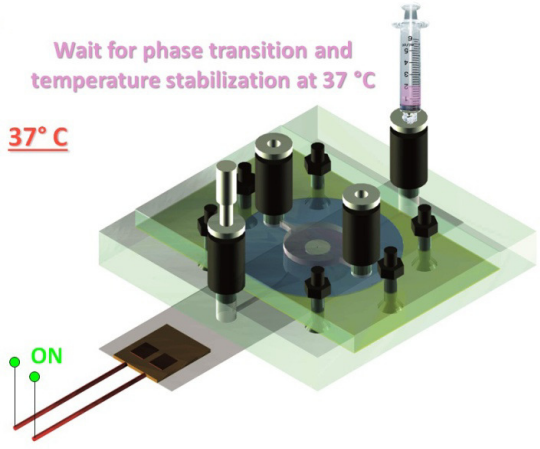
Wait for phase transition and temperature stabilization at 37 °C
37° C
ON

(c)

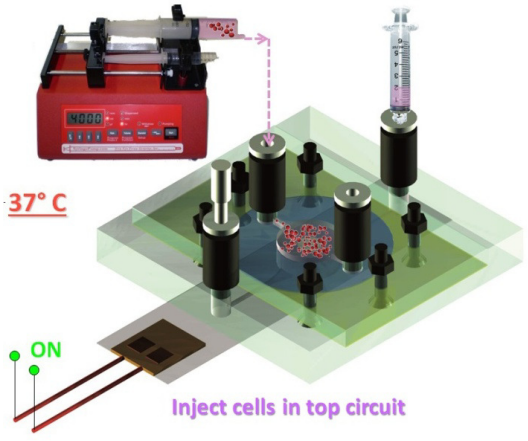
37° C
ON
Inject cells in top circuit

(d)

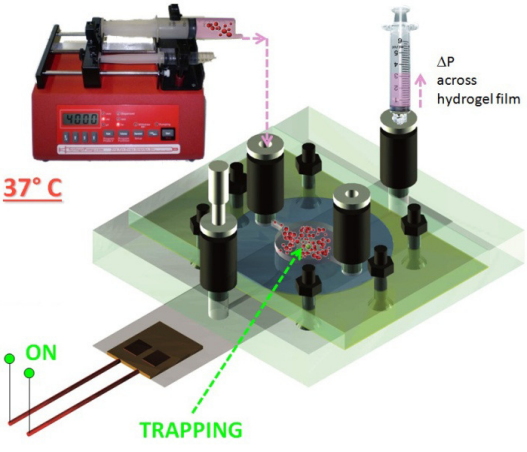
ΔP across hydrogel film
37° C
ON
TRAPPING

(e)

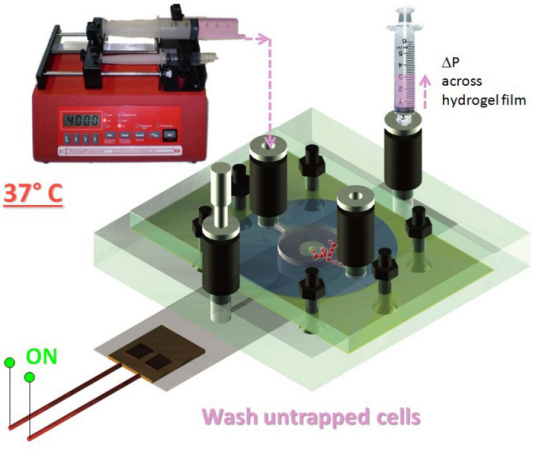
ΔP across hydrogel film
37° C
ON
Wash untrapped cells

(f)

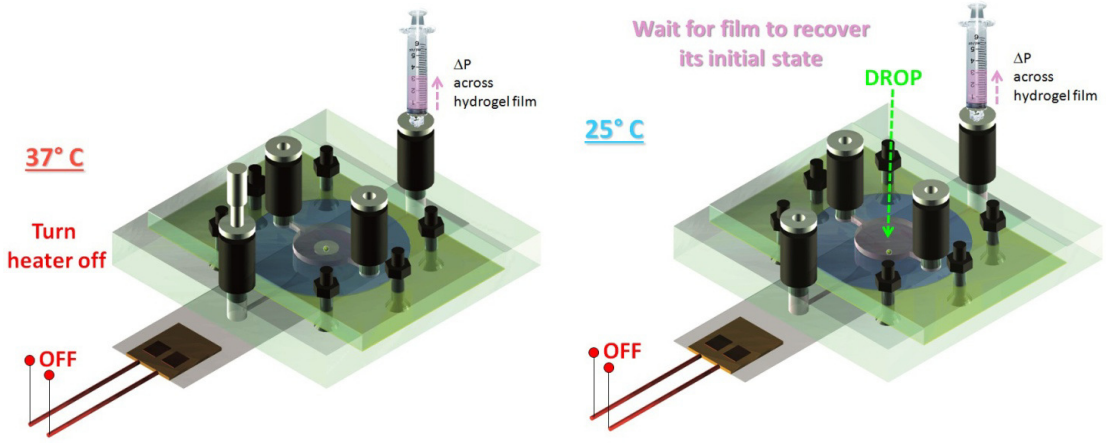


(g) (h)

**Figure 6.13.** Prototype operational principle. a) Once assembled, both top and bottom fluidic circuits are filled with cell medium (or pure water) to keep the hydrogel hydrated. b) The bottom circuit is closed at one end and equipped for suction at the other fluidic connector; the heater is then switched on. c) The system is then brought to 37 °C, promoting PNIPAAm phase transition. d) A cell suspension is injected in the top fluidic circuit using a syringe pump connected to the inlet port. e) When cells are still flowing, suction is promoted by applying a pressure difference across the hydrogel layer through the open port of the bottom fluidic structure, eventually causing the trapping of a cell in the shrunken hole. f) The top fluidic circuit is gently perfused with cell medium to wash out the cells which are not trapped. g) The heater is switched off to bring the thermo-responsive hydrogel back to its initial state. h) The cell is then sorted through the hole in the bottom collecting well.

During the actual sorting tests that were carried out, all of the phases described were conducted in sequence, except the second perfusion of the top chamber after trapping to remove the extra cells which dwelled on the hydrogel around the micro-hole. This was becuse the operation reported in Figure 6.13 – f can be considered as a second order refinment for improving the chip performance, and was therefore not necessary at this stage. Furthermore, by using relatively dilute suspensions, the probability of having a large number of cells around the sorting site after trapping should be reasonably low so that no other cell interferes with the desired sorting mechanism.

## 6.4.3. Working parameters optimization

A captioned picture of the equipment employed for cell sorting tests is shown in Figure 6.14.

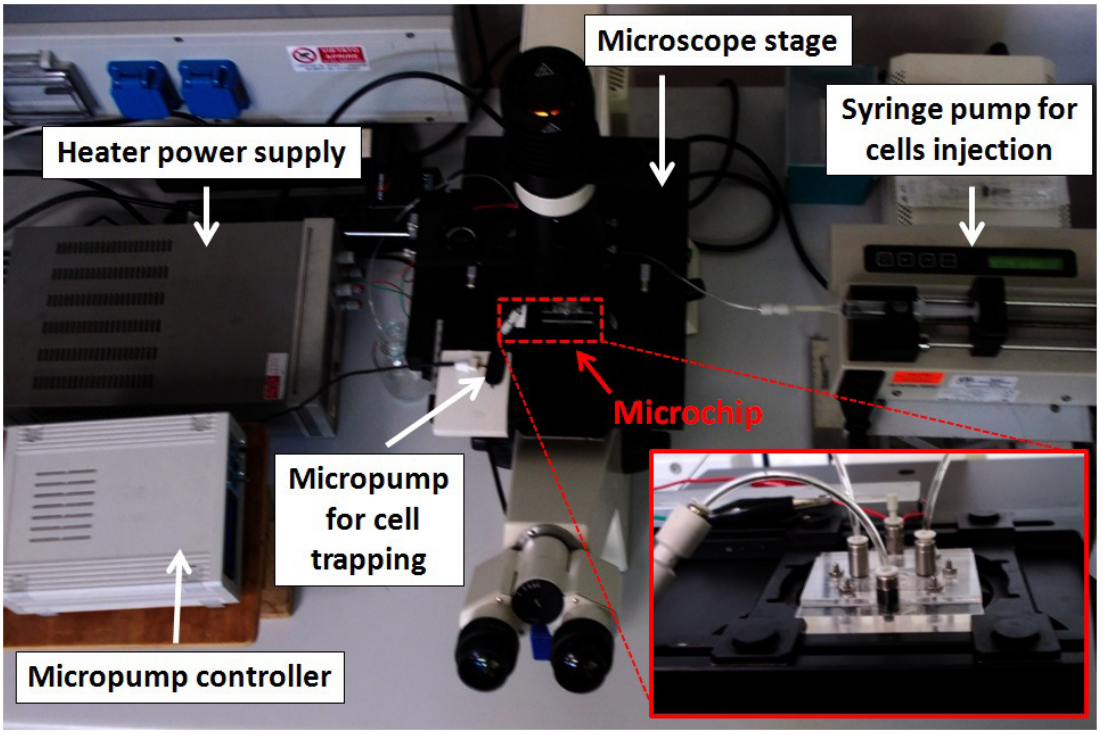


**Figure 6.14.** Experimental setup for testing temperature-triggered cell trapping and sorting on chip. The inset reports a photograph of the prototype equipped with fluidic connectors and tubes for liquid injection and suction.

The experimental setup comprises:

- The Cell-sorter prototype endowed with the assembled transparent heater and the tubing connections. As for the LTD described in 6.3.1., threaded fluidic connectors were purchased from SMC and 2 mm outer diameter polyurethane tubes were used.

- A variable voltage power supply (Hewlett-Packard, model E3615A) connected to the heating element.

- A syringe pump (KD Scientific, model KDS100) connected to the inlet port of the top PMMA component for cell injection.

- A diaphragm micropump (BARTELS Microtechink, model mp-6) connected to one of the ports of the bottom fluidic structure for promoting suction.

- An inverted microscope for real time-imaging.

According to the instrumentation employed, three parameters had to be optimized for running the trapping/sorting tests: the value of the voltage to be imposed at the terminals of the heater to stabilize the system at 37 °C, the flow rate value fixed by the syringe pump so that a laminar flow regime on the top fluidic duct could be established in order to easily visualize and track the cells' movement by optical microscopy and the value of the suction pressure for promoting cell trapping. For the tuning of the power supply, tests at different voltage values were carried out to monitor the stability of the temperature in the device. A k-type thermocouple was employed for measuring the temperature at the central region between the bottom and top chambers of the water filled prototype. The voltage values explored were 2, 5, 7, 10 and 12 V. For this purpose, a 2 mm hollow PDMS spacer embedding the wire of the thermocouple was moulded and then sandwiched between the PMMA components using the screws, so that the active tip of the probe was suspended in the liquid bulk after assembly. The recorded temperature values and a fine tuning of the power supply voltage revealed that by using 11 V as the set point, the temperature of the water could be kept at 37 °C, with good stability (values ranging between 36.5 and 38 °C) for more than an hour. Although in the actual prototype operating configuration the presence of the water-swollen PHEMA/PNIPAAm layer might slightly alter the thermal conditions identified by this calibration, the determined voltage was considered reliable for being employed during the trapping/sorting tests.

From the fluidic point of view, for establishing an optimal value of the pump volumetric flow rate in order to have a laminar flow of the cell suspension injected in the top PMMA layer micro-fluidic structure, an empirical calibration was carried out by monitoring the flow of a

MG63 cell suspension in the device. These cells were chosen as a model cell line due to their spherical shape when suspended in the medium and because of the suitable size of their measured average diameter for the target application, which is around 25 μm as reported in Table 4.1 (Chapter 4). The density of cells was relatively low (5 x $10^3$ cells/mL) and optical microscope image acquisition was used to track their flow. The employed syringe pump has a range of volumetric flow rate values that can be set from 0.1 to 100 mL/h. Flow visualization tests were carried out in two separate sets of tests: the first using a bottom flat PMMA component that sealed to the prototype micro-milled top one using the system of bolts and nuts, the second using the whole prototype assembly. Having a hard substrate instead of the sealing hybrid hydrogel layer did not influence the dynamic of the flow for the rates tested, which were from 6 to 0.1 mL/h. Setting the volume displacement rate at a value of 3 mL/h resulted in a smooth laminar flow of the cells that could be observed and monitored with optical microscopy. Considering the analysis carried out in 6.3.1.2 using the LTD, the determined value of the flow rate is relatively low and a no-leakage regime at the interface between the hydrogel and the thermoplastic is guaranteed. A deep analysis of the fluidic phenomena involved when cell perfusion takes place goes beyond the aim of the present thesis, and so an extensive study about the dynamic of the cell suspension flowing in the chip is not treated in detail. However, the most relevant observations related to the particular design and operational parameters used are reported below. The laminar flow is identified with low Reynolds numbers, Re; this quantity is a parameter which can be calculated knowing the geometrical characteristics of the fluidic duct, the average velocity of the flow and the density and viscosity of the fluid (Eq. 6.1).

$$Re = L\rho v/\eta \qquad [6.1]$$

Where L is the characteristic length of the fluidic conduit, v is the characteristic velocity of the flow (e.g. average velocity), while $\rho$ and $\eta$ are the fluid density and shear viscosity respectively. For $Re < 2300$, the flow can be considered laminar. In microfluidic systems, the small size of the fluidic paths and relatively low velocity values usually brings low Reynolds numbers. In the present case, the cell suspension is injected into a 2.5 mm long rectangular cross-section micro-channel (height x width = 1 x 0.5 $mm^2$) with the volumetric flow rate (Q

= 3 mL/h). The average velocity in the duct is calculated by dividing Q by the cross-section, resulting in <v> = 0.16 cm/s. By describing the cell medium using the density and viscosity values for water at room temperature ($\rho$ = 1 g/cm$^3$ and $\eta$ = $10^{-3}$ Pas, respectively), <v> as the characteristic velocity and considering the 2.5 mm length of the channel as L, the resulting Reynolds number is Re = 4. This confirms the laminar regime which can be reasonably described by a Poiseuille flow for the straight region of the micro-channel, assuming the no-slip boundary conditions i.e. neglecting the effect of the asperities and roughness of the channel walls on the flow. As shown in Figure 6.11, the straight channel was designed so that it starts to diverge when approaching the cylindrical chamber through a 1 mm long region. Using the results obtained from studies on the diverging/converging variable section microchannels at low Reynolds numbers [17, 18, 19], considering that the cross-section of the duct widens from 1x1 mm$^2$ to 1x10 mm$^2$ going from the beginning to the middle of the chamber, the average velocity of the flow is expected to decrease from the calculated value of 0.16 cm/s when reaching the central region where the PNIPAAm film is located. Furthermore, due to the geometry of the system having rectangular cross-section microchannels as fluid inlet and outlet conduits connected to a cylindrical well, the turbulence effects that might take place due to sections discontinuities only showed up in small regions at the side walls of the interface where the cross-sections changes, while the flow is still laminar at the centre of the well [20]. Assuming a Stokes flow [21] and giving the velocity of the cells an upper limit equal to 0.16 cm/s, the average number of cells passing through the center of the cylindrical well in one second is <N> < 80 cells.

Being inspired by cell patch clamp systems on chip, which require the trapping and blocking of single cells in micron-sized holes for electrical transmembrane measurements [22, 23], the working parameters of the micropump were tuned to apply the proper suction from the bottom chamber of the chip. The duty cycle of the diaphragm BARTELS mp-6 can be controlled by two main parameters: the voltage V, which sets the strength of the suction (amplitude of the controlling signal), and the frequency f, which drives the rate at which each single cycle is completed per second (frequency of the controlling signal). First tests were carried out using a water suspension of glass beads with a 250 μm thick hybrid PHEMA/PNIPAAm film moulded with METHOD 2, machined using the 300 μm hole diameter mask. The target of these experiments was to determine the appropriate values of V

and f to trap the particles at room temperature into the exit holes of the patterned layer. The identified set of parameters was then successfully employed in the cell trapping and sorting test using the single hole hydrogel layer and MG63 cells. The holes of the 9x9 array had an average exit hole diameter of about 5 μm, while the nominal average glass bead diameter was 17 μm. After suspension in water, the bead solution was kept in an ultrasonic bath for 30 minutes to disperse possible aggregates and to obtain a homogeneous solution of single spheres. The flow rate Q at which the bead suspension was injected was still 3 mL/h. By gradually exploring a range of values for V and f, keeping the frequency at 10 Hz and increasing the voltage from 50 to 220 V, trapping of the glass spheres was observed only for the maximum value of V available i.e. 220 V. This working regime corresponds to the application of a negative pressure across the hydrogel layer of about 20 kPa. Figure 6.15 shows microscope images of the trapped micro-beads.

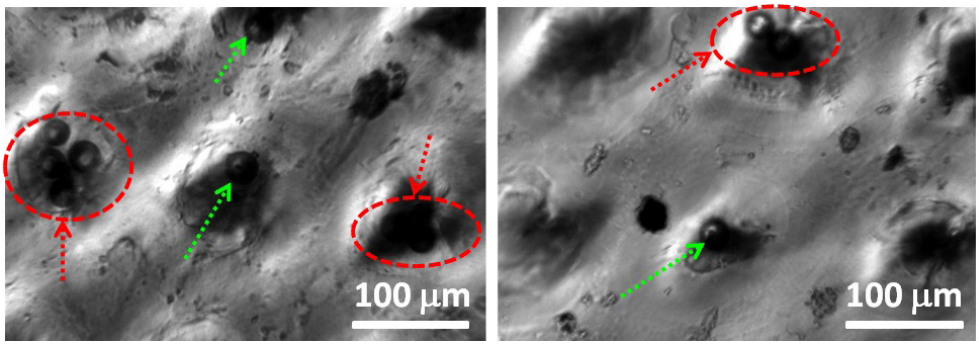


**Figure 6.15.** Microscope images of the glass micro-beads (green arrows) trapped into the exit holes of the array machined in the PNIPAAm region of the hybrid layer. Some spheres are still forming an aggregate (red arrows and circles) despite the ultrasonic treatment.

## 6.4.4. Proving prototype functionality: MG63 cells sorting

MG63 cell suspension of the same concentration as indicated in 6.4.3. was employed for the sorting tests. The assembly procedures and operational working parameters were the same as in 6.4.1. and 6.4.2. The hydrogel employed was a single hole water swollen hybrid PHEMA/PNIPAAm layer, 250 μm thick, having entrance and exit hole diameters of about

220 and 35 μm respectively at room temperature. Once the mechanical fastening was carried out and the system filled with pure water, the heater was switched on and the phase transition of the film took place according to the heating rate imposed. Figure 6.16 shows the evolution of the entrance hole in time. Again, the mechanical constraint caused a partial deformation of the shrinking of the machined structure when the temperature of the system stabilized at 37 °C.

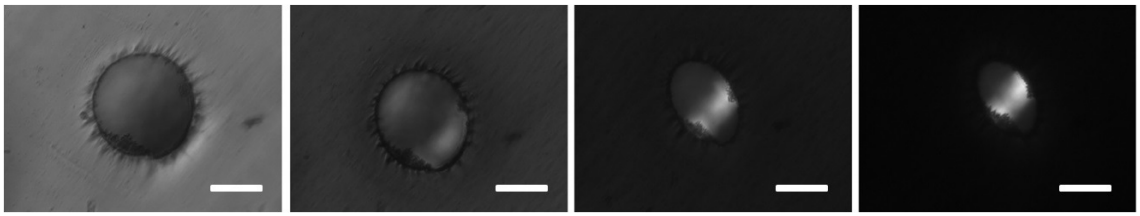


**Figure 6.16.** Transition of the PNIPAAm based component in the prototype. Entrance hole shrinking in time is shown (scale bar is 100 μm). a) Machined structure at room temperature. b) 5 minutes after the heater is switched on. c) After 10 minutes. d) After 15 minutes.

The resulting shrunken elliptical entrance hole size at equilibrium at 37 °C was 170 μm and 120 μm for the long and short axis respectively, while the exit hole changed its size to 18 μm, still bearing a rather circular shape. In this condition, the cell suspension was injected in the top PMMA component of the chip via the inlet port. Because of the phase transition, the PNIPAAm refraction index changes leading to a high opacity of the hydrogel; once transparency is lost, it is difficult to visualize the cells flowing over the layer, but the smoothness of the liquid passage through the micro-fluidic structure can be monitored macroscopically at the tube connected to the outlet port. For microscope imaging, the exit hole of the hydrogel layer was focused continuously. When the liquid reached the outlet port and the suspension started flowing in the connected tube toward the collecting reservoir, the micropump was switched on and suction was applied. In a time window of about one minute, the presence of a cell trapped in the machined structure was observed and the flow of the suspension was then stopped immediately, while keeping the suction active. Figure 6.17 shows microscope images of the trapping process.

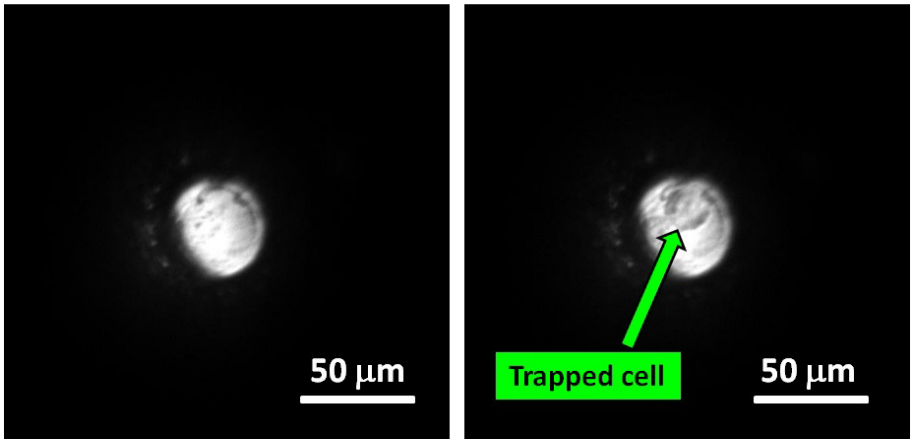


(a) (b)

**Figure 6.17.** Trapping of a MG63 cell visualized at the exit hole of the hydrogel layer. a) Microscope image of the exit hole during cell flow in the top fluidic component before suction is applied. b) After 1.25 minutes of micropump operation to apply a pressure difference across the layer.

The region of the polymer around the exit hole appeared more transparent than the rest of the layer and this is probably due to a decrease in the film thickness surrounding the machined structured, probably caused by light scattering phenomena taking place inside the tapered hole and by material partial overetching during laser ablation. For simplicity and to avoid possible perturbations to the trapped cell, it was chosen not to wash away the cells deposited on the film by a second perfusion and so the sorting was directly tested. The heater power supply was then switched off and the releasing of the cell into the bottom chamber was observed in a 10 minute time window. Figure 6.18 shows the three main phases of the monitored sorting mechanism.

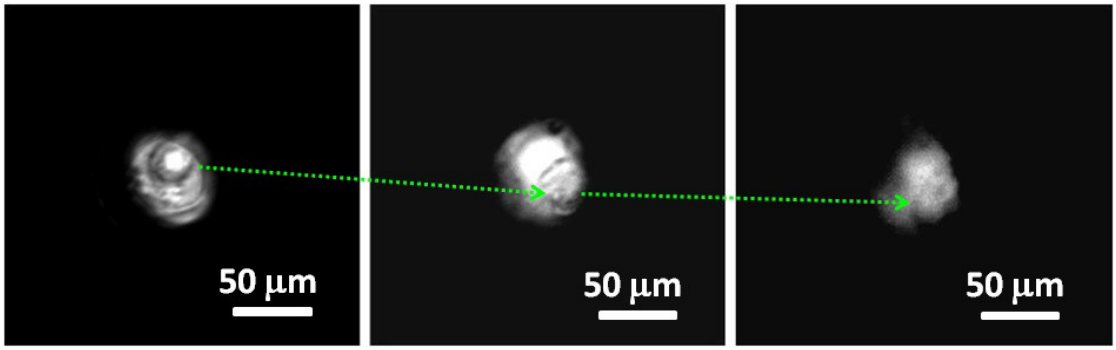


(a) (b) (c)

**Figure 6.18.** Sorting mechanism induced by the recovery of the layer towards its initial state. a) 5 minutes after the heater is switched off, the cell is still trapped. b) 2.5 minutes after (a), the cell is moving through the hole toward the bottom fluidic circuit of the prototype. c) 2 minutes after (b), the cell is approaching the bottom of the collecting well. Arrows indicate each new position of the cell in time.

Though it was difficult to follow the trajectory of the cell passing through the hole, it could be possible to track the main steps of the evolution of the system and see the cell approaching the bottom chamber. No real-time monitoring proof is available at the present time, but the indirect way through which the phenomenon was observed suggests that the prototype has appropriate features and operating capability for properly performing the temperature-triggered trapping/sorting mechanism. At the end of the process, the empty trapping hole and the presence of a MG63 cell in the bottom chamber of the device could be observed, as reported in Figure 6.19.

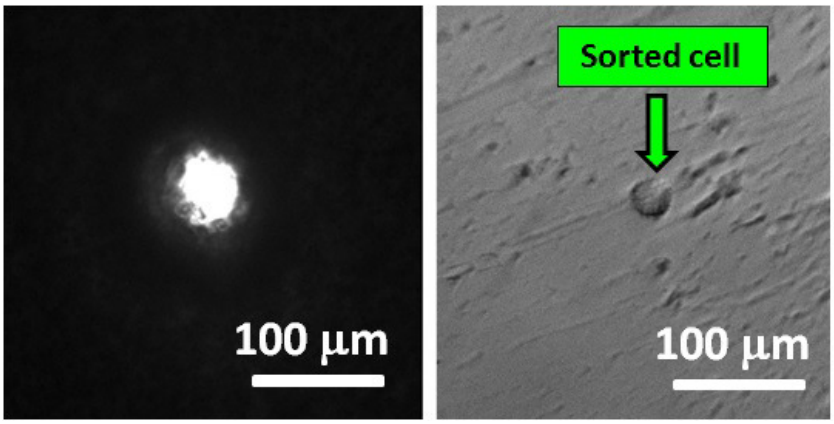


(a) (b)

**Figure 6.19.** Indirect proof of the sorting mechanism. a) Microscope image of the fully recovered exit hole at room temperature. b) MG63 cell visualized at the bottom of the collecting well.

# 6.5. Conclusion

For improving the imaging optical quality and for providing a better visualization of the phenomenon, the use of fluorescence microscopy could be suitable. For this reason, time-lapse and/or video acquisition based monitoring of the sorting experiments involving fluorescent labeled MG63 cells are being set up. As already mentioned in the introduction section of this chapter, no cell viability tests were carried out. The results obtained so far using the designed prototype can be considered satisfactory and promising; the indirect visualization of the device proof of principle suggests the feasibility of the machined micro-structured PHEMA/PNIPAAm hydrogel layers to be used as temperature-triggered smart actuators for cell sorting on-chip. The most advantageous feature of the developed prototype having the polymeric thermo-responsive film integrated as freestanding component relies in the possibility of keeping the transition behavior of the size-modulating machined structures similar to the case where the hydrogel layer would have been free of mechanical constraints. The only effect that the compression based packaging technique employed for the system assembly has on the temperature dependent deswelling/swelling process of the hydrogel is to

slightly deform the shape of the micro-capillary, but a high degree of homogeneity of the transition could be preserved. As already observed in Chapter 5, micro-fluidic devices having micro-patterned PNIPAAm films grafted or chemically attached onto rigid substrates hinders the natural tendency of the polymer to shrink and expand as a function of temperature, due to the in-plane stresses caused by the bonding to the supporting layer [24, 25]. In this sense, using the presented prototype represents a novel approach for exploiting the smart behavior of micro-structured PNIPAAm based hydrogel in the frame of LOC systems for cell biology applications. To further minimize the deformation effects induced by mechanical constraint endured by the hybrid layers, experimental and computational studies to identify the optimum shape of both the PNIPAAm thermo-responsive core and the elastic frame could be carried out. Improving the elasticity of the PHEMA component when subjected to in-plane tensions (e.g. by developing PHEMA based co-polymers) could also be useful for the same target. In the current configuration, not only is the homogeneous behavior of the transition guaranteed, but the mechanical fastened micro-device could provide the appropriate sealing of the hydrogels to the thermoplastic components for fluid manipulation as demonstrated both by the leakage tests and the prototype operation using MG63 cells. The response time of the polymeric actuators is relatively quick, so that the on-chip sorting mechanism can be promoted in a ten minute time window; this could be further improved by reducing the size of the thermo-responsive core during the manufacturing of the hybrid layers. The bulky support instrumentation employed offered a good control over the operational parameters (such as flow rate and system temperature), but a version of the device relying on the use of capillary action for cell flowing instead of using a volume displacement pump and having a calibrated suction actuator (e.g. a syringe-like plastic piston) integrated in the thermoplastic layers would allow the sorting chip to operate in a way which is closer to the original idea of the DDG device, as reported in Chapter 1. At this stage, a single micro-hole was employed for demonstrating the feasibility of the temperature-triggered trapping/sorting mechanism, but the same operation conducted in parallel on a single platform could be considered as an extension of the present case and could be relatively easy to achieve, therefore conferring the desired high throughput feature to the system. The overall results obtained can therefore be considered satisfactory and the perspective of further developments appears promising for next generation hybrid LOC device realization based on the use of a new family of micro-

structured smart hydrogel actuators, able to offer alternative solutions for cells and bioparticle manipulation in miniaturized environments.

## References


[1] Zhao W Santaniello T Gassa F Lenardi C Webb D P and Liu C 2012 *Polym. Int.* **62** 1059–1067

[2] Cardoso P and Davim J P 2012 *Rev.Adv.Mater. Sci.* **30** 98-102

[3] Klank H Kutter J P and Geschke O 2012 *Lab Chip* **2** 242-246

[4] de Mello A 2002 *Lab Chip* **2** 31N–36N

[5] Zhao W Santaniello T Gassa F Webb D P Lenardi C and Liu C *Electronic Components and Technology Conference (ECTC)*, San Diego, California, USA, 29th May – 1st July 2012, pp. 1997-2004

[6] Zhao W Santaniello T Lenardi C Liu C and Wu F *14th International Conference on Electronic Materials and Packaging (EMAP),* Citygate, Lantau Island, Hong Kong, 13-16 Dec. 2012, pp. 1-5

[7] Kaufman J D Morgan E F and Klapperich C M 2008 *J. Mater. Res.* **23**1472-1481

[8] Beatty MF 2006 *Principles of Engineering Mechanics*, Springer Science+Business Media Inc., New York, 151–167

[9] Dow Corning Corporation *Product Information of Electrical insulating Compound from DOWCORNING* Ref. No. 10-1187D-01.

[10] Peppas NA and Benner RE 1980 *Biomaterials* **1** 158–162

[11] Mooney M 1940 J *Appl Phys* **11** 582–592

[12] Rivlin RS 1948 *Large elastic deformations of isotropic materials*, in Further Development of the General Theory, Philos Trans R Soc Lond, A241, 379–397

[13] Mark JE 1999 *Polymer Data Handbook*., Oxford University Press, New York, 430-435

[14] Liu D and Garimella S V 2004 *Journal of Thermophysics and Heat transfer* **18** 65-72

[15] Bruus H 2008 *Theoretical Microfluidics* New York, U.S.A., Oxford University Press 71-84

[16] Vlachopoulou M E Tserepi A Pavli P Argitis P Sanopoulou M and Misiakos K 2009 *J. Micromech. Microeng.* **19** 1-7

[17] Duryodhan V S Singh S G and Agrawal A 2013 *Microfluidics and Nanofluidics* **14** 53-67

[18] Bahrami M Yovanovich M M and Culham J R *Proceedings of ICMM 3rd International Conference on Microchannels and Minichannels*, Toronto, Ontario, Canada, 13-15 June 2005, 1-12

[19] Xuan X and Li D 2006 *J. Micromech. Microeng.* **16** 62-68

[20] Cimetta E Figallo E Cannizzaro C Elvassore N Vunjak-Novakovic G 2009 *Methods* **47** 81–89

[21] Bruus H 2008 *Theoretical Microfluidics* New York, U.S.A., Oxford University Press 60-63

[22] Chen C Y Tu T Y Chen C H Jong D S and Wo A M 2009 *Lab Chip* **9** 2370–2380

[23] Alberti M Snakenborg D and Kutter J P *Twelfth International Conference on Miniaturized Systems for Chemistry and Life Sciences,* San Diego, California, USA, 12-16 October 2008, 519-521

[24] Tekin H Tsinma T Sanchez J G Jones B J Camci-Unal G Nichol J W Langer R and Khademhosseini A
2011 *J. Am. Chem. Soc.* **133** 12944–12947

[25] Yokoyama Y Umezaki M Kishioka T Eiichi T and Takamura Y 2011 *J. Photopolym. Sci. Tech.* **24** 63-70

# 7. Conclusions

In the present work, a manufacturing protocol for producing a new class of micro-structured actuators based on thermo-responsive PNIPAAm was developed. The engineered smart hydrogel layers were then integrated as freestanding components in a designed multilayer LOC device to operate as temperature activated smart cell-sorting interfaces. The research has presented novel and advantageous features which can be summarized as:

i) Establishing a method for the preparation of PNIPAAm layers (50 to 300 μm thick) using an injection/compression moulding (ICM) technique to obtain hydrogel sheets attached to rigid PVC substrates. High repeatability and fine control over the realized hydrogel layers thickness and flatness was achieved which facilitated the subsequent laser patterning procedure. The error in the thickness of the films was kept within the 10% relative to the thickness of the spacer employed in the moulding system;

ii) Improving the relatively poor elastic properties of pure PNIPAAm, by synthesizing hydrogels with different cross-linker and initiator amounts as well as PNIPAAm based co-polymers (PNIPAAm-co-HEMA, PNIPAAm-co-MMA);

iii) Fabricating hybrid PHEMA/PNIPAAm layers having a 5 mm circular thermo-responsive core chemically bonded to a wider PHEMA frame embracing the structure. This enabled a new group of polymeric films having spatially defined regions based on different monomers to be prepared, thereby preserving the PNIPAAm thermo-responsive behaviour in freestanding components when the surrounding elastic PHEMA region was subjected to mechanical constraint;

iv) The application of excimer laser machining (which is traditionally employed for harder polymeric material component fabrication) to micro-pattern soft polymer surfaces with highly resolved geometrical features, without any modification of the polymer's chemistry and without affecting the thermo-responsive properties. A 248 nm wavelength KrF excimer laser was used to fabricate 9x9 arrays of through-holes with entrance diameter of 20 and 30 μm (10 to 20 μm exit holes)

in the hydrogels using an aluminium projection mask. Single hole patterned hybrid PHEMA/PNIPAAm layers were also produced having entrance diameter of 150 μm and exit hole diameter varying from 10 to 30 μm. Laser machining parameters (energy and number of shots) were empirically optimized in order to achieve good resolved features: the best were found to be an initial energy value of 250 mJ, with 5 Hz repetition rate and a number of shots ranging from 400 to 3200 according to the hydrogel thickness and the projection mask employed. The set of chosen parameters was a trade-off between overcoming the ablation threshold of the PNIPAAm and the minimization of debris traces, which were present in a relatively small amount and which did not depend on the number of shots delivered. The fabrication showed good reproducibility and consistency in terms of the geometrical features of the holes, as revealed by metrology characterization (inverted and confocal microscopy).

v) The possibility of easily achieving freestanding micro-structured hydrogel intelligent components by choosing the optimum combination of moulding materials and swelling chemicals was demonstrated. Thermo-responsiveness characterization from 18 °C to 39 °C was carried out on the detached freestanding layers using a thermostatic bath, and samples underwent multiple cycles. As a result of the polymer water loss due to the PNIPAAm phase transition above 32 °C, the shrinkage of the layers caused the pattern to homogeneously shrink without any significant deformation, thus causing the holes to reduce from their original size by a quantity varying from 25% to 50%, depending on the hydrogel structure and composition. The shrinking degree of the hydrogels did not depend on the heating rate imposed, machined hole size or film thickness. A slight deformation of the micro-capillary was induced when the PHEMA/PNIPAAm hybrid layers endured mechanical constraint on the PHEMA elastic frame during the transition, leading to the formation of an elliptical shape at equilibrium in the final state; the micro-through hole could still however reduce its size by around 40% of its initial dimension.

vi) The potential for the hydrogel layers to act as an interface between two PMMA components, providing the appropriate sealing during perfusion of the system

was tested using a three layer micro-fluidic device. The principal focus of these tests was to identify a range of pressure, which the water swollen PHEMA film could undergo when operating as a gasket element. Flow rates chosen were representative for a wide class of microfluidic perfusion devices. Liquid leakage tests were carried out by continuously pumping dyed aqueous solution in the microchannels and monitoring in real time for any leaks at the thermoplastic/hydrogel interface by means of an optical microscope. No liquid leakages at the different material interfaces occurred when the fluid was perfused at relatively low pressure values (from a few Pa to fractions of a kPa) on top of the hydrogel surface and the sealing between the materials was guaranteed for the tested flow rate values, ranging from 100 μL/min to 10 mL/min.

vii) To realize test structures of hydrogel layers supported by PMMA components, mechanical fastening using bolts and nuts was identified as the most appropriate packaging technique for assembly and presents a number of advantages over other assembly/bonding methods, including processing at room temperature, ease of repair / component replacement, low cost and the potential for multiple disassembly. In particular, for micro-fluidic device packaging applications, the technique is less prone to contamination of the components as no glue is involved. To determine whether clamping could damage the layers, compression testing was carried out on PHEMA cylindrical samples in order to measure the ultimate strain and to quantify the material compressive behaviour for the particular material composition. Samples were tested in a liquid environment and the ultimate engineering strain (compression) was estimated to be approximately 45% for a 32 mm diameter sample and 55% for an 18 mm diameter sample, corresponding to ultimate yield strengths of 0.45 MPa to 0.7 MPa respectively.

viii) A multilayer microfluidic system having a single hole KrF excimer laser micro-patterned hybrid PHEMA/PNIPAAm layer integrated as a freestanding component was then designed and built to assess the feasibility of the hydrogels to operate as temperature-triggered cell sorting actuators for single cell assay applications. Still employing mechanical fastening as the packaging strategy, the hydrated hydrogel was sealed between two micro-milled PMMA components,

which provided the fluid access and ducts for the cell suspension to be flowed over the thermo-responsive actuator (top layer) and the well to collect the sorted sample (bottom layer). The device was also fitted with a thin transparent heater to control the microfluidic chip temperature. When the system was assembled, the size of the laser machined micro-structure could be reversibly modulated by inducing the PNIPAAm core phase transition. The reversible thermo-responsive actuation mechanism was exploited to trap a sample cell in the shrunken exit hole on the top of the hydrogel layer by applying a negative pressure across the film via the bottom PMMA component, while keeping the system at 37 °C. Subsequently, the sorting of the trapped cell took place through the micro-capillary when the polymer natural relaxation toward its initial state occurred on cooling. The functionality of the device was demonstrated using MG63 cells as a model cell line, by monitoring the sorting through the size-modulating structure using optical microscopy imaging. The system offered a relatively quick trapping/sorting mechanism according to the PNIPAAm transition (around 10 minutes).

No examples of cell sorting on-chip relying on such actuation nor on the use of smart hydrogel components integrated as freestanding interfaces in multilayer micro-devices have been reported in the literature. The micrometer scale spatial resolution and process repeatability achieved with the fabrication protocols, as well as the relatively low cost of the materials involved, enable hydrogel thin film patterning and integration in LOC devices suitable for manufacturing scale up. Further evolution of the system should now be focused on the miniaturization of the thermo-responsive actuators to decrease the smart hydrogel response time and to confer high-throughput features to the device (i.e. multiple PNIPAAm cores per hydrogel film and therefore multiple sorting per use) to be a reliable and unique solution for label-free cell separation procedures.

# Appendix A

# Alternative manufacturing protocols for hybrid hydrogel layer fabrication: preliminary results

In this appendix, two alternative techniques for hybrid hydrogel layers manufacturing are reported. Both of them were preliminary tested in order to assess their feasibility as possible new fabrication strategies to be further developed.

## A.1. UV cross-linking

UV cross-linking of hydrogel materials has already been discussed in Chapter 2; a light induced polymerization of the hybrid PHEMA/PNIPAAm layers was tested in Fondazione Filarete, using 2,2-dimethoxy-2-phenyl-acetophenone (DIMPA) as the initiator both for PHEMA and PNIPAAm. The monomer to cross-linker and monomer to initiator ratios were kept the same for both polymers as reported in 3.2.2.2 for PHEMA and 3.2.1 for PNIPAAm. No TEMED was employed in the reaction since its action is strictly connected to the specific initiator of the free radical polymerization. The technique that was developed had the same basis as METHOD 1 described in 3.4.2., with the only difference that a transparent lid was employed to replace the aluminium and that compression should be promoted not simply by placing a weight over the lid, but rather using an appropriate clamping system to leave part of the lid's surface exposed to the UV source. UV light was used for promoting the cross-linking of both PHEMA and PNIPAAm; the exposure time determines the degree of cross-linking of the two hydrogels, according to the different reaction kinetics. A scheme of the UV based technique tested is reported in Figure A.1.

*Injection/compression moulding protocol for hybrid PHEMA/PNIPAAm films fabrication:*

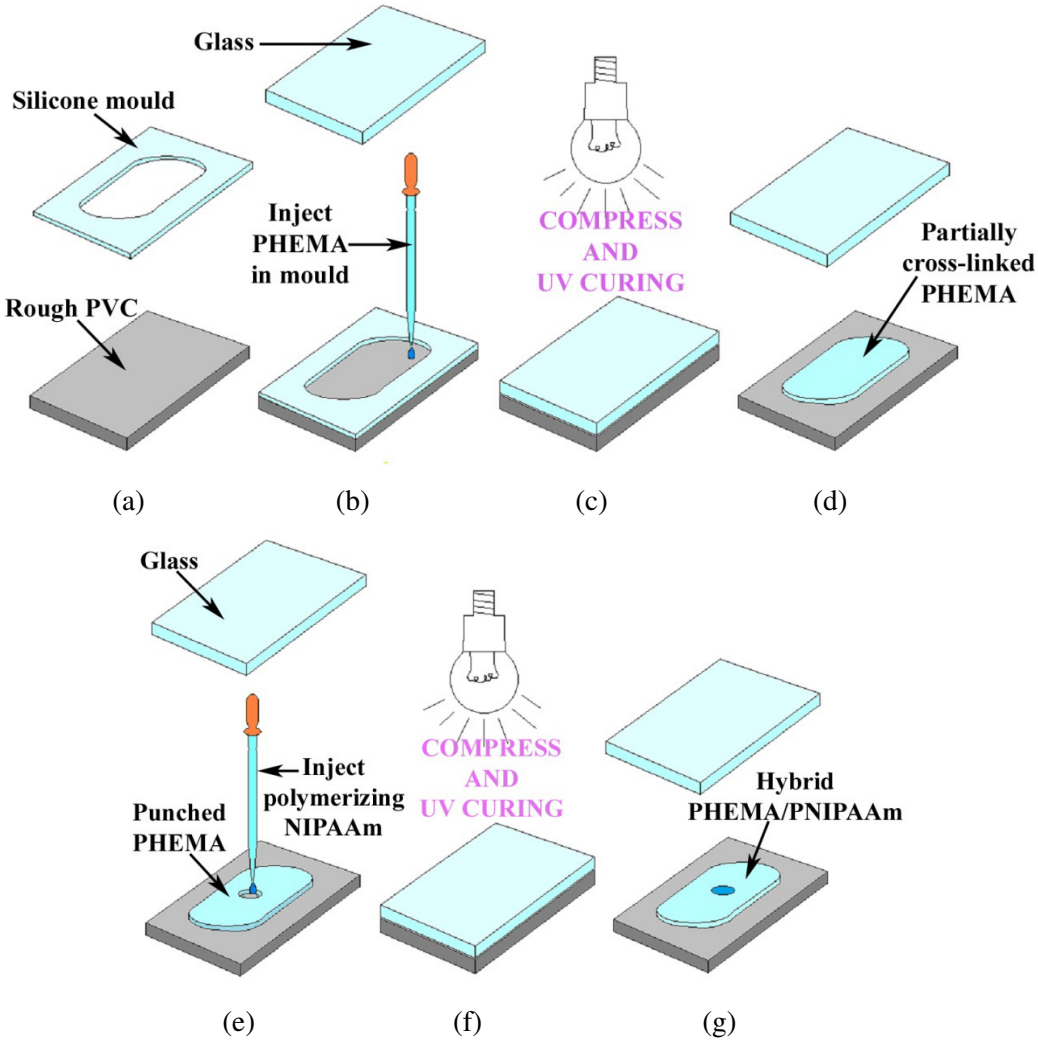


**FIGURE A.1.** Manufacturing protocol for UV cross-linked hybrid hydrogel layers. a) PDMS moulds are positioned over rough PVC. b) PHEMA polymerizing solution is injected in the mould. c) Compression is promoted by using a glass lid; clips are employed to clamp the apparatus (not shown in figure) and the moulding system is exposed to UV light. d) Partially cross-linked PHEMA is recovered on the PVC plate. e) PHEMA layer is punched and the polymerizing PNIPAAm solution is injected in the formed hollow region. f) The moulding system is closed again with a glass lid and exposed to UV light in order to complete both hydrogel polymerization and cross-linking reaction. g) The hybrid layer is formed attached on the PVC substrate.

Reaction kinetic tests on PHEMA and PNIPAAm were carried out prior to moulding and it was observed that the polymerization time was 30 minutes and 20 minutes respectively. The UV lamp employed in these preliminary tests was a Black ray ® B-100AP ($\lambda$ = 365 nm, P = 100 W). This technique also presents advantages and disadvantages that can be summarised as follows:

- ✓ **Advantages:** the main advantage of the UV based technique lies in the possibility of controlling the kinetics of the cross-linking reactions for both the hydrogels by simply changing the exposure time of the samples; in this way, it is possible to easily tune the timing for the fabrication protocol and have good control over the polymerizing solutions' viscosity, which is an important parameter for the injection based fabrication technique, as discussed in Chapter 3.

- ✓ **Disadvantages:** the protocol requires further analysis of the materials employed in the technique. In particular, the transparent lid could constitute a problem, since the choice would probably be limited to glass based materials, due to the relatively high heat developed during the UV curing. Furthermore, PNIPAAm based hydrogels which are synthesized by the use of DIMPA needs to be characterized in terms of thermo-responsitivity; this means that no *a priori* information on their temperature triggered phase transition features are available, although maintaining the same monomer to cross-linker ratio should guarantee a certain compatibility with the chemically induced cross-linked samples already analyzed. The use of a UV lamp also requires the development of a proper experimental set up in terms of the compression technique itself (e.g. compression clamping system) and the curing (e.g. UV exposure protection enclosure).

The obtained layers were detached as reported in 3.4.3 and then swollen in pure water. The most significant difference compared to the samples prepared by the techniques relying on the free radical induced polymerization, was a much higher swelling ratio of the PNIPAAm component, thus dramatically enhancing the 'jellyfish' like effect, as shown in Figure A.2.

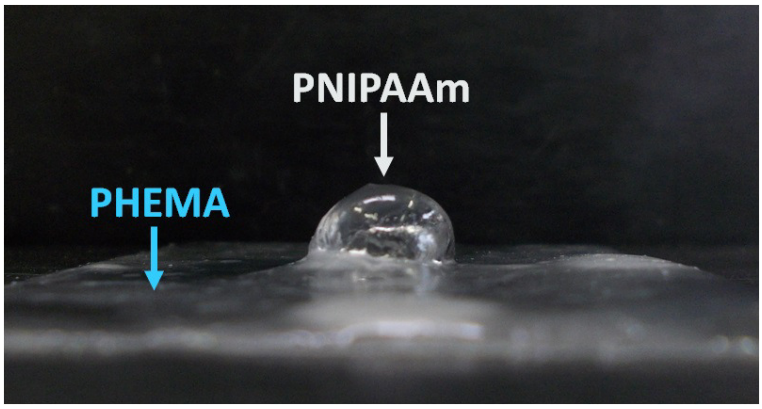


**Figure A.2.** Photograph of a water swollen hybrid hydrogels film fabricated using UV induced cross-linking. The curvature of the PNIPAAm component is dramatically pronounced compared to the layers manufactured using the free radical polymerization protocols.

However, no tearing or damage was present at the hydrogels interface, indicating a tight bonding of the materials in the inter-penetrating network region. Separate qualitative mechanical tests (tensile stretching) were carried out on pure UV cross-linked PNIPAAm layers; the mechanical stability and resistance to the applied stresses of the films was significantly reduced compared to the same type of material synthesized using the free radical induced polymerization. This is probably due to the higher water content embedded in the material as a result of the different network formation mechanism, which also explains the observed difference in the swelling ratio. The tuning of the synthesis parameters is required for the realization of this type of PNIPAAm based hydrogels with suitable mechanical properties.

This technique could also be applied to a manufacturing scheme similar to METHOD 3, by properly changing the moulding apparatus and related equipment, and therefore could constitute a promising route for hybrid hydrogel layers fabrication. The spatial dimensions of the disks could also be scaled down to the sub-millimeter scale, by employing an appropriate patterned mask interposed between the light source and the polymerizing materials in order to cross-link only selected regions of the material.

# A.2. Moulding PHEMA/PNIPAAm interfaces

Another method was developed to increase the strength of the PHEMA/PNIPAAm interface. The basic idea was to realize hybrid layers having an annular region based on PHEMA/PNIPAAm random copolymer bridging the two hydrogels in order to both widen the interfacial area and enhance the bonding of the polymers as well as the mechanical stability of the film. The fabrication scheme can be summarized as follows. A single PNIPAAm disk is formed by standard ICM on a PVC plate; after it is partially cross-linked, the silicone mould is removed and a second hollow PDMS circular layer is positioned on the PVC so that the formed disk is located at its center. An already initiated PHEPAAm10 (or PHEPAAm20) solution is then injected in the interstitial region between the PNIPAAm component and the silicone mould, so that the copolymer can form a relatively wide annular film around the disk. The third step consists in removing the PDMS sheet and then employing a third hollow silicone mould to synthesize the PHEMA frame around the formed co-polymer area. This manufacturing protocol is reported in Figure A.3.

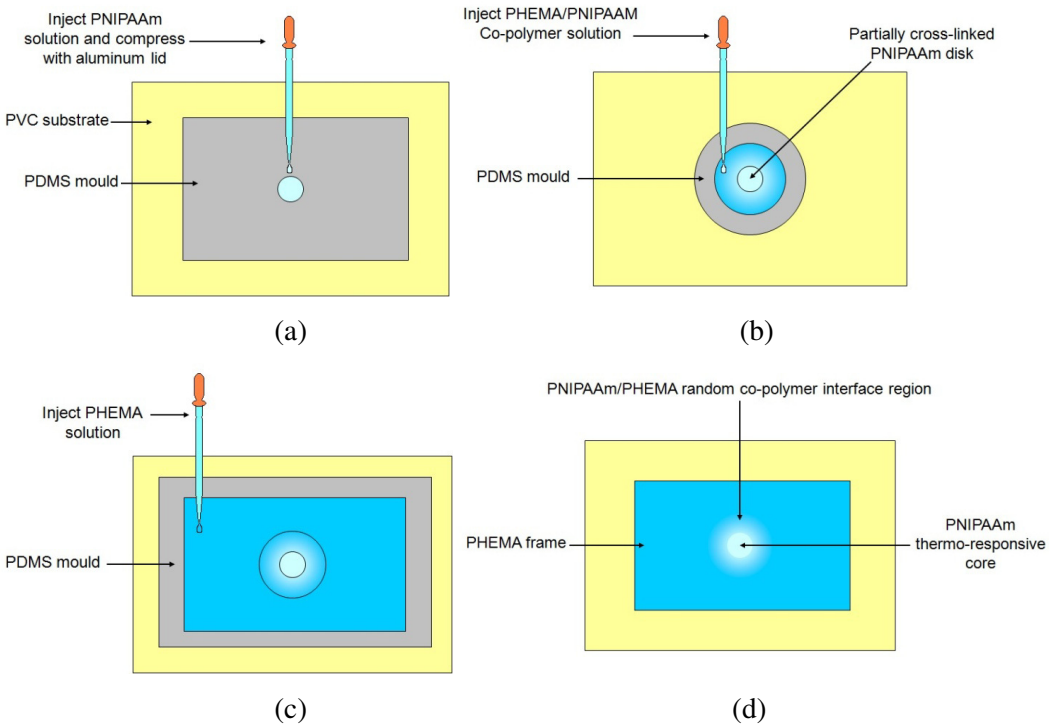

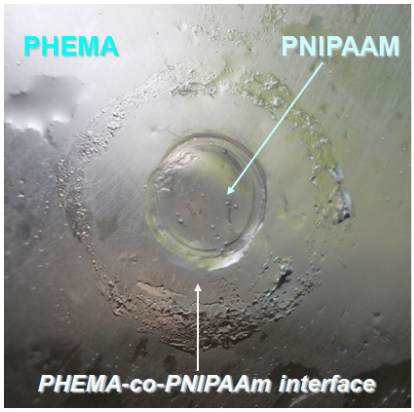


(e)

**Figure A.3.** Scheme representing the fabrication protocol for moulding PHEMA/PNIPAAm interface. a) PNIPAAm disks are realized by standard ICM technique. b) After the disk is formed, an annular silicone mould is positioned on the PVC and a PHEMA-co-PNIPAAm initiated solution is injected in the region between the formed PNIPAAm and the PDMS. c) When the co-polymer is formed, the mould is removed and a second PDMS frame is introduced to inject the PHEMA solution for the final component fabrication. d) The resulting hybrid hydrogel layer is attached to the PVC; its three different regions are indicated. e) Photograph of a realized film, mechanically detached from the substrate.

The main disadvantages of this protocol is that it does not represent a high throughput process, since hybrid layers with only one thermo-responsive core can be fabricated one by one; furthermore, the lack of compression during the second and the third steps, does not provide good control of the overall film thickness, which could constitute a problem during integration on chip. On the other hand, having a wider interface bridging PHEMA and PNIPAAm with intermediate thermo-responsive properties could help to reduce the mechanical stresses between the polymers during the transition.

# Appendix B

# Alternative machining strategies to micro-structure PNIPAAm based hydrogel layers

In this appendix, different alternative techniques for hybrid hydrogel layer micro-patterning are reported. The first two methods rely on the use of other laser based systems: helium-cadmium (HeCd) and neodymium-doped yttrium aluminum garnet (Nd:YAG) lasers were tested to produce a single through-hole on hybrid PHEMA/PNIPAAm layers produced with METHOD 3. Both of these new approaches were tested in order to evaluate the quality of the resulting machining and to check their suitability as alternatives to the excimer laser micro-fabrication, or their feasibility as supporting techniques. On the other hand, a brand new protocol inspired from standard micro-moulding procedures was tested and a futuristic strategy that could be developed based on the results obtained is proposed.

## B.1. HeCd laser machining

The first alternative laser system employed was a continuous HeCd laser, IK 5352 R-D series (KIMMON). Without entering into details of the lasing mechanism taking place in the instrument, a brief description of the system characteristics and of the employed experimental setup are reported below. The available wavelengths at which emission takes place are $\lambda$ = 442 nm and 325 nm. Both of these values fall outside the absorption range of PNIPAAm (190 nm to 270 nm), as reported in 4.1.1. For these tests, the laser was operating at $\lambda$ = 325 nm (relatively close to the PNIPAAm UV/Vis strong absorption region) and with the maximum power available (10 mW). The raw beam was collimated by the laser shutter and it was sent to a mirror and then over a 50 mm focal length lens; the spot was thus focused on the centre of the PNIPAAm region of the film (200 μm thick), which was still attached to the PVC substrate. The position of the sample in respect to the lens was fixed taking care that the

hydrogel layer surface was positioned in the depth of focus determined by the optical system. This location procedure was carried out using a photoactive paper positioned on the film, which allowed a direct visualization of the spot on it, by manually moving the sample until a bright focused spot was seen. Different exposure times (15 and 30 minutes) were chosen to evaluate the effect of the machining. After 15 minutes of exposure, the laser beam caused an evident through-hole in the material (entrance and exit hole diameter was about 120 and 35 μm respectively), bearing the beam's circular profile, shaped by the laser shutter. Furthermore, the polymer looked burned near the feature, having a dark colour in a large surrounding area. When doubling the exposure time, the micro-structure was still present in the hydrogel, but a wider region with evidence of molten re-flowed polymer surrounding the hole was also present. Microscope images of the resulting through-holes are reported in Figure B.1.

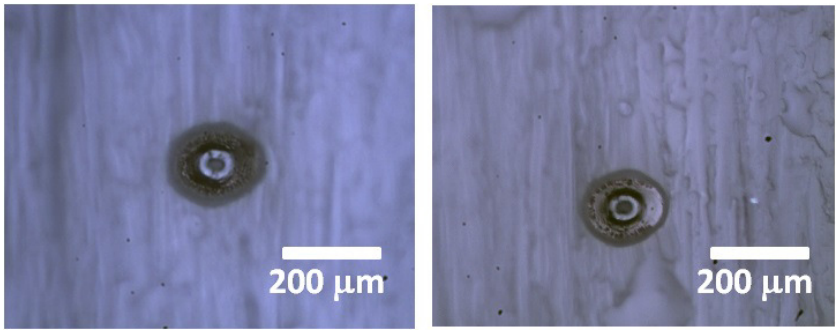


(a) (b)

**FIGURE B.1.** Through-holes produced on a 200 μm thick PHEMA/PNIPAAm layer using a HeCd laser. a) The micro-structure is obtained after exposing the sample to the focused beam for 15 minutes. b) Micro-hole generated on the same sample, doubling the exposure time.

These results were probably determined by the fact that the polymer does not show a significant absorption at the wavelength of the light emitted by the laser, so that disruptive thermal effects are dominating over the photoablation. In this case, the material structure and properties could be changed around the region where the hole is present, so that its thermo-responsive behaviour might be compromised; HeCd laser machining was therefore not found to be a promising technique for processing PNIPAAm based hydrogels.

# B.2. Nd:YAG laser machining

A second laser based technique was developed to machine micro-through-holes in a 200 μm thick PHEMA/PNIPAAm hybrid layer. An Nd:YAG laser (Quanta System, Giant Series, Model G790-20) was used to machine a single through-hole in the PNIPAAm region. Without entering into details of the lasing mechanism taking place in the instrument, a brief description of the system characteristics is reported below. The laser is a Q-switched pulsed laser with fixed repetition rate of 20 Hz, pulse duration of 8 ns and emission at a wavelength of 1064 nm. By using the integrated amplifier and by operating on the system inner optics, a fourth harmonic emission at $\lambda = 266$ nm could be generated, having a nominal initial energy per pulse of 120 mJ. As shown in 4.1.1., a significant absorption of the PNIPAAm films takes place at this wavelength, although its magnitude is decreased by a factor of 7 compared to the operating wavelength of the excimer laser system. The employed experimental setup and the beam focusing on the sample were the same as reported in section B.1. Different exposure times were initially tested; after illuminating the sample for 15, 30, 60 and 120 minutes, no through-hole was observed to be formed on the hydrogel. By dramatically increasing the exposure time to 6 hours, a tapered capillary could be generated in the layer; optical microscope images of the entrance and exit holes in the hydrogel dry state are reported in Figure B.2.

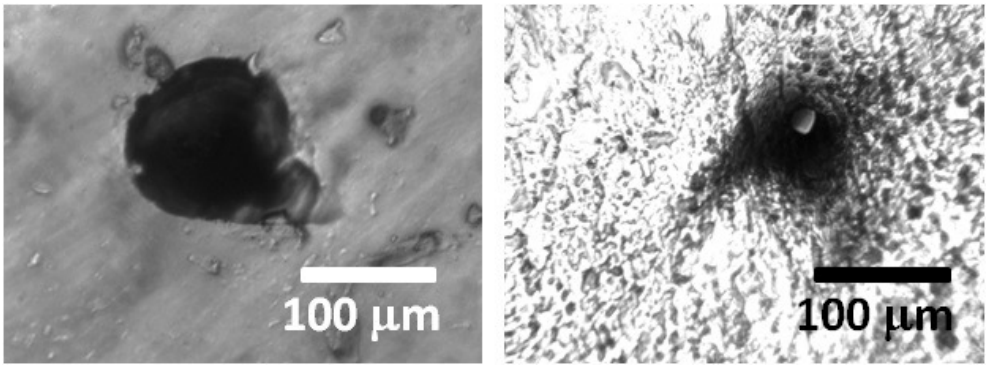


(a) (b)

**FIGURE B.2.** Nd:Yag machined hole on a PHEMA/PNIPAAm hybrid layer moulded with METHOD 3. a) Entrance hole in the dry state. b) Exit hole in the dry state.

As can be seen from the picture, both features present sharp edges and a well defined profile, with minimal debris traces and no presence of molten material in the regions around them. The entrance hole shape is not perfectly circular, but presents a lobe-like structure at one of its sides, reflecting the non circularity of the raw beam itself. The quality of the exit hole is better in terms of shape, though a dark region around it suggests that the bottom surface of the polymeric film was partially over-etched due to the long exposure time. The entrance and exit hole diameters were measured as $<d_{ent}>$ = (96.1±0.9 μm) and $<d_{ext}>$ = (13.9±1.4 μm) respectively. Though the time of machining is definitely too time consuming, the Nd:YAG laser processing seems a suitable technique for producing a single tapered through-hole on the hybrid samples without thermally damaging the material, so it can be considered as a valid supporting fabrication method. Further tests should be carried out in order to achieve more information on the process for exposure times ranging from 3 to 5 hours in order to explore the possibility of reducing the time required for machining the hole.

## B.3. Micro-moulding

A third method for realizing micro-holes in the thermo-responsive core of the hybrid PHEMA/PNIPAAm layers was tested. The technique does not rely on the use of a laser beam to create through-holes in the hydrogels, but on a micro-moulding fabrication scheme. The basic concept of this procedure is to mould the PNIPAAm hydrogel disk around a pre-formed structure, such as a tapered micro-pillar or micro-needle, that is in contact with (or penetrates into) the supporting moulding substrate. After the polymer gelification, the micro-mould would be lifted off from the formed film, thus leaving an empty volume in the hydrogel, with the same geometrical features as the tapered capillaries which are usually machined using the excimer laser. After this step, moulding of the outer elastic PHEMA frame could take place using a procedure similar to the one discussed in 2.A, Appendix A. In this respect, tungsten carbide micro-needles produced by electro-erosion at the Instituto di Tecnologie Industriale e per l'Automazione (ITIA) laboratories (Bari, Italy) were employed as the fixed pre-formed micro-moulds for generating the tapered structures in the forming PNIPAAm hydrogels. These micro-tools were kindly provided as test samples by Dr. Fassi, from the Consiglio

Nazionale delle Ricerche (CNR) engineering division in Milan. Optical microscope images acquired for characterizing the geometrical features of the micro-needles are reported in Figure B.3.

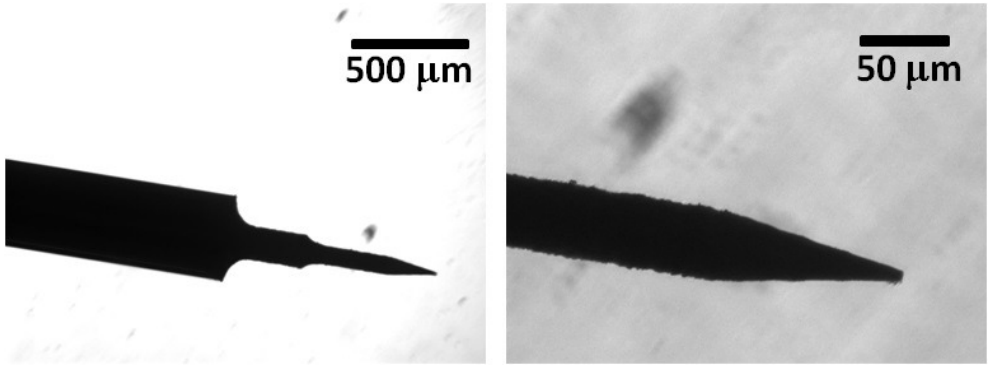


(a) (b)

**FIGURE B.3**. a) Low magnification optical microscope image of a tungsten carbide micro-needle manufactured by electro-erosion at the ITIA's labs. b) Higher magnification showing the needle's tip. The measured tip diameter is about 10 µm.

Tests were carried out fixing a single tungsten carbide needle onto a PTFE substrate by manually promoting a gentle increasing pressure of the tip onto the plate; after this delicate operation, the PNIPAAm disk was moulded around it, using a standard silicone spacer defining the final hydrogel shape. After injection of the polymerizing solution (PNIPAAm4x) in the mould, having the micro-needle positioned at its centre, the whole moulding apparatus was sealed in a chamber where nitrogen gas was flowed at a pressure of 0.2 bar. In this way, the PNIPAAm gelification was dramatically accelerated and happened in a few minutes. Immediately after the gel was formed, a second silicone mould defining the final PHEMA frame was positioned around the disk, still having the micro-tool fixed at its centre, and the polymerizing elastic hydrogel solution was injected. The hybrid film was then recovered on the PTFE plate. This test micro-moulding protocol is reported in Figure B.4.

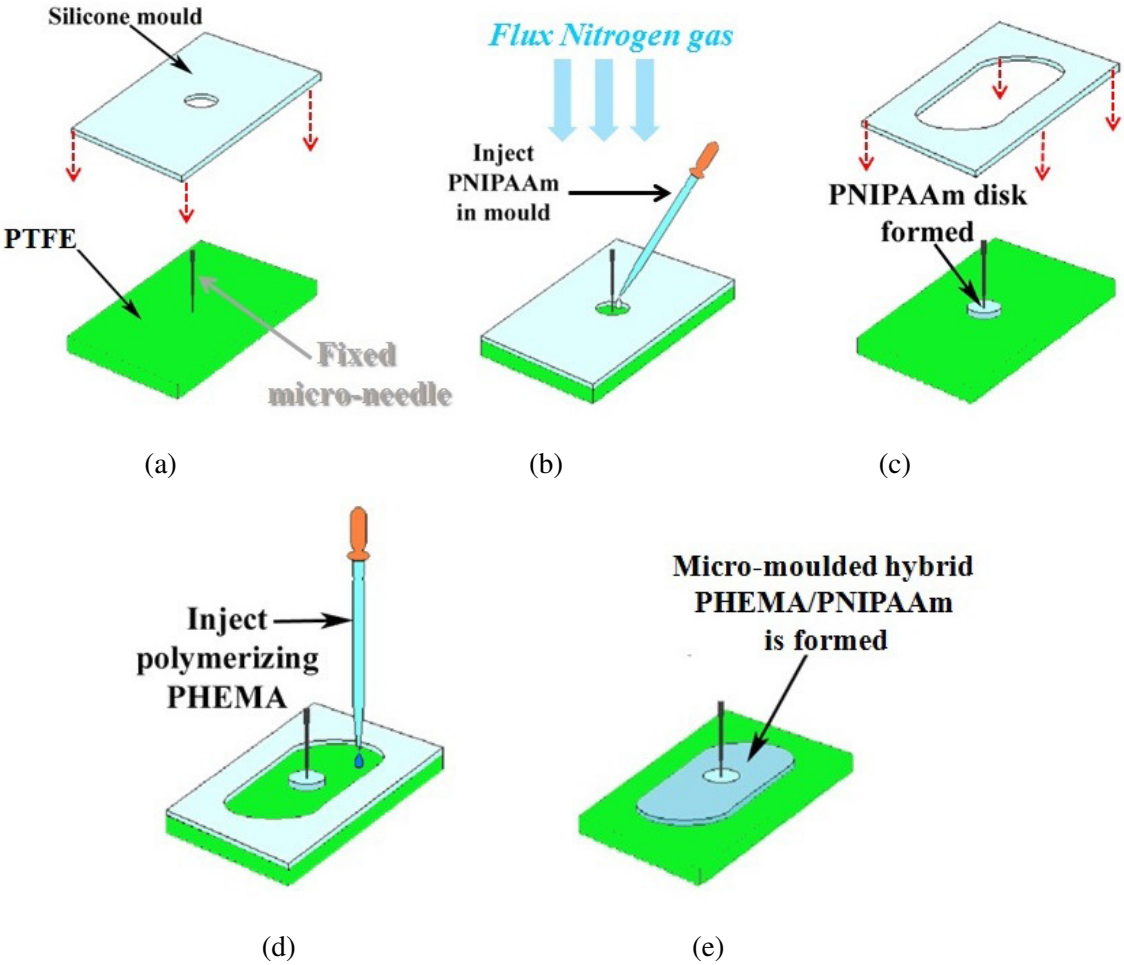


**FIGURE 3.B.**. Hybrid hydrogel layers micro-moulding manufacturing protocol using tungsten carbide micro-needles. a) The needle is fixed onto the PTFE plate and the silicone mould is positioned on top. b) PNIPAAm4x solution is injected in the hollow region of the mould around the needle and the polymerization reaction takes place under nitrogen flow. c) The PNIPAAm disk is formed with the embedded needle and the PDMS spacer for PHEMA moulding is positioned onto the substrate. d) PHEMA polymerizing solution is injected around the disk. e) The micro-moulded hybrid layer is formed on the PTFE plate.

The formed layer could then be mechanically detached from the substrate using a spatula. After removal, the hybrid hydrogel was continuously wetted with MilliQ water using a glass pipette to promote its partial swelling so that the needle could be easily lifted off using a

tweezer. A photograph of the freestanding hydrogel film still having the needle fixed at its centre and optical microscope images of the resulting through-hole formed in the PNIPAAm are shown in Figure B.5.

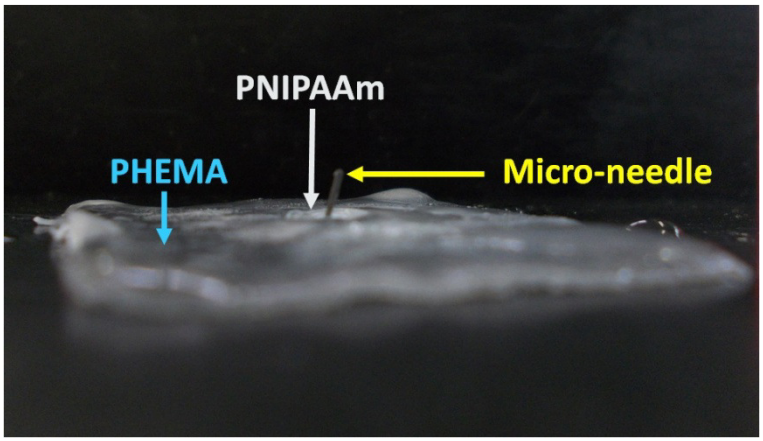


(a)

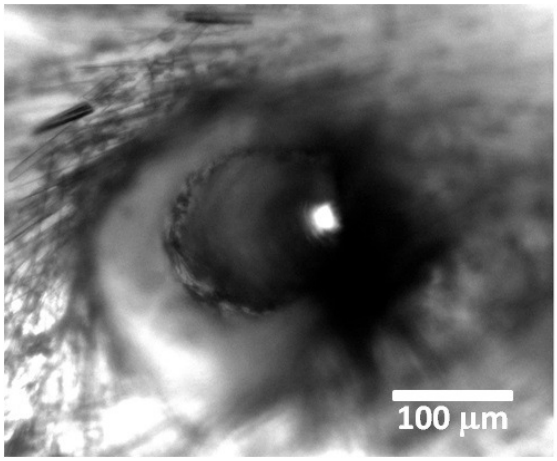


(b)

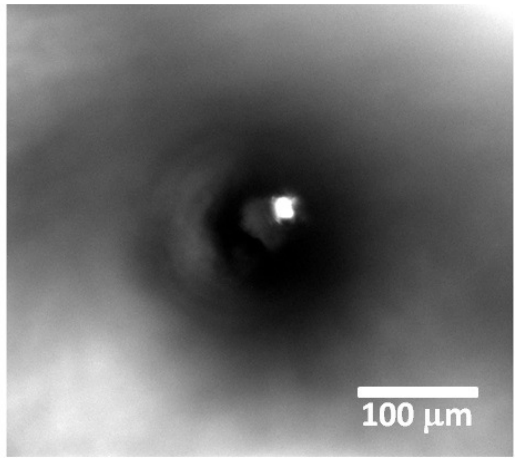


(c)

**FIGURE B.5.** a) Photograph of a partially hydrated PHEMA/PNIPAAm freestanding hybrid layer positioned on a PVC support with an embedded tungsten carbide micro-needle. b) Microscope image of the micro-moulded entrance hole in the polymer dry state; the measured diameter is $\langle d_{ent} \rangle$ = (132.1±2.0 µm). c) Microscope image of the resulting exit hole in the polymer dry state; the measured diameter is $\langle d_{ext} \rangle$ = (17.9±1.2 µm).

The moulded through-hole presents exit and entrance hole diameter values comparable with the ones obtained when excimer laser machining was carried out using the 1.5 mm hole mask, thus demonstrating the suitability of this new fabrication scheme to generate such micro-structures. However, a number of issues derived from this preliminary test can be summarized as follows:

- Only a single through-hole can be fabricated on a single hybrid layer per time, thus not allowing high-throughput manufacturing.
- Though PTFE is a relatively softer plastic compared to the PVC used in the rest of this work, the fixing procedure of the needle is cumbersome and too delicate, causing the breaking of the fragile tungsten carbide tip on many occasions. Furthermore, at this stage there is no control over the positioning and penetration depth of the tip, resulting in a poor control over the exit hole diameter.
- The circularity of the holes is acceptable, but the lift off of the needle caused a protruding region around the entrance hole (Figure B.5 – b) which is probably due to the polymer deformation in the direction of its thickness during this micro-moulding removal procedure.
- For all the above reasons, the protocol was not found to be highly reproducible (< 50% of successes).

Since the characteristic dimensions and relatively good quality of the holes produced were promising with this technique, a more sophisticated apparatus for micro-moulding hybrid hydrogels using this type of tungsten carbide needles was designed, but there was insufficient time to develop it further. To give an idea of the improvements the new system could bring to the manufacturing method tested, a brief summary of its features are described below. The first change would be in refining the control of the tip's movement perpendicularly to the substrate, which would not happen manually, but through a microtranslator, where the tip is assembled on an appropriate support. The system could either be driven manually or through a stepper motor, in order to also control the needle's movement rate as well. In this way, the penetration depth could also be ensured if the system is mounted on a suitable stage and the substrates are sufficiently flat; the use of a 20x objective with high depth of focus connected

to a camera could help monitoring the needle approaching the substrate. To ensure contact between the tip of the needle and the moulding substrate, an electrical signal generated when contact is established would be suitable. In case of non conductive substrates (such as PTFE) gold sputtering over the moulding surface would be sufficient for conferring electrical transport properties to the material. In this way, the tungsten carbide needle and the moulding substrate would act as an electrical switch. A schematic picture resembling these ideas is reported in Figure B.6, where the moulding substrate was considered to be a rough aluminum plate, as used in Chapter 3 (3.3.2), and shown to have the same adhesive properties as rough PVC for physically binding PNIPAAm based hydrogels. In the schematization reported, the micro-moulding would happen in a contact mode between the tip and the substrate and not with the needle penetrating into the moulding plate.

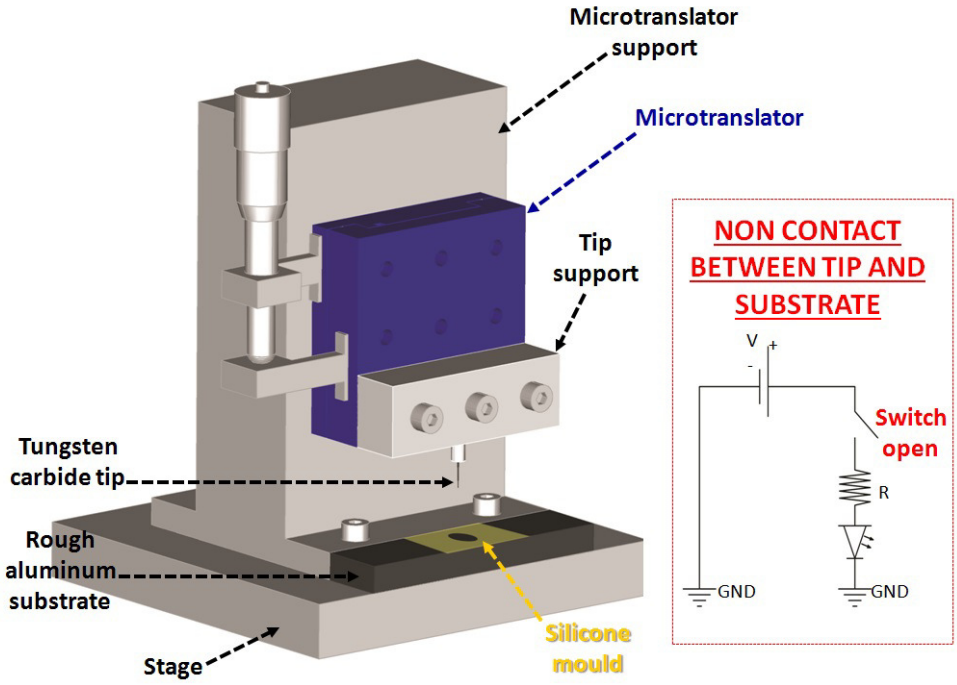


(a)

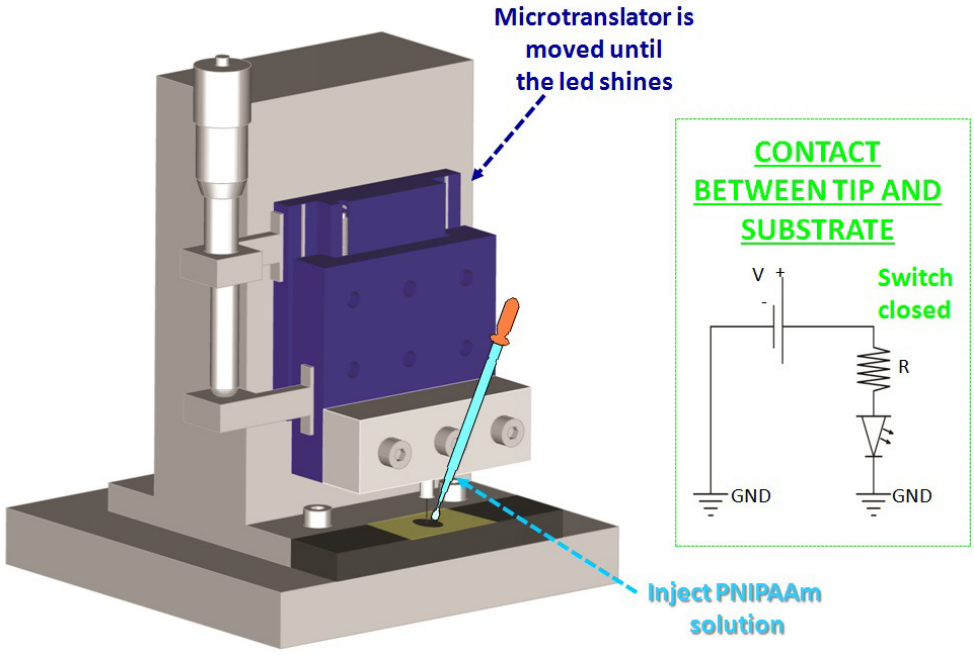


(b)

**FIGURE B.6.** Schematization of the micro-moulding apparatus. a) Assembled system in a non-contact configuration. b) Moulding step when the needle is in contact with the substrate, as indicated by an LED switching on.

In order to continue to consider a moulding procedure where the tip penetrates into a relatively soft substrate (PTFE, rubber or silicone based polymers), the possibility of integrating a heater in the needle support to increase the tip's temperature would promote a more efficient penetration of the substrate, still having the penetration depth controlled by the microtranslator movement. Furthermore, equipping the moulding apparatus with a wider support with a micro-needles array and an integrated injector for delivering the polymerizing solutions directly in the moulds renders this micro-moulding technique more promising for future realization of a high throughput PNIPAAm based hydrogel layer manufacturing process.

# Acknowledgements

This work has been supported by Fondazione CARIPLO for the project 'Hybrid Multifunctional Microdevices to Probe Cell Biology', under the Program 'Promuovere progetti internazionali finalizzati al reclutamento di giovani ricercatori', and by and The Innovative Manufacturing and Construction Research Centre in collaboration with Loughborough University.

# Personal thanks

I wish to thank my supervisors Dr. Cristina Lenardi, Prof. Paul P. Conway and Dr. David A. Hutt for their constant support, effort and helpfulness during the whole period of my Phd. A special thank goes to Dr. Patrick Webb, who has guided me through the first steps of the research as the principal investigator of the project funded by Fondazione CARIPLO and could have made this dual Phd possible. Many thanks to Prof. Paolo Milani and to all the CIMaINa group for useful discussions and support. I also wish to thank Prof. Changqing Liu and Dr. Yang Liu for their kindness and helpfulness during the time I spent in Loughborough and for having supported me during my research. My dear collegues Mr. Yunsong Yan, Dr. Federico Gassa, Dr. Federico Martello, Dr. Alessandro Tocchio, Dr. Weiwei Zhao, Dr. Margerita Tamplenizza and Dr. Carsten Shulte have been fundamental for me to carry on the research because of their constant help in every moment: thank you guys. Loads of thanks go to Francesco Cavaliere and Daniele Viganò from the Mechanical Workshop of the Physics department in Milan, who have realized most of the components and devices which have had a crucial role in my research project. A big thank you also goes to Mr. David Britton, Mr. Lewis Jones, Mr. Mark Capers and Mr. Peter Wileman from the Optical Engineering Lab in Loughborough who have been more than kind all the time and have helped me a lot throughout the laser processing stage. Of course, many thanks to all the technical and administrative staff both in Milan and Loughborough. I also wish to say thanks to all the people at the Mechanical Workshop in Loughborough, to Dr. Daniele Marinotto from the

Optical Laboratories in CIMaINa and to Mr. Andy Sandaver from the specimen preparation and materials lab in Loughborough, without whom I probably would have been lost at the Wolfson School. Many thanks to all of my dear friends in Milan and Loughborough, to my family and to Vale for simply having been there with me all the time, wherever I was. Thank you all.